

Issue 1

2016 | Volume 12

The Journal on Advanced Studies in Theoretical and Experimental Physics,
including Related Themes from Mathematics

PROGRESS IN PHYSICS



“All scientists shall have the right to present their scientific research results, in whole or in part, at relevant scientific conferences, and to publish the same in printed scientific journals, electronic archives, and any other media.” — Declaration of Academic Freedom, Article 8

ISSN 1555-5534

PROGRESS IN PHYSICS

A quarterly issue scientific journal, registered with the Library of Congress (DC, USA). This journal is peer reviewed and included in the abstracting and indexing coverage of: Mathematical Reviews and MathSciNet (AMS, USA), DOAJ of Lund University (Sweden), Scientific Commons of the University of St. Gallen (Switzerland), Open-J-Gate (India), Referativnyi Zhurnal VINITI (Russia), etc.

Electronic version of this journal:
<http://www.ptep-online.com>

Advisory Board

Dmitri Rabounski,
Editor-in-Chief, Founder
Florentin Smarandache,
Associate Editor, Founder
Larissa Borissova,
Associate Editor, Founder

Editorial Board

Pierre Millette
millette@ptep-online.com
Andreas Ries
ries@ptep-online.com
Gunn Quznetsov
quznetsov@ptep-online.com
Felix Scholkmann
scholkmann@ptep-online.com
Ebenezer Chifu
chifu@ptep-online.com

Postal Address

Department of Mathematics and Science,
University of New Mexico,
705 Gurley Ave., Gallup, NM 87301, USA

Copyright © *Progress in Physics*, 2016

All rights reserved. The authors of the articles do hereby grant *Progress in Physics* non-exclusive, worldwide, royalty-free license to publish and distribute the articles in accordance with the Budapest Open Initiative: this means that electronic copying, distribution and printing of both full-size version of the journal and the individual papers published therein for non-commercial, academic or individual use can be made by any user without permission or charge. The authors of the articles published in *Progress in Physics* retain their rights to use this journal as a whole or any part of it in any other publications and in any way they see fit. Any part of *Progress in Physics* howsoever used in other publications must include an appropriate citation of this journal.

This journal is powered by \LaTeX

A variety of books can be downloaded free from the Digital Library of Science:
<http://www.gallup.unm.edu/~smarandache>

ISSN: 1555-5534 (print)

ISSN: 1555-5615 (online)

Standard Address Number: 297-5092
Printed in the United States of America

January 2016

Vol. 12, Issue 1

CONTENTS

Rybicki M. Type Ia Supernovae Progenitor Problem and the Variation of Fundamental Constants	3
Hafeez H. Y., Chifu E. N., Musa I. M. Schrödinger Equation for a Half Spin Electron in a Time Dependent Magnetic Field	15
Consiglio J. On the Absorber in Gravitation	20
Scholkmann F. Power-Law Scaling of the Impact Crater Size-Frequency Distribution on Pluto: A Preliminary Analysis Based on First Images from New Horizons' Flyby ..	26
Gogberashvili M. Standard Model Particles from Split Octonions	30
Zaninetti L. and Scholkmann F. The Impact Crater Size-Frequency Distribution on Pluto Follows a Truncated Pareto Distribution: Results from a First Data Set Based on the Recent New Horizons' Flyby	34
Belyakov A. Determination of the Neutrino Mass	36
Danilov V. On the Nature of the Magnetic Field of the Earth and Other Planets	41
Weng S. A Classical Model of the Photon	49
Potter F. Update on Pluto and Its 5 Moons Obeying the Quantization of Angular Momentum per Unit Mass Constraint of Quantum Celestial Mechanics	56
Belyakov A. On the Deviation of the Standard Model Predictions in the Large Hadron Collider Experiments (<i>Letters to Progress in Physics</i>)	59
Zhang T. X., Wilson C., Schamschula M. P. X-Ray Flares from Sagittarius A* and Black Hole Universe	61
Crothers S. J. On an Apparent Resolution of the Catt Question	68
Catania J. The Roland De Witte Experiment, R. T. Cahill, and the One-Way Speed of Light (<i>Letters to Progress in Physics</i>)	70
Spivey R. J. A Non-anthropocentric Solution to the Cosmological Constant Problem	72
Robitaille P.-M. Further Insight Relative to Cavity Radiation III: Gedanken Experiments, Irreversibility, and Kirchhoff's Law	85
Rybicki M. Mansouri-Sexl Test Theory: The Question of Equivalence between Special Relativity and Ether Theories	89

Information for Authors

Progress in Physics has been created for rapid publications on advanced studies in theoretical and experimental physics, including related themes from mathematics and astronomy. All submitted papers should be professional, in good English, containing a brief review of a problem and obtained results.

All submissions should be designed in L^AT_EX format using *Progress in Physics* template. This template can be downloaded from *Progress in Physics* home page <http://www.ptep-online.com>

Preliminary, authors may submit papers in PDF format. If the paper is accepted, authors can manage L^AT_EX typing. Do not send MS Word documents, please: we do not use this software, so unable to read this file format. Incorrectly formatted papers (i.e. not L^AT_EX with the template) will not be accepted for publication. Those authors who are unable to prepare their submissions in L^AT_EX format can apply to a third-party payable service for LaTeX typing. Our personnel work voluntarily. Authors must assist by conforming to this policy, to make the publication process as easy and fast as possible.

Abstract and the necessary information about author(s) should be included into the papers. To submit a paper, mail the file(s) to the Editor-in-Chief.

All submitted papers should be as brief as possible. Short articles are preferable. Large papers can also be considered. Letters related to the publications in the journal or to the events among the science community can be applied to the section *Letters to Progress in Physics*.

All that has been accepted for the online issue of *Progress in Physics* is printed in the paper version of the journal. To order printed issues, contact the Editors.

Authors retain their rights to use their papers published in *Progress in Physics* as a whole or any part of it in any other publications and in any way they see fit. This copyright agreement shall remain valid even if the authors transfer copyright of their published papers to another party.

Electronic copies of all papers published in *Progress in Physics* are available for free download, copying, and re-distribution, according to the copyright agreement printed on the titlepage of each issue of the journal. This copyright agreement follows the *Budapest Open Initiative* and the *Creative Commons Attribution-Noncommercial-No Derivative Works 2.5 License* declaring that electronic copies of such books and journals should always be accessed for reading, download, and copying for any person, and free of charge.

Consideration and review process does not require any payment from the side of the submitters. Nevertheless the authors of accepted papers are requested to pay the page charges. *Progress in Physics* is a non-profit/academic journal: money collected from the authors cover the cost of printing and distribution of the annual volumes of the journal along the major academic/university libraries of the world. (Look for the current author fee in the online version of *Progress in Physics*.)

Type Ia Supernovae Progenitor Problem and the Variation of Fundamental Constants

Maciej Rybicki

Sas-Zubrzyckiego 8/27, 30-611 Krakow, Poland

E-mail: maciej.rybicki@icloud.com

Cosmological observations strongly suggest our universe is the interior of an expanding black hole. If the constant mass of the universe is assumed then from the equation for Schwarzschild radius: $r_S = 2Gmc^{-2}$ it follows that proportionality constant Gc^{-2} depends linearly on the universe's radius R_u , identified with r_S , i.e. $Gc^{-2} \sim R_u$, $M_u = \text{const}$. Because the Chandrasekhar limit M_{Ch} relates to the speed of light and to the Newton's constant as $M_{Ch} \sim (c/G)^{3/2}$ so expansion involves gradual decrease of M_{Ch} . In result, a single white dwarf can alone become the Type Ia supernova progenitor, which provides a complementary solution to single-degenerate and double-degenerate models for SNe Ia. Both alternative scenarios: $G \sim R_u$ and $c \sim R_u^{-1/2}$ are analyzed in regard of their consistence with observations, and their consequences to cosmology.

1 Introduction

On account of the supposed uniformity of their absolute magnitude, the Type Ia supernovae (SNe Ia) play an important role of “standard candles” in cosmology. A tight correlation between the peak light output and the light-curve width (width-luminosity relation) results from the way SNe Ia originate from white dwarfs (WDs) — the final remnants for low and medium mass stars. According to the current understanding, the carbon-oxygen (CO) thermonuclear fusion triggering the supernova explosion takes place in compact binary systems in either of two principal progenitor channels. A single-degenerate (SD) model (Whelan & Iben [80]) predicts that CO WD accretes matter from the companion, usually the red giant or the main sequence star. Just before approaching the Chandrasekhar mass-limit $M_{Ch} \approx 1.44M_{\odot}$ for which electron degeneracy pressure becomes insufficient to prevent the gravitational collapse, the WD's core reaches the ignition temperature for the runaway carbon and oxygen fusion into heavier elements. In a preceding time lasting usually $\sim 10^6$ yr WD processes the transferred matter falling onto its surface through the accretion disc. In this phase, called “nuclear-burning white dwarf” (NBWD) the hydrogen-helium fusion releases energy in a form of copious X-radiation, observed as “super-soft X-ray source” (Di Stefano [17]).

Instead, the double-degenerate (DD) model (Webbink [79], Iben & Tutukov [37]) predicts that two WDs of the combined mass $\geq M_{Ch}$ form a compact binary system and subsequently spiral towards each other in a common envelope. Eventually, they collide and merge and, after exceeding the Chandrasekhar limit, explode as SN Ia. Unlike in accrete scenario the merging WDs are not expected to be the source of X-radiation until a short time preceding the supernova explosion. The X-ray signatures of SD and DD channels differ significantly, which makes them easy to distinguish. The DD

model admits a broader range of progenitor mass and SNe Ia luminosity; thus is thought to be responsible for the non-standard SNe Ia explosions.

These two basic models (hereinafter collectively referred to as “SNe Ia binary paradigm”) do not however provide a fair explanation to the diversity in the observed characteristics of SNe Ia and the paucity of their potential progenitors. The relevant SNe Ia progenitor problem amounts to the following two items. First is the problem of SNe Ia rate: the total number of potential progenitors seems to be inadequate to the number of observed SNe Ia events. Second is the problem of SNe Ia properties: the observed light-curves and remnants spectra do not match satisfactorily the detailed predictions of SD and DD models.

Our goal here is to provide a solution to the progenitor problem based on assumption of the varying Chandrasekhar mass, a consequence of varying constant Gc^{-2} . It's not been a century yet since one realized our universe has a turbulent history behind and some kind of final fate ahead. Compared with the prior model of eternal and basically invariable universe, this forms quite different ground for thinking about physical fundamental constants. One cannot ascribe logical necessity to any of fundamental constants (class C “universal” constants, according to Uzan's nomenclature (Uzan [74]) as e.g. in the case of mathematical constant π or the Euler's number e). Likewise, one cannot obtain them by pure deduction in a way similar to that Eddington tried (ineffectively) to do with the fine structure constant alpha. For the time being, they work as “free parameters”. Hence, still valid is Dirac's opinion: “It is usually assumed that the laws of nature have always been the same as they are now. There is no justification for this. The laws may be changing, and in particular quantities which are considered to be constants of nature may be changing with cosmological time” (Dirac [16]). Let us complement this opinion with another one: “Ignoring the

possibility of varying constants could lead to a distorted view of our universe and if such a variation is established corrections would have to be applied” (Uzan [74]).

2 The SNe Ia progenitor problem: a brief overview

The question of identity of Type Ia supernovae progenitors is widely considered as the “major unsolved problem in astrophysics” (Maoz & Mannucci [47]). The main problem is the discrepancy between the observed SNe Ia rate and the number of potential progenitors. Taking into account the estimated rate of SNe Ia ($\sim (10^{-3} - 10^{-2})\text{yr}^{-1}$ events in a typical spiral or elliptical galaxy) and the mean/median delay time for the SNe Ia progenitors ($\sim (0.5 - 1)$ Gyr for DD channel and $\sim (2 - 3)$ Gyr for SD channel), X-ray sources should manifest in thousands in any such galaxy including the Milky Way. Meanwhile, the X-ray flux from the sample of six neighboring spiral galaxies obtained from Chandra X-ray Observatory is a factor of 30-50 times fainter than expected (Gilfanov & Bogdan [29]). In some of SNe Ia previously thought to originate in SD channel no remnants of red giant has been observed (Schaeffer & Pagnotta [70], Li et al. [42], Nugent et al. [56]). Generally, in most cases red giants have been excluded as possible ex-companions in binaries. The discrepancy between the observed amount of X-ray sources and the assessed numbers of SNe Ia led to conclusion that accrete scenario is not a primary route to supernovae, giving priority to the merger scenario. Gonzalez Hernandez et al. [30] estimate that fewer than 20% of SNe Ia is produced in SD channel. Gilfanov & Bogdan [29] opt for even more stringent limit $\leq 5\%$ of total population. Di Stefano [17] indicates the lack of 90% – 99% of the required number of X-ray sources. She argues (Di Stefano [18]) that companion stars forming the double degenerates do not age at the same rate and thus do not become WDs at the same time; for that reason the common envelope phase should be preceded by a symbiotic pre-double-degenerate phase with the hydrogen-helium fusion similar to NBWD. Thus, merger channel should also produce X-ray flux comparable to the accrete channel prior to the common envelope phase, which puts into doubt DD model as an effective explanation.

A vital problem is the paucity of the observed white dwarfs mergers. According to Gilfanov [28] “...too few double-white-dwarf systems appeared to exist”. One expects the ESO Supernovae Type Ia Progenitor Survey (SPY) (Napitowzki et al. [54, 55]) and the ongoing Sloan White dwarf Radial velocity data Mining Survey (SWARMS) (Badenes et al. [3], Mullally et al. [53]) to provide evidences for the merger channel (DD) as the main route to SNe Ia. Badenes & Maoz [4] using Doppler techniques isolated 15 WD binaries from a sample of $\approx 4,000$ WDs brought by Sloan Digital Sky Survey (SDSS). They compared the rate of WD binaries with the rate of SNe Ia in the Milky Way-like Sbc galaxies and found a “remarkable agreement” between them. How-

ever, a majority of these WD binaries appeared to be sub-Chandrasekhar, although usually with total mass relatively close to M_{Ch} ($1.1 - 1.2M_{\odot}$).

Some of researches (Hachisu et al. [34], Van Kerkwijk et al. [40], Zhu et al. [82], Maoz & Mannucci [47]) claim that the requirement as to the total mass of merging CO WDs (i.e. $1.4M_{\odot}$) is too restrictive. This would match observations of super-Chandra WD progenitor stars with the combined mass reaching $2.4 - 2.8M_{\odot}$. According to the respective models, the observed number of SNe Ia can be explained provided the wider range of combined mass: smaller than M_{Ch} (sub- M_{Ch} merger channel) or bigger than M_{Ch} (super- M_{Ch} merger channel), dependently on detailed conditions such as rotation, magnetic fields, metallicity and the host galaxy population. This would account for better agreement with observations, both as to the rate of SNe Ia and to the differences in their properties. The controversial point of these models is that they require special fine-tuning to be effective. Maoz & Mannucci [48] attribute some of discrepancies as caused by “deadly sins”, i.e. incorrect or inadequate methods in measuring and analyzing the SNe Ia rates. They admit however the “detailed models still falls short of the observed number (of SNe Ia) by at least factor of a few”.

Di Stefano [18] suggests that, possibly, only a small fraction of accreting WDs can be detected and identified as X-ray sources. This may occur by two reasons: either the winds from a companion giant reprocess the supersoft X-ray radiation into the radiation of longer wavelengths, or the duty cycle of nuclear burning is too low to be detected. However, neither of these solutions has been properly recognized and confirmed as yet. Another proposal (Di Stefano et al. [19]) links the mass of progenitor with the angular momentum gained from the donor star together with matter. The angular momentum prevents the super- M_{Ch} WD from collapse, which widens the potential range of SNe Ia progenitors. The relevant “spin-up/spin-down” models predict the existence of numerous WD “ticking bombs” waiting to explode until their rotation slows down to a proper level.

There is a broad agreement (e.g. Totani et al. [73], Maoz et al. [48], Mennekens et al. [50], Hachisu et al. [33]) as to the key role of “delay time distribution” (DTD) — the number of SNe Ia events in unit time as a function of time elapsed since starburst, in predicting the SNe Ia rates. It seems that DTD (indicated as t^{-1} power law) favors the DD scenario. Hachisu et al. [33] found a good agreement of DTD with SD model either, provided the donor stars are both red giants and the main-sequence stars. Undoubtedly, DTD introduces an indispensable methodological order to the SNe Ia progenitor problem. In general however, regarding DTD did not bring a decisive breakthrough so far in the question of identity of SNe Ia progenitors.

It has gradually become evident that SNe Ia are not “standard candles” in the originally attributed sense. Their intrinsic luminosity is neither considered nor demanded to be ex-

actly uniform, which gives priority to the more “capacious” merger channel. Instead of standard candles, SNe Ia are currently interpreted as “standardizable candles”, which means that utilizing them as the correct distance indicators requires due calibration. This in turn demands better recognizing of their origin and nature. The study by Linden, Virey & Tilquin [43] revealed a likely positive correlation between the SNe Ia absolute brightness and distance, which may put in question the actually determined cosmological parameters. The observed relationship between the intrinsic color and ejecta velocity may help in reducing systematic biases in the estimates of distance (Foley et al. [25]). Instead, Sullivan et al. [72] point to the relationship between the luminosity of SNe Ia and metallicity of their hosts, while metallicity is supposed to depend on redshift. Gallagher et al. [26] comparing the spectra of a sample of 29 early elliptical galaxies of the age exceeding 5 Gyr with the general sample from SDSS including younger galaxies, find a strong correlation between the absolute magnitude of SNe Ia and the age of host galaxies while, most likely, “. . . the observed trend with metallicity is merely an artifact brought about by the evolutionary entanglement of age and metallicity”. These findings may help in recognizing the properties of SNe Ia, which is particularly important for the question of dark energy and the relevant accelerating expansion of the universe (Riess et al. [66], Perlmutter et al. [60]). The supposed correlation between the absolute magnitude and distance suggests the presence of a time dependent factor in the effective SNe Ia progenitor model.

3 Varying Chandrasekhar limit as the postulated main route to SNe Ia

The mass-limit formula for white dwarfs based on the equation of state for ideal Fermi gas (Chandrasekhar [11]) reads

$$M_{Ch} = 4\pi \left(\frac{K_2}{\pi G} \right)^{3/2} \omega_3^0, \quad (1)$$

where ω_3^0 is the numerical constant equal to 2.018, derived from the explicit solution of the Lane-Emden equation for the polytropic index $n = 3$. The constant K in the general case connects pressure and density: $P = K\rho^{(n+1)/n}$ while in the case including white dwarfs (i.e. for $n = 3$) becomes specified as $P = K_2\rho^{4/3}$. Since K_2 is defined as

$$K_2 = \frac{1}{8} \left(\frac{3}{\pi} \right)^{1/3} \frac{hc}{(\mu_e m_H)^{4/3}} \quad (2)$$

(μ_e -mean molecular mass per electron, m_H -mass of hydrogen atom), so substituting gives

$$M_{Ch} = 4\pi \left[\frac{1}{8} \left(\frac{3}{\pi} \right)^{1/3} \frac{hc}{(\mu_e m_H)^{4/3} \pi G} \right]^{3/2} \omega_3^0. \quad (3)$$

Collecting the pure numbers, and considering that $\hbar = h/2\pi$, one gets

$$M_{Ch} \approx 1.11065 \times 10^{54} \mu_e^{-2} m_P^3, \quad (4)$$

where $m_P = (\hbar c/G)^{1/2}$ is the Planck mass. Since CO WDs are mainly composed of carbon-12 and oxygen-16, and because in both cases atomic number equal to half the atomic weight so one has $\mu_e = 2$, leading to $M_{Ch} \approx 1.44 M_\odot$. It is important that Chandrasekhar mass is proportional to the cube of Planck mass:

$$M_{Ch} \sim m_P^3. \quad (5)$$

Assuming $\hbar = const$ it relates to the speed of light and to the Newton’s gravitational constant as

$$M_{Ch} \sim (c/G)^{3/2}. \quad (6)$$

(We use tilde for linear dependence in the cases when the variability of a reference quantity [here: c and G] is hypothetical. Instead, the symbol of proportionality [exact or approximate] \propto is used when variation of a reference quantity is obvious or certain, e.g. cosmic time t or radius of universe R_u).

From this relationship it follows that any cosmological model postulating varying G or/and c (except the case they change accordingly) implies the postulate of varying M_{Ch} . This fact has not been properly explored so far. What we propose here is the “varying Chandrasekhar mass-limit” model (VCM) in which M_{Ch} decreases in cosmic time. VCM postulates that the currently known value of Chandrasekhar limit refers solely to the present epoch while in general:

$$M_{Ch}(\text{past}) > 1.44 M_\odot > M_{Ch}(\text{future}). \quad (7)$$

This determines a scenario for the single WD progenitors of SNe Ia, which can be outlined as follows. Once an individual WD is formed, it keeps its mass approximately constant during the cooling process while the Chandrasekhar limit gradually decreases in time. Eventually, it equates or approaches a given WD’s mass triggering the SN Ia explosion. From a logical point of view, an effect of SN Ia caused by decreasing M_{Ch} reminds bringing water to a boil by reducing the atmospheric pressure without supplying heat. Hence, single WDs are, along with binary WDs, the potential progenitors of SNe Ia.

4 Varying constants and the black-hole cosmology

Varying Chandrasekhar limit, as a hypothesis based on assumption of varying constants c or/and G is closely related to the black-hole cosmology. A constitutive observation of the respective models is the coincidence between the radius of observable universe and the Schwarzschild radius, supposed to be valid over the whole course of the universe’s history. According to a hypothesis advanced by Pathria [58] and Good [31], the universe is the interior of a black hole existing, among many others, within a larger structure called multiverse.

The recent multiverse model by Popławski [64, 65] uses the Einstein-Cartan-Sciama-Kibble theory removing from General Relativity the constraint of symmetry in the affine

connection, and regarding the antisymmetric variable torsion tensor in the Friedmann equations. The relevant cosmological scenario takes an advantage of the fact that most stars have a non-zero angular momentum. When a massive rotating star collapses to a (Kerr) black hole, the torsion of extremely dense matter inside the horizon prevents from the point singularity (replaced by the ring singularity). As a result, the black hole becomes a wormhole to another universe thought to originate in “big bounce”. As far as our own universe is the interior of a black hole existing in another universe, any black hole in our universe is thought to contain (produce) a separate universe. The new universe is interpreted as a “white hole” — a time reversal black hole whose expansion, e.g. such as observed in our universe is driven by the torsion, identified with dark energy. This model predicts the presence of traces of primordial torsion in a form of slight anisotropies in both cosmic and nanoscopic scales. Some reported evidences of the preferred handedness of spiral galaxies (dipole asymmetry of the value 0.0408 ± 0.011 based on SDSS data sample containing 15,158 spiral galaxies with the redshift < 0.085) seem to support the idea of cosmic parity violation (Longo [44]). However, the area covered by this sample is still too small to derive unambiguous conclusions. According to Neta Bahcall “The directional spin of spiral galaxies may be impacted by other local gravitational effects”.

Besides, even if the filaments forming the cosmic web are uniformly distributed, anisotropy connected with rotation will break the homogeneity in a deeper sense. In the isotropic cosmic space, the “center” is a purely relative concept connected with the notion of observable universe. But it is no longer relative in the anisotropic space with the fixed axis of rotation. The spinning universe implies, besides anisotropy, the presence of preferred points. We may think about analogies between directional spin of spiral galaxies and the Coriolis effects on the Earth, e.g. manifesting itself in different spin of hurricanes in north and south hemispheres. Anyway, the question of spinning universe is, in the end, a matter of (further) observations.

The model here proposed (VCM) bases on formal resemblance of our universe with a black hole (and thus we shall use the Schwarzschild equation for radius) yet does not settle whether the universe is a black hole in the literal sense. It seems instead that crucial property of the universe conceived as the interior of a black hole is that its total energy amounts to zero. In this regard, the black-hole cosmologies are close to the “zero-energy universe” theories.

The legitimacy for interpreting the universe in terms of a black hole depends on its parameters, in particular size, density and mass. Recent estimations concerning the radius of observable universe point to the value ≥ 14 Gpc (4.3×10^{26} m) or 28 Gpc in diameter. Cornish et al. [12] analyzing the WMAP data in search of the matched back-to-back circles predicted by various nontrivial topologies, settled the low bound of diameter of the last scattering surface of fun-

damental domain for 24 Gpc. Bielewicz & Banday [6], using similar methods extended this value to 27.9 Gpc. This admittedly does not prejudice the question of size, yet, provided the multi-connected space of universe, constraints the topology scale from below. An additional (though partly linked) difficulty comes out from the potential difference between the notions of entire and observable universe. In principle, entire universe may significantly surpass the observable universe (as inflationary theory predicts), but it can be as well slightly smaller due to nontrivial topology. The respective ratio may also change in time. Presumably, the black hole parameters describe the entire universe, and not just the universe currently observed. However, this distinction becomes important only insofar as “entire”, by virtue of convention, denotes the biggest physically connected object defined according to the horizon problem of the early universe. Assuming the approximately linear rate of expansion after the end of inflationary epoch (or from the beginning), the parameters of the so defined “entirety” should not significantly differ from the “observable” parameters. Bearing in mind the obvious uncertainties, we shall use in calculations the value $10^{27}m$ for the universe’s radius.

The critical density for a flat universe derived from Friedmann equation for the Hubble constant obtained from Planck telescope: $H_0 = 67.15 \text{ kms}^{-1}\text{Mpc}^{-1}$ is $\rho_c = 3H^2/8\pi G \approx 0.85 \times 10^{-26} \text{ kgm}^{-3}$. The resultant total mass for $R_u = 10^{27}m$ amounts to $M_u \approx 1.44 \times 10^{54} \text{ kg}$ (we shall use 10^{54} kg in calculations). Considering the approximated values of gravitational constant: $G \approx 6.7 \times 10^{-11} \text{ m}^3\text{kg}^{-1}\text{s}^{-2}$ and the speed of light: $c \approx 3 \times 10^8 \text{ ms}^{-1}$ ($c^2 \approx 10^{17} \text{ m}^2\text{s}^{-2}$) one obtains the numerical relationship connecting radius and mass:

$$10^{27} = 10^{-10} 10^{54} 10^{-17} (\text{m}), \quad (8)$$

which means that equation for the Schwarzschild radius:

$$r_S = 2Gmc^{-2} \quad (9)$$

apparently applies to the universe as

$$R_u \approx GM_u c^{-2}. \quad (10)$$

We postulate that universe constantly fulfills the “black-hole condition” (BHC), which means that it is always fulfilled:

$$R_u \equiv r_S. \quad (11)$$

Together with assumption $M_u = \text{const}$, and the general assumption of isotropy of cosmic space, BHC implies

$$Gc^{-2} \propto R_u. \quad (12)$$

5 Models with varying constants

In the intensive discussion on the variability of fundamental constants, variation of c is probably the leading topic. A majority of the “variable speed of light” (VSL) models conceived as a challenge to inflation restricts the variation of c

to the early superluminary universe (Moffat [51], Albrecht & Magueijo [2], Magueijo & Smolin [45]). These models do not match BHC since, after restoring the local Lorentz invariance, the light is thought to travel at the presently measured speed. Likewise, assuming the change of c refers totally to the time preceding the structure formation, they would not imply the variability of M_{Ch} .

In some VSL models, the change in c value has been considered as a continuous process spread over the whole lifespan of the universe. Dicke's theory of gravity (Dicke [13]), developing the earlier considerations by Einstein [22, 23] explains the cosmological redshift as a result of c decreasing with time, which somehow corresponds with the steady state theory. However, this model does not predict the change of c to be a measurable effect since it assumes the units of length and time to change accordingly.

In turn, variability of G has been proposed in some scalar-tensor models modifying the Einstein's General Relativity, in particular the Brans-Dicke theory [9] inspired by Mach's principle, with the time and space dependent scalar field ϕ modifying the Newton's constant. A similar as to the general structure and conclusions model by Hoyle & Narlikar [36] originates from considerations concerning the action on distance. Petit [61, 62] advanced a model with joint variation of G , c and h decoding the Hubble's law in a static universe. One of the first models postulating varying G , and likely the most influential one, is the Dirac's "large number hypothesis" (Dirac [15]). From the supposed coincidence between two ratios: radius of universe (expressed as ct) vs. radius of electron, and electrostatic force vs. gravitational force between proton and electron (both of them yielding $\approx 10^{40}$), Dirac derived a conclusion that G changes as the inverse of cosmic time: $G \propto t^{-1}$, while the mass of universe increases as $M_u \propto t^2$. Provided the approximately linear relationship between time and radius ($R_u \propto t$), LNH satisfies BHC. However, LNH also implies $M_{Ch} \propto t^{3/2}$, which compared with the standard assumption of constant G makes the SNe Ia progenitor problem even more puzzling. A model proposed by the present author (Rybecki [69]) has postulated $G \propto R_u$, $M_u = const$, yet then with no reference to BHC and the SNe Ia progenitor problem.

A question underlying the varying constants models is whether the postulated changes in dimensional constants are physically meaningful. A long-lasting controversy over this subject has not been concluded so far. Some physicists (e.g. Barrow [5], Duff [20]) claim that only the (potential) change in dimensionless constants matters, e.g. the coupling constants of fundamental forces such as fine structure constant α , gravitational coupling constant α_G , or the masses of elementary particles related to Planck mass contributing to standard model. Instead, dimensional constants such as \hbar , c , G , e , or k may change in value dependently on the (arbitrary) choice of units, thus being merely the "human constructs" or "conversion factors". Others (Okun [57], Veneziano [76]) consider

as indispensable in shaping the fundamental theories respectively three (G , c and \hbar) and two (c and string length λ_s) dimensional constants.

From the "dimensionless" point of view as applied to BHC, no matter whichever of dimensional constants is thought to vary; only what counts is the change of $\alpha_G = Gm_e^2/\hbar c$. Since we discriminate here between the change of G and c treated as different solutions of BHC, so this question demands a clarifying comment. Let's start with two remarks: 1) There is no doubt that $Gc^{-2} \propto R_u$ implies the variability of α_G ; 2) The fact that dimensional constant changes its numerical value together with the change of unit is trivial, and as such contributes nothing to discussion.

Let the increase of α_G be observed, correlated with the increase of R_u . Assuming $m_e = const$, $\hbar = const$, we conclude that it is either $G \propto R_u$ or $c \propto R_u^{-1}$ which, according to the "dimensionless" paradigm, we treat as fully equivalent (i.e. physically indistinguishable) interpretations of $\alpha_G \propto R_u$. However, from $Gc^{-2} \propto R_u$ it follows: $G \propto R_u \Rightarrow \alpha_G \propto R_u$, and $c \propto R_u^{-1/2} \Rightarrow \alpha_G \propto R_u^{1/2}$, which obviously differs from $\alpha_G \propto R_u$. Thus, G and c cannot be considered as "conversion factors" within BHC.

As we show in next sections, the Planck units of length and time react differently depending on whether G or c is postulated to vary. Besides, each of respective solutions affects entropy in a different way. We thus agree with the anonymous referee cited in Duff's paper: "It is true that if the fundamental "constants" \hbar , c , G , $k \dots$ are truly constant, then they do indeed only act as conversion factors and can e.g. be set equal to unity. However, when they are postulated (or discovered experimentally to vary) in time, then we have to take into account that varying one or the other of these constants can have significant consequences for physics" (Duff [20]).

6 Basics of the VCM hypothesis

Expressed in the here proposed nomenclature, our main idea consists in postulating VCM as being the consequence of BHC. Any model satisfying BHC makes the Planck units variable, and thus determines new parameters of the Planck era.

Identifying the mass in the equation for Schwarzschild radius with Planck mass: $m \equiv m_P$ gives

$$r_S = Gm_P c^{-2} = G(\hbar c G^{-1})^{1/2} c^{-2} = (\hbar G c^{-3})^{1/2} = \ell_P. \quad (13)$$

Accordingly, the black hole becomes the Planck particle. Implementing the Planck mass to the reduced Compton wavelength $\lambda/2\pi = \hbar m^{-1} c^{-1}$ makes the Planck particle the only one black hole whose Schwarzschild radius equals the Compton wavelength

$$\lambda/2\pi = \hbar(G\hbar^{-1}c^{-1})^{1/2} c^{-1} \equiv (\hbar G c^{-3})^{1/2} = \ell_P. \quad (14)$$

Rewriting the Schwarzschild equation for the Planck particle:

$\ell_p \approx Gm_p c^{-2}$ gives the identity

$$(\hbar G c^{-3})^{1/2} \equiv G(\hbar c G^{-1})^{1/2} c^{-2}, \quad (15)$$

which means that Planck particle's property of being a black hole is insensible to the change of G or/and c .

From $Gc^{-2} \propto R_u$ it follows $m_p \propto R_u^{-1/2}$; hence for $R_u \rightarrow 0$ the Planck mass tends to infinity. However, to avoid singularities (and also taking into account that Planck mass should have "realistic" reference), we assume that in the newly defined Planck era (denoted P_0) the Planck mass coincides with the mass of universe:

$$m_{P_0} \equiv M_u. \quad (16)$$

Thus, the initial value of Schwarzschild radius becomes

$$r_{S_0} \approx GM_u c^{-2}. \quad (17)$$

This can be also obtained by expressing the Newton's constant in the equation $R_u = GM_u c^{-2}$ in terms of Planck units, namely: $G = \ell_p m_p^{-1} c^2$. Then

$$R_u = \ell_p M_u m_p^{-1} \quad (18)$$

and so

$$R_u \ell_p^{-1} = M_u m_p^{-1} \quad (19)$$

meaning that identity $R_{u_0} \equiv \ell_{P_0}$ becomes a consequence of the conjecture $M_u m_p^{-1} = 1$. We have thus arrived at conclusion that the universe at its initial stage (here called "primordial Planck era" — PPE) had the form of a quantum mechanical black hole identified with a single one "primordial Planck particle" (PPP), described by equation:

$$\ell_{P_0} = G_0 m_{P_0} c_0^{-2}. \quad (20)$$

Accordingly, the notion of PPP becomes coherent with the concept of the universe emerging from "nothing" due to the Heisenberg uncertainty.

From $M_u \approx 10^{54} kg$, provided $m_{P_0} \equiv M_u$, it follows

$$m_{P_0} m_p^{-1} \approx 10^{62} \quad (21)$$

a factor hereinafter denoted by δ .

Because $M_{Ch} \sim m_p^3$ so

$$M_{Ch_0} M_{Ch}^{-1} = \delta^3. \quad (22)$$

Obviously, M_{Ch_0} as related to the early universe, is a formal entity only. To be a physically meaningful concept, Chandrasekhar limit demands a proper physical "environment" (atoms, elements, stars). It belongs then to the epoch of structure formation starting from Population III stars. Provided the universe expanded in a roughly uniform rate, BHC can be expressed as the approximate function of cosmic time: $Gc^{-2} \propto t$. From the whole range of possible BHC scenarios, the two deserve special attention, namely: 1) $G \propto R_u$ i.e. $G \propto t$, $c = const$, and 2) $c \propto R_u^{1/2}$, $G = const$, both analyzed in the next sections.

7 Assumption $c \propto R_u^{-1/2}$, $G = const$: collision with the second law of thermodynamics

The initial value of speed of light derived from $m_{P_0} = (\hbar c_0 / G)^{-1/2}$ and $m_{P_0} \equiv M_u \approx 10^{54} kg$ becomes $c_0 = 10^{132} ms^{-1}$, yielding $c_0 / c \approx 10^{124} = \delta^2$. The respective Planck length is (hereinafter, SI units always when omitted)

$$\ell_{P_0} = (\hbar G / c_0^3)^{-1/2} \approx 10^{-220} \quad (23)$$

a value equal to the Schwarzschild radius

$$r_S = Gm_{P_0} / c_0^2 \approx 10^{-220} \quad (24)$$

and to the Compton wavelength

$$\lambda_0 = \hbar M_u^{-1} c_0^{-1} \approx 10^{-220}. \quad (25)$$

The initial Planck time would amount to

$$t_{P_0} = (\hbar G / c^5)^{-1/2} \approx 10^{-352}. \quad (26)$$

From $E = m_{P_0} c_0^2$ it follows

$$\hbar = E t_{P_0} (10^{-34} = 10^{318} 10^{-352}). \quad (27)$$

As derived from $c \propto t^{-1/2}$, with the age of universe $\approx 13.8 \times 10^9$ yr the current rate of decrease in the speed of light becomes

$$\dot{c}/c \approx -2.7 \times 10^{-11} yr^{-1}. \quad (28)$$

Let us compare this prediction with the results obtained from observations of gas clouds spectra intersecting the distant quasars, the Oklo natural uranium fission reactor, and atomic clocks. In agreement with the VSL paradigm, the supposed change of α is usually interpreted as the change of c . For the approximate emission time connected with the observational data samples concerning quasars: $t_{EM} \approx 0.25 t_0 / 0.85 t_0$ covering ≈ 8.3 Gyr (here t_0 stands for the present moment), the reported values suggesting the change are: $\Delta c(t)/c = (-0.57 \pm 0.10) \times 10^{-5}$ (Webb et al. [77]), and $\Delta c(t)/c = (-1.09 \pm 0.17) \times 10^{-5}$ (Webb et al. [78]). At the same time, other groups (e.g. Chand et al. [10]) reported no detectable change in α value over the last 10-12 billion years. In the case of Oklo, for the respective operating time $t_{prev}/t_0 \approx 0.87$, Petrov et al. [63] obtained $\dot{\alpha}/\alpha = (-4 + 3) \times 10^{-17} yr^{-1}$, in fact signifying no detectable change. In turn, Lamoreaux & Torgerson [41] reported a decrease in alpha at the level -4.5×10^{-8} over the last 2 billion years, which consequently should be interpreted as the increase of the speed of light. Observations based on atomic clocks give a direct insight to the possible current rate of change. Peik et al. [59], using cesium atomic clock set the limit of annual change of the present variation of alpha for $\dot{\alpha}/\alpha = (-1.2 \pm 4.4) \times 10^{-15} yr^{-1}$. In turn, Rosenband et al. [67], based on the frequency ratio of Al^+ and Hg^+ in a single ion atomic clocks obtained a bound: $\dot{\alpha}/\alpha = (-1.6 \pm 2.3) \times 10^{-17} yr^{-1}$.

Except the data provided by Webb et al. suggesting decrease of c at the level 10^{-15}yr^{-1} , and the opposite one (as to general conclusion) provided by Lamoreaux & Torgerson, all other results seem to point the zero change. This suggests the failure of assumption $c \propto R_u^{-1/2}$. Besides, the question of entropy provides us with an additional argument against declining c . As is known, entropy is proportional to the horizon surface area, which normally (i.e. by assumption $G = \text{const}$, $c = \text{const}$) implies linear dependence on the squared mass. Let us apply the Bekenstein-Hawking formula for the entropy of black hole:

$$S_{BH} = Akc^3(4G\hbar)^{-1} \quad (29)$$

or, written in terms of Planck length,

$$S_{BH} = Ak(4\ell_P^2)^{-1}, \quad (30)$$

where A is the surface area for event horizon, and k the Boltzmann constant. For the spherically symmetrical black hole, the surface area is $A = m^2 8\pi G^2 c^{-2}$ so entropy becomes $S_{BH} = m^2 2\pi G k c \hbar^{-1}$. Thus, despite increasing surface area $A = m^2 8\pi G^2 c^{-2}$, at the assumption $m \equiv M = \text{const}$, $G = \text{const}$ and $c \propto R_u^{-1/2}$, the entropy decreases according to $S_{BH} = m^2 2\pi G k c \hbar^{-1}$ being dependent on the decreasing speed of light: $S_{BH} \sim c$. One obtains therefore

$$S_{BH(\text{present})}/S_{BH(\text{primordial})} = \delta^{-2}, \quad (31)$$

which violates the second law of thermodynamics applied to the universe as a whole. This does not exclude VSL models in general; in particular, does not exclude VSL applied to the very early universe. However, BHC is not agreeable with VSL conceived as a continuous process. Therefore, in the further considerations, we shall specify BHC as a model defined by the assumption $G \propto R_u$, $c = \text{const}$. We shall also treat this model as a right basis for the VCM hypothesis and the respective quantitative predictions.

8 Assumption $G \propto R_u$, $c = \text{const}$: parameters of the universe at Planck era

Provided $m_{P_0} \equiv M_u \approx 10^{54}$ kg, the initial value of Newton's constant derived from $m_{P_0} = (\hbar c/G_0)^{-1/2}$ is $G_0 \approx 10^{-134}$, yielding $G/G_0 = \delta^2$. The initial Planck length becomes

$$\ell_{P_0} = (\hbar G_0/c^3)^{-1/2} \approx 10^{-97} \quad (32)$$

equal to the Schwarzschild radius:

$$r_S = G_0 M_u c^{-2} \approx 10^{-97} \quad (33)$$

and to the (constant) value of Compton wavelength for the universe:

$$\lambda_0 = \hbar M_u^{-1} c^{-1} \approx 10^{-97}. \quad (34)$$

All three quantities apply to the initial size of universe R_{u_0} :

$$R_{u_0} \equiv \ell_{P_0} \equiv r_S \equiv \lambda_0. \quad (35)$$

The initial Planck time is

$$t_{P_0} = (\hbar G_0 c^{-5})^{1/2} \approx 10^{-105}. \quad (36)$$

Hence,

$$\hbar = E_{P_0} t_{P_0} \approx 10^{-34}, \quad (37)$$

where $E_{P_0} = M_u c^2 \approx 10^{71}$. The invariability of Planck constant is a consequence of the fact that, although individually Planck energy and Planck time change in time, their product remains constant:

$$E_{P(\text{variable})} \times t_{P(\text{variable})} = \hbar_{(\text{constant})}. \quad (38)$$

In general, initial values of the base Planck units relate to their present equivalents as

$$m_{P_0}/m_P = \ell_P/\ell_{P_0} = t_P/t_{P_0} = \delta. \quad (39)$$

The horizon problem in PPE is solved so to speak by definition, since

$$c t_{P_0} = \ell_{P_0}, \quad (40)$$

which means that the whole primordial universe fits in a light cone.

The density in the primordial Planck era is

$$\rho_{(PPE)} = M_u \ell_{P_0}^{-3} \approx 10^{344} \quad (41)$$

equal to initial Planck density:

$$\rho_{P_0} = c^5 \hbar^{-1} G^{-2} \approx 10^{344}. \quad (42)$$

Let us compare this with the critical density derived from the Friedmann equation: $\rho_c = 3H^2(8\pi G)^{-1}$, as calculated for PPE. The current value of Hubble constant (≈ 70 kms⁻¹/Mpc) expressed in SI units amounts to

$$H_{(\text{now})} \approx 2.27 \times 10^{-18} \text{ s}^{-1} \quad (43)$$

yielding the respective value of the Hubble constant in PPE:

$$H_{(PPE)} = H_{(\text{now})} \times \delta^2 \approx 10^{106} \text{ s}^{-1}. \quad (44)$$

Approximating $8\pi G_0 \approx 10^{-133}$, one obtains the PPE critical density:

$$\rho_{c(PPE)} \approx 10^{212} 10^{133} \approx 10^{345}. \quad (45)$$

Hence, it is likely that also in PPE

$$\rho_{(PPE)} \equiv \rho_c \quad (46)$$

which solves the flatness problem.

In contrast to the previously considered assumption $c \propto R_u^{-1/2}$, $G = \text{const}$, the thermodynamic arrow of time becomes well defined. Considering $G/G_0 = \delta^2$, from $S_{BH} = m^2 2\pi G k c \hbar^{-1}$ it follows

$$S_{BH(\text{present})}/S_{BH(\text{primordial})} = \delta^2. \quad (47)$$

In the cosmological scenario based on assumption $G \propto R_u$, $c = \text{const}$, the expansion is linear, or roughly linear, including the early epoch. This means that $G \propto R_u$ is tantamount to $G \propto t$; in particular, $G_0(10^{-134})$ coincides with $t_{p_0}(10^{-105})$. At some additional assumptions, this scenario could be modified so as to regard nonlinear expansion during early epochs. However, considering that basic motives for invoking inflation (horizon problem and flatness problem) are absent in BHC scenario, inflation appears to be basically redundant.

9 Assumption $G \propto R_u$, $c = \text{const}$: question of consistency with observational tests of G variability

Provided the approximately uniform rate of Hubble flow, the derived from $G \propto R_u$ current rate of increase of G becomes a simple inverse of the age of universe. In fact, the Hubble time does not significantly differ from estimations of the age of universe derived from Friedman equation equipped with definite values of k and Λ . Whereas these estimations range from ≈ 13.798 Gyr (Lambda-CDM concordance model based on data from Planck satellite and WMAP) to ≈ 13.82 Gyr (Planck mission), the Hubble time ranges between ≈ 13.7 Gyr and ≈ 14.26 Gyr according to the current extreme estimates of the Hubble constant: ≈ 72 and ≈ 67 $\text{kms}^{-1}\text{Mpc}^{-1}$ respectively. Thus, on the average, the Hubble time only slightly exceeds the supposed age of universe. Interpreting $G \propto R_u$ as $G \propto t$ and estimating the age of the universe for $\approx 13.8 \times 10^9$ yr gives the current rate of change:

$$\dot{G}/G \approx 7.25 \times 10^{-11} \text{yr}^{-1}. \quad (48)$$

Let us compare this prediction with the constraints put upon G variation, derived from different sources (paleontology and geophysics, celestial mechanics, stellar physics, cosmology). A handful of representative results covering the whole range are:

- paleontological data connected with Earth temperature: $|\dot{G}/G| < 2.0 \times 10^{-11} \text{yr}^{-1}$ (Eichendorf & Reinhardt [21]);
- increase of Earth radius: $\dot{G}/G = (-0.5 \pm 2) \times 10^{-11} \text{yr}^{-1}$ (Blake [8]);
- stability of the radii of Earth, Moon and Mars: $-\dot{G}/G \leq 8 \times 10^{-12} \text{yr}^{-1}$ (McElhiny et al. [49]);
- stability of the orbit of Mars (Mariner 9 and Mars orbiter data): $\dot{G}/G = (-2 \pm 10) \times 10^{-12} \text{yr}^{-1}$ (Shapiro [71]);
- systematic deviations from the Keplerian orbital periods of Moon: $\dot{G}/G \leq (3.2 \pm 1.1) \times 10^{-11} \text{yr}^{-1}$ (Van Flantern [75]);
- lunar laser ranging (LLR): $|\dot{G}/G| < 6 \times 10^{-12} \text{yr}^{-1}$ (Dickey et al. [14]); LLR: $\dot{G}/G \leq (4 \pm 9) \times 10^{-13} \text{yr}^{-1}$ (Williams et al. [81]);
- spin-down of pulsar JP1953: $-\dot{G}/G < 5.8 \pm 1 \times 10^{-11} \text{yr}^{-1}$ (Mansfield [46]);
- pulsar timing PSR B1913+16: $\dot{G}/G \leq (4 \pm 5) \times 10^{-12} \text{yr}^{-1}$ (Kaspi et al. [38]);

- luminosity function of white dwarfs (cooling age): $-\dot{G}/G \leq 3_{-3}^{+1} \times 10^{-11} \text{yr}^{-1}$ (Garcia-Berro et al. [27]);
- pulsating white dwarf data G117-B15A: $|\dot{G}/G| \leq 4.10 \times 10^{-10} \text{yr}^{-1}$ (Biesiada & Malec [7]);
- SNe Ia luminosity vs. redshift: $\dot{G}/G = (-3, +7.3) \times 10^{-11} \text{yr}^{-1}$ (Mould & Uddin [52]);
- helioseismology: $|\dot{G}/G| \leq 1.6 \times 10^{-12} \text{yr}^{-1}$ (Guenther et al. [32]);
- big bang nucleosynthesis (BBN): $|\dot{G}/G| \leq 9. \times 10^{-13} \text{yr}^{-1}$ (Accetta et al. [1]); BBN: $|\dot{G}/G| \leq 1.7 \times 10^{-13} \text{yr}^{-1}$ (Rothman & Matzner [68]).

One can easily notice that BHC prediction hardly matches the minority of the above bounds. However, a closer insight into methodology reveals various circumstances hidden behind the digits. We shall discuss them now, one by one.

9.1 Accuracy of the constraints on G variation and accuracy in measurements of the value of G

Unlike in the case of other fundamental constants, the increasing precision of measurements of G value is accompanied by increasing discrepancy of the obtained results. This led the CODATA to widen the uncertainty range from 0.013% to 0.15%. We ask whether this uncertainty may impinge on the G variability tests. This question does not seem groundless taking into account the ratio between typical bound put on the annual rate of change of G ($\sim 10^{-11}$) and the uncertainty range of G value (1.5×10^{-3}), roughly ten-billionth! To better realize the scale, imagine we test the Wegener's continental drift theory (btw unaccepted for a long time) by settling a constraint on the annual rate of relative motion between two continents, say, America and Europe. Assume we determine two points (measuring devices) placed on each of these continents, and estimate the distance between them for 5 thousand kilometers. However, due to hypothetical imperfection of measuring techniques, this distance is only known with the relative uncertainty 0.15%, which translates into 7.5 km. Assume next that, undeterred by this immense inaccuracy, we derive the constraint for the drift rate for 10^{-11}yr^{-1} , i.e. 0.05 mm/year, while the drift rate estimated by the theory amounts to $7.25 \times 10^{-11} \text{yr}^{-1}$, i.e. 0.36 mm/year (in fact, Wegener estimated the speed of drift for 2.5 m/year, while the currently observed rate amounts to about 2.5 cm/year).

Obviously, measuring a given value and measuring a change in this value are, basically, two different things; yet the mentioned discrepancy is too significant to be ignored. This in particular happens when a constraint depends on assumptions that are themselves encumbered by sizeable uncertainty (see subsection 9.3). In the above fictional example, before drawing ultimate conclusions as to the correctness of Wegener's idea, one should certainly aim at eliminating the distance uncertainty or try to find its hidden sources. Otherwise, any ultimate conclusions as to the change of distance

could not be considered reliable. There is no reason to assume the question of variability of Newton's constant should subject to different rules.

9.2 Differences in notation and the question of autonomy of particular constraints

There is no unique notation for the constraints on G variation; for different reasons, particular constraints (or their groups) are expressed in different mathematical forms. Revealing their meaning provides us with a better insight into the question of autonomy. The (here called) canonical form, $\dot{G}/G \leq (a \pm b) \times 10^{-c} \text{yr}^{-1}$ (a positive/negative, b, c positive) reads: "An annual rate of increase/decrease of G , not greater than $a \times 10^{-c}$ has been observed, with the uncertainty range equal to $\pm b \times 10^{-c}$ ". If $a = 0$, it means that no change has been observed, although b still describes the range of uncertainty of that finding. Expression $-\dot{G}/G$, instead of \dot{G}/G , means that given constraint concerns solely (is design to detect) the decrease rate of G . This takes place when a theory predicting the decrease of G (e.g. Dirac's LNH) is tested, and thus respective assumptions are the base of derivation. In turn, the form $|\dot{G}/G|$ reads: "The possibility of G variation (including increase and decrease in equal degree) fits in the range..." However, $|\dot{G}/G|$ is sometimes used as equivalent to $-\dot{G}/G$, in particular when aimed at testing Dirac's hypothesis (e.g. Eichendorf & Reinhardt [21]). This form implies a to be indistinguishable from b , i.e. treats expressions "(rate) not greater than" and "with the uncertainty range" as tantamount to each other. Another way to identify the range of possible change with the range of uncertainty is the form $\dot{G}/G = (-b_1, +b_2) \times 10^{-c} \text{yr}^{-1}$, $b_1 \neq b_2$. Although apparently similar to $|\dot{G}/G|$, this form indicates the observed tendency (i.e. increase or decrease) and thus seems to be basically equivalent to the canonical form; e.g. the term $(-2, +4)$ could be expressed as (1 ± 3) . An alternative use of the relation symbols $<$, \leq and $=$ in each of the above forms can be interpreted (dependently on the context) as a gradable expression of conviction as to the observed tendency. In particular, symbols $<$ and \leq , when used in the canonical form, play the role of additional proviso (apart of b term) due to general uncertainty; for example, if $|a|$ is greater than b then using $=$ unambiguously points to the observed change of G . Instead, using $<$ or \leq weakens this statement, suggesting the change to be only probable.

Let us assume that, generally, all observations meet the criteria of scientific rigor. Apart of proper methodology and precision, this would also mean the unbiased standpoint as to the principal question, i.e. whether the Newton's constant is a true constant. Provided that, the postulate of autonomy says that each constraint should be interpreted in accordance with the sense of its notation and with regard to the underlying assumptions (usually not reflected in notation). In particular, weaker constraints should not be treated as "worse" than the

stronger ones but, for the most part, as speaking in favor of variability.

9.3 Dependence on the employed theory and assumptions

Many factors involved in determination of the bounds put on G variation are theory or assumption dependent. For example, stringent constraints derived from BBN (Accetta et al. [1], Rothman & Matzner [68]) are valid only for Brans-Dicke theory; likewise, the constraint derived by Guenther et al. [32] bases on the Brans-Dicke type theory with varying G . Most of constraints, even when not visibly shown in their notation, base on observations testing Dirac's LNH, i.e. are focused on the possible decrease of G . This in particular concerns the results derived from geophysical and paleontological data: impact of the Earth surface temperature on ancient organisms, expansion of Earth and the relevant difference in paleolatitudes between two sites of known separation (allowing to deduce the paleoradius), spin-down of the Earth due to its expansion, recession of the Moon and its impact on tides reflected in fossils. The respective data depend on too many conditions to repose excessive trust in their precision, and thus to consider them as fully reliable assumptions. In his extensive review study, Uzan [74] pays attention on these other sources of uncertainty connected with particular constraints.

9.4 Variation of Newton's constant and the age of universe

Assuming that increase of G extends the age of universe, the rate of G variation would be smaller than the here quoted value $7.25 \times 10^{-11} \text{yr}^{-1}$ thus better fitting observations. However, according to the Friedmann equation

$$H^2 = \left(\frac{\dot{a}}{a}\right)^2 = \frac{8\pi G}{3} \rho - \frac{kc^2}{a^2} + \frac{\Lambda c^2}{3}, \quad (49)$$

variation of G has a negligible impact on the age of universe. For $k = 0$ (flat universe) and $\Lambda = 0$, density becomes critical ($\rho_c = 3H^2(8\pi G)^{-1}$), and thus Friedmann equation reduces itself to identity $H^2 \equiv H^2$ becoming insensible to the change of G . In such a case, the age of universe simply equals the inverse of Hubble's constant ($t = H^{-1}$). However, for $\Lambda \neq 0$, currently estimated for $\Lambda_{(const)} \approx 10^{-52} \text{m}$, dark energy (in a form of cosmological constant) predominates from a certain moment, so that t and H^{-1} more and more diverge. In an accelerating universe driven by dark energy, the rate of increase of G determined by $G \propto R_u$ also accelerates, which means that its declining in the unit time gradually slows down. Hence, in the far future, $G \propto R_u$ will translate to $G \propto H^{-1}$ rather than to $G \propto t$.

9.5 Equivalence of gravity and inertia

As is known, there are (currently) four notions of mass: 1) active gravitational mass — measure of ability to create gravi-

tational field or curvature, 2) passive gravitational mass — measure of “sensing” the gravitational field by a body (in the Newtonian depiction, respectively: measure of the force exerted by a body and measure of the force experienced by a body), 3) inertial mass — measure of resistance against the force accelerating a body (including the force of gravity), and 4) mass as a measure of energy according to $E = mc^2$. Numerous experiments performed over a long time up to present days have shown with increasing precision that inertial mass and passive gravitational mass are proportional to each other: $m_{(inert)} \sim m_{(pass)}$ (weak equivalence principle). In turn, since active and passive gravitational masses are interchangeable according to the Newton’s third law, so also active gravitational mass and inertial mass are proportional to each other:

$$m_{(act)} \sim m_{(inert)}. \quad (50)$$

The active gravitational mass is proportional to the Newton’s constant: $m_{(act)} \sim G$. In fact $m_{(act)}$ is inseparable from G , which means that any change in the active mass should be interpreted as the change in the Newton’s constant. Consequently, inertial mass is thought to follow the putative variation of G :

$$\Delta G \rightarrow \Delta m_{(inert)}. \quad (51)$$

This would make the so-called “inertial reaction force” always (i.e. also in the time-slice experiments) equivalent to the gravitational force. At the same time, variation of the Newton’s constant would not affect the mass interpreted as the source of positive energy. Accordingly, the tests on G variation derived from celestial mechanics (e.g. LLR) would be basically ineffective, while the other ones (e.g. based on stellar physics) would still remain valid.

10 Quantitative predictions of the varying Chandrasekhar limit hypothesis, based on $G \propto R_u$, $c = const$

We shall now consider the VCM hypothesis in the form related to the BHC specified as $G \propto R_u$ i.e. $G \propto t$. On the assumption that the rate of Hubble expansion is approximately uniform, the Chandrasekhar limit depends on cosmic time as $M_{Ch} \propto t^{-3/2}$. This determines characteristic “delay time” for a single white dwarf, defined as the time needed to reach the WD’s mass by the decreasing M_{Ch} . It makes thereby a basis for the quantitative predictions of VCM as to the rate of supernovae events, interpreted as a function of cosmic time. While, in general, the anticipated by VCM ability of a single WD to become the supernova meets the problem of the paucity of SNe Ia progenitors, the detailed predictions obviously demand more circumstantial investigation. One has to regard: 1) the number of single WDs within a given area (in particular, the number of their representative sample); 2) the mean/median mass of this sample; 3) the respective “delay time” for the median mass, determined by $M_{Ch} \propto t^{-3/2}$. Besides, in predicting the rate of distant SNe Ia one should also regard the related to distance intrinsic time

of the observed events, and a corresponding value of Chandrasekhar limit. Once a distance is well defined, the respective limit should be treated as constant, considering the negligible (compared with the assumed rate of change in M_{Ch}) time devoted to observation. Instead, for the nearby SNe Ia one may fairly assume $M_{Ch} \approx 1.4M_{\odot}$.

Let us apply the above to our Galaxy. For the sake of simplicity (an also taking into account the uncertainty in all data), we shall not regard the contribution of SNe Ia originated in binaries. We aim to estimate the present rate of SNe Ia, deriving it from accessible data, according to the above quoted three points. As is known, the Galaxy contains roughly 100-400 billion stars, above 97% of them supposed to end as white dwarfs, which however includes both actual WDs and the potential ones. According to the estimations based on SPY project, the space density of WDs within the radius of 20 pc is $(4.8 \pm 0.5) \times 10^{-3} \text{ pc}^{-3}$ while the corresponding mass density amounts to $(3.2 \pm 0.3) \times 10^{-3} M_{\odot} \text{ pc}^{-3}$, which gives the overall mean mass $(M)_{WD} \approx 0.665 M_{\odot}$ (Holberg et al. [35]). Instead Kepler et al. [39], basing on catalog elaborated by Eisenstein et al. [24] from the SDSS Data Release 4, found significant difference in the WD’s mean mass between DA and DB stars (hydrogen and helium layers, respectively); namely $(M)_{DA} \approx 0.593 M_{\odot}$ and $(M)_{DB} \approx 0.711 M_{\odot}$. Considering the number of DA and DB in the sample (7167 and 507, respectively), one gets the $(M)_{WD} \approx 0.6 M_{\odot}$. We shall use this value in the further calculations.

In order to estimate the total number of white dwarfs in the Milky Way, we have to multiply the WD’s space density by the Galaxy volume. Certainly, such an extrapolation is encumbered by significant uncertainty, as it is doubtful whether the sample obtained from the relatively close neighborhood (thin disc, in general) is typical for the whole Galaxy including thick disc, halo and the galactic bulge. Different parts of Galaxy vary in age, so WD’s population is likely inhomogeneous in age and density. Evaluating the radius for 15,000 pc and the mean thickness for 5,000 pc and multiplying this by WDs’ local density, one obtains: $(3.5 \times 10^{12} \text{ pc}^3) \times (5 \times 10^{-3}) \approx 1.7 \times 10^{10}$. This gives an insight into the actual number of WDs, consistent with a list brought by the Research Consortium on Nearby Stars (RECONS). According to the latter, 8 of the nearest 100 stars are the white dwarfs, which, provided this to be the representative ratio, gives the total number between 0.8×10^{10} to 3.2×10^{10} , dependently on the assumed total number of stars (100-400 billion).

The next step is to derive the “mean delay time” $(T)_{del}$ for the WD’s mean mass $(M)_{WD}$. The respective algorithm reads

$$(T)_{del} = \left(\frac{t}{T_u} + 1 \right)^{2/3} \times T_u - T_u \quad (52)$$

T_u -age of universe, t – an auxiliary delay time not regarding

the power index, yielding

$$t = \frac{T_u}{(M_{Ch}/\Delta M_{WD}) - 1}, \quad (53)$$

where $\Delta M_{WD} = M_{Ch} - (M)_{WD}$. After conversion, one has

$$(T)_{del} = \left(\frac{M_{Ch}}{(M)_{WD}} \right)^{2/3} \times T_u - T_u. \quad (54)$$

Inserting $M_{Ch} = 1.4M_{\odot}$, $(M)_{WD} = 0.6M_{\odot}$ and $T_u = 13.8$ Gyr, one obtains $(T)_{del} \approx 10$ Gyr. Dividing the number of white dwarfs in Galaxy by that time gives the rate of roughly 1-3 events per year, a frequency exceeding the observed rate by a factor $> 10^2$. However, this prediction does not concern the present rate but a hypothetic rate averaged over the above calculated $(T)_{del}$. One should not identify (or confuse) “averaged” with “uniform” mainly because WD’s masses subject, in general, to the Gaussian distribution:

$$f(x, \mu, \sigma) = \frac{1}{\sigma \sqrt{2\pi}} e^{-(x-\mu)^2/2\sigma^2} \quad (55)$$

(σ -standard deviation, μ -mean of the distribution) and the respective probability function:

$$Prob[a \leq x \leq b] = \int_a^b f(x) dx. \quad (56)$$

The observed standard deviation is significantly smaller than one ($\sigma^2 \ll 1$) yielding substantial peak around the median mass $0.6M_{\odot}$. Obviously, only WDs of the mass close to $1.4M_{\odot}$, corresponding with the relatively short mean delay time, contribute to the present rate of SNe Ia. We assume that any single white dwarf of the mass close to M_{Ch} is, dependently on specific conditions (rotation, chemical composition), a potential SN Ia at any moment during the slated delay time. Admittedly, the most massive known WD only slightly exceeds $1.3M_{\odot}$; this however should be associated with the fact that less than one-millionth of the whole population of WDs in Galaxy are identified so far. A similar difficulty concerns specifying the expression “close to $1.4M_{\odot}$ ”. Bearing in mind an inevitable uncertainty, let us determine the respective range for $[b - a] \approx 0.1M_{\odot}$, assuming that, dependently on detailed conditions, any WD of the mass between $1.3 - 1.4M_{\odot}$ may become the SNe-Ia. For that mass range, the unit normal distribution yields less than 0.1% of the entire population, say, $\approx 10^7$. The mean mass of this “representative sample” is $1.35M_{\odot}$. It follows:

$$T_{del} \approx (1.4/1.35)^{2/3} \times 13.8 - 13.8 \approx 0.34 \text{ (Gyr)}. \quad (57)$$

The respective rate is then

$$\frac{10^7}{3 \times 10^8} = 3 \times 10^{-2} \text{ (yr}^{-1}\text{)}. \quad (58)$$

This still slightly exceeds the observed rate, provided the latter is ≤ 1 events per 100 years. However, considering the mentioned above reservations, it would not be reasonable to attach excessive importance to this or that particular number. The real number of single WDs from the representative sample may prove to be much smaller than 10^7 . The mass-range of potential progenitors may appear slightly narrower or wider. In general, more accurate data may support or falsify our hypothesis.

11 Conclusion

We have considered the SNe Ia progenitor problem in the context of general problem of the constancy of fundamental constants. Basing on arguments derived from the black-hole cosmology, we have singled out the Newton’s constant as the most probable candidate for “inconstant constant”. Since the increase of G involves the decrease in the value of Chandrasekhar limit M_{Ch} , both questions meet together yielding a hypothesis according to which a single white dwarf can alone become the progenitor of SN Ia.

Admittedly, the ongoing progress in observational techniques together with an improvement in stellar physics may bring solution to the progenitor problem dispensed with violating the constancy of Chandrasekhar limit. A tacit heuristic strategy connected with searching for the SNe Ia progenitors consists in attempts of making the SD and DD models flexible enough to eliminate the observed discrepancies. For the time being however the problem still exists, which makes solutions going beyond the binary paradigm justifiable and noteworthy.

The unbiased estimations seem to support the main thesis of this article, i.e. that M_{Ch} decreasing according to $G \propto R_u$ may explain the paucity of SNe Ia progenitors. It is to be noted that, predicted by $G \propto R_u$ immense growth of the Newton’s constant from the initial to present value ($G/G_0 = \delta^2 \approx 10^{124}$) almost completely applies to the very early and early universe, preceding structure formation. Since the oldest SNe Ia detected so far: SN UDS1 0Wil (Wilson) and SN 1997ff reach about 11 Gyr the part of increase of the Newton’s constant shaping the Chandrasekhar limit does not exceed the one order of magnitude, being much smaller in the case of overwhelming majority of the observed events.

Submitted on June 11, 2014 / Accepted on October 22, 2015

References

1. Accetta F.S., Krauss L.M., & Romanelli P. *Phys. Lett. B*, 1990, v.248, 146.
2. Albrecht J. & Magueijo J. *Phys. Rev. D*, 1999, v.59, 043516.
3. Badenes C. et al. *ApJ*, 2009, v.707, 971.
4. Badenes C. & Maoz D. *ApJ*, 2012, v.749, L11.
5. Barrow J.D. *The Constants of Nature; from Alpha to Omega*. Pantheon Books, New York, 2002.
6. Bielewicz P., & Banday A.J. *MNRAS*, 2011, 412(3), 2104.
7. Biesiada M., & Malec B. *MNRAS*, 2004, v.520(2), 644.

8. Blake G.M. *MNRAS*, 1977, v.181, 41.
9. Brans C.H., Dicke R.H. *Phys. Rev.*, 1961, v.123, issue 3, 925.
10. Chand H., et al. *A&A*, 2004, v.417, 853.
11. Chandrasekhar S. Nobel Prize lecture, 1983.
12. Cornish N.J. et al. *Phys. Rev. Lett.*, 2003, v.92, 201302.
13. Dicke R. *Rev. Mod. Phys.*, 1957, v.29, 363.
14. Dickey J.O. et al. *Science*, 1994, 265, 482.
15. Dirac P.A.M. *Nature*, 1937, 139, 323.
16. Dirac P.A.M. Lecture on the International Symposium on Contemporary Physics, Trieste, June 1968.
17. Di Stefano R. *ApJ*, 2010a, v.712, 728.
18. Di Stefano R. *ApJ*, 2010b, v.719, 474.
19. Di Stefano R., Voss R., Claeys J.S.W. *ApJL*, 2011, v.738(1).
20. Duff M.J. 2004, arXiv: hep-th/020809v3.
21. Eichendorf W. & Reinhardt M. *Mitt. Astron. Ges.*, 1977, v.42, 89.
22. Einstein A. *Annalen der Physik*, 1911, v.35, 898.
23. Einstein A. *Annalen der Physik*, 1912, v.38, 355.
24. Eisenstein D.J. et al. *ApJS*, 2006, v.167, 40.
25. Foley R.J. et al. *AJ*, 2012, v.143(5), 113.
26. Gallagher J.S. et al. *ApJ*, 2008, v.685(2), 752.
27. Garcia-Berro E. et al. *MNRAS*, 1995, v.277, 801.
28. Gilfanov M. Press conference, Chandra Press Room, NASA, Feb. 17, 2010.
29. Gilfanov M. & Bogdan A. *Nature*, 2010, v.463, 924.
30. Gonzalez Hernandez J.I. et al. *Nature*, 2012, v.489, 533.
31. Good I.J. *Physics Today*, 1972, v.25(7), 15.
32. Guenther D.B., Krauss L.M., & Demarque P. *ApJ*, 1998, v.498, 871.
33. Hachisu I., Kato M., Namoto K. *ApJ*, 2008, v.683, L127.
34. Hachisu I. et al. *ApJ*, 2012, v.744, 69.
35. Holberg J.B. et al. *AJ*, 2008, v.135, 1225.
36. Hoyle F. & Narlikar J.V. *Proceedings of the Royal Society of London A*, 1964, v.282, issue 1389, 19.
37. Iben I. Jr. & Tutukov A.V. *ApJS*, 1984, v.54, 335.
38. Kaspi V.M., Taylor J.H., & Riba M.F. *ApJ*, 1998, v.498, 871.
39. Kepler S.O. et al. *MNRAS*, 2007, v.375(4), 1315.
40. Kerkwijk Van M.H. et al. *ApJ*, 2010, v.722, L157.
41. Lamoreaux S.K. & Torgerson J.R. *Phys. Rev. D*, 2004, v.69, 121701.
42. Li W. et al. *Nature*, 2011, v.480, 348.
43. Linden S., Virey J.-M., Tilquin A. *A&A*, 2009, v.506(3), 1095.
44. Longo, M.J. 2011, *Phys. Lett. B*, 699 (4), 224
45. Magueijo, J., & Smolin, L. 2002, *Phys. Rev. Lett.* 88, 190403
46. Mansfield, V.N. 1976, *Nature*, 261, 560
47. Maoz D. & Mannucci F. *Publications of the Astron. Soc. of Australia*, 2012, v.29(4), 44.
48. Maoz D., Mannucci F., & Brandt T.D. *MNRAS*, 2012, v.426, 3282.
49. McElhiny N.W., Taylor S.R., & Stevenson D.J. *Nature*, 1978, v.271, 316.
50. Mennekens N. et al. *A&A*, 2010, v.515, A89.
51. Moffat J. *Int. J. Mod. Phys. D2*, 1993, 351.
52. Mould J. & Uddin S.A. To appear in PASA, 2014, arXiv: 1402.1534.
53. Mullally F. et al. *ApJL*, 2009, v.707, L51.
54. Napiwotzki R. et al. *Messenger*, 2003, v.112, 25.
55. Napiwotzki R. et al. *ESO Astrophysics Symposia*, 2003, v.134.
56. Nugent P. et al. *Nature*, 2011, v.480, 344.
57. Okun L.B. *Usp. Fiz. Nauk*, 1991, v.161, 177 (*Sov. Phys. Usp.*, 1991, v.34, 818).
58. Pathria R.K. *Nature*, 1972, v.240, 298.
59. Peik E. et al. *Phys. Rev. Lett.*, 2004, v.93(17), 170801.
60. Perlmutter S. et al. *ApJ*, 1999, v.517(2), 565.
61. Petit J.P. *Mod. Phys. Lett.*, 1988, v.A3, issue 16, 1527.
62. Petit J.P. *Mod. Phys. Lett.*, 1988, v.A3, issue 18, 1733.
63. Petrov Y.V. et al. *Phys. Rev. C*, 2006, v.74(6), 064610.
64. Popławski N.J. *Physics Letters B*, 2010, v.687(2), 110.
65. Popławski N.J. *Physics Letters B*, 2010, v.694(3), 181.
66. Riess A.G. et al. *AJ*, 1998, v.116(3), 1009.
67. Rosenband T. et al. *Science*, 2008, v.319, issue 5871, 1808.
68. Rothman T. & Matzner R. *ApJ*, 1982, v.257, 450.
69. Rybicki M. *Apeiron*, 2008, v.15(4), 465.
70. Schaefer B.E. & Pagnotta A. *Nature*, 2012, v.481, 7380.
71. Shapiro I.I. In *General Relativity and Gravitation*, ed. by N. Ashby, D.F. Bartlett and W. Wyss, Cambridge University Press, 1990.
72. Sullivan M. et al. *MNRAS*, 2010, v.406(2), 782.
73. Totani T. et al. *PASJ*, 2008, v.60, 1327.
74. Uzan J.-P. *Rev. Mod. Phys.*, 2003, v.75, 403.
75. Van Flandern T.C. In: *Precision Measurements and Fundamental Constants II*, NBS circular, 1981, v.617, 625.
76. Veneziano G. *Europhysics Lett.*, 1986, issue 2, 199.
77. Webb J.K. et al. *Phys. Rev. Lett.*, 1999, v.82(5), 884.
78. Webb J.K. et al. *Phys. Rev. Lett.*, 2001, v.87(9), 091301.
79. Webbink R.F. *ApJ*, 1984, v.277, 355.
80. Whelan J. & Iben I. *ApJ*, 1973, v.186, 1007.
81. Williams P.J., Newhall X.X., & Dickey J.O. *Phys. Rev. D*, 1996, v.53, 6730.
82. Zhu C. et al. *ApJ*, 2013, v.767, 164.

Schrödinger Equation for a Half Spin Electron in a Time Dependent Magnetic Field

Hafeez Y. Hafeez¹, E. N. Chifu², and Ibrahim M. Musa³

Physics Department, Federal University Dutse, P.M.B 7156, Jigawa State, Nigeria.

¹E-mail: hafezyusufhafeez@gmail.com

²E-mail: ebenechifu@yahoo.com

³E-mail: baffapet@yahoo.com

The behaviour of an electron with mass m_e and half spin when passing through a magnetic field with fixed strength B_0 is studied. The motion of the particle is restricted to a ring with radius R , thus assuming periodic boundary conditions. We also focused on magnetic field evolving adiabatically in time, the magnetic field is expressed as a function of angle ϕ and θ i.e only the direction of the magnetic field vectors change while the strength B_0 is kept fixed. Expression for eigenenergies were drawn for a fixed energy and sample values of α , ω , θ and $x = mR^2/\hbar^2$.

1 Introduction

An intriguing example emerging from asymmetric spin-interactions are skyrmion lattices. In 1989 Alexey Bogdanov predicted that for anisotropic chiral magnets there is a new magnetic order consisting of topologically stable spin whirls, named skyrmions after the English particle physicist Tony Skyrme, who showed that localized solutions to non-linear quantum field theories may be interpreted as elementary particles. Briefly speaking, skyrmions are topologically stable whirls in fields.

In 2009, a new magnetic order was observed in Manganese Silicide (MnSi) for specific temperatures and magnetic fields by Mühlbauer et al [1]. The physics of an electron moving through the magnetic field can be analyzed from two different points of view:

From the point of view of the electron, i.e. considering the problem in terms of emergent electric and magnetic fields, the change in spin orientation is equal to an effective Lorentz force acting on the electron, which is perpendicular to its motion [2]. As a result, the magnetic field induces a deflection of the electron, which can be measured by making use of the topological Hall-effect [3]. Because of the electron carrying an electric charge, a potential may be measured perpendicular to the direction of the current. Since the magnetic structure of the skyrmion lattice is very smooth, the adjustment of the spin of the electron to the magnetization of the skyrmion lattice can be considered an adiabatic process.

On the other hand, there must be a corresponding counterforce acting on the skyrmion. This force, arising from the transfer of angular momentum from the conduction electrons to the local magnetic structure (cf. [4]), can for example result in a drift of the domains of the lattice. A 1-D model of an electron passing over a static magnetic field has previously been investigated in the Bachelor's thesis of M. Baedorf [5]. Berry phase physics and spin-scattering in time-dependent magnetic fields has been studied by Sarah Maria Schroeter [6].

In this work, the behaviour of an electron with mass m_e , when passing through a magnetic field with a fixed strength B_0 is studied.

2 Formulation of the problem

The behaviour of a half spin particle, more specifically an electron, when passing through a magnetic field with a fixed strength B_0 is considered. The parameter ϕ sets the position where the particular magnetic field is measured. At every position ϕ on border of the circle, we attach an imaginary 3D-sphere which determines the direction of the field vector. In effect, the magnetic field is constituted by mere spherical coordinates. In addition, we allow variation of both angle ϕ and θ in time with frequency of ω_1 and ω_2 respectively:

$$B(r, t) = B_0 \hat{n}(\phi, \theta, t) \quad (1)$$

$$B(r, t) = B_0 \begin{bmatrix} \sin(\theta - \omega_2 t) \cos(\phi - \omega_1 t) \\ \sin(\theta - \omega_2 t) \sin(\phi - \omega_1 t) \\ \cos(\theta - \omega_2 t) \end{bmatrix} \quad (2)$$

$$B(r, t) = B_0 \begin{bmatrix} \sin(\tilde{\theta}) \cos(\tilde{\phi}) \\ \sin(\tilde{\theta}) \sin(\tilde{\phi}) \\ \cos(\tilde{\theta}) \end{bmatrix} \quad (3)$$

where $\tilde{\phi} = \phi - \omega_1 t$ and $\tilde{\theta} = \theta - \omega_2 t$. The Hamiltonian is made up of a kinetic part and a part arising from the interaction of particle with the magnetic field:

$$H_0(r, t) = \frac{\hat{p}^2}{2m_e} + B(r, t) \frac{g_s |\mu_B|}{\hbar} S \quad (4)$$

where S is the electron spin, g_s is the spin g-factor and μ_B is the Bohr magneton

$$|\mu_B| = \frac{|e|\hbar}{2m_e}$$

We confine ourselves to the xy -plane, with the real space parameter $\theta = \pi/2$ and radius R kept fixed. The nabla-operator

is simplified as:

$$\nabla = \hat{e}_r \frac{\partial}{\partial r} + \hat{e}_\theta \frac{1}{R} \frac{\partial}{\partial \theta} + \hat{e}_\phi \frac{1}{R \sin \theta} \frac{\partial}{\partial \phi} \quad (5)$$

which becomes

$$\nabla^2 = \left(\frac{1}{R} \frac{\partial}{\partial \phi} \right)^2. \quad (6)$$

Thus, we can now rewrite the Hamiltonian H_0 as

$$H_0 = -\frac{\hbar^2}{2mR^2} \left(\frac{\partial}{\partial \phi} \right)^2 + |\mu_B| B_0(r, t) \sigma \quad (7)$$

where σ is a vector of Pauli matrices and for any unit vector \hat{n} , we find a rotation matrix \mathfrak{R} such that $\mathfrak{R} \hat{\phi} = \hat{n}$ so that (7) can be rewritten as

$$H_0 = \frac{\hbar^2}{mR^2} \left(-\frac{1}{2} \left(\frac{\partial}{\partial \phi} \right)^2 + \frac{|\mu_B| B_0}{\hbar^2/mR^2} \hat{n} \sigma \right) \quad (8)$$

$$H_0 = \frac{\hbar^2}{mR^2} \left(-\frac{1}{2} \left(\frac{\partial}{\partial \phi} \right)^2 + \alpha \hat{n} \sigma \right) = \frac{\hbar^2}{mR^2} \tilde{H}_0 \quad (9)$$

where

$$\alpha = \frac{|\mu_B| B_0}{\hbar^2/mR^2}; S = \frac{\hbar}{2} \sigma; g_s = 2.$$

Combining the operators generating the translation and rotation gives

$$g = -i\hbar \frac{\partial}{\partial S} 1 + \frac{\hbar}{2R} \sigma_z = -\frac{i\hbar}{R} \frac{\partial}{\partial \phi} 1 + \frac{\hbar}{2R} \sigma_z \quad (10)$$

$$\tilde{g} = -i \frac{\partial}{\partial \phi} 1 + \frac{\sigma_z}{2} \quad (11)$$

where \tilde{g} is a rescaled version of g . By careful construction of g , \tilde{H}_0 and \tilde{g} commute, consequently H_0 and g indeed commute.

$$[\tilde{H}_0, \tilde{g}] = \left[-\frac{1}{2} \left(\frac{\partial}{\partial \phi} \right)^2 + \alpha \hat{n} \sigma, -i \frac{\partial}{\partial \phi} 1 + \frac{\sigma_z}{2} \right] \quad (12)$$

$$[\tilde{H}_0, \tilde{g}] = \left[-\frac{1}{2} \left(\frac{\partial}{\partial \phi} \right)^2, -i \frac{\partial}{\partial \phi} \right] + \left[\alpha \hat{n} \sigma, -i \frac{\partial}{\partial \phi} \right] + \left[-\frac{1}{2} \left(\frac{\partial}{\partial \phi} \right)^2, \frac{\sigma_z}{2} \right] + \left[\alpha \hat{n} \sigma, \frac{\sigma_z}{2} \right] \quad (13)$$

$$[\tilde{H}_0, \tilde{g}] = i\alpha \left(\frac{\partial}{\partial \phi}, \hat{n} \sigma \right) + \frac{\hbar \sigma}{2} \left([\sigma_x, \sigma_z], [\sigma_y, \sigma_z], [\sigma_z, \sigma_z] \right) \quad (14)$$

with

$$[\sigma_i, \sigma_j] = 2i \epsilon_{ijk} \sigma_k.$$

$$[\tilde{H}_0, \tilde{g}] = i\alpha \left[\frac{\partial}{\partial \phi} \left(\sin \tilde{\theta} \cos \tilde{\phi} \sigma_x + \sin \tilde{\theta} \sin \tilde{\phi} \sigma_y + \cos \tilde{\theta} \sigma_z \right) + i\alpha \hat{n} (-\sigma_y, \sigma_x, 0) \right] \quad (15)$$

$$[\tilde{H}_0, \tilde{g}] = i\alpha \left(-\sin \tilde{\theta} \sin \tilde{\phi} \sigma_x + \sin \tilde{\theta} \cos \tilde{\phi} \sigma_y \right) + i\alpha \hat{n} (-\sigma_y, \sigma_x, 0) \quad (16)$$

$$[\tilde{H}_0, \tilde{g}] = 0. \quad (17)$$

We have shown that \tilde{H}_0 and \tilde{g} possess the same system of eigenfunctions, with that, we regard \tilde{g} as a generalized momentum operator.

2.1 Solution to momentum operator

We now establish the eigenfunctions of \tilde{g} solving the eigen-system

$$\left(-i \frac{\partial}{\partial \phi} 1 + \frac{\sigma_z}{2} \right) |\psi\rangle = K |\psi\rangle \quad (18)$$

$$-i \frac{\partial}{\partial \phi} 1 |\psi\rangle = \left(K - \frac{\sigma_z}{2} \right) |\psi\rangle = \begin{pmatrix} K - \frac{1}{2} & 0 \\ 0 & K + \frac{1}{2} \end{pmatrix} |\psi\rangle \quad (19)$$

with eigenvalues

$$\lambda_{\pm} = \left(K \mp \frac{1}{2} \right) \quad (20)$$

and the respective eigenfunctions

$$|\psi_1\rangle = \begin{pmatrix} 1 \\ 0 \end{pmatrix} e^{i(K - \frac{1}{2})\phi} = \begin{pmatrix} \psi_1 \\ 0 \end{pmatrix} \quad (21)$$

$$|\psi_2\rangle = \begin{pmatrix} 0 \\ 1 \end{pmatrix} e^{i(K + \frac{1}{2})\phi} = \begin{pmatrix} 0 \\ \psi_2 \end{pmatrix}. \quad (22)$$

As we study the motion of a particle on a ring, we require $|\psi(\phi)\rangle$ to fill periodic boundary condition

$$|\psi(\phi)\rangle = |\psi(\phi + 2\pi)\rangle e^{i(K \mp \frac{1}{2})2\pi} = 1K = n + \frac{1}{2}; n \in Z \quad (23)$$

This means that the momentum is quantized. The general solution to (18) is linear combination of both eigenfunctions

$$|\psi(\phi)\rangle = C_1(t) |\psi_1(\phi)\rangle + C_2(t) |\psi_2(\phi)\rangle = \begin{pmatrix} C_1(t) |\psi_1(\phi)\rangle \\ C_2(t) |\psi_2(\phi)\rangle \end{pmatrix} \quad (24)$$

where $C_1(t)$ and $C_2(t)$ do not depend on ϕ .

2.2 Solution to the time-dependent Hamiltonian

Ultimately, we are interested in computing the time-dependent coefficients $C_1(t)$ and $C_2(t)$ in order to receive full solution of the Schrödinger equation when solving the time-dependent Schrödinger equation, we employ the solution to

the momentum operator in order to simplify the eigensystem associated with \tilde{g} as follows:

$$i\hbar\partial_t|\psi\rangle = H_0|\psi\rangle = \frac{\hbar^2}{mR^2} \left(-\frac{1}{2} \left(\frac{\partial}{\partial\tilde{\phi}} \right)^2 + \alpha\hbar\sigma \right) |\psi\rangle. \quad (25)$$

See the last page for intermediate equations (26) and (27)

$$i\hbar\partial_t|\psi\rangle = H_{0,K,\tilde{\phi}}(t)|\psi\rangle \quad (28)$$

where $H_{0,K,\tilde{\phi}}(t)$ is defined by equation (27).

2.2.1 Setting up the Schrödinger equation for the time-dependent coefficients

To set up the Schrödinger equation for the time-dependent coefficients $C_1(t)$ and $C_2(t)$ is by transforming the Schrödinger equation for $|\psi\rangle$:

$$\begin{aligned} i\hbar\partial_t|\psi\rangle \begin{pmatrix} C_1(t)\psi_1 \\ C_2(t)\psi_2 \end{pmatrix} &= H_0(t) \begin{pmatrix} C_1(t)\psi_1 \\ C_2(t)\psi_2 \end{pmatrix} \\ i\hbar\partial_t|\psi\rangle \begin{pmatrix} C_1(t) \\ C_2(t)\frac{\psi_2}{\psi_1} \end{pmatrix} &= H_0(t) \begin{pmatrix} C_1(t) \\ C_2(t)\frac{\psi_2}{\psi_1} \end{pmatrix}. \end{aligned} \quad (29)$$

Employing the equation (27) computed solution to the momentum operator, we know that $\frac{\psi_2}{\psi_1} = e^{i\theta}$ and may write (see the last page for intermediate equations (30) and (31)):

$$i\hbar\partial_t \begin{pmatrix} C_1(t) \\ C_2(t) \end{pmatrix} = H_{0,K,\omega} \begin{pmatrix} C_1(t) \\ C_2(t) \end{pmatrix} \quad (32)$$

where $H_{0,K,\omega}$ is defined by equation (31).

2.3 Moving into a rotating coordinate system

To solve the eigensystem, we transform $H_{0,K,\omega}(t)$ by changing into a coordinate system rotating clockwise with a frequency $\omega = \omega_1$

$$\begin{pmatrix} C_1\tilde{(t)} \\ C_2\tilde{(t)} \end{pmatrix} = e^{-\frac{i}{\hbar}S_z\omega t} \begin{pmatrix} C_1(t) \\ C_2(t) \end{pmatrix} = e^{-\frac{i}{2}\sigma_z\omega t} \begin{pmatrix} C_1(t) \\ C_2(t) \end{pmatrix}. \quad (33)$$

In another way, (33) becomes

$$\begin{pmatrix} C_1(t) \\ C_2(t) \end{pmatrix} = e^{\frac{i}{2}\sigma_z\omega t} \begin{pmatrix} C_1\tilde{(t)} \\ C_2\tilde{(t)} \end{pmatrix} \quad (34)$$

where

$$\begin{aligned} e^{\frac{i}{2}\sigma_z\omega t} &= \sum_n \frac{\left(\frac{i}{2}\sigma_z\omega t\right)^n}{n!} = \sum_n \frac{\left(\frac{i}{2}\omega t\right)^n}{n!} \begin{pmatrix} 1^n & 0 \\ 0 & (-1)^n \end{pmatrix} \\ &= \begin{pmatrix} e^{\frac{i}{2}\omega t} & 0 \\ 0 & e^{-\frac{i}{2}\omega t} \end{pmatrix}. \end{aligned}$$

Substituting of (32) in (34) gives:

$$\begin{aligned} i\hbar\partial_t \begin{pmatrix} e^{\frac{i}{2}\omega t} & 0 \\ 0 & e^{-\frac{i}{2}\omega t} \end{pmatrix} \begin{pmatrix} C_1\tilde{(t)} \\ C_2\tilde{(t)} \end{pmatrix} \\ = H_{0,K,\omega} \begin{pmatrix} e^{\frac{i}{2}\omega t} & 0 \\ 0 & e^{-\frac{i}{2}\omega t} \end{pmatrix} \begin{pmatrix} C_1\tilde{(t)} \\ C_2\tilde{(t)} \end{pmatrix}. \end{aligned} \quad (35)$$

Multiplying L.H.S of (35) by $e^{\frac{i}{2}\sigma_z\omega t}$, we obtain

$$\begin{pmatrix} e^{-\frac{i}{2}\omega t} & 0 \\ 0 & e^{\frac{i}{2}\omega t} \end{pmatrix} \begin{pmatrix} e^{\frac{i}{2}\omega t} \left(-\frac{\hbar\omega}{2} + i\hbar\partial_t \right) & 0 \\ 0 & e^{-\frac{i}{2}\omega t} \left(\frac{\hbar\omega}{2} + i\hbar\partial_t \right) \end{pmatrix} \begin{pmatrix} C_1\tilde{(t)} \\ C_2\tilde{(t)} \end{pmatrix} = \begin{pmatrix} -\frac{\hbar\omega}{2} & 0 \\ 0 & -\frac{\hbar\omega}{2} \end{pmatrix} \begin{pmatrix} C_1\tilde{(t)} \\ C_2\tilde{(t)} \end{pmatrix} + i\hbar\partial_t \begin{pmatrix} C_1\tilde{(t)} \\ C_2\tilde{(t)} \end{pmatrix}.$$

Also multiplying R.H.S of (35) by $e^{\frac{i}{2}\sigma_z\omega t}$ we have:

$$\begin{pmatrix} e^{-\frac{i}{2}\omega t} & 0 \\ 0 & e^{\frac{i}{2}\omega t} \end{pmatrix} H_K \begin{pmatrix} e^{\frac{i}{2}\omega t} & 0 \\ 0 & e^{-\frac{i}{2}\omega t} \end{pmatrix} \begin{pmatrix} C_1\tilde{(t)} \\ C_2\tilde{(t)} \end{pmatrix} = \begin{pmatrix} \frac{1}{2} \left(K - \frac{1}{2} \right)^2 + \alpha \cos \tilde{\theta} & \alpha \sin \tilde{\theta} \\ \alpha \sin \tilde{\theta} & \frac{1}{2} \left(K + \frac{1}{2} \right)^2 - \alpha \cos \tilde{\theta} \end{pmatrix} \begin{pmatrix} \tilde{C}_1(t) \\ \tilde{C}_2(t) \end{pmatrix}.$$

As a consequence, (35) yields (see the last page for intermediate equation (36))

$$i\hbar\partial_t \begin{pmatrix} \tilde{C}_1(t) \\ \tilde{C}_2(t) \end{pmatrix} = C \begin{pmatrix} \tilde{C}_1(t) \\ \tilde{C}_2(t) \end{pmatrix}. \quad (37)$$

Comparing (37) with the corresponding static Schrödinger equation for time-independent coefficients, one observes that C is the Hamiltonian one receives when considering static magnetic field (cf. [5]) combined with an additional matrix

$$\begin{pmatrix} \frac{\omega m R^2}{2\hbar} & 0 \\ 0 & -\frac{\omega m R^2}{2\hbar} \end{pmatrix}.$$

We now deal with time-independent $\tilde{\theta}$ and time-dependent $\tilde{\phi}$, so that $\tilde{\theta} = \theta = \text{constant}$. As eigenvalues of the operator C we get (see the last page for equation (38)), which correspond to the energies of the lower and upper band. E_- corresponds to a magnetic moment which is parallel to the magnetic field.

2.4 Determining the rotated time-dependent coefficients

To determine the solution to (36) i.e find a representation of the rotated time-dependent coefficients $\tilde{C}(t)_1$ and $\tilde{C}(t)_2$, an equation of the form

$$i\hbar\partial_t \begin{pmatrix} \tilde{C}_1(t) \\ \tilde{C}_2(t) \end{pmatrix} = C \begin{pmatrix} \tilde{C}_1(t) \\ \tilde{C}_2(t) \end{pmatrix}$$

can immediately be found to have the solution

$$\begin{pmatrix} \tilde{C}_{1+}(t) \\ \tilde{C}_{2+}(t) \end{pmatrix} = e^{-iE_+t} X_+ \quad (39)$$

$$\begin{pmatrix} \tilde{C}_{1-}(t) \\ \tilde{C}_{2-}(t) \end{pmatrix} = e^{-iE_-t} X_- \quad (40)$$

where E_+ , E_- and X_+ , X_- are the eigenvalues and corresponding normalized eigenvectors of the matrix C respectively.

More precisely, the later are found to be given by equation (41) and normalization factor (42) given on the last page.

2.5 Establishing the solution to the initial Schrödinger equation

Combining (39) and (40) with already computed static parts of the wave function (21) and (22) as well as multiplying the respective components with the e factor which sets the wave function back into a non-rotating coordinate system (see (34)), we receive the exact solutions to the initial Schrödinger equation (27)

$$|\psi\rangle_{K,+} = e^{-iE_+t} \begin{pmatrix} x_{1,+} e^{i(K-\frac{1}{2})\phi} e^{i\frac{\omega}{2}t} \\ x_{2,+} e^{i(K+\frac{1}{2})\phi} e^{-i\frac{\omega}{2}t} \end{pmatrix}; \quad (43)$$

$${}_{+,K}\langle\psi|\psi\rangle_{K,+} = 1$$

$$|\psi\rangle_{K,-} = e^{-iE_-t} \begin{pmatrix} x_{1,-} e^{i(K-\frac{1}{2})\phi} e^{i\frac{\omega}{2}t} \\ x_{2,-} e^{i(K+\frac{1}{2})\phi} e^{-i\frac{\omega}{2}t} \end{pmatrix}; \quad (44)$$

$${}_{-,K}\langle\psi|\psi\rangle_{K,-} = 1$$

The solutions (43) and (44) specific to energies E_- and E_+ (and respective bands + and -) corresponding to the solution to one K , hence the indices.

3 Numerical solution to the eigenenergies

First, let us turn back to the exact eigenenergies we computed in section 2.2, equation (38). We consider an incoming wave function with a fixed energy ϵ (given on the last page). For a fixed energy $\epsilon_n = \epsilon_o + n\omega$ there are maximal four real solutions for $K(n, \sigma, \delta)$, which correspond to the propagation directions $\delta = l, r$ and the two possible eigenenergies of the respective wave functions, i.e. the alignment of the spin $\sigma = +, -$ with respect to the magnetic field, (see Fig. 1).

4 Discussion

The Schrödinger equation for a half spin particle in a time dependent magnetic field is presented. Depending on the energy, there are up to four real solutions for K . The energy function $E_+(K)$ lies below the function $E_-(K)$ for all specific K , (see Fig. 1). For a fixed energy below the minimum of E_- there are no real solutions. For a fixed energy between both minima there are two real solutions which correspond to a spin aligned in the direction of the magnetic field and waves propagating towards the left or the right. For an energy above two minima there are four real solutions. In this case, both directions of propagation and both spin orientations occur.

5 Conclusion

In this paper, the exact wave function of a particle moving through a non-colinear time-dependent magnetic field is computed. Also, it is confirmed that the motion of a half spin of an electron through the chosen magnetic field is an adiabatic problem evolving with time. We found that for a time-dependence of the position of the electron, there are no emergent electric fields since the undisturbed Hamiltonian can be mapped onto a time-independent one by unitary transformations.

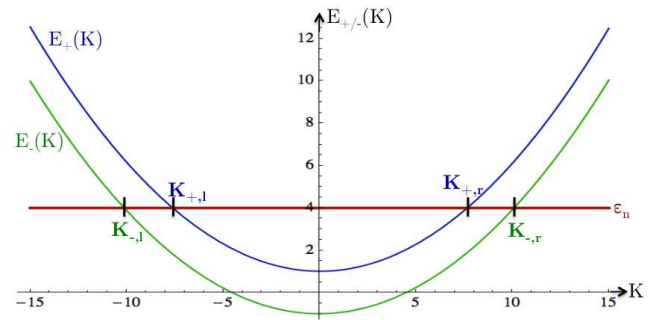


Fig. 1: Eigenenergies $E_{\pm}(K)$ plotted versus the momentum eigenvalue K for sample values of α , ω , θ and $x = mR^2/\hbar^2$. The points of intersection K_i with a fixed energy ϵ determine the propagation direction and the spin alignment of the wave function. We set $\alpha = 10$, $\omega = 0.1$, $\theta = \pi$ and $x = mR^2/\hbar^2 = 10$.

Acknowledgements

The authors wish to thank Sarah Maria Schroeter for her time, useful discussions to this problem.

Submitted on October 10, 2015 / Accepted on October 17, 2015

References

1. Mühlbauer S., Binz B., Jonietz F., Pfleiderer C., Rosch A., Neubauer A., Georgii R., Boni P. Skyrmion Lattice in a Chiral Magnet. *Science*, 2009, v. 323, 915–919.
2. Pfleiderer C. and Rosch A. Single skyrmions spotted. *Nature*, 2010, v. 465 (7300), 880–881.
3. Neubauer A., Pfleiderer C., Binz B., Rosch A., Ritz R., Niklowitz P. G., and Boni P. Topological Hall Effect in the A Phase of MnSi. *Phys. Rev. Lett.*, 2009, v. 102, 186602.
4. Everschor K. Current-Induced Dynamics of Chiral Magnetic Structures. Ph.D. thesis, University of Cologne, 2012.
5. Baedorf M. Berry-Phase und Spinstreuung. Bachelor's thesis, University of Cologne, 2011.
6. Schroeter S.M. Berry Phase Physics and Spin-Scattering in Time-Dependent Magnetic Fields. Bachelor's thesis, University of Cologne, 2012.

$$i\hbar\partial_t|\psi\rangle = \frac{\hbar^2}{mR^2} \begin{pmatrix} -\frac{1}{2}\left(\frac{\partial}{\partial\tilde{\phi}}\right)^2 + \alpha\cos\tilde{\theta} & \alpha\sin\tilde{\theta}e^{-i\tilde{\phi}} \\ \alpha\sin\tilde{\theta}e^{i\tilde{\phi}} & -\frac{1}{2}\left(\frac{\partial}{\partial\tilde{\phi}}\right)^2 - \alpha\cos\tilde{\theta} \end{pmatrix} |\psi\rangle \quad (26)$$

$$i\hbar\partial_t|\psi\rangle = \frac{\hbar^2}{mR^2} \begin{pmatrix} \frac{1}{2}\left(K - \frac{1}{2}\right)^2 + \alpha\cos\tilde{\theta} & \alpha\sin\tilde{\theta}e^{-i\tilde{\phi}} \\ \alpha\sin\tilde{\theta}e^{i\tilde{\phi}} & \frac{1}{2}\left(K + \frac{1}{2}\right)^2 - \alpha\cos\tilde{\theta} \end{pmatrix} |\psi\rangle \quad (27)$$

$$i\hbar\partial_t \begin{pmatrix} C_1(t) \\ C_2(t)\frac{\psi_2}{\psi_1} \end{pmatrix} = \frac{\hbar^2}{mR^2} \begin{pmatrix} \left(\frac{1}{2}\left(K - \frac{1}{2}\right)^2 + \alpha\cos\tilde{\theta}\right)C_1(t) + \alpha\sin\tilde{\theta}e^{-i\tilde{\phi}}C_2(t)e^{i\phi} \\ \alpha\sin\tilde{\theta}e^{i\tilde{\phi}}C_1(t) + \left(\frac{1}{2}\left(K - \frac{1}{2}\right)^2 - \alpha\cos\tilde{\theta}\right)C_2(t)e^{i\phi} \end{pmatrix} \quad (30)$$

$$i\hbar\partial_t \begin{pmatrix} C_1(t) \\ C_2(t) \end{pmatrix} = \begin{pmatrix} \frac{1}{2}\left(K - \frac{1}{2}\right)^2 + \alpha\cos\tilde{\theta} & \alpha\sin\tilde{\theta}e^{i\omega_1 t} \\ \alpha\sin\tilde{\theta}e^{-i\omega_1 t} & \frac{1}{2}\left(K + \frac{1}{2}\right)^2 - \alpha\cos\tilde{\theta} \end{pmatrix} \begin{pmatrix} C_1(t) \\ C_2(t) \end{pmatrix} \quad (31)$$

$$i\hbar\partial_t \begin{pmatrix} \tilde{C}_1(t) \\ \tilde{C}_2(t) \end{pmatrix} = \frac{\hbar^2}{mR^2} \begin{pmatrix} \frac{1}{2}\left(K - \frac{1}{2}\right)^2 + \alpha\cos\tilde{\theta} + \frac{\omega mR^2}{2\hbar} & \alpha\sin\tilde{\theta} \\ \alpha\sin\tilde{\theta} & \frac{1}{2}\left(K + \frac{1}{2}\right)^2 - \alpha\cos\tilde{\theta} - \frac{\omega mR^2}{2\hbar} \end{pmatrix} \begin{pmatrix} \tilde{C}_1(t) \\ \tilde{C}_2(t) \end{pmatrix} \quad (36)$$

$$E_{\pm} = \frac{\hbar^2}{mR^2} \left(\frac{K^2 + \frac{1}{4}}{2} \pm \sqrt{\frac{\left(K - \frac{\omega mR^2}{2\hbar}\right)^2}{4} - \alpha\left(K - \frac{\omega mR^2}{2\hbar}\right)^2 \cos\theta + \alpha^2} \right) \quad (38)$$

$$X_{\pm} = \begin{pmatrix} x_{1,\pm} \\ x_{2,\pm} \end{pmatrix} = \frac{1}{N_{\pm}} \begin{pmatrix} \frac{\hbar^2}{mR^2} \left(-\frac{1}{2}\left(K + \frac{1}{2}\right)^2 + \alpha\cos\theta \right) + \frac{\hbar\omega}{2} + E_{\pm} \\ \frac{\hbar^2}{mR^2} \alpha\sin\theta \end{pmatrix} \quad (41)$$

$$N_{\pm}^2 = \left(\frac{\hbar^2}{mR^2} \left(-\frac{1}{2}\left(K + \frac{1}{2}\right)^2 + \alpha\cos\theta \right) + \frac{\hbar\omega}{2} + E_{\pm} \right)^2 + (\alpha\sin\theta)^2 \quad (42)$$

$$E_{\pm} = \frac{\hbar^2}{mR^2} \left(\frac{K^2 + \frac{1}{4}}{2} \pm \sqrt{\frac{\left(K - \frac{\omega mR^2}{2\hbar}\right)^2}{4} - \alpha\left(K - \frac{\omega mR^2}{2\hbar}\right)^2 \cos\theta + \alpha^2} \right) = \text{const} = \epsilon_o \quad (45)$$

On the Absorber in Gravitation

Jacques Consiglio

52 Chemin de Labarthe, 31600 Labastidette, France
E-mail: Jacques.Consiglio@gmail.com

Assuming the big-bang is a periodic 4-dimensional event, we show that the main parameters of the Λ CDM model, namely matter, dark energy and total density, can be computed straightforwardly from Mach's principle and that the existence of dark matter is not necessary. As a result, we find that the cosmos expansion is the origin of mass and energy — but not the big-bang as a singular event.

1 Introduction

The object of this note is to show that once assumed that the big bang is a periodic event, and using absorber theory, the dark matter field is un-necessary in cosmology, and the dark energy is the natural free field of the absorber.

2 The Absorber and cosmology

Mach's principle states in a very general manner: *local physical laws are determined by the large scale structure of the universe*. This principle is the basis of the Wheeler-Feynman absorber theory [1, 2]. They suppose that the energy of particles is given by a time-symmetrical field; this interpretation was made by Tetrode and assumes that particles are not self-interacting. The main equations go as follows:

$$E_{total}(x_j, t) = \frac{\sum_{n \neq j} (E_n^{ret}(x_j, t) + E_n^{adv}(x_j, t))}{2}, \quad (2.1)$$

$$E_{damping}(x_j, t) = \frac{E_j^{ret}(x_j, t) - E_j^{adv}(x_j, t)}{2}, \quad (2.2)$$

$$E_{total}(x_j, t) = E_{damping}(x_j, t) + \sum_{n \neq j} E_n^{ret}(x_j, t). \quad (2.3)$$

They define the energies of the damping (2.2) and the total field (2.1–2.3), from advanced and retarded components for each particle (index j). The central idea is that the advanced field not being causal, it can only have damping effects while energetic interactions are causal. The theory was designed in electrodynamics but here we assume the field at the origin of gravitation and energy (including mass-energy and inertia), and propagating on the light cone.

The standard model of cosmology is based on general relativity theory (GRT). The idea is that the cosmos is self-contained (no outer realm), and internal metric expansion. However, it requires a unique event at its beginning, the so called big bang, resulting in the conceptual problem of its cause. Here we use Mach's principle on a larger scale: we assume the observed cosmos part of a wider 4-dimensional area. A 4-space denoted universe which we assume Euclidean with its own time and evolves as follows:

- A central location exists at the origin of the cosmos; we shall call it the emitter;

- A new cosmos or membrane is emitted periodically; the membranes separation is constant;
- The membrane progression is radial; the emitter produces more membranes and so on.

This structure is reminiscent of a wave; it is a manner to solve the problems of origin (the system is permanent); the membranes separation, if large enough, avoids the problem of instantaneous inflation. It also has the elegance of simplicity and the expansion is immediately linear. The idea at the basis of this concept was triggered-off by the recent observation of cosmological oscillations by Ringermacher and Mead [3].

3 Gravitation and energy

Now evidently, we have to build a theory from scratch; that is to say from experimental evidences. We shall use the following: we know from experimental gravitation physics that fixed clocks at different heights in the field have different rates; and the pulsation of photons and material system are constant in free fall. Equivalently, it is said that gravitation defines the context in which the rest of physics lives. According to Mach's principle it implies only a local variation of density which depends on the structure of the universe.

Denoting the density g , it varies according to $1/r$ as it addresses energy. This is classically written with:

$$g(r) = g^\infty \left(1 - \frac{f(M)}{r}\right), \quad (3.1)$$

where $f()$ is an undefined function of mass. The Newton potential reads:

$$\Gamma = \Gamma^0 - \frac{GM}{r}. \quad (3.2)$$

Then G depends on $f()$, and Γ^0 is usually an arbitrary constant and the rest energy of a mass m is $E^0 = mc^2$. But now energy is given by the absorber mechanism and then the constant is $\Gamma^0 = c^2$. Then we write:

$$E = m \left(c^2 - \frac{GM}{r} \right). \quad (3.3)$$

Therefore the density g defined in (3.1) is linked to mass-energy and to the velocity of light.

In a relativistic manner we can for instance define a variable c^* , use invariant masses and write:

$$c^{*2} = c^2 - \frac{2GM}{r}. \quad (3.4)$$

Since frequencies and wavelengths evolve conversely in the gravitational field, we write:

$$c^2 d\tau^2 = c^{*2} dt^2 - \frac{c^2}{c^{*2}} dr^2. \quad (3.5)$$

Substituting from (3.4) this is the Schwarzschild metric. The pulsations of photons and of material systems in free fall are constant and then this equation applies identically to any form of energy. The concept is different from general relativity (GRT) but the equation is experimentally verified exactly in the same manner — that is to say uniquely in the solar system since all other verifications lead to suppose the existence of dark matter.

4 Dark energy and matter density

The absorber is time-symmetrical with causal effects; it concerns the total currents within the event horizon, say M_A c^2 the absorber “free” mass/energy. Equilibrium exists in the absorber process, and then the currents interfering with a mass m depend on m/M_A . We assume linear expansion; the visible cosmos radius is then $R_U = c/H = cT$ where H is the Hubble parameter and T the age of the membrane. Then by symmetry, we write:

$$\frac{E_m}{M_A c^2} = \frac{m}{M_A} \times \left(1 - \frac{MR_U}{M_A r}\right). \quad (4.1)$$

This is the Newton potential but the standard cosmological model is based on GRT which gives a factor $2GM$ like from (3.4–3.5), then in the standard theory the absorber free energy will be estimated from:

$$\frac{R_U}{2M_A} = \frac{G}{c^2}. \quad (4.2)$$

Using c , G and H we can now compute the absorber free energy; we find:

$$M_A = \frac{R_U c^2}{2G} = 8.790 \times 10^{52} \text{ Kg}. \quad (4.3)$$

Considering visible energies $M_V c^2$, the ratio M_V/M_A is geometrical as it corresponds to the surface of a 4-sphere ; it is then $1/2\pi^2$. Then the factor 2 in (4.2) becomes $4\pi^2$ in 3+1D where masses interact. It gives:

$$2M_A = 4\pi^2 M_V \rightarrow M_V = 4.453 \times 10^{51} \text{ Kg}. \quad (4.4)$$

Summing (4.3–4.4), we get the total energy of the cosmos:

$$M_{total} = M_A + M_V = 9.236 \times 10^{52} \text{ Kg}. \quad (4.5)$$

It corresponds to a density $\rho = 9.91 \times 10^{-27} \text{ Kg/m}^3$ and the visible part (4.2) is 4.82% of the total. The benchmark at this time is the Plank mission results [4] which is $\rho = 9.90 \times 10^{-27} \text{ Kg/m}^3$ and 4.9% of visible energy.

Hence according to the most favored model in cosmology we get three valid quantities in (4.3, 4.4, 4.5) which are *deduced* from the absorber symmetry and depend on geometry, c , G and $H = 1/T$. We do not get any dark matter, and assuming those results are significant we cannot afford any — though one could think that it may hide in M_A . But here the concept is different; the field is time-symmetrical and it cannot be an independent field as its relative amplitude is given by geometry.

With the results in this section we face two possibilities:

- The Λ CDM model parameters are tuned to match a linear expansion and it results in (4.3, 4.4, 4.5); which is a little surprising.
- A simple coincidence for M_A , but maybe a relevant result for M_V .

One way to make our mind is to develop the theory and check if the field needs dark matter.

5 The short range gravitational field

In (4.1) it appears that either G or M_V is variable; if we consider M_V constant, then G is a scale factor in proportions of R_U , but it is scale-independent on cosmological scales where R_U/r is constant.

In standard physics, one uses G , c and masses constant; we can then use the same constant quantities and it should give the differences between the Newton theory and the gravitational field given by our equations, at least a short range. In this section we consider that only t evolves and $T \gg t > 0$; it is linked to the Hubble factor H or R_U since the scenario of emission gives:

$$H(T) R_U(T) = c \rightarrow H(T) = \frac{c}{(R_0 + cT)} \approx \frac{1}{T}, \quad (5.1)$$

where $R_0 = R_U(T = 0)$ and T is the elapsed time since the separation of our membrane. Then from (4.2–5.1), denoting $R_U(T) \rightarrow R_U$ we can also write:

$$\frac{GM_A}{(R_U - ct)} = c^2. \quad (5.2)$$

Now all is constant except t and we can take a second order limited development; then denoting $H(T) \rightarrow H$, and using (5.1–5.2) we get:

$$\frac{GM_A H}{c} \times \left(1 + \frac{Hr}{c} - \frac{H^2 r^2}{c^2}\right) = c^2. \quad (5.3)$$

Multiplying G in the Newton potential by the terms of the limited development in (5.3) we introduce retarded interaction and then causality in the field (which is not in Newton’s

theory). The potential is extended as:

$$\Gamma = \Gamma^0 - \frac{GM}{r} - \frac{GMH}{c} + \frac{GMH^2 r}{c^2}. \quad (5.4)$$

Let us analyze how this potential works:

It first adds a constant negative energy term $(-GMH/c)$ with no gravitational impact. It is then the contribution of the mass M to the constant c^2 ; it is the free absorber field and M must be summed to $2M_A$. Using (4.2) it leaves a negative constant $-c^2$ on the right-hand side. We get:

$$\Gamma = \Gamma^0 - c^2 - \frac{GM}{r} + \frac{GMH^2 r}{c^2}.$$

Then $\Gamma^0 = c^2$ is immediate and the physical origin of energy is the expansion, not the big-bang.

The next term is then of identical nature and we sum again M to $2M_A$. Using (4.2) again yields $GM_A H^2 r/c^2 = Hcr$ (giving an acceleration Hc). We now get:

$$\Gamma = \Gamma^0 - c^2 - \frac{GM}{r} + Hcr. \quad (5.5)$$

But $\Gamma^0 = c^2$ and $\Gamma < 0$; then rescaling notations with $\Gamma + c^2 \rightarrow \Gamma$ and using (4.2) we choose to write:

$$\frac{\Gamma}{c^2} = 1 - \frac{MR_U}{2M_A r} + \frac{r}{R_U}. \quad (5.6)$$

It is well-known that stars at galaxies borders experience an anomalous centripetal acceleration in the range Hc . This acceleration is the origin of the dark matter hypothesis by Oort in 1932.

Here the potential c^2 and the acceleration Hc are the effects of expansion and retarded interaction; it must be seen as the origin of energy and the known problem of conservation related to this acceleration is inexistent.

A second classical objection is that this anomaly is not observed in the solar system; however, we assume the absorber at the origin of mass/energy and the immediate consequence is that it transform in acceleration. We can directly transform the density g ; that is, with acceleration Hc in any direction, a transformation L exists verifying:

$$L\left(Hc, g\left(T - \frac{r}{c}\right)\right) = g(T). \quad (5.7)$$

The following transformation holds:

$$g\left(T - \frac{r}{c}\right) \times \left(1 + \frac{Hr}{c}\right) = g(T). \quad (5.8)$$

Because once extended to any acceleration A in place of Hc , and replacing $r \rightarrow ct$, the non relativistic case gives:

$$g(T-t) \frac{A}{c} = \frac{g(T) - g(T-t)}{t}.$$

The right-hand of this equation is a time derivative, hence:

$$\frac{gA}{c} = \frac{dg}{dt} \rightarrow \frac{g}{c} = \frac{dg}{dv}. \quad (5.9)$$

It shows that a density obeying (5.8) creates resistance to acceleration and that mass increases with velocity. Hence the field is not Galilean, it is then a-priori relativistic. The equation (5.8) is equivalent to (and also justified by) the equation (5.2), but symmetrical where the field transforms in acceleration. This calculus shows, by symmetry, that a cosmological acceleration of the sun and its satellites in the direction of the galaxy core rescales the density and eliminates the term Hcr ; hence no second cosmological acceleration of its satellites can exist directed to the sun (and so on with planet's satellites).

6 Energy and the quantum world

6.1 Correspondence with the classical field

In this section, we shall continue using G constant and masses variable with time. The non-reduced Plank units and the Schwarzschild radius will be useful to the discussion. Recall:

$$M_P = \sqrt{\frac{hc}{G}}, \quad l_P = \sqrt{\frac{hG}{c^3}}, \quad t_P = \sqrt{\frac{hG}{c^5}}, \quad R_S = \frac{2Gm}{c^2}.$$

The equation (4.2) is equivalent to saying that the visible cosmos is defined by the Schwarzschild radius of M_A . The unique property of the Plank mass is that its Schwarzschild radius and wavelength are equal; it is then pivotal and using (4.2), we first write:

$$\frac{2M_A}{M_P^2} = 4\pi^2 \frac{M_V}{M_P^2} = \frac{R_U c}{h}. \quad (6.1)$$

A similar equation can be written for any material system of mass m using its Schwarzschild radius:

$$\frac{2m}{M_P^2} = \frac{R_S c}{h}.$$

Hence, one could think that (6.1) is nothing new, but this is interesting firstly because this equation uses M_A and R_U , and not M_{total} as we may classically expect. It shows that any mass m and M_A come from the same mechanism, but in a reciprocal manner since the two quantities define opposite limit radius and obey the same equation. A complimentary equation gives unit-less ratios:

$$\frac{2M_A}{M_P} = \frac{R_U c^2}{G} \times \sqrt{\frac{G}{hc}} = \frac{R_U}{l_P} = \frac{T}{t_P}. \quad (6.2)$$

It expresses the same link with quantum physics; the system of units $[2M_A, R_U, T]$ is the time integral of the Plank system $[M_P, l_P, t_P]$. Again, it can be written with any mass m , but

not with M_V or M_{total} . Now using $h = c = G = 1$ we have $M_P = t_P = l_P = 1$, and the only evolving quantities are:

$$T = R_U = 2 M_A = 4\pi^2 M_V. \quad (6.3)$$

In the most natural system of units the cosmos energy is trivial and it appears to evolve. This is due to the choice of G constant. In facts, the cosmos expands exactly of one Compton wavelength of any massive system during one period of its pulsation (this is just $\lambda = hc/E$). The system $[2 M_A, R_U, T]$ is just a time integral, and a system of units its differential. Consequently, the physical link with the quantum world is also trivial: *The cosmos expansion gives an action h at each period of any system pulsation.* It gives a very natural origin to the basics of quantum physic where energy is a time differential, $E = h \nu$.

We find identity of expansion, wave and energy, in perfect agreement with the results of the previous section.

6.2 The field

The Plank mass is pivotal in (6.1–6.2) then we model the absorber with an evolving field ϕ given by:

$$2 M_A M_\phi = M_P^2 \rightarrow E_\phi = \frac{hc}{R_U} \approx 1.52 \times 10^{-51} \text{ J}. \quad (6.4)$$

This is the energy of a field of wavelength R_U ($\approx 10^{-32}$ eV). Its energy is proportional to $1/R_U$ and decreases with time. But the laws of nature do not change; hence (6.4) is scale dependent but valid at any epoch and it is legitimate to write:

$$E_\phi(r) = \frac{hc}{r}, \quad P_\phi(r) = \frac{h}{r}, \quad (6.5)$$

which addresses identically a hypothetical cosmos of radius r , and the field at a distant r of any mass.

A spherically inflating membrane defines a frame which is moving at velocity $v = cr/R_U$ at distance r from the attractive body M ; then notice:

$$\frac{h}{M_\phi v} = r, \quad \frac{h}{M_\phi(r) v} = R_U, \quad (6.6.1)$$

$$P_\phi(r) = \frac{h}{r} = M_\phi \frac{c^2}{v}. \quad (6.6.2)$$

The two expressions in (6.6.1) are equivalent to a de Broglie wavelength and in (6.6.2) momentum transfers on the light cone but in proportions of the phase velocity of the de Broglie wave. Now on top of the potential c^2 , gravitation can be seen as a negative energy field. The equation (6.6.2) then corresponds to negative momentum on the light cone where the exchanged quantum is given by the de Broglie wave phase velocity $V = c^2/v$, and its emission rate is the Compton frequency of its source. In this way, we can write the field equations in an interesting semi-classical manner where all quantities depend on pulsation and momentum:

$$\frac{G}{c^2} = \frac{1}{P_\phi(R_U)} \times \frac{1}{v_A(T)} = \text{const}, \quad (6.7)$$

$$F = -\frac{P_\phi(r)^2}{P_\phi(R_U)} \times \frac{v_M(T) v_m(T)}{v_A(T)} = -\frac{GMm}{r^2}, \quad (6.8)$$

$$\frac{\Gamma}{c^2} = 1 - \frac{P_\phi(r)}{P_\phi(R_U)} \times \frac{v_M(T)}{v_A(T)} = 1 - \frac{GM}{rc^2}, \quad (6.9)$$

where notations are trivial for the Compton frequencies of the masses m , M , and $2 M_A$ at the epoch T . From (6.4), the denominator is time independent, and then the choice of G constant is legitimate. (Though the alternate choice M_V constant where G is a scale factor also holds.)

6.3 Advanced and retarded components

Now let us show that the equations (6.8–6.9) are approximate and come from causality. Using constant masses, G is a scale factor and we can use the same limited development as before but with little interest; instead we shall use the absorber equations in section 2. In (6.8–6.9) the denominator is constant but the masses at the numerator evolve in proportion of time. Then using first (6.9) without the potential c^2 , consider the distance $r = ct$ constant; at the time T the retarded and advanced momentum from M will be felt by m respectively like $P_\phi(r) v_M(T-t)$ and $P_\phi(r) v_M(T+t)$ in proportion of m . Recall also $v_M(T) = kT$, then we first write the damping potential; it gives the participation of M to the potential c^2 which we sum to the absorber mass:

$$\begin{aligned} \frac{\Gamma_{damping}}{c^2} &= -\frac{P_\phi(r) v_M(T-t) - P_\phi(r) v_M(T+t)}{2 P_\phi(R_U) v_A(T)} \\ &= +\frac{P_\phi(r) v_M(t)}{P_\phi(R_U) v_A(T)} = +\frac{v_M(T)}{v_A(T)} \rightarrow +1. \end{aligned} \quad (6.10.1)$$

Now the retarded potential:

$$\begin{aligned} \frac{\Gamma_{retarded}}{c^2} &= -\frac{P_\phi(r) v_M(T-t) + P_\phi(r) v_M(T+t)}{2 P_\phi(R_U) v_A(T)} \\ &= -\frac{P_\phi(r)}{P_\phi(R_U)} \times \frac{v_M(T)}{v_A(T)}. \end{aligned} \quad (6.10.2)$$

Of course their sum is causal and it gives:

$$\frac{\Gamma_{retarded}}{c^2} + \frac{\Gamma_{damping}}{c^2} = 1 - \frac{P_\phi(r)}{P_\phi(R_U)} \times \frac{v_M(T)}{v_A(T)}, \quad (6.10.3)$$

which is causal, agrees with (6.9), and now includes the potential c^2 from integration; but it misses the acceleration Hc . A similar exercise is then needed on energy but we shall use forces as it will give the orientation of the acceleration; here we have to evaluate these on the full system (m plus M) exerted by all masses of the cosmos at the instant T . We shall do as if M and m were in a circular orbit at equal distance r of a third object (or their center of mass) as it is a representative test case. The retarded force on the system corresponds to the force from $M(T-t)$ to $m(T+t)$, summed with the force from $m(T-t)$ to $M(T+t)$; using again $r = ct$ we get:

$$\frac{F_{ret}}{c^2} = -P_\phi(2r)^2 \frac{v_M(T-t) v_m(T+t) + v_M(T+t) v_m(T-t)}{P_\phi(R_U) v_A(T)}.$$

The advanced forces are identical and exerted at $T-t$; we get:

$$\frac{F_{adv}}{c^2} = -P_\phi(2r)^2 \frac{v_M(T+t)v_m(T-t) + v_M(T-t)v_m(T+t)}{P_\phi(R_U)v_A(T)}.$$

The damping force is null as it is the difference between those two expression; the retarded force is their sum and we extract the part related to $v_M(t)v_m(t)$ as the rest of the expression is identical to the potential; we get:

$$\Delta F = +P_\phi(r)^2 \frac{v_M(t)v_m(t)}{P_\phi(R_U)v_A(T)} > 0.$$

To simplify this expression we replace each momentum by its value (6.5) and use the linearity of $m(t) = m(T) \times t/T$:

$$\Delta F = + \frac{v_M(T) \times h v_m(T)}{v_A(T)R_U} \rightarrow -H c m(T) < 0. \quad (6.10.4)$$

This expression depends only on T and we sum (for instance) M to get the effect on m of all masses of the cosmos; the sum is valid since the expression is independent of r . The sign of the force is negative since the masses in the sum are geometrically external to the system (except for the system itself which is negligible).

6.4 The Plank scale potential

At the Plank scale, (6.5) yields:

$$E_\phi(l_P) = \frac{h c}{l_P} = M_P c^2. \quad (6.11)$$

This is the expected result in particles physics. But here the field is dependent on its source and this energy level does not pervade all space, the potential is c^2 and just multiplied by mass. Then, and more subtly, from (6.9), the main terms of the field potential cancel exactly at the Plank scale.

This section show the coherence of the classical field discussed in section 5 with the quantum world because the only equation introduced here is $Et = h$ or equivalently $P = h/r$.

7 Oscillations, expansion, black holes

A membrane of this kind has large thickness and the emission of the next membranes can be imprinted in the observable cosmos geometry; this imprint must be damped in proportions of the number of membranes existing between the emitter and ours. The oscillation recently observed by Ringermacher and Mead [3] corresponds to 7 minima and 6.5 ± 0.5 phases. The amplitude of the oscillations increases with distance. We interpret the minima as successive membrane emissions, and ≈ 6.5 visible oscillation phases for 7 membranes correspond to $\approx 50\%$ of our membrane emission logically invisible, as a descending phase preceding its emission.

Now we want to understand the observation of 1A supernova since it leads to accelerated expansion and dark energy.

The Chandrasekhar limit gives the mass of the type 1A supernova on which luminosity depends:

$$M_{limit} = \frac{k M_P^3}{(\mu_e m_h)^2},$$

where k is a constant factor, M_P the Plank mass, μ_e the average molecular weight per electron, and m_h the mass of a hydrogen atom. Hence, with variable masses, M_{limit} evolves like $1/T^2$, which is in contradiction with observation (constant chemistry and atomic physics). Therefore, as it should in a gravitation theory, the field defines the context in which the rest of physics lives. It means that the same field is also at the origin of all charges interaction; not only of mass but of all forms of energy.

Consider then M_{limit} constant; the expression is epoch-independent and then also the emission luminosity. Now assume all measured red-shift are given by linear expansion (neglecting oscillations). Then photons will disperse more than with a decelerating expansion. A linear expansion is almost in perfect agreement with observation as shown by Perlmutter & al [5] and more recent works.

The Λ CDM model also uses baryonic acoustic oscillations to evaluate the size of the large structures of the cosmos; it requires dark matter and our equivalent is the acceleration Hc which becomes infinite when $T \rightarrow 0$. Then, large anisotropies of matter density should already be present at a very early epoch and primordial black-holes are also possible.

At the Schwarzschild radius the field potential reads:

$$\frac{\Gamma}{c^2} = 1 - 1 + \frac{R_S}{R_U}. \quad (7.1)$$

The field is then compatible with the existence of black holes, which is obvious, but also with their stability since R_S/R_U is epoch-independent. Since the exchanges are time-symmetric it creates neither black holes inflation (a known problem of pushing gravity) nor deflation.

8 Conclusion

We showed that the theory holds with no dark matter. It comes as a pressure field given by the very first quantum equation $P = h/r$; the gravitational field agrees with GRT results on a short scale and cosmology is straightforward. The field is coherent with Mach's principle; the emitter creates dissymmetry and the differential between the advanced and retarded field components create energy, gravitation, and the acceleration Hc .

Interestingly, this field necessarily defines the context in which the rest of physics lives; hence it is also the origin of particles interaction and therefore it interacts with charges. Firstly the potential c^2 comes as a pressure field and can be interpreted as the Poincaré stress [6] and secondly it implies bottom-up unification.

9 Addendum

Still considering G constant, and since $H = 1/T$ and $m(T) = kT$, the force in (6.10.4) is time-invariant. In this equation, summing $m(T)$ to the absorber mass M_A gives:

$$\Delta F_{MA} = H c M_A(T) = \frac{c^4}{2G} = \frac{M_p c^2}{2l_p}, \quad (9.1)$$

which is half the Plank force; it also reads:

$$2 \Delta F_{MA} l_p = M_p c^2. \quad (9.2)$$

This is the work of a force $2\Delta F_{MA}$ over the Plank length. We also have $M_p c^2 = h c/l_p$, and then:

$$2 \Delta F_{MA} l_p^2 = h c, \quad (9.3)$$

which is the natural constant of the Yukawa interaction of the SM Higgs field. It also gives:

$$2 \Delta F_{MA} l_p t_p = h. \quad (9.4)$$

This is the action of a force $2\Delta F_{MA}$ over the Plank length in the Plank time. Those equations read as if in a cosmos which radius is expanding at light speed (of length l_p in time t_p), a scalar field of constant hc is creating an additional dark energy $M_p c^2/2$ with an action h ; then the total energy created by ΔF_{MA} since the big bang is:

$$M = \frac{M_p R_u}{2l_p} \rightarrow M = M_A, \quad (9.5)$$

which, of course, is identical to (4.2). Finally, we have just separated the forces of energy creation from the usual gravitation and then energy conservation.

This reasoning is circular as we introduce M_A at the beginning of the calculus; but there is no naturalness problem in the cosmology outlined here with respect to the constants of quantum physics (the cosmological constant and the so called “why now” problems are nonexistent). The novelty is the immediate significance of the Plank units and the permanence of energy creation; its power is constant and can easily be computed, it is half the Plank power which is then a constant of nature, and corresponds roughly to 2.4 W/Kg of dark or visible energy at the present epoch.

Submitted on October 30, 2015 / Accepted on November 1, 2015
Corrected on December 22, 2015

References

1. Wheeler J.A., Feynman R.P. Interaction with the Absorber as the Mechanism of Radiation. *Reviews of Modern Physics*, 1945, v. 17(2–3), 157–161.
2. Wheeler J.A., Feynman R.P. Classical Electrodynamics in Terms of Direct Interparticle Action. *Reviews of Modern Physics*, 1949, v. 21(3), 425–433.
3. Ringermacher H.I. and Mead L.R. Observation of discrete oscillations in a model-independent plot of the cosmological scale factor versus loopback time and scalar field. *Astronomical Journal*, 2015, v. 149, no. 4.
4. The Plank Collaboration. Planck 2015 results. I. Overview of products and scientific results. arXiv: 1502.01582
5. Perlmutter S. et al. Measurements of Omega and Lambda from 42 high redshift supernovae. *Astrophysical Journal*, 1999, v. 517(2), 565–86; arXiv: astro-ph/9812133.
6. Poincaré H. Sur la dynamique de l'électron. *Rendiconti del Circolo Matematico di Palermo*, 1903, v. 21, 129-176.

Power-Law Scaling of the Impact Crater Size-Frequency Distribution on Pluto: A Preliminary Analysis Based on First Images from New Horizons' Flyby

Felix Scholkmann

Research Office of Complex Physical and Biological Systems (ROCoS), Bellarairain 10, 8038 Zürich, Switzerland
E-mail: felix.scholkmann@gmail.com

The recent (14th July 2015) flyby of NASA's New Horizons spacecraft of the dwarf planet Pluto resulted in the first high-resolution images of the geological surface-features of Pluto. Since previous studies showed that the impact crater size-frequency distribution (SFD) of different celestial objects of our solar system follows power-laws, the aim of the present analysis was to determine, for the first time, the power-law scaling behavior for Pluto's crater SFD based on the first images available in mid-September 2015. The analysis was based on a high-resolution image covering parts of Pluto's regions *Sputnik Planum*, *Al-Idrisi Montes* and *Voyager Terra*. 83 impact craters could be identified in these regions and their diameter (D) was determined. The analysis revealed that the crater diameter SFD shows a statistically significant power-law scaling ($\alpha = 2.4926 \pm 0.3309$) in the interval of D values ranging from 3.75 ± 1.14 km to the largest determined D value in this data set of 37.77 km. The value obtained for the scaling coefficient α is similar to the coefficient determined for the power-law scaling of the crater SFDs from the other celestial objects in our solar system. Further analysis of Pluto's crater SFD is warranted as soon as new images are received from the spacecraft.

1 Introduction

The first close-up images of Pluto from NASA's New Horizons spacecraft, received in mid-September 2015, show a complex surface structure of Pluto never seen before in this detail. During the spacecraft's flyby of Pluto on 14th July 2015, images were taken by New Horizons' Long Range Reconnaissance Imager (LORRI) with a cooled 1024×1024 pixel CCD camera from a distance of approx. 12,500 km making it possible to obtain high-resolution images of Pluto's surface. Due to the slow transmission (about 1–2 Kbps), it will take around 16 months for all flyby images of Pluto to be received in full [1].

Many phenomena in astrophysics follow a power-law, i.e. the relationship between features exhibits a scale-invariance. Examples are the characteristics of the channel network on Mars [2], the relationship between solar flare occurrence and total flare energy [3], the correlation between a supermassive black hole mass and the host-galaxy bulge velocity dispersion ("M-sigma relation") [4], the distribution of initial masses for a population of stars ("initial mass function") [5], Kepler's third law, or the distribution of galaxies in the universe [6–8].

Size-frequency distributions (SFD) of natural objects also follow in general a power-law. Examples are the SFD of fragment sizes due to a fragmentation process [9], the SFD of landslides [10], the particle SFD of volcanic ash [11], the mass distribution objects of the Kuiper belt [12] — or the SFD of impact crater diameters on celestial objects.

Already in 1940 Young showed that the impact crater SFD on the Earth's Moon can be described by two power-laws with different scaling exponents. Further studies extended the analysis to other celestial objects, e.g. Earth [13], Mars

[14–16] and Mercury [17].

Due to the lack of high-resolution images available, it has not been possible until now to analyze the impact crater SFD of Pluto. With the first images now available from NASA's New Horizons mission, the aim of the present paper was to conduct such a first, preliminary, analysis.

2 Materials and methods

2.1 Data

For the present analysis the raw images* obtained by the New Horizons' LORRI as of 14th September 2015 were visually inspected in order to find an image showing impact craters of Pluto with the highest resolution possible. An additional selection criterion was that the image had to be taken by LORRI at an angle capturing the region of interest maximally parallel to the camera, minimizing geometrical distortions of the features in the image.

The image lor_0299174809_0x630_sci_4 (in the following denoted as LOR-0299174809) was selected as fulfilling these criteria (see Figure 1(b)). LOR-0299174809 displays a particular area covering parts of Pluto's regions *Sputnik Planum*, *Al-Idrisi Montes* and *Voyager Terra*. The image was taken by LORRI on 14th July 2015, 10:14:50 UTC, with an exposure time of 150 ms.

2.2 Determination of crater diameter values

The image LOR-0299174809 was analyzed in Adobe Illustrator (version CS5; Adobe Systems, CA, USA) by first visually

*LORRI Images from the Pluto Encounter, <http://pluto.jhuapl.edu/soc/Pluto-Encounter>

identifying the craters on the image and measuring their diameters (D). The obtained values were then rescaled to give the final values in the unit km. To do so, the information given on NASA's website* was used. Information on the website indicated that image number three (from top), which covers the region displayed in LOR-0299174809, is 470 km in width.

2.3 Statistical analysis

For the statistical analysis we used the mathematical framework provided by the Santa Fe Institute [18, 19]. The data were analyzed in Matlab (version 2010a; Mathworks Inc., Natick, MA, USA).

2.3.1 Estimation of the lower-bound and exponent of the power-law model

A quantity x shows power-law scaling if it stems from a probability distribution $p(x) \sim x^{-\alpha}$, with the exponent α defining the characteristics of the scaling. To test if an empirically obtained probability distribution follows a power-law, classically a histogram is calculated and the distribution is analyzed on a doubly logarithmic plot. Since $p(x) \sim \alpha \ln(x) + \text{const.}$, a power-law distributed quantity x follows a straight line in the plot. Besides the fact that this method was (and is still) used to investigate power-law scaling of different quantities this approach can generate significant systematic errors [18]. Therefore, for the present analysis we used a framework presented by Clauset et al. [18] that circumvents these errors and also offers the possibility of estimating the lower bound of the power-law (x_{\min}). The determination of x_{\min} is crucial when analyzing empirical data for power-law scaling since often the power-law behavior applies only for the tail region of the distribution, i.e. for values greater than the threshold value x_{\min} .

For the obtained crater diameter (D) data ($= x$) the power-law threshold value D_{\min} ($= x_{\min}$) was determined based on the method described by Clauset et al. [18] which uses the Kolmogorow-Smirnov (KS) statistics. The scaling exponent α was then calculated with a maximum likelihood fitting method also described by Clauset et al. [18].

2.3.2 Determination of the statistical significance of the power-law fit

In order to determine if the fitted power-law can be considered statistically significant, a goodness-of-fit test described by Clauset et al. [18] was employed. To this end, power-law distributed synthetic data was generated with values of α and x_{\min} that are equal to the values obtained by fitting the empirical data to the power-law model. Each synthetic data set is then fitted to the model and the KS statistics determined. Based on the occurrences of times the KS statistic is larger

than for the empirical values, a p -value is calculated. For $p < 0.1$ the fit of the power-law model to the empirical data is considered to be statistically not significant, i.e. it can be ruled out that the empirical distribution obeys a power-law scaling. Thus, the p -value in this case represents a measure of the hypothesis that is tested for validity. A high value of p corresponds to a good fit.

3 Results, discussion and conclusion

83 impact craters could be identified and their diameter values were determined, ranging from 0.84 km to 37.77 km. Using the obtained 83 D values and the methods described in Section 2.3.1, the scaling coefficient α was determined to be $\alpha = -2.4926 \pm 0.3309$ and the scaling threshold value to be $D_{\min} = 3.75 \pm 1.14$ km. Thus, for D in the range $[3.75 \pm 1.14 \text{ km}, 37.77 \text{ km}]$ the values follow a power-law. The log-likelihood (L) of the data $D \geq D_{\min}$ under the fitted power law was determined to be $L = 104.5688$.

The statistical test, as described in Section 2.3.2, employing 10,000 synthetic data sets revealed a p value of 0.2241. Thus, according to the test the hypothesis cannot be refuted that the data follows a power-law, i.e. Pluto's crater SFD shows a power-law scaling. Figure 1(c) visualizes the power-law behavior of the crater SFD.

How do the results of the presented analysis relate to the findings about characteristics of the crater SFD of other celestial objects? As mentioned in the introduction, it well established that the crater SFD of all investigated celestial bodies in our solar system exhibit a power-law scaling.

For example, according to an analysis performed by Robertson and Grieve from 1975 the crater SFD of the Earth is characterized by $\alpha \approx -2$ (for $D \geq 8$ km) [13]. An own analysis using the updated data of impact craters on Earth ($n = 188$) based on the Earth Impact Database[†] revealed $\alpha = 2.0286$ (for $D \geq 7$ km). The Earth Moon's crater SFD has been intensively investigated since the 1940's when Young [20] initially showed that for large D the crater SFD follows a power-law with $\alpha = -3$, and for small D the scaling is described by $\alpha = -1.5$. Subsequent studies described the scaling with laws governed by $\alpha = 2$ (for $D = [\sim 2 \text{ km}, 70 \text{ km}]$) [21], as well as $\alpha = -2$ (for $D < 100$ m) and $\alpha = -2.93$ (for $D > \text{a few } 100 \text{ m}$) [22], for example. Further studies showed that the scaling-relations of the lunar crater SFD need to include the observation that multiple power-laws are necessary to describe the whole SFD spectrum, i.e. α depends on D [23, 24]. A solution for optimally fitting the crater SFD was described based on the idea of using a polynomial function to fit the SFD data in the log-log space, i.e. it could be shown that a polynomial function of 7th degree fit the data well for $D = [300 \text{ m}, 20 \text{ km}]$. The polynomial function included an extra term accounting for the fact that the scaling function also depends on the geological charac-

*<http://tinyurl.com/n9k5mmc>

[†]<http://www.passc.net/EarthImpactDatabase>

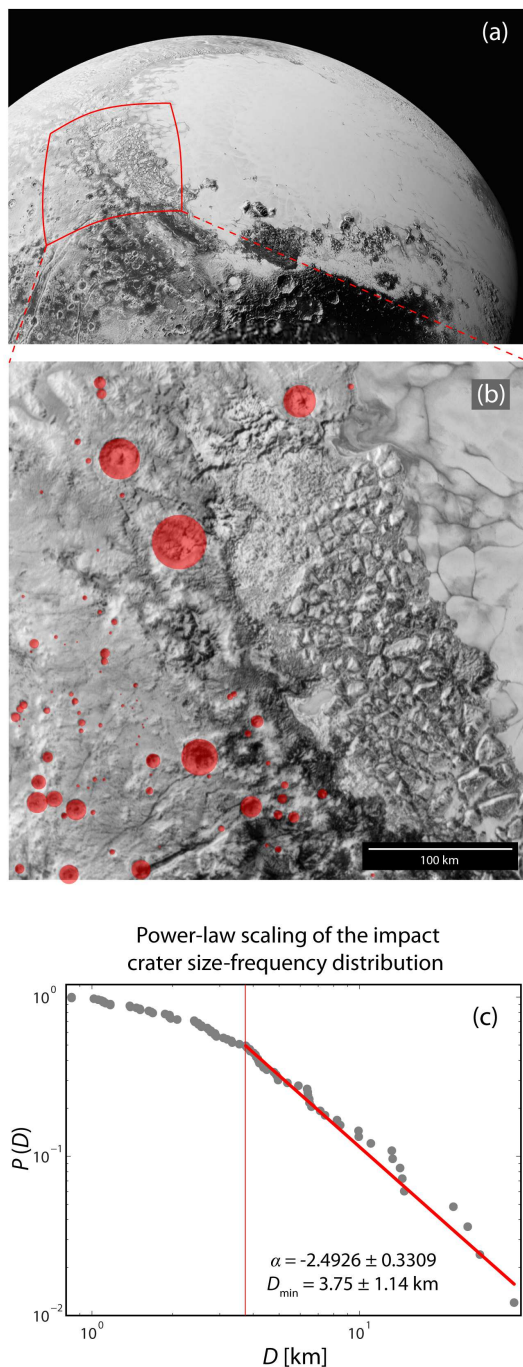


Fig. 1: (a) View of Pluto taken in July 2015 by LORRI on board NASA's New Horizons spacecraft. In the field of view the western lobe of the Tombaugh region is depicted. (b) LORI image lor0299174809_0x630_sci_4 showing a particular area covering parts of Pluto's regions *Sputnik Planum*, *Al-Idrisi Montes* and *Voyager Terra*. (c) Visualization of the power-law scaling of the impact crater size distribution. $P(D)$: complementary cumulative distribution function; D : crater diameter. Images (a) and (b) were obtained from NASA, Johns Hopkins University Applied Physics Laboratory, Southwest Research Institute.

teristics of the region investigated — a finding also made by other studies (e.g., [24–26]). For an extended range of D , in later work a 11th degree polynomial function was published by Neukum [27] valid for $D = [10 \text{ m}, 300 \text{ km}]$ and covering scaling exponents in the range of $\alpha = [-1, 4]$. For the Martian satellites Phobos and Deimos, the crater SFD was determined as being described by a power-law with $\alpha \approx 1.9$ for $D = [44 \text{ m}, 10 \text{ km}]$ [16].

Thus, the finding of the present analysis concerning the power-law characteristics (i.e., $\alpha = 2.4926 \pm 0.3309$ for $D = [3.75 \pm 1.14 \text{ km}, 37.77 \text{ km}]$) of the crater SFD of Pluto is comparable to the power-laws observed for the other celestial bodies. That Pluto's diameter scaling for $D < 3.75 \pm 1.14 \text{ km}$ does not follow the $\alpha = -2.4926$ scaling relies most probably on the fact that small craters are much faster deteriorated due to erosion and that counting of craters with small D was not perfectly possible due to the limited resolution of the available image. The lowest D value ($3.75 \pm 1.14 \text{ km}$) for which the power law holds might interpreted as related to a transition from simple to complex craters. Interestingly, such a “transition diameter” was predicted for Pluto to be in the range of 4–5 km [28–30].

This analysis, of course, should be regarded only as a preliminary study for further follow-up as soon as the full set of images from Pluto is available and the images have been processed to deliver a high-resolution picture of Pluto's surface morphology. A limitation of the present analysis is that only one high-resolution image with sufficient craters was available. It was therefore only possible to obtain a relatively low number of crater diameter values ($n = 83$).

Knowledge of Pluto's crater SPF will not only give insights in the universality of the crater SFD scaling relations but necessarily will also help in the understanding of the history of Pluto and the characteristics of the Kuiper belt which Pluto is part of.

Acknowledgements

I thank Rachel Scholkmann for proofreading the manuscript, and the New Horizons project team at the Johns Hopkins University Applied Physics Laboratory for discussion concerning the copyright status of the publicly released LORRI images.

Submitted on October 15, 2015 / Accepted on November 6, 2015

References

1. Rieni G. How exactly does New Horizons send all that data back from Pluto? Available from: <http://hub.jhu.edu/2015/07/17/new-horizons-data-transmission>
2. Caldarelli G., De Los Rios P., Montuori M., Servedio V.D.P. Statistical features of drainage basins in mars channel networks. *The European Physical Journal B*, 2004, v. 38 (2), 387–391.
3. Hudson H.S. Solar flares, microflares, nanoflares, and coronal heating. *Solar Physics*, 1991, v. 133 (2), 357–369.
4. Ferrarese L., Merritt D. A fundamental relation between supermassive black holes and their host galaxies. *The Astrophysical Journal*, 2000, v. 539 (1), L9–L12.

5. Kroupa P., Weidner C., Pflamm-Altenburg J., Thies I., Dabringhausen J., Marks M., Maschberger T. The stellar and sub-stellar initial mass function of simple and composite populations. In *Planets, Stars and Stellar Systems*, Oswalt T.D., Gilmore G. (Editors), 2013, Springer Netherlands, 115–242.
6. Watson D.F., Berlind A.A., Zentner A.R. A cosmic coincidence: The power-law galaxy correlation function. *The Astrophysical Journal*, 2011, v. 738 (1), 1–17.
7. Baryshev Y.V., Labini F.S., Montuori L., Pietronero L., Teerikorpi P. On the fractal structure of galaxy distribution and its implications for cosmology. *Fractals*, 1998 v. 6 (3), 231–243.
8. Joyce M., Sylos Labini F., Gabrielli A., Montuori M., Pietronero L. Basic properties of galaxy clustering in the light of recent results from the Sloan Digital Sky Survey. *Astronomy & Astrophysics*, 2005, v. 443 (1), 11–16.
9. Turcotte D.L. Fractals and fragmentation. *Journal of Geophysical Research*, 1986, v. 91 (B2), 1921–1926.
10. Stark C.P., Hovius N. The characterization of landslide size distributions. *Geophysical Research Letters*, 2001, v. 28 (6), 1091–1094.
11. Wohletz K.H., Sheridan F., Brown W.K. Particle size distributions and the sequential fragmentation/transport theory applied to volcanic ash. *Journal of Geophysical Research*, 1989, v. 94 (B11), 15703–15721.
12. Bernstein G.M., Trilling D. E., Allen R. L., Brown K. E., Holman M., Malhotra R. The size distribution of transneptunian bodies. *The Astrophysical Journal*, 2004, v. 128 (3), 1364–1390.
13. Robertson P.B., Grieve R.A.F. Impact structures in Canada — Their recognition and characteristics. *The Journal of the Royal Astronomical Society of Canada*, 1975, v. 69, 1–21.
14. Bruckman W., Ruiez A., Ramos E. Earth and Mars crater size frequency distribution and impact rates: Theoretical and observational analysis. *arXiv:1212.3273*, 2013.
15. Barlow N.G. Crater size-frequency distributions and a revised martian relative chronology. *Icarus*, 1988, 75, 285–305.
16. Thomas, P. Veverka, J. Crater densities on the satellites of Mars. *Icarus*, 1980, v. 41, 365–380.
17. Strom R.G., Chapman C.R., Merline W.J., Solomon S.C., Head J.W. Mercury cratering record viewed from Messenger's first flyby. *Science*, 2008, v. 321 (5885), 79–81.
18. Clauset A., Shalizi C.R., Newman M.E.J. Power-law distributions in empirical data. *SIAM Review*, 2009, v. 51 (4), 661–703.
19. Virkar Y., Clauset A. Power-law distributions in binned empirical data. *Annals of Applied Statistics*, 2014, v. 8 (1), 89–119.
20. Young, J., A Statistical Investigation of Diameter and Distribution of Lunar Craters. *Journal of the British Astronomical Association*, 1940, v. 50, 309–326.
21. Cross C.A. The size distribution of lunar craters. *Monthly Notices of the Royal Astronomical Society*, 1966, v. 134, 245–252.
22. Shoemaker E.M., Hait M.H., Swann G.A., Schleicher D.L., Dahlem D.H., Schaber G.G., Sutton R.L. Lunar regolith at tranquillity base. *Science*, 1970, v. 167 (3918), 452–455.
23. Chapman C.R., Haefner, R.R. A critique of methods for analysis of the diameter-frequency relation for craters with special application to the Moon. *Journal of Geophysical Research*, 1967, v. 72 (2), 549–557.
24. Neukum G., König B., Arkani-Hamed J. A study of lunar impact crater size-distributions. *The Moon*, 1975, v. 12 (2), 201–229.
25. Baldwin R.B. On the history of lunar impact cratering: The absolute time scale and the origin of planetesimals. *Icarus*, 1971, v. 14, 36–52.
26. Head J.W., Fassett C.I., Kadish S.J., Smith D.E., Zuber M.T., Neumann G.A., Mazarico E. Global distribution of large lunar craters: implications for resurfacing and impactor populations. *Science*, 2010, v. 329 (5998), 1504–1507.
27. Neukum, G. Meteoritenbombardement und Datierung planetarer Oberflächen. *Habilitationsschrift*. 1983, München, Germany: Universität München.
28. Moore J.M., Howad A.D., Schenk P.M., McKinnon W.B., Pappalardo R., Ryan E., Bierhaus E.B., et al. Geology before Pluto: Pre-encounter considerations. *Icarus*, 2014, v. 246, 65–81.
29. Bray V.S., Schenk P.M. Pristine impact crater morphology on Pluto — Expectations for New Horizons. *Icarus*, 2015, v. 246, 156–164.
30. Zahnle K., Schenk P., Levison H., Donnes L. Cratering rates in the outer Solar System. *Icarus*, 2003, v. 163, 263–289.

Standard Model Particles from Split Octonions

Merab Gogberashvili

Javakishvili Tbilisi State University, 3 Chavchavadze Avenue, Tbilisi 0179, Georgia
 Andronikashvili Institute of Physics, 6 Tamarashvili Street, Tbilisi 0177, Georgia
 E-mail: gogber@gmail.com

We model physical signals using elements of the algebra of split octonions over the field of real numbers. Elementary particles are corresponded to the special elements of the algebra that nullify octonionic norms (zero divisors). It is shown that the standard model particle spectrum naturally follows from the classification of the independent primitive zero divisors of split octonions.

The algebra of octonions [1–3] is interesting mathematical structure for physical applications (see reviews [4–7]). In this paper we suggest that split octonions over the reals form proper mathematical framework to describe elementary particles and show that some physical properties, like the variety of their spices, naturally follows from the structure of the algebra.

In [8–10] different aspects of geometrical applications of split octonions over the reals were considered. It is suggested to use split octonions as universal mathematical structure in physics, instead of vectors, tensors, spinors, etc. In this approach world-lines (paths) of particles are parameterized by the elements of split octonions,

$$s = \omega + \lambda^n J_n + x^n j_n + ctI . \quad (n = 1, 2, 3) \quad (1)$$

Here a pair of repeated upper and lower indices implies a summation, i.e. $x^n j_n = \delta_{nm} x^n j^m$, where δ^{mm} is Kronecker's delta.

Four of the eight real parameters in (1), t and x^n , denote the ordinary space-time coordinates, and ω and λ^n are interpreted as the phase (classical action) and the wavelengths associated with the octonionic signals.

The eight octonionic basis units in (1) are represented by one scalar (denoted by 1), the three vector-like objects J_n , the three pseudo vector-like elements j_n and one pseudo scalar-like unit I . The squares (inner products) of seven of the hypercomplex basis elements of split octonions give the unit element with the different signs,

$$J_n^2 = 1 , \quad j_n^2 = -1 , \quad I^2 = 1 . \quad (2)$$

It is known that to generate a complete basis of split octonions the multiplication and distribution laws of only three vector-like elements J_n are enough [1–3]. The three pseudo vector-like basis units, j_n , in (1) can be defined as the binary products,

$$j_n = \frac{1}{2} \varepsilon_{nmk} J^m J^k , \quad (n, m, k = 1, 2, 3) \quad (3)$$

where ε_{nmk} is the totally antisymmetric unit tensor, and thus describe orthogonal planes spanned by vector-like elements

J_n . The seventh basis unit I (the oriented volume) is defined as the triple product of all three vector-like elements and has three equivalent representation in terms of J^n and j^n ,

$$I = J_1 j_1 = J_2 j_2 = J_3 j_3 . \quad (4)$$

So the complete algebra of all non-commuting hypercomplex basis units has the form:

$$\left. \begin{aligned} J_n J_m &= -J_m J_n = \varepsilon_{nmk} j^k \\ j_n j_m &= -j_m j_n = \varepsilon_{nmk} J^k \\ J_m J_n &= -J_n J_m = \varepsilon_{nmk} J^k \\ J_n I &= -I J_n = j_n \\ j_n I &= -I j_n = J_n \end{aligned} \right\} . \quad (5)$$

The conjugation of vector-like octonionic basis units,

$$J_n^\dagger = -J_n , \quad (6)$$

can be understand as reflections. Conjugation reverses the order of J_n in products, i.e.

$$\left. \begin{aligned} j_n^\dagger &= \frac{1}{2} (\varepsilon_{nmk} J^m J^k)^\dagger = \frac{1}{2} \varepsilon_{nmk} J^{k\dagger} J^{m\dagger} = -j_n \\ I^\dagger &= (J_1 J_2 J_3)^\dagger = J_3^\dagger J_2^\dagger J_1^\dagger = -I \end{aligned} \right\} . \quad (7)$$

So the conjugation of the pass function (1) gives

$$s^\dagger = \omega - \lambda_n J^n - x_n j^n - ctI . \quad (8)$$

Using (2), (5) and (8) one can find the norm (interval) of the pass function (1),

$$N^2 = s s^\dagger = s^\dagger s = \omega^2 - \lambda^2 + x^2 - c^2 t^2 , \quad (9)$$

which is assumed to be non-negative. A second condition is that for physical events the vector part of (1) should be time-like [10],

$$c^2 t^2 + \lambda_n \lambda^n > x_n x^n . \quad (10)$$

One can represent rotations in the space of the split octonions (1) by the maps,

$$s' = e^{\theta/2} s e^{-\theta/2} , \quad (11)$$

where θ is some real angle and ϵ denotes the (3+4)-vector defined by the seven basis units J_n, j_n and I [1–3, 10]. The set of transformations (11), which satisfy the conditions (9) and (10), form the group $SO(3, 4)$ of passive transformations of the coordinates x^n, λ^n and t [11]. However, to represent the active rotations in the space of s , which preserves the multiplicative structure (5) as well, we would need the transformations to be automorphisms. It means not all tensorial transformations of the coordinates λ_n, x_n and t , represent real rotations, only the transformations that have a realization as associative multiplications should be considered. Automorphisms of split-octonions form subgroup of $SO(3, 4)$, the noncompact form of Cartan’s smallest exceptional Lie group G_2^{NC} [12, 13].

Infinitesimal transformations of coordinates, which correspond to the action of the main geometrical group of the model, G_2^{NC} , can be written as [10]:

$$\left. \begin{aligned} x'_n &= x_n - \epsilon_{nmk} \alpha^m x^k - \theta_n ct + \\ &+ \frac{1}{2} (\epsilon_{nmk} \phi^m + \epsilon_{nmk} \theta^m) \lambda^k + \left(\varphi_n - \frac{1}{3} \sum_m \varphi_m \right) \lambda_n \\ ct' &= ct - \beta_n \lambda^n - \theta_n x^n \\ \lambda'_n &= \lambda_n - \epsilon_{nmk} (\alpha^m - \beta^m) \lambda^k + \beta_n ct + \\ &+ \frac{1}{2} (\epsilon_{nmk} \phi^m - \epsilon_{nmk} \theta^m) x^k + \left(\varphi_n - \frac{1}{3} \sum_m \varphi_m \right) x_n \end{aligned} \right\}, \quad (12)$$

with no summing over n in the last terms of x'_n and λ'_n . From the 15 parameters (five 3-angles: $\alpha^m, \beta^m, \phi^m, \theta^m$ and φ^m) in (12), due to the condition

$$\sum_n \left(\varphi_n - \frac{1}{3} \sum_m \varphi_m \right) = 0, \quad (13)$$

only 14 are independent.

The transformations (12) can be divided into several distinct classes [10]. For instance, the G_2^{NC} -rotations by the angles α^n, β^n and θ^n of the space-time coordinates only, imitate the ordinary infinitesimal Poincaré transformations of (3+1)-Minkowski space,

$$\left. \begin{aligned} ct' &= ct - \theta_n x^n + a_0 \\ x'_n &= x_n - \epsilon_{nmk} \alpha^m x^k - \theta_n ct + a_n \end{aligned} \right\}, \quad (14)$$

where the space-time translations are defined as:

$$\left. \begin{aligned} a_0 &= -\beta_n \lambda^n \\ a_n &= \frac{1}{2} \epsilon_{nmk} \theta^m \lambda^k \end{aligned} \right\}. \quad (15)$$

Time translations a_0 are smooth, since β_n are compact angles, but θ^n are hyperbolic and for the spatial translations a_n we have the Rindler-like horizons.

Note that Poincaré-like transformations (14) do not form subgroup of G_2^{NC} (the subgroup structure of G_2^{NC} one can be find, for example, in [13]), since we had neglected rotations of the extra time-like parameters λ_n . Complete G_2^{NC} -transformations reveal some new features in compare to the Minkowski case, like parity violations [10].

Another class of automorphisms,

$$\left. \begin{aligned} x'_n &= x_n + \left(\varphi_n - \frac{1}{3} \sum_m \varphi_m \right) \lambda_n \\ t' &= t \\ \lambda'_n &= \lambda_n + \left(\varphi_n - \frac{1}{3} \sum_m \varphi_m \right) x_n \end{aligned} \right\}, \quad (16)$$

represent rotations through hyperbolic angles, φ_1, φ_2 and φ_3 (of the three, due to (13), only two are independent) of the pairs of space-like and time-like coordinates x_n and λ_n , into the orthogonal planes $(x_1 - \lambda_1), (x_2 - \lambda_2)$ and $(x_3 - \lambda_3)$. It is convenient to define 2-parameter Abelian subalgebra of G_2^{NC} by the generators of two independent rotations in these planes. It is known that the rank of G_2^{NC} is two, as of the group $SU(3)$ [13, 14]. In terms of the two parameters, K_1 and K_2 , which are related to the angles φ_n as

$$\left. \begin{aligned} K_1 &= \frac{1}{3} (2\varphi_1 - \varphi_2 - \varphi_3) \\ K_2 &= -\frac{1}{2\sqrt{3}} (2\varphi_3 - \varphi_1 - \varphi_2) \end{aligned} \right\}, \quad (17)$$

the transformations (16) can be written more concisely,

$$\begin{pmatrix} \lambda'_1 + Ix'_1 \\ \lambda'_2 + Ix'_2 \\ \lambda'_3 + Ix'_3 \end{pmatrix} = e^{(K_1 \Lambda_3 + K_2 \Lambda_8) I} \begin{pmatrix} \lambda_1 + Ix_1 \\ \lambda_2 + Ix_2 \\ \lambda_3 + Ix_3 \end{pmatrix}, \quad (18)$$

where I is the vector-like octonionic basis unit ($I^2 = 1$) and Λ_3 and Λ_8 are the standard 3×3 Gell-Mann matrices [10]. Then one can classify irreducible representations of G_2^{NC} by two fundamental simple roots of the algebra (K_1 and K_2) and using analogies with $SU(3)$ interpret them as corresponding to the spin and hypercharge of particles. It is known that all quarks, antiquarks, and mesons can be imbedded in the adjoint representation of G_2^{NC} [14].

In the approach [8–10] the norm (9) can be viewed as some kind of space-time interval with four time-like dimensions. The ordinary time parameter, t , corresponds to the distinguished octonionic basis unit, I , while the other three time-like parameters, λ_n , have a natural interpretation as wavelengths, i.e. do not relate to time as conventionally understood. Within this picture, in front of time-like coordinates in the expression of pseudo-Euclidean octonionic intervals there naturally appear two fundamental physical parameters, the light speed and Planck’s constant. Then from the requirement of positive definiteness of norms under G_2^{NC} -transformations,

together with the introduction of the maximal velocity, there follow conditions which are equivalent to uncertainty relations [9, 10]. Also it is known that a unique physical system in multi-time formalism generates a large variety of “shadows” (different dynamical systems) in (3+1)-subspace [15–19]. One can speculate that information of multi-dimensional structures, which is retained by these images of the initial system, might take the form of hidden symmetries in the octonionic particle Lagrangians [10].

Split algebras contain special elements with zero norms (zero divisors) [1], which are important structures in physical applications [20]. For the coordinate function (1) we can define the differential zero divisor,

$$\frac{d}{ds} = \frac{1}{2} \left[\frac{d}{d\omega} - J_n \frac{d}{d\lambda_n} - j_n \frac{d}{dx_n} - I \frac{d}{cdt} \right], \quad (19)$$

such that its action upon s is:

$$\frac{ds}{ds} = 1. \quad (20)$$

The operator (19) annihilates s^\dagger , while the conjugated derivative operator,

$$\frac{d}{ds^\dagger} = \frac{1}{2} \left[\frac{d}{d\omega} + J_n \frac{d}{d\lambda_n} + j_n \frac{d}{dx_n} + I \frac{d}{cdt} \right], \quad (21)$$

is zero divisor for s , i.e.

$$\frac{ds^\dagger}{ds} = \frac{ds}{ds^\dagger} = 0. \quad (22)$$

From these relations it is clear that the interval (9) is a constant function for the restricted left octonionic gradient operators,

$$\left. \begin{aligned} \frac{d}{ds_L} (s^\dagger s) &= \left(\frac{ds^\dagger}{ds} \right) s = 0 \\ \frac{d}{ds_L^\dagger} (s s^\dagger) &= \left(\frac{ds}{ds^\dagger} \right) s^\dagger = 0 \end{aligned} \right\}, \quad (23)$$

and the invariance of the intervals,

$$ds^2 = ds ds^\dagger = ds^\dagger ds, \quad (24)$$

in the space of split octonions can be viewed as an algebraic property.

The octonionic wavefunctions Ψ , in general, should depend on s and on s^\dagger as well. Thus we need the condition of analyticity of functions of split octonionic variables,

$$\frac{d\Psi(s, s^\dagger)}{ds^\dagger} = 0, \quad (25)$$

which is similar to the Cauchy-Riemann equations from complex analysis. It can be shown that the system of eight algebraic conditions (25), in certain cases [21], lead to the octonionic Maxwell and Dirac equations [8].

Now consider non-differential zero divisors. These type of quantities are distinct elements of the algebra and thus in physical applications could be corresponded to the unit signals (elementary particles). In the algebra of split octonions two types of primitive zero divisors, idempotent elements (projection operators) and nilpotent elements (Grassmann numbers), can be constructed [1, 10]. There exist four classes (totally eight) of primitive idempotents,

$$\left. \begin{aligned} D_n^\pm &= \frac{1}{2} (1 \pm J_n), \quad (n = 1, 2, 3) \\ d^\pm &= \frac{1}{2} (1 \pm I) \end{aligned} \right\}, \quad (26)$$

which obey the relations:

$$\left. \begin{aligned} D_n^\pm D_n^\pm &= D_n^\pm \\ d^\pm d^\pm &= d^\pm \end{aligned} \right\}. \quad (27)$$

The pairs (D_n^+, D_n^-) and (d^+, d^-) are zero divisors for each other,

$$\left. \begin{aligned} D_n^\pm D_n^\mp &= 0 \\ d^\pm d^\mp &= 0 \end{aligned} \right\}, \quad (28)$$

and thus commute,

$$[D_n^+, D_n^-] = [d^+, d^-] = 0. \quad (29)$$

We have also twelve classes (twenty four in total) of primitive nilpotents,

$$\left. \begin{aligned} G_{nm}^\pm &= \frac{1}{2} (J_n \pm j_m), \quad (n, m = 1, 2, 3) \\ g_n^\pm &= \frac{1}{2} (I \pm j_n) \end{aligned} \right\}, \quad (30)$$

which are zero divisors for themselves,

$$\left. \begin{aligned} G_{nm}^\pm G_{nm}^\pm &= 0 \\ g_n^\pm g_n^\pm &= 0 \end{aligned} \right\}. \quad (31)$$

We see that separately the quantities (30) can be considered as the Grassmann numbers, but do not commute with their conjugates,

$$\left. \begin{aligned} G_{nm}^\pm G_{nm}^\mp &= d^\mp \\ G_{nm}^\pm G_{nm}^\mp &= \epsilon_{nmk} D_k^\pm, \quad n \neq m \quad (n, m, k = 1, 2, 3) \\ g_n^\pm g_n^\mp &= D_n^\pm \end{aligned} \right\}, \quad (32)$$

in contrast to the case of projection operators (29). The quantities G_{nm}^\pm and g_n^\pm are the elements of so-called algebra of Fermi operators with the anti-commutators,

$$\left. \begin{aligned} G_{nm}^\pm G_{nm}^\mp + G_{nm}^\mp G_{nm}^\pm &= 1 \\ g_n^\pm g_n^\mp + g_n^\mp g_n^\pm &= 1 \end{aligned} \right\}, \quad (33)$$

which is some syntheses of the Grassmann and Clifford algebras.

We want to emphasize that the number of distinct primitive idempotents (four) and nilpotents (twelve), and there conjugates, coincides with the number of particle/antiparticle species (bosons and fermions, respectively) of the standard model. This justifies our assumption that primitive zero divisors, which describe unit signals in the space of split octonions, can be corresponded to the elementary particles. The properties that the product of two projection operators reduces to the same idempotent (27), while the product of two Grassmann numbers is zero (31), naturally explains the validity of the Bose and Fermi statistics for the corresponding particles. In this picture distinct statistics follows from the existence of the two types of “light-cones” in the octonionic (4+4)-space (9), what shows itself in the definitions of the primitive zero divisors (26) and (30). Also note that the number of the standard model particle generations and the amount of spatial dimensions, both follow from the structure of the algebra of split octonions and are connected with the existence of the three fundamental vector-like elements J_n .

To conclude, in this paper geometrical applications of real split octonions are considered and elementary particles are connected with zero divisors, the special elements of the algebra which nullify octonionic intervals. It is shown that the standard model particle spectrum naturally follows from the classification of the independent primitive zero divisors of the algebra.

Acknowledgments: This research was supported by the Shota Rustaveli National Science Foundation grant ST09_798.4 – 100.

Submitted on November 18, 2015 / Accepted on November 19, 2015

References

1. Schafer R. Introduction to Non-Associative Algebras. Dover, NY 1995.
2. Springer T.A and Veldkamp F.D. Octonions, Jordan Algebras and Exceptional Groups. Springer Monographs in Mathematics, Springer, Berlin 2000.
3. Baez J.C. *Bull. Am. Math. Soc.*, 2002, v.39, 145, arXiv: math/0105155 [math.RA].
4. Okubo S. Introduction to Octonion and Other Non-Associative Algebras in Physics. Cambridge Univ. Press, Cambridge, 1995.
5. Finkelstein D. Quantum Relativity: A Synthesis of the Ideas of Einstein and Heisenberg. Springer, Berlin 1996.
6. Gürsey F. & Tze C. On the Role of Division, Jordan and Related Algebras in Particle Physics. World Scientific, Singapore 1996.
7. Löhmus J., Paal P. & Sorgsepp L. Nonassociative Algebras in Physics, Hadronic Press, Palm Harbor 1994; *Acta Appl. Math.*, 1998, v.50, 3.
8. Gogberashvili M. *Int. J. Mod. Phys. A*, 2006, v.21, 3513, arXiv: hep-th/0505101; *J. Phys. A*, 2006, v.39, 7099, arXiv: hep-th/0512258.
9. Gogberashvili M. arXiv: hep-th/0212251; *Adv. Appl. Clif. Alg.*, 2005, v.15, 55, arXiv: hep-th/0409173; *Adv. Math. Phys.*, 2009, 483079, arXiv: 0808.2496 [math-ph].
10. Gogberashvili M. & Sakhelashvili O. *Adv. Math. Phys.*, 2015, 196708, arXiv: 1506.01012 [math-ph].
11. Manogue C.A. & Schray J. *J. Math. Phys.*, 1993, v.34, 3746.
12. Cartan É. Sur la structure des groupes de transformations finis et continus. Thèse, Paris 1894, p.146; *Ann. Sci. Ecole Norm. Sup.*, 1914, v.31, 263; Reprinted in: *Oeuvres complètes*, Gauthier-Villars, Paris 1952.
13. Beckers J., Hussin V. & Winternitz P. *J. Math. Phys.*, 1986, v.27, 2217.
14. Günaydin M. & Gürsey F. *J. Math. Phys.*, 1973, v.14, 1651; *Lett. Nuovo Cim.*, 1973, v.6, 401; *Phys. Rev. D*, 1974, v.9, 3387.
15. Cole E.A.B. *Nuov. Cim. A*, 1977, v.40, 171; *J. Phys. A*, 1980, v.13, 109.
16. Gogberashvili M. *Phys. Lett. B*, 2000, v.484, 124, arXiv: hep-ph/0001109.
17. Gogberashvili M. & Midodashvili P. *Phys. Lett. B*, 2001, v.515, 447, arXiv: hep-ph/0005298; *Europhys. Lett.*, 2003, v.61, 308, arXiv: hep-th/0111132.
18. Christian J. *Int. J. Mod. Phys. D*, 2004, v.13, 1037, arXiv: gr-qc/0308028; in *Relativity and the Dimensionality of the World*, ed. V. Petkov, Springer, NY 2007, arXiv: gr-qc/0610049.
19. Velev M.V. *Phys. Essays*, 2012, v.25, 3.
20. Sommerfeld A. *Atombau und Spektrallinien*, II Band. Vieweg, Braunschweig 1953.
21. Gogberashvili M. *Eur. Phys. J. C*, 2014, v.74, 3200, arXiv: 1410.4136 [physics.gen-ph].

The Impact Crater Size-Frequency Distribution on Pluto Follows a Truncated Pareto Distribution: Results from a First Data Set Based on the Recent New Horizons' Flyby

Lorenzo Zaninetti¹ and Felix Scholkmann²

¹ Dipartimento di Fisica, University of Turin, Via Pietro Giuria 1, 10125 Turin, Italy. E-mail: zaninetti@ph.unito.it

² Research Office of Complex Physical and Biological Systems (ROCoS), Bellariairain 10, 8038 Zürich, Switzerland
E-mail: felix.scholkmann@gmail.com

Recently it could be shown (Scholkmann, *Prog. in Phys.*, 2016, v. 12(1), 26-29) that the impact crater size-frequency distribution of Pluto (based on an analysis of first images obtained by the recent New Horizons' flyby) follows a power law ($\alpha = 2.4926 \pm 0.3309$) in the interval of diameter (D) values ranging from 3.75 ± 1.14 km to the largest determined value of 37.77 km. A reanalysis of this data set revealed that the whole crater SFD (i.e., with values in the interval of 1.2–37.7 km) can be described by a truncated Pareto distribution.

1 Introduction

The recent flyby of NASA's New Horizons spacecraft allowed high-resolution images of Pluto's surface morphology to be obtained, thus enabling a first determination of the impact crater size-frequency distribution (SFD) of a specific region, i.e., covering parts of Pluto's regions *Sputnik Planum*, *Al-Idrisi Montes* and *Voyager Terra* [1].

The first analysis of the crater SFD used a power law of the type $p(x) \sim x^{-\alpha}$ to model the data. In the present paper we show the results of an extended analysis. The inverse power law scaling is known as the Pareto distribution $p(x) \sim x^{-(c+1)}$. In the present paper we tested the hypothesis that an upper truncated Pareto distribution (i.e., a Pareto distribution in which the probability range is limited rather than infinite) can improve the modelling of the empirical crater SFD presented in [1].

We review the properties of the Pareto and the truncated Pareto distributions in Section 2, and report in Section 3 the results of applying the truncated Pareto distribution to the novel Pluto crater SFD data set.

2 From the Pareto to the truncated Pareto distribution

In the following we report the definitions of the probability density function (PDF), the distribution function (DF), the survival function (S) and the maximum likelihood estimator (MLE) for the two distributions analyzed here. The sample is made by crater diameter (D) values ($n = 83$) denoted by x_i .

2.1 The Pareto distribution

The Pareto PDF is given by

$$f(x; a, c) = ca^c x^{-(c+1)}, \quad (1)$$

with $c > 0$; the Pareto DF is defined as

$$F(x; a, c) = 1 - a^c x^{-c}, \quad (2)$$

and the survival function is given by

$$S(x; a, c) = 1 - F(x; a, c). \quad (3)$$

The parameter values can be estimated by applying the MLE:

$$a = \min(x_i), \quad (4a)$$

$$\frac{1}{c} = \left(\frac{1}{n}\right) \sum_{i=1}^n \ln\left(\frac{x_i}{\tilde{a}}\right). \quad (4b)$$

More details can be found in [2].

2.2 The truncated Pareto distribution

An upper truncated Pareto random variable is defined in the interval $[a, b]$, and the PDF is given by

$$f_T(x; a, b, c) = \frac{ca^c x^{-(c+1)}}{1 - \left(\frac{a}{b}\right)^c}; \quad (5)$$

and the truncated DF is defined as

$$F_T(x; a, b, c) = \frac{1 - \left(\frac{a}{x}\right)^c}{1 - \left(\frac{a}{b}\right)^c}. \quad (6)$$

The MLE determines the parameters according to

$$a = \min(x_i), \quad (7a)$$

$$b = \max(x_i), \quad (7b)$$

$$0 = \frac{n}{\tilde{c}} + \frac{n \left(\frac{a}{b}\right)^{\tilde{c}} \ln\left(\frac{a}{b}\right)}{1 - \left(\frac{a}{b}\right)^{\tilde{c}}} - \sum_{i=1}^n [\ln x_i - \ln a], \quad (7c)$$

where the value of \tilde{c} can be found using Brent's method to find a root of a nonlinear function, i.e., by applying the FORTRAN subroutine ZBRENT [3]. More details can be found in [4].

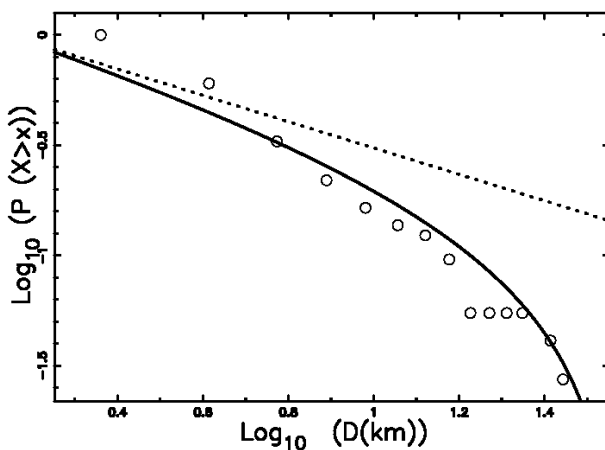


Fig. 1: Survival function (S) in a log-log plot for crater size in $D = [1.38 \text{ km}, 37.77 \text{ km}]$. Empty circles: empirical data, full line: S of the truncated Pareto PDF, dotted line: S of the Pareto PDF. The K-S test for the truncated Pareto gave $P_{KS} = 0.128$ and $d_{max} = 0.134$. The K-S test for the Pareto gave $P_{KS} = 0.0075$ and $d_{max} = 0.192$.

3 Data analysis and results

For statistical testing the Kolmogorov–Smirnov (K-S) test [5–7] was employed which does not require data binning. The K-S test, as implemented by the FORTRAN subroutine KSONE [3], finds the maximum distance (d_{max}) between the theoretical and the empirical DF as well the significance level P_{KS} (see equations 14.3.5 and 14.3.9 in [3]). A value of $P_{KS} \geq 0.1$ assures that the fit is acceptable.

When using the impact crater SFD data of Pluto with $D = [3.75 \text{ km}, 37.77 \text{ km}]$ the Pareto PDF gave $c = 1.5299$ and thus $\alpha = 2.5299$ (similar to the value $\alpha = 2.4926$ reported by [1]), and the K-S test gave $P_{KS} = 0.866$ and $d_{max} = 0.091$. Figure 1 shows the empirical and the two fitted distributions when the interval of crater size values is enlarged so that all D values are included in the fitting, i.e., $D = [1.2 \text{ km}, 37.77 \text{ km}]$. The truncated Pareto distribution describes the empirical crater SFD quite accurately over the whole interval of D values available.

4 Conclusions

The distribution of crater diameters of planets is commonly modeled by a power law. A small modification of the “simple” PDF by a truncated Pareto PDF (as given by equation (5)) allows the dichotomy of the infinite rather than finite range of existence to be avoided and provides better K-S test statistics with respect to the Pareto PDF (i.e., a “simple” power law), see captions of Figure 1.

In conclusion, we were able to show that the empirical impact crater SFD of Pluto (using a first data set based on recent New Horizons flyby) closely agrees with a truncated Pareto distribution. Applying the same modelling approach to an extended data set of Pluto’s crater values is warranted to

confirm our results – a task to be done as soon as new images of the New Horizon spacecraft are available.

Submitted on November 30, 2015 / Accepted on December 2, 2015

References

1. Scholkmann F. Power-law scaling of the impact crater size-frequency distribution on pluto: A preliminary analysis based on first images from New Horizons flyby. *Progress in Physics*, 2016, v. 12(1), 26–29.
2. Evans M., Hastings N. and Peacock B. *Statistical Distributions* (third edition). John Wiley & Sons Inc, New York, 2000.
3. Press W. H., Teukolsky S. A., Vetterling W. T. and Flannery B. P. *Numerical Recipes in FORTRAN. The art of scientific computing*, Cambridge University Press, Cambridge, UK, 1992.
4. Zaninetti L. and Ferraro M. On the truncated Pareto distribution with applications. *Central European Journal of Physics*, 2008, v. 61, 1–6.
5. Kolmogoroff A. Confidence limits for an unknown distribution function. *The Annals of Mathematical Statistics*, 1941, v. 12(4), 461–463.
6. Smirnov N. Table for estimating the goodness of fit of empirical distributions. *The Annals of Mathematical Statistics*, 1948, v. 19(2), 279–281.
7. Massey F.J. Jr. The Kolmogorov-Smirnov test for goodness of fit. *Journal of the American Statistical Association*, 1951, v. 46 (253), 68–78.

Determination of the Neutrino Mass

Anatoly V. Belyakov

E-mail: belyakov.lih@gmail.com

The neutrino mass in four different independent formulations have been successfully calculated on the basis of the mechanistic interpretation of J. Wheeler's geometrodynamics concept. Mechanical analogue of the weak interaction is presented. Its adequacy is confirmed by the various variants for calculating the neutrino mass. The calculated mass agrees well with the indirect estimation of the neutrino mass obtained on the basis of cosmological data. It has been established that neutrinos can change its structure and properties, in particular, a magnetic moment, that leads to changes in the power of detected neutrinos flow (neutrino oscillations). The time constant of neutrino oscillations is calculated.

1 Introduction

The geometrodynamics of the famous scientist John Archibald Wheeler, who passed away in 2008, does not seem to find favor among modern physicists.

According to J. Wheeler's geometrodynamics concept charged microparticles are considered therein as singular points located in a non-unitary coherent two-dimensional surface and connected to each other through "wormholes", current tubes, or current force lines of the input-output (source-drain) kind in an additional dimension, thus forming a closed contour. However, "wormholes" in space, if they are not considered as purely mathematical constructions, in its physical embodiment can only be vortex formations of some kind substance that has the properties of an ideal fluid.

Assuming their existence, consistently developing and complicating the concept, one has managed to develop the mechanistic model, in which the properties of objects in both the microcosm and space scales are grounded and defined by using only the most general physical laws [1–4]. The determination of the neutrino mass and the calculation of other characteristic parameters provided out later in this article are the final confirmation of the correctness of the chosen model.

Experiments on the direct measurement of the neutrino mass, based on the kinematics of weak decays, to date do not give the exact value of neutrino masses, but only set the upper limit for it (the limit is permanently decreasing). The lowest limit is obtained indirectly by studying cosmological data on the relict radiation, the galaxies recession and other. According Adam Moss and Richard Battye's analysis of the data of Planck Space Telescope and their comparison with gravitational lensing observations on distant galaxies gives an upper limit for the total amount of neutrino masses of about 0.320 ± 0.081 eV [5].

2 Initial conditions

Recall that, in the proposed model, from a purely mechanistic viewpoint the *charge* only manifests the degree of the nonequilibrium state of physical vacuum; it is proportional to the momentum of physical vacuum in its motion along the

contour of the vortical current tube. Respectively, the *spin* is proportional to the angular momentum of the physical vacuum with respect to the longitudinal axis of the contour, while the *magnetic interaction* of the conductors is analogous to the forces acting among the current tubes [1].

In such a formulation the electric constant ε_0 makes sense the linear density of the vortex current tube

$$\varepsilon_0 = \frac{m_e}{r_e} = 3.233 \times 10^{-16} \text{ kg/m}, \quad (1)$$

and the value of *inverse magnetic constant* makes sense of the centrifugal force

$$\frac{1}{\mu_0} = c^2 \varepsilon_0 = 29.06 \text{ n} \quad (2)$$

appearing due to rotation of an element of the vortex tube having the mass m_e and the classical radius r_e with the light velocity c ; this force is equivalent to the force acting between two elementary charges at the given radius.

Elementary particles are like vortex structures in an ideal fluid which can stay in two extreme forms: the vortex *at the surface* along the X-axis (let it be the analogue of a fermion of the mass m_x), and the vortex thread or a *sub-surface* vortical current tube having of the peripheral velocity v , the radius r and the length l_y along the Y-axis (let it be the analogue of a boson of the mass m_y). These structures oscillate inside a real medium, passing through one another (forming an oscillation of oscillations) showing that a mass (an energy) can have two states and pass from one form to another.

In paper [2], proceeding from the conditions of conservation of charge and constancy parameters μ_0 and ε_0 , the parameters of the vortex thread m_y , v , r for an arbitrary p^+e^- -contour were defined as

$$m_y = (an)^2 m_e, \quad (3)$$

$$v = \frac{c_0^{1/3} c}{(an)^2}, \quad (4)$$

$$r = \frac{c_0^{2/3} r_e}{(an)^4}, \quad (5)$$

where n is the quantum number, a is the inverse fine structure constant, c_0 is the dimensionless light velocity $c/[m/sec]$.

Wherein, referring to the constancy ε_0 (linear density), it is clear that the relative length of the tube current in the units of r_e is equal the boson mass m_y in the units of m_e , i.e.

$$l_y = m_y = (an)^2. \quad (6)$$

In the framework of the model, the particles themselves are a kind of a contour of a subsequent order, formed by the intersection of the X-surface with the current tube, and they have their own quantum numbers defining the influence zone of these microparticles.

In [2] we determined that

$$n_p = \left(\frac{2c_0}{a^5}\right)^{1/4} = 0.3338 \quad (7)$$

for a proton, while for the electron we have $n_e = (n_p)^{1/2} = 0.5777$.

To calculate the mass of an arbitrary fermion m_i a formula was obtained

$$m_i = m_e \left(\frac{n_e}{n_i}\right)^{14}. \quad (8)$$

Hereinafter all the numerical values of the mass, size and speed are given in dimensionless units: as the respective proportions of the electron mass m_e , its radius r_e and the speed of light c .

It is important to note that the vortex tube contour (which the vortex thread fills helically) can be regarded as completely “stretched”, i.e. elongated proportionally to $1/r$ or, contrary, extremely “compressed” i.e. shortened proportionally to $1/r$ and filling all the vortex tube of the radius r_e . In the latter case its compressed length $L_p = l_y r$ is numerically equal to the energy of the contour boson mass in the mass-energy units $m_e c^2$.

Indeed, because $r = v^2$, the numerical values of the aforementioned quantities (expressed in dimensionless units) are in all cases identical, and for an arbitrary axis are

$$L_{p_i} = l_i r_i = m_i r_i = m_i v^2 = \frac{c_0^{2/3}}{(an_i)^2}. \quad (9)$$

It is obvious that the mass of an arbitrary boson in the mass-energy units matches its own numerical value m_y only in the case of ultimate excitation of the vortex tube wherein we have $r \rightarrow r_e$ and $v \rightarrow c$.

When considering a closed contour having contra-directional currents from the balance of the magnetic and gravitational forces recorded in a “Coulombless” form, the characteristic size of the contour comes as a *geometric mean* of two linear values [2], which in the r_e units has the form:

$$l_k = (l_i r_i)^{1/2} = \left(\frac{z_{g1} z_{g2}}{z_{e1} z_{e2}}\right)^{1/2} (2\pi\gamma\rho_e)^{1/2} \times [sec], \quad (10)$$

where $z_{g1}, z_{g2}, z_{e1}, z_{e2}, r_i, l_i$ are gravitational masses and charges expressed through the mass and charge of the electron, the distance between the current tubes and their length, γ is the gravitational constant, while ρ_e is the electron density $m_e/r_e^3 = 4.071 \times 10^{13} \text{ kg/m}^3$.

In the $p^+ - e^-$ -contour, proton quarks become an active part of the proton mass, and are involved in the circulation. Their mass as z_g enters into the equation (10). When a proton and an electron are approaching, for example, in the case of e -capture, the contour becomes deformed and reduced.

3 Determination of the neutrino mass from the conditions of weak interaction

Let the neutrino is a particle having fermion and boson parts; the latter is separated in the weak interaction process (for example, when electron-proton absorption occurs) from the proton-electron X-contour into the region Y; see Figure 1. Let us find the neutrino mass *on the basis on the parameters of the neutrino vortex tube*.

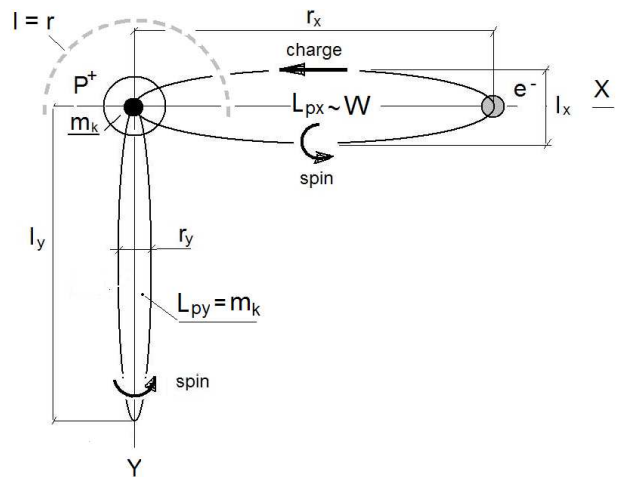


Fig. 1: Scheme of formation of the neutrino.

For the X-contour, referring to (9), its energy-mass in units of $m_e c^2$ is

$$L_{p_x} = \frac{c_0^{2/3}}{(an_x)^2}. \quad (11)$$

It is necessary to define the same parameters n_y and L_{p_y} for the neutrino. Because of the special stability of the neutrino, one can assume that its structure is characterized by all possible balances and symmetries.

Proceeding from energy balance, we assume that the active part of the proton, i.e. the quark energy-mass, is equal to the neutrino boson vortex tube energy-mass

$$m_k = L_{p_y} = \frac{c_0^{2/3}}{(an_y)^2}. \quad (12)$$

For the $p^+ - e^-$ -X-contour it is accepted: $z_{g_1}/z_{e_1} = 1$, $z_{e_2} = 1$ and $z_{g_2} = m_k = L_{p_y}$. Then, using (9), from (10) we get:

$$\frac{L_{p_x}}{L_{p_y}} = 2\pi\gamma\rho_e \times [\text{sec}^2]. \quad (13)$$

Assume, due to symmetry, that the contour large axis along X-axis and the neutrino vortex tube along Y-axis are equal, i.e., $r_x = l_y$. Then, referring to (5) and (6), the relation between the quantum parameters X and Y-contours is

$$n_y n_x^2 = \frac{c_0^{1/3}}{a^3}. \quad (14)$$

Proceeding from the formulas (11–14), as a result, we have

$$L_{p_x} = c_0^{4/9} (2\pi\gamma\rho_e \times [\text{sec}^2])^{1/3} = 1.51 \times 10^5 \text{ (77 GeV)}, \quad (15)$$

$$L_{p_y} = m_k = \frac{c_0^{4/3}}{L_{p_x}^2} = 8.83 \text{ (4.51 MeV)}, \quad (16)$$

as well as the quantum parameter of the neutrino vortex tube

$$n_y = \frac{c_0^{1/3}}{aL_{p_y}^{1/2}} = 1.643. \quad (17)$$

Now, according to the equation (8) the neutrino fermion mass is found:

$$m_v = \left(\frac{n_e}{n_y}\right)^{14} = \left(\frac{0.5777}{1.643}\right)^{14} = 4.39 \times 10^{-7} \text{ (0.225 eV)}. \quad (18)$$

Additional sequels appear: the X-contour energy-mass is very close to a W-boson mass (80 GeV), and the estimated mass of a quark agrees well with that of the d-quark (4.8 MeV).

In more detailed consideration of the weak interaction, process the possibility of finding the neutrino mass *from the conservation of energy and symmetry* is detected. In the process of e^- -capture, the proton-electron X-contour is reduced and deformed in the Y-region. Being already the neutrino Y-contour, it contains the neutrino mass instead of the electron mass. Let us assume that at some intermediate state, before the allocation in the vortex tube form, Y-contour still maintains its momentum (the unit charge). In this case the formula (15) includes a neutrino mass m_v (in the m_e units), and, at $z_{e_2} = 1$, applies to the neutrino contour. It has the form:

$$(L_{p_x})_v = c_0^{4/9} m_v^{1/3} (2\pi\gamma\rho_e \times [\text{sec}^2])^{1/3}. \quad (19)$$

At the same time the X-contour initial energy-mass L_{p_x} has been transformed into the proton active part energy-mass (i.e., the quark mass $(L_{p_y})_v$). Then, referring to (16), we can write

$$L_{p_x} = (L_{p_y})_v = \frac{c_0^{4/3}}{(L_{p_x})_v^2}. \quad (20)$$

As a result, considering (15) and (19) from (20) we obtain:

$$m_v = (2\pi\gamma\rho_e \times [\text{sec}^2])^{-3/2} \quad (21)$$

that gives 4.5×10^{-7} (0.23 eV), the amount actually coincided with the result of the formula (18). With making the similar actions under the condition of the short axes equality $r_y = l_x$, then the same result has been got. In this case, contrary, $L_{p_y} = (L_{p_x})_v$ that apparently corresponds to the inverse process of the neutron in proton transformation.

Finally, the neutrino mass can be derived from the *conditions of complete symmetry*, i.e. from the state that is intermediate between the neutron and the proton when the X and Y-contours merge into one symmetrical contour at the zero point coordinates. This state apparently occurs only under some distinctive amount of the neutrino contour charge, namely — it is the charge value per one structure unit of the standard contour (per one photon) or e_0/a [1].

Indeed, since for a symmetrical contour $n_x = n_y$, $l = r = c_0^{2/9}$ and $L_{p_x} = L_{p_y} = c_0^{4/9}$, then by introducing into the initial formula (10) $z_{e_2} = 1/a$ from (19) we obtain

$$m_v = a^{-1} (2\pi\gamma\rho_e \times [\text{sec}^2])^{-1}, \quad (22)$$

that gives 4.28×10^{-7} (0.219 eV), the same amount as the resulting from the formulas (18) and (21).

Note that if a single photon has a linear size of $1/a$ of the standard contour length, i.e. the value of $c_0^{2/3}/a$, then the neutrino has a similar size of $c_0^{2/3} m_v$ or $0.192 r_e$. This value is about 1/3 of the proton diameter; it is the linear quark dimension along the axis X. Indeed, since for the quark we have $n = 0.48$, then $r_x = c_0^{2/3}/(an)^{3.5} = 0.194 r_e$ [2]. This coincidence additionally points to the correctness of the proton quark model, as set out earlier.

Full symmetry and the combining of the $p^+ - e^-$ -contour and the neutrino contour are possible only in a special excited state of the nucleon. In reality, the electromagnetic interaction (nominal axis X) and weak interaction (nominal axis Y) are realized separately, and then only in a certain scale range, forming three generations of elementary particles [2]. That is, here is a *mechanical analogue of spontaneous electroweak symmetry breaking in the SM*.

Thus, the proposed model clearly describes the process of the weak interaction (how a proton absorbs an electron). The proton-electronic contour is reduced until the energy-mass becomes equal to the energy of W-particles. Then it transmits this energy and momentum (charge) to the proton, transforming it into an excited state (the neutron); further the contour is allocated into Y-region as the neutrino vortex tube with the parameter $n_y = 1.643$, keeping its spin and having the value of energy-mass equal to that of the light d-quark.

4 Determination of the neutrino mass from the limit conditions

At last, the neutrino mass is possible to be found directly from the magnetic-gravitational equilibrium conditions; from the equation (10), by substituting the limit conditions.

A vortex thread or tube in a non-viscous medium can be either closed or having an output to the surface of X, that is having a charge. The neutrino has no detectable charge and, therefore, it represents a closed structure or a contour.

Assume that Planck's size $r_h = (\hbar\gamma/c^3)^{1/2}$ has a physical meaning and it is the minimum size of the elementary neutrino vortex contour, i.e., $r_i = r_h = 1.616 \times 10^{-35}$ m or $5.735 \times 10^{-21} r_e$. Then, taking into account (5) and (6), a geometric mean is obtained from (10) as

$$l_k = c_0^{1/6} r_h^{1/4}. \quad (23)$$

In [2] it is shown that any electron vortex tube includes three vortex zones. But as one of the zones needs to be double, there should in general be four vortex threads each containing one-quarter of the electron total momentum (charge). Therefore, the elementary neutrino should be viewed as a pair of the closed vortex threads. Accordingly, two types of neutrinos are possible there: a pair of left-right rotation and, conversely, a pair of right-left rotation, obviously, as a neutrino and an antineutrino.

For a pair of the vortex threads at $z_{e1} = z_{e2} = \frac{1}{4} e_0$ and at $z_{g1} = z_{g2}$, having in mind (23), from (10) it should be:

$$z_g = m_v = \frac{c_0^{1/6} r_h^{1/4}}{(32\pi\gamma\rho_e \times [\text{sec}^2])^{1/2}}, \quad (24)$$

that gives 4.31×10^{-7} (0.220 eV), the amount actually coinciding with the results of the formulas (18), (21), and (22). It should be noted that these results are only the ones of its kind since these formulas include only the fundamental constants.

Thus, the two states of the neutrino are obtained — *at the moment of birth in the form of a vortex tube and in its ultimate state in the form of a closed structure*, and the fermion neutrino mass in the initial state turned out equal to the gravitational mass of the neutrino vortex threads in the ultimate state. Is it possible to reconcile these very different states? Perhaps, it must be admitted that since the neutrino's vortex tubes initially contain all four single vortex threads then further the neutrino transforms into two potentially possible final forms (neutrino and antineutrino) maybe passing some intermediate states.

As for the muon and the tau-neutrinos, the electron mass in the formula (10) can be formally replaced by the masses of the muon and the tau-particles, provided that the linear density of the contour tube remains unchanged (that is not obvious). Then, as follows from the above formulas, the contours' parameters are changed, and the contours are deformed "stretching" along their axes; the X-contour energy-mass increases as the cube root of the relative weight of the

microparticle. For the muon contour $L_{p_x} = 456$ GeV, which is equal to twice the value of the total energy-mass of the standard $p^+ - e^-$ -contour (229 GeV) [1]. For the τ -contour $L_{p_x} = 1170$ GeV. This value is the sum of the neutrino energy and that of the expected boson energy-mass of the third generation, the heaviest one, which is not yet registered in experiment; that is, having the value of about 1000 GeV, which matches to the value defined earlier in [2]. As follows from the above formulas masses of the muon and the tau-neutrinos must be much less than that of the electron neutrino, and the resulting formulas give different results that may indicate instability of these neutrinos, like other particles of the second and third generations.

The fact of the neutrino transformation is derived from the model and confirmed by the experimentally detected neutrino oscillations.

5 Neutrino magnetic properties and its oscillations

The neutrino boson vortex tube retains the electron spin, and has a magnetic moment μ . The magnetic moment is determined relative to the axis Y. By definition, the μ is the product of the charge \times the velocity \times the path. Suppose that for the vortex thread the peripheral speed is v , while the path is πr . Revealing v and r through (4) and (5), as a result we obtain

$$\mu = \frac{\pi c_0 c e_0 r_e}{(an)^6} \text{ Am}^2. \quad (25)$$

(Ampere at a "Coulombless" system is equivalent to the acting force.)

The neutrino magnetic moment in the moment of its allocation μ_{v_0} according to formula (25) at $n_y = 1.643$ is 9.81×10^{-31} Am². Moreover, it appears that this value with high accuracy is equal to the geometric mean of the proton magnetic moment μ_p and the vortex tube magnetic moment with average parameter l_k (Compton wavelength), which complies to $n_y = 8.07$ [2]. Its magnetic moment $\mu_k = 6.99 \times 10^{-35}$ Am², which corresponds to 0.75×10^{-11} Bohr's magneton. That is,

$$\mu_{v_0} = (\mu_p \mu_k)^{1/2}. \quad (26)$$

Such a large magnetic moment of neutrinos are not detected, but what is significant, it is the magnetic moment μ_k close to 10^{-11} Bohr's magneton that requires the neutrino to explain the anticorrelation of the registered neutrino flow with the magnetic flow near the sun surface. It is assumed that the neutrino magnetic moment interacts with the magnetic field in the outer convective layers of the sun, which leads to the spin precession of neutrinos changing its helicity from left to right; and the right neutrinos are not registered by detectors [6, 7]. The same neutrino magnetic moment is required because of some astrophysical limitations regarding the dynamics of stars [7].

So it is logical to assume that the neutrino magnetic moment, an originally very large magnitude, rapidly decreases

to the value of about 10^{-11} Bohr's magneton at the intersection of the Sun's surface, and in the neutrino ultimate state it becomes absolutely negligible. The reason for this is the transformation of the neutrino contour, which is analogous to the process of the transformation of a neutron into a proton.

Indeed, if the counter comprises several vortex threads with co-directed currents, they must be rotated relative to the longitudinal axis. At the same time, since by definition an elementary unit of the model medium (vortex thread) is absolutely inelastic and at the same time is absolutely deformed, the closed counter must be deformed ("turned out") in different structures by changing its parameters.

From the equality of the magnetic and inertial (centrifugal) forces for the vortex threads the peripheral rotation speed relative to the longitudinal axis of the contour is obtained

$$v_0 = \frac{(z_{e_1} z_{e_2})^{1/2} r_e}{(2\pi)^{1/2} \times [\text{sec}]} . \quad (27)$$

This speed does not depend on the length of the vortex threads and distances between them and for the unit charges is 1.124×10^{-15} m/sec.

Earlier [2], it was found that the *time constant* of the transformation process (the ratio of the counter size to the peripheral speed) has appeared equal to the neutron lifetime.

Similarly, the time constant for the neutrino can be expressed in the forms $\tau_v = r_y/v_0$. Then, referring to (5), with $n = 1.643$, we obtain $\tau_v = 4.37 \times 10^{-4}$ sec (the time constant should be increased with the decrease of the residual charge of the neutrino). During this time the neutrinos having the speed of light move away from the source at a distance of 1.31×10^5 m. If they would transform to another form, a decrease in their number would be registered when the detector would be displaced from the source at a distance not less than the calculated value.

It is the distance the largest neutrino detector KamLAND (Kamioka Liquid Scintillator Anti-Neutrino Detector, Honshu island, Japan) has registered a decrease of the neutrino flow in the nuclear reactor antineutrino experiments [8]); see Figure 2 (the data are taken from [8]).

6 Conclusion

Thus, one value of the neutrino mass has been derived by theoretical methods. Moreover, the same result was then obtained in four different formulas and three of them on the basis of the classical mechanistic model (actually through the analogue of spontaneous electroweak symmetry breaking in the SM). The results coincided with the indirect estimate of the neutrino mass derived from cosmological data. It was established that neutrinos may exist in various forms. It arises in the form of the electron neutrino with the mass of about 0.22 eV and further during the transition to its final state with the same mass may possibly change its parameters like the mass and magnetic moment, which results in the changes of

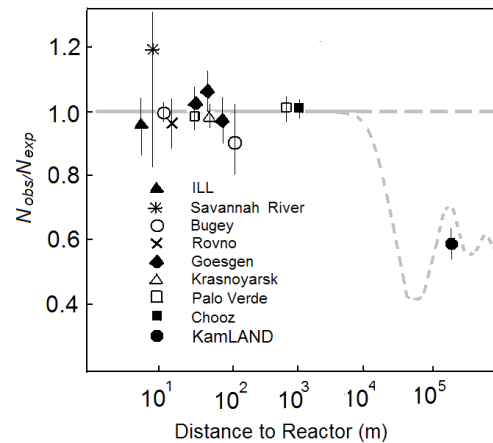


Fig. 2: The ratio of the measured neutrinos flows in the expected ones if there is no oscillations for experiments with reactor neutrinos.

a detectable power neutrino flow (oscillations). It is possible that the muon-neutrinos and tau-neutrinos are not stable. Apparently, they are the intermediate states of the totally stable electron neutrino.

The fact that the same neutrino mass is obtained in several ways may indicate that the values of other fundamental constants can also be obtained through the neutrino mass, which apparently is a key element of matter.

Submitted on October 14, 2015 / Accepted on November 17, 2015

References

1. Belyakov A.V. Charge of the electron, and the constants of radiation according to J. A. Wheeler's geometrodynamics model. *Progress in Physics*, 2010, v. 6, issue 4, 90–94.
2. Belyakov A.V. Macro-analogies and gravitation in the micro-world: further elaboration of Wheeler's model of geometrodynamics. *Progress in Physics*, 2012, v. 8, issue 2, 47–57.
3. Belyakov A.V. Evolution of stellar objects according to J. Wheeler's geometrodynamics concept. *Progress in Physics*, 2013, v. 9, issue 1, 25–40.
4. Belyakov A.V. Nuclear power and the structure of a nucleus according to J. Wheeler's geometrodynamics concept. *Progress in Physics*, 2015, v. 11, issue 1, 89–98.
5. Battye R.A., Adam M. Evidence for massive neutrinos from CMB and lensing observations. arXiv: 1308.5870, August 27, 2013.
6. Wolfenstein L., Bayer Yu.U. Neutrino oscillations and solar neutrinos. *Physics Today*, July 1989, v. 42, no. 7, 28–36.
7. Derbin A.V. The search for the magnetic moment of the neutron. *Particle Physics and Nuclear Physics*, Petersburg Nuclear Physics Institute at Gatchina, Russia, 2001, v. 32, v. 3, 734–749.
8. Orekhov D.I. Toolkit for neutrino physics. Dept. of Physics, Moscow State University, August 27, 2006.

On the Nature of the Magnetic Field of the Earth and Other Planets

Vladimir Danilov

E-mail: danvlad@bk.ru

This study presents a hypothesis of the origin and maintain of the magnetic field of the Earth and the planets. The mechanism of the tides on the opposite side of the Earth from the Moon is considered. The possible causes that enforce the continents to displace are discussed in couple with the causes that distort the shape of the Earth, and the causes of the jumps of the astronomical time. A mechanism of earthquakes is proposed, as well as a version of the appearance of the “magnetic tubes” in the Sun. The source of the forces causing the equatorial current and wind is shown.

Contents

1. Introduction
2. Tides
3. Currents
4. Earthquakes
5. Time jumps and killer waves
6. Causes of a dip appearing in the gravity graph during the Sun’s passage across the sky
7. On motion of the magnetic poles
8. Conclusion

Appendix. A short comparison of the planets’ magnetic fields depending on the number of their moons and other properties

Books of physics are full of complicated mathematical formulae. But thought and ideas, not formulae, are the beginning of every physical theory.

Albert Einstein

That hypothesis which explains the current world with the fewest assumptions and means should have an advantage, because it is less arbitrary.

Empedocles, *On Nature, the Law of Economy*

The form of development of natural science, in so far as it thinks, is the hypothesis... If one should wait until the material for a law was in a pure form, it would mean suspending the process of thought in investigation until then and, if only for this, reason, the law would never come into being.

Friedrich Engels, *Dialectics of Nature*

1 Introduction

The Earth’s magnetic field makes our planet habitable — there would be no life on the planet without it. It protects the Earth’s biological envelope from the hostile lifeless space and devastating effects of cosmic-ray particles. The habitability-determining need for a magnetic field reduces the number of

potentially habitable planets. It is hard to enumerate all the effects of the field on inhabitants of the planet. Its properties are used by both humans and animals, while the scientific community has no unambiguous approach to understanding the mechanism of the field’s creation and maintenance, as well as on the factors affecting its behavior.

One of the most popular hypotheses trying to explain the nature of the field is the dynamo theory. It proposes that convective and/or turbulent motions of conductive fluid in the core trigger self-excitation of a magnetic field and maintain the field stable.

However, it is hard to imagine the core steadily moving up to the surface in the same direction due to temperature — if it is convective motion; or the turbulence created by rotation being so stable that it could maintain self-excitation, and even in the same direction. Though, the nature of turbulence is not clear either. Over time, in the absence of external forces, the inner substance of the Earth will also rotate together with the shell due to its viscosity. The origin of the potentials in the core is also unclear. Why are they not compensated, if the substance is conductive? The authors of this hypothesis themselves thought it was a far cry from being proven. Although the hydrodynamic dynamo hypothesis explains many well-known facts, it is clear that the power triggering the “dynamo” has been defined incorrectly.

Another hypothesis proposes that the magnetic field is created in the ionosphere by the solar wind.

The third one says about salt-water flows in the oceans.

None of these theories can be applied to all the planets of the Solar System free of contradictions. For example, Jupiter spins in the same direction as the Earth does, but Jupiter’s magnetic field is directed opposite to the Earth’s one. Venus and Mars have no strong fields.

Anyway, it is not fair to believe that the Earth owns some unique features that no other planet has. After all, it is not the only planet that has a magnetic field, and it is not quite the thing to do to come up with its own mechanism for creating a magnetic field for each planet either. So what could be right? There should be a single physics of this phenomenon.

It just manifests itself somewhat differently because of different conditions of existence of different planets.

I would like to note here that the modern model of the Earth (with a hard core inside, surrounded by liquid alloy) is based on the study of behavior of acoustic (seismic) waves and their ability to pass in solid and liquid media differently. High-temperature plasma with close-packed nuclei will conduct seismic waves as a solid (crystalline) material, which is consistent with the measured data, and the adopted boundary of the solid core may be a boundary of transition to the plasma state. Generally it is hard to imagine — without inventing new forms and states — that some substance would “float” in a hard form in the same melted substance without melting itself.

This article presents a hypothesis of emergence and maintenance of the planet’s magnetic field taking into account its own travel (axial inclination) in the solar ecliptic and the properties of the planet itself and its moons, if any. It shows that the outer shell of the planet is “independent” from the processes occurring in the planet’s interaction with other bodies, thus allowing the magnetic poles to move, up to their inversion.

Attempts to find the answers to the following questions

1. What is the origin of the Earth’s and other planets’ magnetic fields?
2. Why does the far side of the Earth furthest from the Moon has tides too?
3. Why do the Moon and most moons keep the same side turned to their planets?
4. What force causes the continents to move?
5. What causes earthquakes?
6. Why is the Earth not round?
7. What are the reasons for sharp changes in astronomical time?
8. How do “killer-waves” occur?
9. Why is there a dip in the gravitation graph during the Sun’s passage across the sky?
10. What are the reasons for periodic variations of geophysical fields and seismic activity?
11. What gives rise to and maintains major ocean currents and equatorial winds?

have given rise to the following hypothesis:

The main reason for all of the above phenomena is the gravitational interaction of the Sun and moon(s) with a moving core of the planet.

The main proof of the hypothesis is the clear connection in the chain “**planet — satellite(s) — planet’s magnetic field**” for various planets of the Solar System, bearing in mind that each planet is a moon of the Sun in its turn.

Thus, it can be noted that:

1. The magnetic field is effective if a planet has a moon or more. The field is small if the planet has no moons (e.g., Venus and Mercury have no moons, and their magnetic fields are very small);
2. If the planet cooled down and does not have a liquid core, it does not have a magnetic field either (e.g., the Moon);
3. Direction and shape of a planet’s magnetic field depends on both the direction of rotation of the planet itself in the ecliptic plane and the orbit of the moon revolving around the planet (e.g., Mars and Uranus have reverse rotation of moons and reverse magnetic fields);
4. In the presence of multiple moons, the field becomes complex, and priority in the field’s direction is determined by the more closely spaced or the more massive moon (for example, Uranus or Neptune);
5. Direction of the main winds and location of dust clouds on most of the planets in the Solar System coincides with the direction of their moons’ motion.

In addition, the fact that the most moons revolve around their planets turning one side on them, and the rotation of planets such as Venus and Mercury is synchronized with the motion of the Earth (the two planets turn the same hemisphere to the Earth when approaching it), shows that cosmic bodies interact with each other not as uniform bodies, but as bodies with misplaced centers of mass. At the same time, in the case of a liquid core, the center can move within the hard shell of the planet.

Let’s consider the mechanism of occurrence of a magnetic field (MF) in the example of the Earth. It will be the same for any Earth-like planet.

Imagine the Earth as a fixed sphere filled with substances of various densities and various specific gravity, and the Sun as a source of gravity affecting these substances. It is obvious that the heavier structures will gravitate to the shell of the sphere that is closest to the source of gravity, and distribution of density and mass within the Earth will be uneven not only in depth, but also towards the Sun (see Fig. 1).

According to modern theories of the Earth structure, substances below the lower mantle are in a liquid state (metallic phase) — plasma — where electrons are separated from the

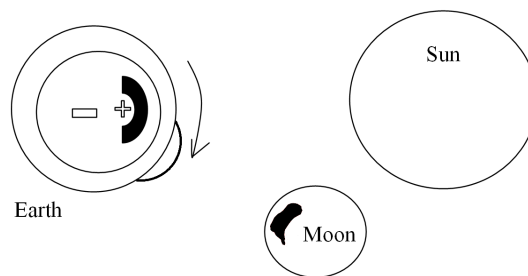


Fig. 1: Mass distribution.

nuclei. But, as the nuclei are much heavier than the electrons, it is clear that these are “precipitating” nuclei. Then a division inside the Earth’s core occurs not only by mass but also by electric potential. The core of the Earth has become a dipole with the center of mass shifted significantly, where “+” and the bulk mass of the core are closer to the Sun.

While the Earth rotates, this part of the Earth’s core follows the Sun and thereby create directed motion of electrically charged particles and circular, cyclic displacement of the center of mass of the Earth relative to its shell.

In 1878, Henry A. Rowland proved that charges moving on a moving conductor are identical in their magnetic effect to conduction current in a conductor at rest. Thus, in our case, the right-hand rule is generally appropriate, as evidenced by the direction of motion of the core part carrying a positive charge and the force lines of the Earth’s magnetic field.

It certainly does not mean that one side of the sphere is pure “+” and the other is “-”. Otherwise there would be no magnetic field formed in rotation of such a dipole because of the mutual compensation. There are just different motion radii, and different linear speeds respectively, and hence current potentials are different too. There may occur some compensation in motion of various charges, but “+” prevails.

More information on polarization of plasma in massive astronomical objects due to gravitational forces and their interaction with Coulomb forces is available in works by Igor Iosilevskiy (for example, in his publications [1, 2]).

By the way, if we accept the proposed hypothesis, the formation of the dipole inside the planet is a practical proof of the theoretical assumptions made by Iosilevskiy.

Of course, besides the Sun, the behavior of the charged core is also influenced by all the planets and the Moon in particular (see the section on tides).

Another proof of the hypothesis are daily and annual changes in the magnetic field direction, i.e., dependence of the field on the Earth’s position relative to other objects affecting division by mass, charge, and trajectory of the core. (In the case of the now accepted hypothesis of a hydrodynamic dynamo, there should be no such influence.)

In fact, the heavy part of the core moves from East to West and in spirals from North to South and back with changes in axial inclination (change of season).

A very interesting measured data were provided by Yury P. Malyshkov and Sergey Yu. Malyshkov [3] on the basis of their research done in the Institute of Monitoring Climatic and Ecological Systems, Russian Academy of Sciences.

Based on years of research on natural pulse electromagnetic fields of the Earth (NPEMFE) in seismically active areas of the Baikal Lakeside, they came to a conclusion on the motion of the planet’s core and related natural phenomena — seismic activity, impact on the human body and so forth. The figures showing intensity of NPEMFE changes at different points in time exactly repeat the expected movement pattern of the dipole’s heavy part.

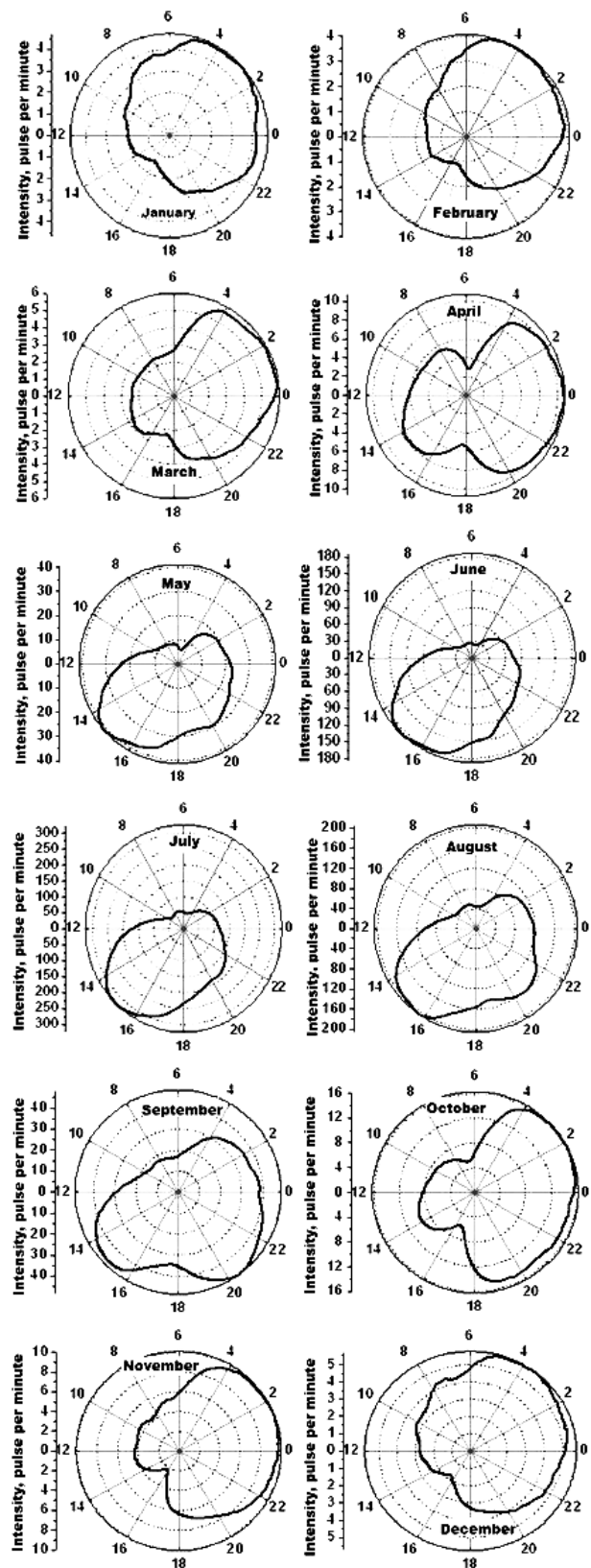


Fig. 2: Average rounded daily variations in NPEMFE in polar coordinates for the period from 1997 to 2004.

These figures show the way the intensity of the electromagnetic field disturbances is changing during the time of day depending on the season. We can see that the intensity is significantly reduced in winter months with its maximum at night, that is when it is day time and summer in the Southern Hemisphere, where the heavy part of the core is, and there are more storms.

It is very sad that such an enormous result obtained by Y.P. Malyshkov and S. Yu. Malyshkov [3] on these measurements, systematization, analysis and so on cannot be continued because of lack of funding.

It becomes clear how the Earth's magnetic field is formed and why other planets and the Sun have magnetic fields too, if they have moons, or no magnetic fields, if they don't (eg., Venus has a very slow spin — 243 Earth days — that is there are no gravitational forces to create a moving charge), or if the planet cooled down and has no liquid core (Moon), as well as reversal of polarity with reversed rotation of the moon(s) (Mars), and presence of a complex field due to the planet's complex relationship with moons (Uranus and Neptune). It is interesting that Mercury, while having no moons, has a field similar to the Earth's one, though much smaller. However, it itself is a moon of the Sun, and the closest one. It quickly orbits the Sun — in 89 Earth days. Mercury's field is symmetric and directed along the axis of rotation. Its equator is only 0.1 degree tilted to the orbit plane.

A good illustration of the influence of the planet-moon system on a magnetic field's form is a comparison of the fields of Jupiter and Earth. Jupiter's field is more like a flat disk — even most of its moons rotate in correct circular orbits in the equatorial plane — and the axis of rotation of the planet itself is negligibly tilted. There is no change of seasons. On the other hand, the form of the Earth's field resembles an apple, and the planet itself swings relative to the plane of the ecliptic. This can be compared as fields from two different electromagnetic coils — one loop-to-loop wound around the coil-tube and the other being similar to a cassette tape.

Thus, the charges forming the magnetic field of a planet having a liquid core are created and propelled by the total gravitational force from its moons, the Sun, and other planets moving nearby relative to the planet. The charges also influence on the field shape. Of course, MF depends on the distance between the planet and the Sun. Influence of the latter is paramount. For example, as shown by Alexander L. Chizhevsky, "Taking into account the diameter of the Sun equal to 1,390,891 km* and the tremendous power of physical and chemical processes occurring on the Sun, it must be recognized that the Globe is under its enormously intensive influence" [4].

A short comparison of the planets' magnetic fields depending on the number of their moons and other properties is

*According to recent data, the Sun's diameter is 1,392,000 kilometers, while the Earth is located at 107 Sun diameters from the Sun.

given in Appendix.

The generated pulsating (for a point on the surface) — with a day-and-night period — magnetic field of the Earth is supported by the magnetic properties of the planet's body that smooths and stabilizes its behavior, and sometimes distorts, creating local anomalous areas.

According to the research conducted by Hrvoje Tkalčić, College of Physical and Mathematical Sciences, Australian National University [5], he found that spins of different layers of the Earth are not synchronic. The red-hot core of the Earth inexplicably begins to gain momentum and then slow down, and spins faster or slower than the Earth does. To detect the desynchronization phenomenon, the researchers used a very effort-consuming method of studying double earthquakes, i.e. the earthquakes that occur in the same place at intervals of two weeks to decades. Comparison of seismic waves made it possible to reveal changes in the deep layers of the Earth and learn about changing spin speed of the planet's core.

It is quite hard to measure the spin speed in discrete measurements as, in this case, we need some kind of a marker on the core's surface; all the more so as said that the speed is unstable and variable. We can only determine that there is a position change. If changing the model of the Earth's internal structure, the measured result change too. However, the fact that these changes take place also verifies the hypothesis, and it can broadly explain the physics of motion.

2 Tides

Let's consider the effect of gravitational force in the example of the Earth. The primary influence is caused by the Sun and the Moon. The Sun's influence is (according to various data) 30 to 200 times stronger than the Moon's. However, despite the fact that the Sun's gravitational force is almost 200 times greater for the Globe than the gravitational force of the Moon, the tidal forces generated by the Moon are almost twice as much as generated by the Sun. This is due to the fact that the tidal forces do not depend on the magnitude of the gravitational field and its degree of heterogeneity. With increasing distance from the source of the field, heterogeneity decreases more rapidly than the size of the field itself. Since the Sun is almost 400 times farther from Earth than the Moon, the tidal forces caused by the solar gravitation are weaker.

In other words we can say that the tidal force of the Moon is more "superficial", local, and more affecting the ocean and the upper mantle, whereas the solar gravity is more uniform, affecting the whole body of the planet. The solar gravity can be considered roughly equal anywhere on the Earth. It is the solar gravity that makes the core move and separate into charges. Naturally, this mechanism will slightly vary for other planets, but the physics of the phenomenon is the same.

With spin of the Earth, these two forces are added and the tidal wave, which has the shape of an ellipsoid, is a superposition of two *double-humped waves*, formed as a result

of gravitational interaction of the Earth-Moon planetary pair and the gravitational interaction of the pair with the central luminary — the Sun.

Thus, the words *lunar tide* hereinafter mean a tide caused by the cumulative influence of the Sun and Moon on the body of the planet.

In addition to the tides on the Earth’s side facing the Moon, there are tides on the other side. They are about the same in magnitude. In literary sources, the existence of this phenomenon is explained by reduced gravity of the Moon and the centrifugal forces created by rotation of the Earth-Moon pair. But then there would be a tide on the other side of the Moon too, and this would happen there all the time, especially as the Moon moves at the larger distance from the center of mass than the other side of the Earth does. We know about the shifting center of mass and elongation of the Moon towards the Earth, but there are no tides on the far side. In addition, as it was said above, the tides are caused not only by the Moon, but by the Sun and the Moon together, so we have to find now the center of mass for three planets.

If we compare the forces affecting the Earth’s surface in low-tide areas (Point 2) and high-tide areas of the *dark* side of the Earth (Point 1), the gravity forces in the *dark* should be stronger, as the gravity of the Earth’s center is added (though weakened) the gravity of the Moon and the Sun. This means that the sea level in Point 1 should be lower than the sea level at low tide in Point 2, but it is actually almost the same as it is in Point 3. How else can it be explained?

Following the hypothesis, we can assume that the heaviest part of the Earth’s core following the Moon and the Sun is displaced so far from the opposite edge of the Earth, that the square of the distance has its effect, and the gravity force of the core on the surface is weakened thus causing a tidal effect. In other words, the force of gravity at the point on the Earth depends not only on the position of the Moon and the Sun, but also the center of mass of the Earth (see Fig. 3 and Fig. 4).

Apparently, these processes occurred on the Moon too. When cooling, the heavy mass of the inner substance clustered mostly in the side of the planet facing the Earth, thus making the Moon a kind of Roly-Poly and forcing it to turn the same heavy side to us.

This is also confirmed by the fact that earlier, as it is known, it had a strong magnetic field which now exists only in residual form.

Thus, the force of the Earth’s gravity (together with the Moon’s gravity force) not only holds the Moon in the moon orbit, but also makes it spin thus requiring energy. Perhaps this interaction further heats the inner substance of the planet, preventing it from cooling down. This can refute the theory of a thermonuclear source maintaining the planet’s core in a “warm” state. Otherwise, at least we would have long been bald.

The same core makes the Earth to “bulge” at the equator, giving it a form other than a sphere. The same bulging is a

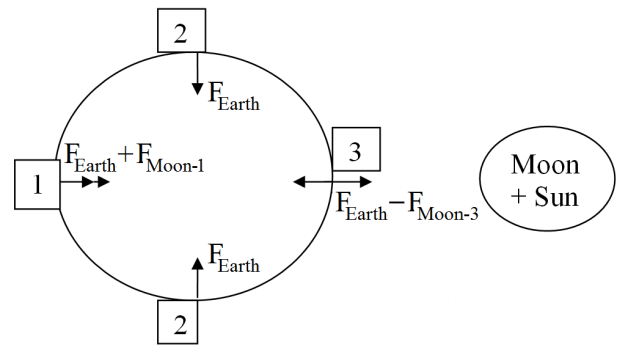


Fig. 3: The forces affecting the points on the Earth’s surface with uniform mass distribution.

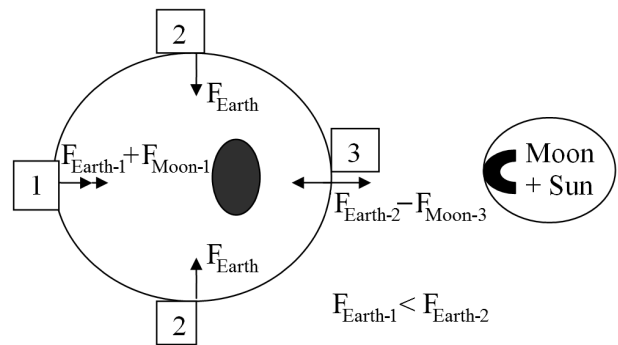


Fig. 4: The forces affecting the points on the Earth’s surface with the shifted center.

characteristic of Jupiter with its high speed of spin, where this is further contributed by centrifugal forces.

A similar phenomenon seems to be happening with the Sun and its moon-planets.

If we imagine that the “heavy” center of the Sun following the moon-planets “floats” on the surface with a strong gravitational pull of planets, is charged with the electric potential, and is in motion, this may cause *magnetic flux tubes* on the surface, i.e. output points of the both poles of the magnetic field.

Over many years of research on the impact of solar activity on the biosphere, Chizhevsky has clearly shown a direct relationship of these processes, assuming that the perturbations observed as *sunspots* are causing radiation that reaches the Earth’s surface and penetrates into it affecting all the living and non-living things [5]. The proposed hypothesis can explain the appearance of wide-frequency-range electromagnetic radiation as a result of abruptly changing fluxes of charged solar material.

3 Currents

Literature sources used to explain the nature of the equatorial currents by the winds constantly blowing in the same direction, while the nature of the winds was explained by surface heating and spinning of the Earth. Of course, this does affect

the ocean and the air masses too, but, in my opinion, they are primarily influenced by the gravity force from moving *Earth core — the Moon* and *Earth core — the Sun* pairs affecting everything that gets between them and that is carried from East to West by their gravity force. It should not be regarded as a process with tight fixing. It is more similar to stirring a teaspoon in a large pot in the same direction — not hard, but for a long time.

4 Earthquakes

There is still no clear definition of the nature of earthquakes. It is quite possible that it may look as follows: Employ your imagination — Where will a body located at the center of the planet gravitate at the slightest deviation from the center?

If a substance is distributed unevenly (assume that it is denser to the center), it is just like as written in textbooks. But what forces draw it in the center? It should be a substance having infinite density. It sounds more like fiction.

If the Earth had the form of an empty sphere, there would be no gravity force inside it. The point inside the Earth would be influenced by the gravity forces of external bodies — the Moon, the Sun, etc. This point would tend to follow the direction of the sum vector of the forces of these bodies.

If the Earth had uniform distribution of substance by density, then (if the substance is liquid) it would be the same.

In both cases, the substance inside the hard shell will gravitate to the shell from the inside toward the outside forces from other planets.

All the above was said without taking pressure into account, but let's consider the pressure's behavior upon submersion — naturally it increases in the beginning (as the mass "over the head" increases), but further on the gravity force decreases and the pressure gradually "stabilizes". In the end we have a closed space with approximately even pressure throughout volume, and its influence may be small compared to the gravity forces. It is just the same as in ordinary life — the atmospheric column presses down on all of us, but it still lets the gravity forces to drop an apple on the ground.

It turns out that the interior of the Earth can be similar in structure to a chicken egg and have the same distribution of substance by density as it is on the surface — solid-liquid — and all these at enormous pressure and temperature.

Now, if we imagine, the glowing mass exposed to various — addable or deductible — gravitational forces from various planets is moving in the "inner" surface of the earth, constantly blending and running into irregularities. At the same time, the interior of the Earth's shell is constantly exposed to momentum which is transmitted to the tectonic plates, forcing them to move gradually, thereby moving the continents. This is confirmed by the fact that the continents are moving in the latitudinal direction (East-West) and do not move in the longitudinal one (South-North).

Sometimes the forces are added in such a way that parts

of the core get into the central zero-gravity zone and, after breaking away from the bulk mass, "fall" on the opposite side of the sphere, which might cause an earthquake. A very good illustration of such a case is behavior of water in a zero-gravity environment shot by US astronauts. Behavior of water balls in a "bubble" could well be similar to that of the inner core of the planet.

By the way, the zero-gravity zone is not fixed in a permanent place, but is following the main mass of the core in rough circles.

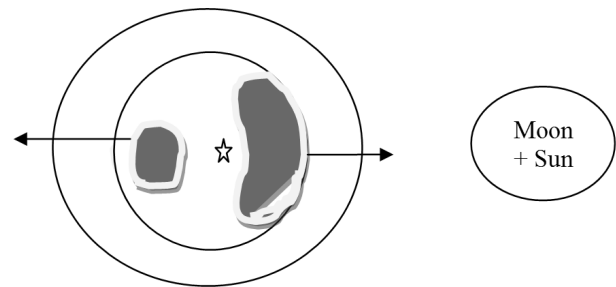


Fig. 5: A part of the core falls on the opposite side of the Earth's shell after it has separated and moved to a gravity-equilibrium zone.

There may also occur a sort of a wave with a crest when climbing an inner roughness, with a further collapse, which may also cause an earthquake.

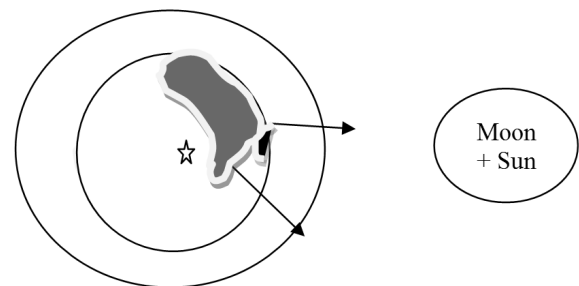


Fig. 6: Collapse of a core part.

This mechanism of earthquakes may be even more likely, since the majority of seismic focuses are located at the boundaries of tectonic plates or in areas of geological irregularities.

These two phenomena can cause shifts in the surface layers of the mantle triggering creation of additional seismic focuses and aftershocks.

It should be also noted that, as is known, magnetic storms on the Earth are accompanied with low-frequency vibrations of the Earth's body, and vice versa, earthquakes are accompanied by electromagnetic radiation, i.e. these two phenomena are interrelated. This can also serve as a verification of the suggested hypothesis, as there are surges of electric charge (current), and the transition process (as we know) has a wider range than direct current.

5 Time jumps and killer waves

With the advent of new, more precise time measuring means, it was observed that sometimes the celestial (stellar) time flows changing relative to the reference atomic one in jumps*. How can this be explained but through the Earth being exposed to forces, turning it at a certain angle? We see no external forces of such a power, so we have internal ones left.

It is quite possible that, when running into an internal “roughness”, the core “pushes” the main body of the planet, altering astronomical time relative to the stable reference one.

Mariners now a natural phenomenon known as the “killer wave” (also known as periodic wave, monster wave, rogue wave, freak wave, onde scelerate, or galejade). Some ten to fifteen years ago, scientists believed that seafarers’ stories about giant killer waves that emerged from nowhere and took down ships were nothing but maritime folklore.

The existence of sea waves twenty to thirty meters high contradicts the laws of physics and does not fit into any mathematical model of formation of waves. It should be noted that these waves appear on relatively calm water surface. They can be a crest or a trough, single one or coming in a set.

The proposed hypothesis can logically explain the mechanism of their occurrence through the same interactions between the moving core and the internal irregularities of the planet’s body, which are carried over to the sea surface.

6 Causes of a dip appearing in the gravity graph during the Sun’s passage across the sky

Following the work with a new directional gravimeter, Evgeny Orlov presented some interesting data. As shown in his article [6], round-the-clock registration of gravimeter readings made it possible to determine the original geometrical shape of the solar gravitational signal (see Fig. 7).

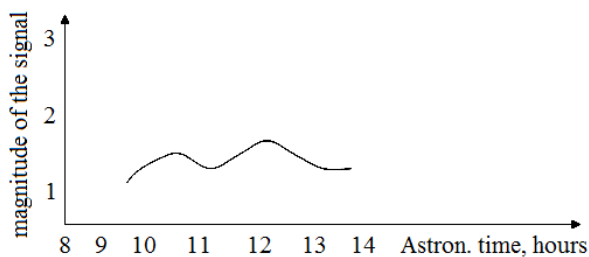


Fig. 7: The original geometrical shape of the solar gravitational signal as registered by Orlov [6].

It is registered in the daytime, in the form of double-humped curve with a dip in the range from 11 a.m. to 01 p.m., so the dip comes where the Sun would draw the load the hardest. The author of the article explains this by the fact that the volume of the gravitating mass of the planet facing the Sun on both sides of the planet exceeds the gravitating

mass at its center. However, in my opinion, it is determined by the fact that the hardest part of the core comes closer to the Earth’s surface and the distance to the measuring part of the gravimeter is reduced, thereby increasing the gravity to the Earth and compensating the gravity to the Sun.

7 On motion of the magnetic poles

It also turns out that the outer shell of the Earth is weakly related to the processes taking place between the planets causing appearance of a magnetic field, and therefore is “free” to move relative to the center of mass (it is similar to rotation of the outer rim of a bearing with internal one being fixed), while changing the position of the magnetic poles on the surface of the Earth, but without changing the position in space. At the same time, the position of the outer sphere of the Earth depends on the interaction strength of the core magnetic field and the magnetic properties of the sphere itself, which, among other things, may be affected by anthropogenic factors. A shift occurs before the mantle comes into one of the local stability points. It does not have to be a complete polarity reversal.

8 Conclusion

The suggested hypothesis is not loaded with mathematical calculations for yet for a number of reasons, including the following:

1. There are too many factors affecting the field;
2. One can always bring math under any theory by introducing correction factors and hiding the lack of physics of the phenomenon.

Of course, this hypothesis is presented in yet “unfledged” form and requires much to be done to verify and expand understanding of the physics of the processes.

Submitted on November 24, 2015 / Accepted on December 5, 2015

References

1. Iosilevskiy I.L. Plasma polarization in massive astrophysical objects. *Journal of Physics A: Mathematical and Theoretical*, 2009, v.42, 214008.
2. Iosilevskiy I.L. Plasma polarization in high gravity astrophysical objects. *Contrib. Plasma Phys.*, 2009, v. 49, no. 10, 755–759.
3. Malyskov Yu.P., Malyskov S.Yu. Periodic variations in geophysical fields and seismic activity, and their possible connection with motion of the Earth’s core. *Geology & Geophysics*, 2009, v. 50, no. 2, 152–172 (in Russian).
4. Chizhevsky A. Physical Factors of the Historical Process. *Cycles*, Special Issue, January 1971, 11–27.
5. Tkalčić H., Young M.K., Bodin T., Ngo S., and Sambridge M., The shuffling rotation of the Earth’s inner core. *Nature Geoscience*, 2013, v. 6, 497–502.
6. Orlov E.F. Experimental propagation speed of the gravitational interaction. Part 1. *Researches in Science*, May 2013, no. 5 (in Russian, accessed from <http://science.snauka.ru>)

*Please do not confuse it with a correction of calendar time.

Appendix. A short comparison of the planets' magnetic fields depending on the number of their moons and other properties

Planet	Moons	Magnetic field
Mercury	No	One percent of the Earth's field; of dipole-type, directed along the axis of rotation which is perpendicular to the orbit plane. Comment: The intensity of Mercury's magnetic field is 100 times smaller than that of the Earth. Mercury's magnetic field has a dipole structure and is highly symmetrical. Its axis is only two degrees tilted from the spin axis of the planet.
Venus	No	Almost absent: the planet's spin is very slow. Comment: Since the planet's own magnetic field is absent, it should be assumed that there is no motion of charged particles — electric current — in its iron core that could cause a magnetic field. Therefore, the core substance does not move.
Mars	2	The planet's magnetic field is 500 times weaker than the Earth's one. The field's polarity is reverse to that of the Earth. Phobos rises in the West and goes down in the East. Its size is very small. The influence of Deimos is weaker because of its remoteness. Comment: Mars has a magnetic field, but it is weak and extremely unstable. In various parts of the planet, its intensity may vary from 1.5 to 2 times. Its magnetic poles do not coincide with physical ones.
Jupiter	17 + ring	Twenty times as strong as the Earth's. The polarity is reverse to that of the Earth. Comment: Jupiter's moon system consists of at least 67 moons, including four large moons. Jupiter has a strong magnetic field. The dipole axis is tilted to the axis of rotation at 10°. Its polarity is reverse to the polarity of Earth's magnetic field. All the major moons of Jupiter rotate synchronously and always keep the same face turned to Jupiter due to the influence of powerful tidal forces of the giant planet. Jupiter's rotation speed is so high that the planet bulges along the equator.
Saturn	18 + ring	Almost equal to the Earth's and reverse in direction. Comment: By its strength, Saturn's magnetic field is in the middle between the magnetic field of the Earth and the more powerful field of Jupiter. The magnetic field is nearly a dipole, similar to that of the Earth, with north and south magnetic poles. The north magnetic pole is located in the northern hemisphere, and the south one is in the South, unlike Earth, where the location of the geographic poles is reverse to that of magnetic ones. Saturn has 62 known moons. Most of the moons, except Hyperion and Phoebe, spin synchronously — they always keep the same side turned to Saturn.
Uranus	21 + ring	Less than that of the Earth and has axial tilt at 60 degrees. The polarity is reverse to the Earth's. Uranus rotates reversely. The moons rotate reversely too. The moons' orbits are steeply tilted to the ecliptic. Comment: The equatorial plane of Uranus is tilted to the plane of its orbit at an angle of 97.86° — that is, the planet rotates "lying on its side." This gives the season changing process completely different from the other planets of the Solar System. If other planets may be compared to a spinning top, Uranus is more like a rolling ball. Uranus has a very specific magnetic field that is not directed from the geometric center of the planet, but is tilted towards the axis of rotation by 59 degrees. In fact, the magnetic dipole is shifted from the center to the south pole of the planet about one third of the planet's radius. This unusual geometry results in a very asymmetric magnetic field.
Neptune	8	A complex magnetic field Comment: Neptune resembles Uranus in its magnetosphere, with a magnetic field strongly tilted relative to its rotational axis at 47°. Neptune has 13 known moons. Triton is the largest Neptunian moon, comprising more than 99.5% of the mass in orbit around Neptune, and it is the only one massive enough to be spheroidal. Unlike all other large planetary moons in the Solar System, Triton has a retrograde orbit. It is close enough to Neptune to be locked into a synchronous rotation, and it is slowly spiraling inward because of tidal acceleration.

A Classical Model of the Photon

Shixing Weng

11 Metzack Dr., Brampton, Ontario L6Z 4N3, Canada
E-mail: wengs2015@gmail.com

A desired solution of the four-potential is presented for free-space photons, obtained with wave equations derived from the Maxwell equations and the Lorenz condition. The solution shows that an electromagnetic field in wave form propagating at the speed of light with a fixed internal phase may exist as a particle taking a limited space at a specific point of time. It reveals the existence of electric charge distributed as an electric capacitor on the parallel cylindrical surface of constant radius to the central axis of the solution. And the charge distribution has a phase change both in the azimuthal angle and along the direction of the wave propagation. The solution is applied to the case of a model photon to determine several parameter values of the solution, which in turn provides a view on the model photon.

1 Introduction

The year of 2015 has been the International Year of Light and Light-Based Technologies, designated by the United Nations Educational, Scientific, Cultural Organization (UNESCO). This designation further emphasizes the importance of light to people's life. As a part of the support for the designation, we present in this paper a theoretical model for the elements of light, photons, based on our knowledge of classical electrodynamics, classical mechanics and mathematical method for quantization rules.

In this paper we consider a single free photon in which photon-photon interactions [1] are neglected. A photon [2] is a quantum of light which is a wave form of the electromagnetic radiation and is characterized by its speed c and wavelength λ . It is known that a photon has both physical properties of wave and particle.

As a particle, the photon has a certain energy and momentum. In the study of the black body radiation [3], Max Planck proposed that the energy ϵ of a radiation oscillator was quantized and each energy was proportional to its vibrational frequency ν as

$$\epsilon = h\nu, \quad (1)$$

where h is the Planck constant. Then Einstein applied the idea to the light and proposed that light was made of quanta, inseparable entities, with the energy ϵ in terms of the frequency being given in Eq. (1), which successfully explained the photoelectric effect [4].

The Compton Scattering Experiment [5] further demonstrated that a photon had a certain energy as specified in Eq. (1) as well as a momentum in the direction of its motion. And the magnitude of the momentum p is given by

$$p = \frac{\epsilon}{c} = \frac{h\nu}{c} = \frac{h}{\lambda}, \quad (2)$$

where the relation $\nu = c/\lambda$ is used.

Furthermore it is known from quantum mechanics [6], that there is an angular momentum difference involved in the

magnitude of integral \hbar between the two transitional atomic states, where \hbar is the reduced Planck constant which equals to the Planck constant h divided by 2π . In the case of light emission this angular momentum difference may be transferred to the photon.

On the other hand the Young's two slit experiment [7] shows the wave property of light. In a typical Young's experiment one observes the interference pattern of light from a monochromatic light source of wavelength λ passing through two small-spaced parallel slits, which demonstrates the wave property of light.

It is also known that light is a form of the electromagnetic wave. In the electromagnetism [8], the set of Maxwell equations for vacuum gives relationships among the electric field \mathbf{E} , magnetic field \mathbf{B} , electric charge density ρ , and electric current density \mathbf{J} as following:

$$\nabla \cdot \mathbf{E} = \frac{\rho}{\epsilon_0}, \quad (3)$$

$$\nabla \cdot \mathbf{B} = 0, \quad (4)$$

$$\nabla \times \mathbf{E} + \frac{\partial \mathbf{B}}{\partial t} = 0, \quad (5)$$

$$\nabla \times \mathbf{B} - \frac{1}{c^2} \frac{\partial \mathbf{E}}{\partial t} = \mu_0 \mathbf{J}, \quad (6)$$

where ϵ_0 is the permittivity of vacuum and μ_0 is the permeability of vacuum; ∇ represents the differential operator and $\nabla = \hat{\mathbf{i}} \frac{\partial}{\partial x} + \hat{\mathbf{j}} \frac{\partial}{\partial y} + \hat{\mathbf{k}} \frac{\partial}{\partial z}$ in Cartesian coordinates with $\hat{\mathbf{i}}, \hat{\mathbf{j}}, \hat{\mathbf{k}}$ being unit vectors for the Cartesian coordinates; t represents the time and x, y, z are, respectively, the Cartesian components; the “ \times ” symbol represents the cross operation and the “ \cdot ” represents the dot operation. In this paper we use SI units. And for simplicity we shall consider in the following the medium to be vacuum. For vacuum where $\rho = 0$ and $\mathbf{J} = 0$, the following equations may be obtained for the electric field \mathbf{E} and the magnetic field \mathbf{B} from Eqs. (3) to (6),

$$\frac{1}{c^2} \frac{\partial^2 \mathbf{E}}{\partial t^2} - \nabla^2 \mathbf{E} = 0, \quad (7)$$

$$\frac{1}{c^2} \frac{\partial^2 \mathbf{B}}{\partial t^2} - \nabla^2 \mathbf{B} = 0, \quad (8)$$

where c is the speed of light, which is equal to $1/\sqrt{\epsilon_0\mu_0}$ for vacuum, and ∇^2 is the Laplacian operator. Eqs. (7) and (8) are wave equations with the propagation speed equal to the speed of light, which shows the light to be a form of the electromagnetic wave. But we believe that the achieved solution from Eqs. (7) and (8) so far for free-space photon is limited to one-dimension and our current view on the photon is limited.

As we know that an electric field or a magnetic field has energy. And the total energy density η is equal to the sum of the electric field energy density η_E and the magnetic field energy density η_B and is given by

$$\eta = \eta_E + \eta_B = \frac{1}{2} \epsilon_0 |\mathbf{E}|^2 + \frac{1}{2\mu_0} |\mathbf{B}|^2, \quad (9)$$

where $|\mathbf{E}|$ is the magnitude of the electric field and $|\mathbf{B}|$ the magnitude of the magnetic field.

The Poynting vector \mathbf{S} , which is the energy current density of the electromagnetic wave, is given by

$$\mathbf{S} = \frac{1}{\mu_0} \mathbf{E} \times \mathbf{B}. \quad (10)$$

The Poynting vector is perpendicular to both \mathbf{E} and \mathbf{B} vectors and is in the direction of the thumb while using the right-hand-rule turning fingers from \mathbf{E} to \mathbf{B} .

Both the electric field \mathbf{E} and the magnetic field \mathbf{B} can be expressed in terms of the four-potential, a scalar electric potential ψ plus a magnetic vector potential \mathbf{A} as following,

$$\mathbf{B} = \nabla \times \mathbf{A}, \quad (11)$$

$$\mathbf{E} = -\nabla\psi - \frac{\partial \mathbf{A}}{\partial t}. \quad (12)$$

The Lorenz condition [9], named after the Danish mathematician and physicist, L. V. Lorenz, provides a covariant form of the four-potential and is given by

$$\nabla \cdot \mathbf{A} + \frac{1}{c^2} \frac{\partial \psi}{\partial t} = 0. \quad (13)$$

Eq. (13) appears similar to the continuity equation and may represent a ‘‘local form’’ of the conservation of electric potential energy for a point charge in the electromagnetic field. With the Lorenz condition, both the scalar potential ψ and the vector potential \mathbf{A} satisfy the following equations, respectively,

$$\frac{1}{c^2} \frac{\partial^2 \psi}{\partial t^2} - \nabla^2 \psi = \frac{\rho}{\epsilon_0}, \quad (14)$$

$$\frac{1}{c^2} \frac{\partial^2 \mathbf{A}}{\partial t^2} - \nabla^2 \mathbf{A} = \mu_0 \mathbf{J}. \quad (15)$$

The purpose of the paper is to present a model view of the photon by obtaining a three-dimensional solution from

Eqs. (14) and (15) for vacuum without external electric charge nor external electric current. The three-dimensional solution hence is theoretical analyzed to reveal its physics meaning. It is finally applied to the case of a model photon to gain a deep insight into the photon, which is new since we are not aware of such a report in the literatures.

This paper is organized as these: Introduction, Solution, Discussions, and Conclusion. The Introduction section provides a brief overview on our fundamental understandings of light and photon. In the Solution section, two expressions of the four-potential as a solution for three-dimensional space are presented, which are obtained from Eqs. (14) and (15) for vacuum without external electric charge nor external electric current. The characteristic of the solution shows that its quantities are in limited space at a specific point of time, which is desirable for photons. In the Discussions section, expressions for the electric field and the magnetic field are derived from the four-potential solution. An analysis of the electric field reveals the existence of electric charge distributed on the parallel cylindrical surface of constant radius to the central axis of the solution. The solution then is applied to the case of a model photon to determine the constant parameter values of the solution from physical quantities of the photon, which in turn provides a view on the model photon. The Conclusion section provides a brief summary of the paper together with some comments.

2 Solution

In vacuum where electric charge density $\rho = 0$ and electric current density $\mathbf{J} = 0$, Eqs. (14) and (15) are reduced respectively to

$$\frac{1}{c^2} \frac{\partial^2 \psi}{\partial t^2} - \nabla^2 \psi = 0, \quad (16)$$

$$\frac{1}{c^2} \frac{\partial^2 \mathbf{A}}{\partial t^2} - \nabla^2 \mathbf{A} = 0. \quad (17)$$

Eqs. (16) and (17) are wave equations and their solutions for one-dimensional space are easily obtained and are known as a traveling wave,

$$\psi = \psi_0 \sin(kx - \omega t), \quad (18)$$

$$A = A_0 \sin(kx - \omega t), \quad (19)$$

where ψ_0 represents the amplitude of the scalar potential, A_0 the amplitude of the vector potential, ω is the angular frequency which equals to $2\pi\nu$ and ν is the wave frequency, and k is the wavenumber and $k = \omega/c = 2\pi/\lambda$. The reason to choose the sine function instead of the cosine function here is arbitrary, but with no difference, since the sine and cosine functions are different by a phase difference of $\pi/2$, they may represent the same physical wave. Also as we know that the electric potential is a measurable quantity which is real, we shall restrict the solution to the real number domain in this paper.

In the following, Eqs. (16) and (17) are solved for three-dimensional space to reveal more features of the solution. First we choose the circular cylindrical coordinates (or cylindrical polar coordinates) as in Fig. 1 for our coordinate system [10]. Here we use the r symbol to represent the polar axis since the ρ symbol is used for the electric charge density. And ϕ represents the azimuthal angle and z represents the central axis and is the same as the Cartesian z axis. Their respective unit vectors are $\hat{\mathbf{r}}$, $\hat{\phi}$, and $\hat{\mathbf{z}}$ as in Fig. 1.

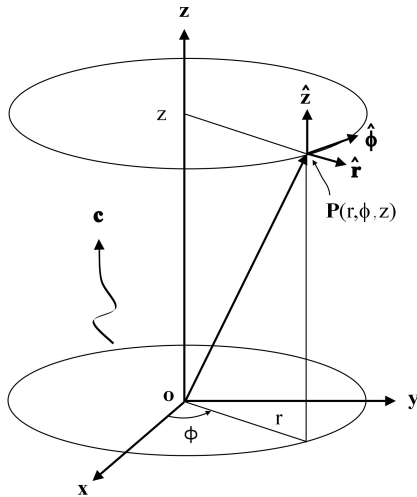


Fig. 1: A drawing of the circular cylindrical coordinate system with respect to the Cartesian coordinates, where $\hat{\mathbf{r}}$, $\hat{\phi}$, and $\hat{\mathbf{z}}$ are unit vectors for the coordinate system. The wave symbol represents a photon moving in the direction of the positive z axis at the speed of light c .

The Laplacian operator ∇^2 in the cylindrical coordinates is expressed as

$$\nabla^2 = \frac{1}{r} \frac{\partial}{\partial r} \left(r \frac{\partial}{\partial r} \right) + \frac{1}{r^2} \frac{\partial^2}{\partial \phi^2} + \frac{\partial^2}{\partial z^2}, \quad (20)$$

and hence we get a solution of the four-potential from Eqs. (16) and (17) as following

$$\psi = \psi_0 \sin(kz + m\phi - \omega t) \begin{cases} \left(\frac{r}{r_0}\right)^m & r < r_0, \\ \left(\frac{r_0}{r}\right)^m & r > r_0, \end{cases} \quad (21)$$

$$\mathbf{A} = \hat{\mathbf{z}} A_0 \sin(kz + m\phi - \omega t) \begin{cases} \left(\frac{r}{r_0}\right)^m & r < r_0, \\ \left(\frac{r_0}{r}\right)^m & r > r_0, \end{cases} \quad (22)$$

where we choose the wave to propagate along the positive z axis, ψ_0 is a strength constant for the scalar potential and A_0 is a strength constant for the vector potential whose direction is in that of the wave propagation, r_0 is a constant polar radius to be determined in the next section by the wavelength

of the photon, m is a positive integer to satisfy the 2π periodic boundary condition of the azimuthal angle. Here m is a quantum number which may be associated with the angular momentum of the wave. Again the choice of the sine function instead of the cosine function here is arbitrary but has no physics difference. The solution at r_0 is not defined but has finite quantities. r_0 is a boundary of the solution and in the following treatment we shall let the boundary thickness to approach to zero so the solution is approximately defined at r_0 .

Eqs. (21) and (22) represent a traveling wave propagating along the positive z axis. The solution by the two expressions is desirable since its quantities are limited in the polar axis. It is worthwhile to mention that this solution may be for individual photons free from interactions with each other. The study of photon interactions is out of the scope of this paper. In the following section we will analyze the solution to reveal its physics meaning.

3 Discussions

Applying the Lorenz condition, Eq. (13), to Eqs. (21) and (22), we have

$$A_0 = \frac{\psi_0}{c}. \quad (23)$$

Hence the vector potential and the scalar potential are related to each other, only one of them is independent.

Now applying Eqs. (11) and (12) to the solution Eqs. (21) and (22) and using Eq. (23), we may have for the electric field \mathbf{E} and the magnetic field \mathbf{B} as following:

$$\mathbf{E} = -m\psi_0 \begin{cases} \left(\frac{r^{m-1}}{r_0^m}\right) \left(\hat{\mathbf{r}} \sin(kz + m\phi - \omega t) + \hat{\phi} \cos(kz + m\phi - \omega t) \right) & r < r_0, \\ \left(\frac{r_0^m}{r^{m+1}}\right) \left(-\hat{\mathbf{r}} \sin(kz + m\phi - \omega t) + \hat{\phi} \cos(kz + m\phi - \omega t) \right) & r > r_0, \end{cases} \quad (24)$$

$$\mathbf{B} = mA_0 \begin{cases} \left(\frac{r^{m-1}}{r_0^m}\right) \left(\hat{\mathbf{r}} \cos(kz + m\phi - \omega t) - \hat{\phi} \sin(kz + m\phi - \omega t) \right) & r < r_0, \\ \left(\frac{r_0^m}{r^{m+1}}\right) \left(\hat{\mathbf{r}} \cos(kz + m\phi - \omega t) + \hat{\phi} \sin(kz + m\phi - \omega t) \right) & r > r_0, \end{cases} \quad (25)$$

where $\hat{\mathbf{r}}$ is the unit vector for the polar axis, $\hat{\phi}$ is the unit vector for the azimuthal angle. From Eqs. (24) and (25) we know that both the electric field \mathbf{E} and the magnetic field \mathbf{B} are traveling in the direction of the positive z axis and are perpendicular to the direction of the wave propagation. Furthermore we have $\mathbf{E} \cdot \mathbf{B} = 0$, meaning that the electric field and the magnetic field are perpendicular to each other, which is consistent with the basic electromagnetic theory for free-space.

For better understanding of the fields, in the following discussions we shall restrict ourself to the case of the angular momentum number $m = 1$, which may correspond to the case of the photon we know. For general case of $m > 1$, following treatments are similarly applicable. Hence Eqs. (24) and (25) become

$$\mathbf{E} = -\psi_0 \begin{cases} \frac{1}{r_0} \left(\hat{\mathbf{r}} \sin(kz + \phi - \omega t) + \hat{\phi} \cos(kz + \phi - \omega t) \right) & r < r_0, \\ \frac{r_0}{r^2} \left(-\hat{\mathbf{r}} \sin(kz + \phi - \omega t) + \hat{\phi} \cos(kz + \phi - \omega t) \right) & r > r_0, \end{cases} \quad (26)$$

$$\mathbf{B} = A_0 \begin{cases} \frac{1}{r_0} \left(\hat{\mathbf{r}} \cos(kz + m\phi - \omega t) - \hat{\phi} \sin(kz + m\phi - \omega t) \right) & r < r_0, \\ \frac{r_0}{r^2} \left(\hat{\mathbf{r}} \cos(kz + m\phi - \omega t) + \hat{\phi} \sin(kz + m\phi - \omega t) \right) & r > r_0. \end{cases} \quad (27)$$

From Eqs. (26) and (27), for $r > r_0$ both field strengths are inversely proportional to r^2 and approach to zero as r goes to infinity, which is a desirable result because a photon takes a limited space at a specific point of time. The electric field \mathbf{E} at r_0 , or on the parallel cylindrical surface in a three-dimensional view, is not continue in the radial direction, meaning charge may exist on the surface. To derive an expression for the surface charge density σ , apply Eq. (3) to Eq. (26), we have

$$\sigma = 2\epsilon_0\psi_0 \frac{1}{r_0} \sin(kz + \phi - \omega t). \quad (28)$$

Hence the charge density is also in the form of a traveling wave, moving uniformly in the direction of the positive z axis with a fixed internal phase both in the azimuthal angle and along the z axis.

To get a precise sense of the fields and charge distribution, we simplify Eqs. (26), (27), and (28) by letting $z = 0$, and $t = 0$, which allows us to better understand the solution at the specific point of time and space. And hence we have

$$\mathbf{E} = \psi_0 \begin{cases} -\frac{1}{r_0} \hat{\mathbf{j}} & r < r_0, \\ \frac{r_0}{r^2} \left(\hat{\mathbf{i}} \sin(2\phi) - \hat{\mathbf{j}} \cos(2\phi) \right) & r > r_0, \end{cases} \quad (29)$$

$$\mathbf{B} = A_0 \begin{cases} \frac{1}{r_0} \hat{\mathbf{i}} & r < r_0, \\ \frac{r_0}{r^2} \left(\hat{\mathbf{i}} \cos(2\phi) + \hat{\mathbf{j}} \sin(2\phi) \right) & r > r_0, \end{cases} \quad (30)$$

and

$$\sigma = 2\epsilon_0\psi_0 \frac{1}{r_0} \sin \phi, \quad (31)$$

where $\hat{\mathbf{i}}$ is the unit vector for the x axis and $\hat{\mathbf{j}}$ is the unit vector for the y axis. In deriving Eqs. (29) and (30), we use the following relations for unit vector transformations between the polar and Cartesian coordinates

$$\hat{\mathbf{r}} = \hat{\mathbf{i}} \cos \phi + \hat{\mathbf{j}} \sin \phi, \quad (32)$$

$$\hat{\phi} = -\hat{\mathbf{i}} \sin \phi + \hat{\mathbf{j}} \cos \phi. \quad (33)$$

The electric field \mathbf{E} , magnetic field \mathbf{B} , and the surface charge density σ at $z = 0$ and $t = 0$ are shown in Fig. 2.

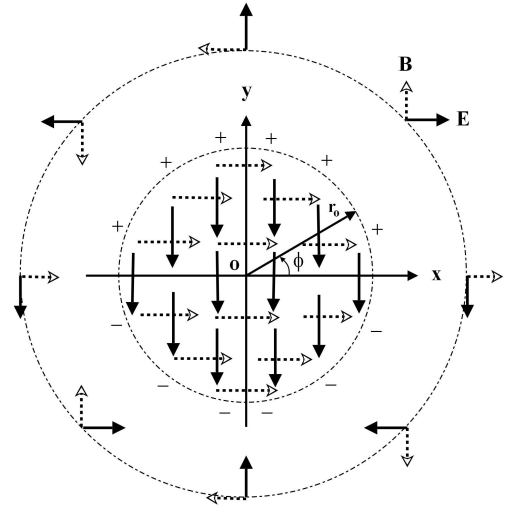


Fig. 2: A schematic diagram of the electric field \mathbf{E} (solid lines), magnetic field \mathbf{B} (dash lines), and charge distribution (“+” for positive charge and “-” for negative charge) on an imaging cylindrical surface ($r = r_0$) of the solution in the x - y plane, where $z = 0, t = 0$. The wave is propagating along the positive z axis (pointing out of the x - y plane). r_0 is the constant radius, and ϕ is the azimuthal angle.

As we know from Eqs. (29) and (30), both the electric field \mathbf{E} and the magnetic field \mathbf{B} are constant inside of the circle r_0 ; For outside of the r_0 both fields decreases as the radius squared, r^2 , increases, and the field direction changes two times as fast as the azimuthal angle ϕ (Fig. 2). The distribution of the surface charge density σ is described by the sine function of the azimuthal angle, and the total charge by the r_0 circle is zero. Referring to Fig. 2, the charge distribution is polarized, i.e., the positive charge on its corresponding half-circle at r_0 is distributed symmetrically to the negative charge on the other half-circle, or vice versa. The total charge distribution appears as an electric capacitor made of circularly distributed electric dipoles.

In the following discussions we apply the solution to a model photon and shall use the physical quantities of the photon to determine the values of the constants used in the solution.

For $z \neq 0$ and $t = 0$ the electric field \mathbf{E} , the magnetic field \mathbf{B} and the surface electric charge density σ are distributed around the central axis z with a certain phase. And the phase

change depends on both the azimuthal angle ϕ and the z axis. We show the charge distribution for $z < 0$ and $t = 0$ in Fig. 3.

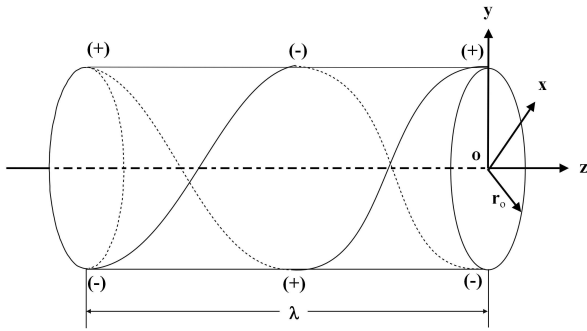


Fig. 3: A schematic diagram showing the surface charge distribution (“+” for positive charge and “-” for negative charge) on the surface of $r = r_0$ in the z axis direction for one wavelength λ , where $t = 0$, the model photon is moving along the positive z axis at the speed of light c and r_0 is the constant radius. For clarity we only show two lines of charges here.

The charge distribution appears as a circularly distributed electric dipole “twisted” in the azimuthal angle and along the z axis. The twisting phase change is exactly the same as that of the photon (one cycle of the charge phase change by one wavelength λ). The model photon picture in Fig. 3 represents a “frozen” view at $t = 0$. For $t \neq 0$, by the phase analysis of the sine wave (Eq. (28)), the model photon is doing a displacement along the positive z without changing its internal phase. Now imagining that if we place an observer facing the incoming photon at a fixed z position, it may see the circularly distributed charge rotating counter-clockwise (in the direction of the azimuthal angle) around the photon’s central axis. Since this rotation represents a certain angular momentum, the photon may carry an angular momentum in the phase of the charge distribution.

In the following we shall assume that the length of the model photon, l , equals to $n\lambda$, where n is a positive integer to satisfy the periodic condition in the propagation direction. Here n may be considered as a quantum number and its minimum value is one, which makes a minimum complete cycle.

Now applying Eq. (23) to Eqs. (26) and (27), we find that the electric field energy density $\eta_{\mathbf{E}}$ and the magnetic field energy density $\eta_{\mathbf{B}}$ (Eq. (9)) are equal to each other for the photon. And we have the total energy density η as following

$$\eta = \epsilon_0 |\mathbf{E}|^2 = \epsilon_0 \psi_0^2 \begin{cases} \frac{1}{r_0^2} & r < r_0, \\ \frac{r_0^2}{r^4} & r > r_0, \end{cases} \quad (34)$$

where $|\mathbf{E}|$ is the magnitude of the electric field. The energy density is constant for $r < r_0$ and is inversely proportional to r^4 for $r > r_0$. The photon energy (Eq. (1)) may be equal to the integration value of Eq. (34) in the photon space at time

$t = 0$. The integration path for r is 0 to r_0 and r_0 to ∞ , for z is $-n\lambda$ to 0, and for ϕ is 0 to 2π . And hence we find the ψ_0 to have the following relationship

$$\psi_0 = \sqrt{\frac{\hbar c}{\epsilon_0 n}} \frac{1}{\lambda}. \quad (35)$$

In deriving Eq. (35) we used Eq. (1). It is interesting to note that the potential strength constant, ψ_0 , is inversely proportional to the wavelength λ .

By using Eqs. (10), (26), and (27), the Poynting vector is

$$\mathbf{S} = \hat{\mathbf{z}} \frac{\psi_0 A_0}{\mu_0} \begin{cases} \frac{1}{r_0^2} & r < r_0, \\ \frac{r_0^2}{r^4} & r > r_0. \end{cases} \quad (36)$$

According to Eq. (36), the photon energy flows in the direction of the positive z axis, which is consistent with the photon direction of motion. The total energy by the Poynting vector for the photon is $h\nu$, which may be calculated by integrating out the Poynting vector, Eq. (36), for the photon and using Eqs. (23) and (35). This is an expected result.

Since the charge is distributed in the r_0 cylindrical surface, which generates a surface electric current by the displacement of the photon at the speed of light, the density of the photon self energy may also be expressed in the following relationship,

$$\eta' = \frac{1}{2} \sigma \psi + \frac{1}{2} \mathbf{A} \cdot \mathbf{J}', \quad (37)$$

where η' represents the surface energy density, σ the surface charge density, ψ the electric potential, \mathbf{A} the vector potential, and \mathbf{J}' represents the surface electric current density. For the photon, $\mathbf{A} \cdot \mathbf{J}' = AJ'$ and $J' = \sigma c$, the second term is equal to the first term on the right hand side of Eq. (37) and we have.

$$\eta' = \sigma \psi. \quad (38)$$

Using Eqs. (28), (21) for $m = 1$, and (35), we may calculate the photon energy ϵ by integrating out Eq. (38) on the r_0 cylindrical surface of length $n\lambda$,

$$\begin{aligned} \epsilon &= \int_{-n\lambda}^0 \int_0^{2\pi} \eta' dS = \int_{-n\lambda}^0 dz \int_0^{2\pi} \sigma \psi r_0 d\phi \\ &= \int_{-n\lambda}^0 dz \int_0^{2\pi} 2\epsilon_0 \psi_0^2 \sin^2(kz + \phi) d\phi \\ &= \int_{-n\lambda}^0 dz \int_{kz}^{kz+2\pi} 2\epsilon_0 \psi_0^2 \sin^2(\phi') d\phi' \\ &= n\lambda 2\epsilon_0 \psi_0^2 \pi = h\nu, \end{aligned} \quad (39)$$

where dS represents an infinite small area on the r_0 cylindrical surface, the time $t = 0$, and a variable change, $kz + \phi = \phi'$. Hence we get that the energy is $h\nu$. This result indicates that

it is equivalent to consider the photon energy being stored in the r_0 cylindrical surface.

Now we evaluate the value of the constant length of the polar radius, r_0 , of the model photon. We first assume that r_0 is proportional to the wavelength λ as

$$r_0 = \frac{\lambda}{2\pi}. \quad (40)$$

Then we support it by two reasons. The first reason is that with this assumption the phase velocity of the charge distribution on the r_0 cylindrical surface is equal to the speed of light c , i.e., $\omega r_0 = 2\pi\nu\lambda/2\pi = \nu\lambda = c$. This is consistent with the nature of the photon. This velocity may be physically experienced by an electron in an atom as in light absorption.

The second reason is that the angular momentum carried by the photon is \hbar , which is consistent with the angular momentum number $m = 1$. To evaluate the angular momentum, we use following expression

$$d\mathbf{J} = \mathbf{r}_0 \times d\mathbf{P}, \quad (41)$$

where we consider the angular momentum to be generated in the r_0 cylindrical surface, $d\mathbf{J}$ represents an infinite small quantity of angular momentum, $d\mathbf{P}$ represents an infinite small quantity of momentum in the cylindrical surface, and \mathbf{r}_0 is the polar radius vector pointing to the cylindrical surface where the small momentum is considered. Referring to Fig. 3, an observer like an electron in an atom may experience a rotational force from the photon, which corresponds to a momentum in the direction of the azimuthal angle ϕ . This momentum may generate an angular momentum in the direction of the positive z axis.

Similar to Eq. (2), the magnitude of the infinite small quantity of momentum dP may be written as

$$dP = \frac{d\epsilon}{c}, \quad (42)$$

where $d\epsilon$ represents an infinite small amount of energy in the cylindrical surface and c is the speed of light. Using Eq. (38), we have for the $d\epsilon$,

$$d\epsilon = \eta' dS = \sigma\psi dS, \quad (43)$$

where dS represents an infinite small area on the r_0 cylindrical surface. And finally we have for the magnitude of the infinite small quantity of the angular momentum dJ as

$$dJ = \frac{r_0}{c} \sigma\psi dS, \quad (44)$$

where r_0 is given in Eq. (40). The direction of the angular momentum is in the positive z axis.

By integrating out Eq. (44) for the photon on the r_0 cylindrical surface at the time $t = 0$, as has been done in Eq. (39), we get that the total angular momentum of the photon is indeed \hbar . Hence from the second reasoning we prove that the constant radius r_0 of the photon cylindrical surface is $\lambda/2\pi$.

This angular momentum, derived from the classical mechanics, may be considered as the spin angular momentum of the photon since it is generated by the self-rotation around its central axis.

Now based on the solution of Eqs. (21) and (22), we have built a consistent three-dimensional model of the photon: a quantized electromagnetic wave of length $n\lambda$ with a charged cylindrical surface core of radius $\lambda/2\pi$. Such a model may be tested for it is expected that the photon is very hard to pass a pinhole of radius less than $\lambda/2\pi$.

4 Conclusion

Conclusion by summarizing what have been presented in the paper. First a desirable solution was shown in terms of the two expressions, Eqs. (21) and (22), for the four-potential, obtained from wave Eqs. (16) and (17) derived by using the Maxwell equations together with the Lorenz condition. Although we assumed the medium to be vacuum in the solution for simplicity, our solution may be extended to the case of a homogeneous medium by using the medium parameters of the permittivity, permeability, and the speed of light. Also for clarity we limited our consideration in the Discussions section to the case of $\phi \geq 0$ and $t \geq 0$, but the solution itself is equally applicable if we substitute ϕ by $-\phi$ or t by $-t$. In the case of ϕ , the \pm signs respectively may represent the right or left spin state of the photon.

Then the solution was analyzed for understanding its characteristics, which showed that an electromagnetic field in isolated wave form at the speed of light might exist in a limited space at a specific point of time. The solution requires the existence on the r_0 cylindrical surface of electric charge distributed in certain phase with the azimuthal angle ϕ and along the direction of the light propagation. The solution was specifically studied for the case of the angular momentum number $m = 1$.

We then applied the solution to the case of a model photon and determined the constant values of the solution in terms of the photon quantities. By doing that, a detailed theoretical three-dimensional model of the photon was achieved. We showed that the angular momentum of the photon might be considered as coded in the r_0 cylindrical surface by the phase of the charge distribution.

Notice that we have solved a special case of Eqs. (16) and (17) by restricting the angular momentum of the photon in the direction of the light propagation. Furthermore, the length of the photon was assumed to be $n\lambda$, but the upper bound of n was not determined specifically.

Finally it is theoretically interesting to mention that by letting the angular momentum number $m > 1$ in the solution, which could correspond to a photon with spin larger than one, we may get similar results as the spin one photon in terms of the wave taking a limited space at a specific point of time.

Acknowledgements

The author would like to express his thanks to all teachers for his education up to the post-doctoral position. Helpful discussions with Dr Wing-Ki Liu are acknowledged.

Submitted on November 10, 2015 / Accepted on December 7, 2015

References

1. Glauber R.J. The quantum theory of optical coherence, *Physical Review*, 1963, v. 130(6), 2529.
2. Kragh H. Photon: New light on an old name. arXiv:1401.0293.
3. Planck M. *Verhandl. Dtsch. Phys. Ges.*, Berlin, 1900, v. 2, 237. (English translation: Planck M. On the theory of the energy distribution law of the normal spectrum. In: *The Old Quantum Theory*, ed. by D. ter Haar, Pergamon Press, 1967, 82.)
4. Einstein A. *Annalen der Physik* (in German), 1905, v. 17(6), 132. (English translation: Einstein A. On a heuristic point of view concerning the production and translation of light. In: *The Swiss Years: Writings, 1900–1909*, v. 2, 86.)
5. Compton A.H. A quantum theory of the scattering of X-rays by light elements. *Physical Review*, 1923, v. 21 (5), 483.
6. For example: Davydov A.S. *Quantum Mechanics*. 2nd ed., Translated by D. Ter Haar, Pergamon Press, New York, 1988, p. 22.
7. For example: Kenyon I.R. *The Light Fantastic*. Oxford University Press, New York, 2008.
8. For example: Jackson J.D. *Classical Electrodynamics*. 3rd ed., John Wiley & Sons Inc., New York, 1999.
9. Lorenz L. V. On the identity of the vibrations of light with electrical currents. *Philos. Mag.*, Ser 3, 1867, v. 34, 287.
10. Arfken G. *Mathematical Methods for Physicists*, 3rd Ed., Academic Press, Inc., New York, 1985, 95.

Update on Pluto and Its 5 Moons Obeying the Quantization of Angular Momentum per Unit Mass Constraint of Quantum Celestial Mechanics

Franklin Potter

Sciencegems.com, 8642 Marvale Drive, Huntington Beach, CA 92646 USA
E-mail: frank11hb@yahoo.com

In July, 2015, the New Horizons spacecraft passing by Pluto did not discover any more moons. Therefore, we know the Pluto system total angular momentum to within 2.4%, more accurately than any other system with more than two orbiting bodies. We therefore update our previous analysis to determine whether a definitive test of the quantum celestial mechanics (QCM) angular momentum constraint can now be achieved.

1 Introduction

In 2012 we analyzed the angular momentum properties of the Pluto system with its 5 moons [1] not knowing the total angular momentum in the system. The New Horizons spacecraft passing by Pluto and its large moon Charon in July, 2015, did not discover any more moons than its earlier discovery of 4 additional tiny moons. Therefore, the Pluto system that we know is the final configuration of orbiting bodies, so we now know its total angular momentum to within 3%. Consequently, we can consider this gravitationally bound system as a possible definitive test of the theory called quantum celestial mechanics (QCM) first proposed in 2003 by H. G. Preston and F. Potter [2].

They derived a new gravitational wave equation from the general relativistic Hamilton-Jacobi equation for a test particle of mass μ as given by Landau and Lifshitz:

$$g^{\alpha\beta} \frac{\partial S}{\partial x^\alpha} \frac{\partial S}{\partial x^\beta} - \mu^2 c^2 = 0, \quad (1)$$

where $g^{\alpha\beta}$ is the metric of the general theory of relativity (GTR) and S is the action. This general relativistic Hamilton-Jacobi equation becomes a scalar wave equation via the transformation to eliminate the squared first derivative, i.e., by defining the wave function $\Psi(q, p, t)$ of position q , momentum p , and time t as

$$\Psi = e^{iS'/H} \quad (2)$$

with $S' = S/\mu c$. The H is defined as the Preston distance characterizing the specific gravitational system and is a function of *only two physical parameters* of the system

$$H = \frac{L_T}{M_T c}, \quad (3)$$

where M_T is the total mass of the system and L_T its total angular momentum. Only these two parameters of the system are required to define all the stable quantization states of the gravitationally bound system. We call the resulting theory quantum celestial mechanics or QCM.

The end result of the transformation is the new scalar "gravitational wave equation" (GWE)

$$g^{\alpha\beta} \frac{\partial^2 \Psi}{\partial x^\alpha \partial x^\beta} + \frac{\Psi}{H^2} = 0. \quad (4)$$

One can now consider the behavior of the test particle in different gravitational metrics. In the Schwarzschild metric, we find good agreement with predictions for all systems to which the QCM constraints have been applied.

There have been numerous applications of QCM to gravitationally bound systems, including multi-planetary exosystems [3], the Solar System [2], the five moons of Pluto [1], the S-stars at the galactic center [4], and circumbinary systems [5, 6] with planets. All these systems have been shown to obey the quantization of angular momentum per unit mass constraint dictated by QCM in the Schwarzschild metric approximation for each orbiting body μ_i , i.e.,

$$\frac{L_i}{\mu_i} = m_i c H. \quad (5)$$

Of course, one assumes that the body in consideration has been in an equilibrium orbit for at least tens of millions of years. Then if one knows the semi-major axis r , the eccentricity e , and the period of orbit, the QCM value for L_i in the specific equilibrium orbit equals the Newtonian value $L = \mu \sqrt{GM_T r (1 - e^2)}$. The value of M_T is nearly the central body mass for most cases.

Knowing the period of orbit is an additional constraint that allows one to determine a set of integers m for the QCM angular momentum per unit mass linear regression fit, with $R^2 > 0.999$, which we seek in all cases. Moreover, if one knows the total angular momentum for the gravitationally bound system, then a unique set of m values is possible. However, if the system total angular momentum is unknown, then several sets of integers could meet the linear regression fit, in which case we will accept the set beginning with the smallest integer.

From the slope of the resulting plot of $L/\mu c$ vs. m for all

the known orbiting bodies in the system, one can calculate the predicted QCM total system angular momentum L_T and therefore can predict whether additional mass orbiting the star is needed to account for this total angular momentum value. Many m values for the gravitationally bound system will be unoccupied, for the occupancy of the specific QCM orbits depends upon the history of formation and the subsequent evolution of the planetary system.

For simplicity, applications have concentrated on circular or near-circular orbits only. Whereas in GTR and its Newtonian approximation all allowed circular or nearly-circular orbits about a massive central object are equilibrium orbits, QCM dictates that only a subset of these equilibrium orbits are permitted by the quantization of angular momentum per unit mass constraint.

With any new theory, one needs a definitive test. Until now there has been no laboratory test of QCM. Finding a convincing, definitive test for QCM has not been successful. As of this date, the satellites of Pluto actually offer the best test of QCM and its quantization of angular momentum per unit mass prediction. Why? Because the total angular momentum of the Pluto-Charon system with its 4 tiny moons is well-known now to within 2.4%.

One would expect that the Solar System as a whole or the many satellites of the Jovian planets would be a better test. However, one does not know the total angular momentum to within 10% of either the Solar System or each of the Jovian planets. The Jovian planets themselves dominate the angular momentum contributions in their systems but their internal differential rotations lead to large uncertainties in their total angular momentum.

And, unfortunately, we do not know the total angular momentum of the Solar System to within 10%. Why not? Because the Oort Cloud dominates the Solar System angular momentum [7], providing about 50 times the total angular momentum contribution from the Sun and the planets! The total mass of the Oort Cloud is unknown but can be estimated by assuming perhaps 100 Earth masses of ice chunks at more than 40,000 AU. The dominance of the Oort Cloud can be verified by estimating the Newtonian value of its angular momentum.

Although we have determined excellent linear regression fits to all planetary-like systems by the QCM angular momentum constraint, there remain two limitations of the fits: (1) they are not unique and (2) all integers are candidates for m , i.e., there being no upper limit. For example, even with a linear regression fit $R^2 = 1.000$ for the set of m values 3, 5, 8, 14, 17, for a 5 planet system, the set of double values 6, 10, 16, 28, 34, fits equally well. The slope of the graph of $L/\mu c$ versus m is used to predict the total angular momentum of the system, the former set predicting twice the angular momentum. However, if one knows the total system angular momentum value, such as we do now for the Pluto system, then the set of m values is unique.

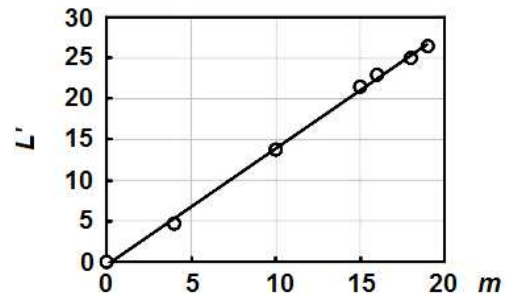


Fig. 1: The Pluto System fit to QCM.

	$r \times 10^6$ m	Period (d)	m	P_2/P_1	$(n_2/n_1)^3$
Pluto	2.035	6.38723	4		
Charon	17.536	6.38723	10	1	1
Styx	42.656	20.16155	15	3.156	3.077
Nix	48.694	24.85463	16	3.891	3.691
Kerberos	57.783	32.16756	18	5.036	5.153
Hydra	64.738	38.20177	19	5.981	6.011

Table 1: Pluto system orbital parameters and QCM m values.

2 Pluto and its 5 moons

Will a *random* set of orbital distances fit the QCM angular momentum quantization constraint? Yes, because there is no upper limit to the integers available for the m values. One can always fit the constraint using very large integers! This possibility is eliminated when the total angular momentum is known. If one uses this random set of orbital distances with a specific mass for the central star but the other masses are unknown, the system obeys Newton's law of universal gravitation and the angular momentum *per unit mass* is known but the unique set of integer values for m cannot be achieved.

The New Horizons spacecraft passing Pluto in July, 2015, did not discover any more moons. The Pluto satellite system [8] has five moons, Charon, Styx, Nix, Kerberos, and Hydra, which are nearly in a 1:3:4:5:6 resonance condition! The orbital behavior of the five moons is considered by using distances from the Pluto-Charon barycenter. The important physical parameters of the Pluto system satellites are given in Table 1. The orbits are very close to circular.

The system total mass is essentially the combined mass of Pluto (13.05×10^{21} kg) and Charon (1.52×10^{21} kg). The QCM values of m in the fourth column were determined by the linear regression fit ($R^2 = 0.998$) to the angular momentum quantization per mass equation as shown in Figure 1 with $L' = L/\mu c$ plotted against m with resulting slope $H = 1.43$ meters. The uncertainty bars are within the circles. Our previous fit [1] of these Pluto moons proposed the m values 2, 6, 9, 10, 11, 12, with $R^2 = 0.998$ also.

This new value of H produces a total angular momentum value $L_T = 6.28 \times 10^{30}$ kg m²/s that is commensurate with the total angular momentum of $6.26(\pm 0.14) \times 10^{30}$ kg m²/s for the

known Pluto system when both orbital and rotational angular momentum are included.

In QCM the predicted period ratios for the orbital resonance conditions in the last column of Table 1 are calculated from the m values using

$$\frac{P_2}{P_1} = \frac{(m_2 + 1)^3}{(m_1 + 1)^3}. \quad (6)$$

With Charon as the reference, this system of moons has nearly a 1:3:4:5:6 commensuration, with Kerberos having the largest discrepancy of about 5.2%.

These moons have distances from the barycenter that are within 2.4% of their QCM equilibrium orbital radii. If in the next few million years they adjust their orbital semi-major axes, their positions on the plot may improve to increase the R^2 value but their m values will remain the same. Dynamic analysis via the appropriate QCM equations could be done to predict their possible movements.

Note that some additional extremely tiny moons of Pluto may be found at some of the non-occupied m values, but their angular momentum contributions will be very small. The formation history of Pluto determines which m values are actually occupied by orbiting bodies.

3 Discussion

QCM predicts the quantization of angular momentum per unit mass for all orbiting bodies in gravitationally bound systems. Unfortunately, the total angular momentum of planetary-like systems is usually not known to within 10%. Fortunately, the New Horizons spacecraft passing by Pluto in 2015 did not discover any additional moons of Pluto, so we now know the extent of this system and its total angular momentum to within 2.4%.

We have determined the best set of m integers for a fit to the QCM angular momentum constraint, and the predicted resonances in its moon system are in agreement with the measured period ratios to within 5.2%.

Therefore, we claim to have a definitive test of QCM in the Schwarzschild metric in a planetary-like system because the best understood system, Pluto and its 5 moons, obeys the quantization of angular momentum per unit mass constraint. Consequently, we expect that all such systems obey QCM, and in the future we will search for systems that seem to violate the angular momentum constraint.

One would prefer the ability to vary the parameters in a gravitationally bound system, but we do not have that luxury in astronomical systems. A laboratory test would allow the variation of the system parameters in a controlled manner and should be undertaken with perhaps a pendulum in a vacuum chamber near to a rotating mass. In the ideal case one would expect the maximum repulsion of the pendulum to occur when the angular momentum constraint is met and its magnitude to be comparable to the Newtonian attraction.

This type of additional definitive test of QCM might be able to achieve an reduced uncertainty down to about 0.1%.

Acknowledgements

We thank Sciencegems.com for continuing to encourage this research into the applications of QCM to gravitational systems.

Submitted on December 7, 2015 / Accepted on December 9, 2015

References

1. Potter F. Pluto moons exhibit orbital angular momentum quantization per mass. *Progress in Physics*, 2012, v.8(4), 3–4.
2. Preston H.G., Potter F. Exploring large-scale gravitational quantization without \hbar in planetary systems, galaxies, and the Universe. arXiv: gr-qc/0303112.
3. Potter F. Multi-planet exosystems all obey orbital angular momentum quantization per unit mass predicted by Quantum Celestial Mechanics (QCM). *Progress in Physics*, 2013, v.9(3), 60–61.
4. Potter F. Galaxy S-stars exhibit orbital angular momentum quantization per unit mass. *Progress in Physics*, 2012, v.8(4), 29–30.
5. Potter F., Preston H.G. Kepler-16 circumbinary system validates Quantum Celestial Mechanics. *Progress in Physics*, 2012, v.8(1), 52–53.
6. Potter F. Kepler-47 circumbinary planets obey angular momentum quantization per unit mass predicted by Quantum Celestial Mechanics (QCM). *Progress in Physics*, 2014, v.10(1), 19–20.
7. Weissman P.R. The angular momentum of the Oort cloud. *Icarus*, 1991, v.89, 190–193.
8. Youdin A.N., Kratter K.M., Kenyon S.J. Circumbinary chaos: using Pluto's newest moon to constrain the masses of Nix & Hydra. arXiv: 1205.5273v1.

LETTERS TO PROGRESS IN PHYSICS

On the Deviation of the Standard Model Predictions in the Large Hadron Collider Experiments

Anatoly V. Belyakov

E-mail: belyakov.lih@gmail.com

The newest Large Hadron Collider experiments targeting the search for New Physics manifested the possibility of new heavy particles. Such particles are not predicted in the framework of Standard Model, however their existence is lawful in the framework of another model based on J. A. Wheeler's geometrodynamics.

The main task of the Large Hadron Collider is to look for true deviations from the Standard Model (SM) if any. The collider has done hundreds of such experiments already. Some experimental results of these really deviate from the theoretical results predicted in the framework of SM. The newest Large Hadron Collider experiments done in look for New Physics manifested the possibility of new heavy particles.

The ATLAS collaboration team and the CMS collaboration team reported on the experimental search for heavy particle-resonances [1–3]. So, the ATLAS team, while experimental search for heavy resonances of a mass in the scale from 1 to 3.5 TeV decaying into a pair of bosons (i.e., into WW-, WZ-, or ZZ-pairs), discovered an anomalous number of events having an invariant mass of ~ 2 TeV. While the CMS team looked for the events in which many hadrons and an electron-positron pair were born then scattered with high energies. In the scale of invariant masses of ~ 2 TeV, they registered an anomalous many events. The obtained picture is like the production and decay of new heavy particles.

Such particles are not predicted in the framework of SM. However their existence is lawful in the framework of a model based on J. A. Wheeler's geometrodynamics concept.

In this geometrodynamics model, any elementary particle is considered as a trace appeared due to that a vortical tube (Wheeler's wormhole) transits the surface of our world (i.e. as a fermion), and also as a contour or a vortical tube (i.e. as a boson). So there can be connected contours of the first and higher order, which give birth to a few generations of the elementary particles [4]. As a result, any particle corresponds to two quantum numbers depending on that the particle is considered either as a fermion (an analogy of a proton joined into the large contour of the next family of particles), or as the boson mass of the contour of the previous family of particles.

In this way, only three families of the elementary particles can exist.

The first generation of the particles is a proton contour (a proton itself) having the same fermionic and bosonic masses, the sum of which is approximately equal to the sum of all π -mesons and K-mesons (1899 MeV).

The second generation is the standard proton-electron contour (the μ -analogy of the proton) having a bosonic mass close to the summary mass of the W and Z-bosons (229 GeV; the fermionic masses of the contour and those of the following contour are neglected).

The third generation is the largest contour wherein the parameters of the vortical tube reach its critical numerical values (the τ -analogy of the proton). The mass of the vortical tube is 3.1 TeV. It is logically lawful to guess that, in analogy to the second generation, this mass consists as well of three bosons (the average mass of each is 1 TeV).

According to the formulae obtained in [4] on the basis of Wheeler's geometrodynamics, the aforementioned mass can be expressed in the $m_e c^2$ units as

$$M_y = \frac{1}{3} \left(\frac{2a^3}{c_0^{1/3}} \right)^{7/4} = 2.1 \times 10^6 (1.07 \text{ TeV}), \quad (1)$$

where a is the reverse fine structure constant, while c_0 is the dimensionless light speed.

The characteristic mass close to 1 TeV can also be found proceeding from other consideration. As was found in [5, 6], the mass of the active part of the proton (the mass of its quark) enrolled into a circulation contour having a quantum contour parameter n_y answers the relation $m_k = c_0^{2/3} / (an_y)^2$. It is shown in [4, 6] that not only 1/3 but also 1/4 of this value can be the minimally possible charge (mass). Thus, in the ultimate small value can be $m_k = \frac{1}{4} m_e$. As a result, the ultimate heavy bosonic mass of the contour (in its excited state) is equal to

$$M_y = (an_y)^2 = 4c_0^{2/3} = 1.79 \times 10^6 (0.916 \text{ TeV}). \quad (2)$$

At last, it was found in [6] while considering the process of appearance of the neutrino that, if the mass-energy of a $p^+ - e^-$ -contour is close to the mass of a W-boson, replacing the electron mass with the τ -particle mass we obtain

$$\begin{aligned} M_y &= c_0^{4/9} m_\tau^{1/3} (2\pi\gamma\rho_e \times [\text{sec}^2])^{1/3} = \\ &= 2.29 \times 10^6 (1.17 \text{ TeV}) \end{aligned} \quad (3)$$

that corresponds to the mass of the guessed boson of the third generation. Herein, m_τ is the τ -particle mass in the m_e units, γ is the gravitational constant, ρ_e is the density inside the electron ($m_e/r_e^3 = 4.071 \times 10^{13}$ kg/m³).

Thus, proceeding from the viewpoint of the suggested model, such heavy particles decaying into the boson pair having a summary mass of ~ 2 TeV are very possible.

Submitted on November 10, 2015 / Accepted on November 11, 2015

References

1. ATLAS Collaboration. Search for high-mass diboson resonances with boson-tagged jets in proton-proton collisions at $\sqrt{s} = 8$ TeV with the ATLAS detector. arXiv: 1506.00962; CERN Report: CERN-PH-EP-2015-115.
2. CMS Collaboration. Search for massive WH resonances decaying to $\ell\nu b\bar{b}$ final state in the boosted regime at $\sqrt{s} = 8$ TeV. CERN Report: CMS-PAS-EXO-14-010.
3. CMS Collaboration. Search for heavy neutrinos and W bosons with right-handed couplings in proton-proton collisions at $\sqrt{s} = 8$ TeV. arXiv: 1407.3683; CERN Reports: CMS-EXO-13-008, CERN-PH-EP-2014-161.
4. Belyakov A.V. Macro-analogies and gravitation in the micro-world: further elaboration of Wheeler's model of geometrodynamics. *Progress in Physics*, 2012, v. 8, issue 2, 47–57.
5. Belyakov A.V. Nuclear power and the structure of a nucleus according to J. Wheeler's geometrodynamics concept. *Progress in Physics*, 2015, v. 11, issue 1, 89–98.
6. Belyakov A.V. Determination of the neutrino mass. *Progress in Physics*, 2016, v. 12, issue 1, 34–38.

X-Ray Flares from Sagittarius A* and Black Hole Universe

T. X. Zhang, C. Wilson, and M. P. Schamschula

Department of Physics, Alabama A & M University, Normal, Alabama 35762, USA

E-mail: tianxi.zhang@aamu.edu

Sagittarius (Sgr) A* is a massive black hole at the Milky Way center with mass of about 4.5 million solar masses. It is usually quite faint, emitting steadily at all wavelengths including X-rays. Since the beginning of this century, rapid and intensive X-ray flares are regularly detected from Sgr A* at a rate of about once a day. Conventionally, these mysterious events daily occurred at the Milky Way center are believed to be caused by the falling of objects such as asteroids, comets, and planets onto the massive black hole. However, the physical process of how the falling objects to produce the observed X-ray flares is still poorly understood. It is unclear why the gases, formed by tearing the falling objects apart, can be heated up to 100 million degrees Celsius so suddenly on a regular basis. This study develops a new alternative mechanism and provides a possible explanation for the observations of X-ray flares from Sgr A*, in accordance with the black hole universe model that was recently proposed by Zhang. The results obtained from this study indicate that X-ray flares from the Milky Way center can be understood as emissions of the dynamic massive black hole (i.e. Sgr A*). A massive or supermassive black hole, when accreting matter or objects from the outside, becomes dynamic and breaks its event horizon, which leads to the inside hot (or high-frequency) blackbody radiation leaking and produces X-ray flares or bursts. The energies and spectra of X-ray flares that Sgr A* can produce when it accretes objects with various sizes including asteroids, comets, planets, and stars are theoretically analyzed and numerically calculated. In terms of results obtained from these analyses and calculations, we explain the current measurements of X-ray flares from Sgr A*, predict events that will possibly occur at our galactic center in future, and compare the extremely intensive events predicted with the strong X-ray flares measured from other normal and active galactic centers. This study develops a new physical mechanism for the origin of X-ray flares from galactic centers and deepens our understanding to the black hole dynamics, galactic activities, and cosmological evolutions.

1 Introduction

Sagittarius (Sgr) A* is a compact astronomical radio source that was first discovered by [1] at the center of the Milky Way, near the border of the constellations, Sagittarius and Scorpius. The orbital motions of stars around the Milky Way center indicate the presence of a massive black hole with about 4.5 million solar masses, which is spatially coincident with Sgr A* [2–3].

In general, Sgr A* is very faint and emits steadily at all wavelengths, especially in the range of soft X-rays (2–10 keV) with luminosity about 2×10^{33} erg/s [4]. Recently, NASA Chandra X-ray Observatory and other missions such as Swift, NuStar, XMM-Newton, and Roast have discovered intensive and rapid X-ray flares at a rate of about once a day from Sgr A*, with luminosity at the peak up to a few times 10^{35} erg/s [5–7]. The brightest X-ray flare ever observed so far emits in total $\sim 10^{39} - 10^{40}$ ergs of X-rays (2–10 keV) and last a few thousand seconds or hours [8–9]. The X-ray echoes recently discovered reveal that Sgr A* would have been a very violent past with luminosity of $\sim 10^{39}$ erg/s (i.e., a mil-

lion times brighter than its present normal emission) during the X-ray outbursts of the past few hundred years [10]. X-ray outbursts from some other inactive galaxies can be even much more intensive with luminosity $\sim 10^{44}$ erg/s [11–12]. Luminosities of an active galactic nuclei or a quasar can be extremely high up to 10^{46} erg/s [13–15].

To explain the mysterious X-ray flares, astronomers have suggested that there exists a gas cloud around Sgr A* containing hundred-trillions of asteroids, comets, and planets that are stripped from their parent stars by the tidal forces of the massive black hole. When these objects rain down or are accreted onto the massive black hole, X-ray flares take place via physical processes such as the non-thermal synchrotron emission [16], the inverse-Compton scattering [17], and stochastic electron acceleration [18]. To emit the high-energy X-rays detected, an object that was striped from its parent star had to be torn apart into gases during its falling and the gases when arriving nearly at the massive black hole had to spike to hundreds of million degrees Celsius, which is ten or more times hotter than the center of the Sun. However, why the gases heats up so suddenly and efficiently on a regular ba-

sis is still poorly understood. One possible heating scenario recently guessed is based on the physics of solar flares by considering that the lines of magnetic energy contained in the gas flowing into Sgr A* got tangled and the reconnection of magnetic lines leads [19-20], but there still lacks of a quantitative study on this magnetic mechanism. Especially, Sgr A* may not be able to gravitationally tear an asteroid into parts as small as a human body, because the gravitational field difference between the head and feet of a 2-meter height person, who stands on Sgr A* surface is only 10^{-3} m/s^2 . Up to the date, astronomical communities are still out on what really caused these giant X-ray flares from Sgr A*. The mechanism for the origin of X-ray flares from the galactic center is still a mystery and in pending for a physical explanation.

Recently, postulating the equivalence between a spacetime and a black hole, Zhang [21–22] developed a new cosmological model called black hole universe, which is consistent with Mach's principle, governed by Einstein's general relativity with the cosmological principle of spacetime isotropy and homogeneity, and able to explain the existing observations of the universe without encountering difficulties such as the flatness, horizon, inflation, dark matter, and dark energy problems. The studies that have been conducted so far have explained the origin, structure, evolution, expansion, cosmic microwave background radiation, quasar formation and emission, gamma ray bursts (GRBs), and acceleration of black hole universe [15, 22–27]. According to this new cosmological model, the universe originated from a star-like black hole with several solar masses, grew up through a supermassive black hole with billions of solar masses to the present state with hundred sextillions of solar masses by accreting ambient matter and merging with other black holes. More aspects about the black hole universe model have been presented in a sequence of American Astronomical Society (AAS) meetings [28–37]. The black hole universe model establishes a complete new understanding to the dynamics of black holes, so that offers a unique explanation to the observations of various events that relate to the activities of black holes such as quasars [15], gamma ray bursts [25], and X-ray flares from galactic centers (this paper).

This study will focus our investigations on the physical mechanism of X-ray flares from Sgr A*, a massive black hole at the Milky Way center, and provides an alternative explanation for the energy and spectrum measurements of X-ray flares according to the black hole universe model. The results indicate that X-ray flares from the galactic center can be understood as emissions of the dynamic massive black hole. As pointed out in Zhang's early studies, a black hole, when it accretes its ambient matter or objects, becomes dynamic. A dynamic black hole has a broken event horizon and thus cannot hold the inside hot (or high-frequency) blackbody radiation, which leaks out and produces a gamma ray burst if it is a star-like black hole or an X-ray flare if it is a massive or supermassive black hole. The energies and spectra of X-rays

obtained by this study for the X-ray emissions from Sgr A* when it accretes appropriate size objects such as asteroids, comets, and planets can be consistent with the measurements.

2 X-ray emissions of dynamic massive black holes

In accordance with the black hole model of the universe developed recently by [21–22], a black hole constructs an individual spacetime (spatially singular and temporally noncausal to the outside) and a spacetime encloses a black hole. Black hole and spacetime are equivalent. According to this equivalence, our four-dimensional (4D) spacetime universe is a fully grown extremely supermassive black hole. The observed star-like, massive, and supermassive black holes are subspaces of our black hole universe. Upon the view from the outside, a star-like or supermassive black hole is a singular sphere, from which no matter and radiation can escape. In general, a star-like (or larger) black hole can be considered as an ideal blackbody, with the following Mach-Schwarzschild mass-radius (M-R) relation

$$\frac{2GM}{c^2R} = 1, \quad (1)$$

where c is the light speed in the free space and G is the gravitational constant.

The temperature inside a star-like black hole, though it cannot be measured from outside, should be as high as that of a neutron star because both types of objects are comparably compact. At the moment of its birth via a supernova explosion, a neutron star can reach 10^{12} K and then quickly cools down to about 10^8 K because of its strong radiation and neutrino emission [38]. A black hole can hold the high temperature reached at the moment of its birth because it does not radiate significantly. When a star-like black hole accretes matter and radiation from outside, it expands and cools down. As a star-like black hole grows up as big as the present universe, the inside temperature decreases from 10^{12} K to about 3 K . In the black hole universe model, the observed 3 K cosmic microwave background radiation is the internal blackbody radiation of the black hole universe, an ideal blackbody [23, 29].

The spectral energy density of blackbody radiation within a black hole including the black hole universe can be determined according to Planck's law as

$$u(\nu, T) = \frac{8\pi h\nu^3}{c^3} \frac{1}{\exp\left(\frac{h\nu}{kT}\right) - 1}, \quad (2)$$

where ν is the radiation frequency, T is the temperature, h is the Planck constant, and k is the Boltzmann constant. In the SI unit system, the unit of $u(\nu, T)$ is $\text{J/m}^3/\text{Hz}$, which is equivalent to $2.41 \times 10^{17} \text{ J/m}^3/\text{keV}$. Figure 1 plots the spectral energy density as a function of photon energy $\epsilon = h\nu$ at temperature equal to 10^6 , 10^7 , 10^8 , and 10^9 K , respectively. It is seen that the spectral energy density significantly varies with the temperature and photon energy. Inside a black hole

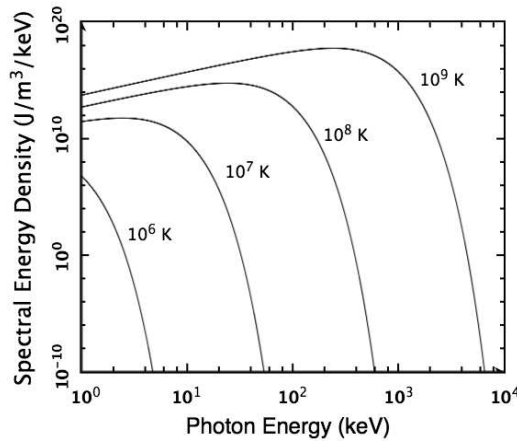


Fig. 1: The spectral energy density of blackbody radiation as a function of radiation energy at temperature equal to 10^6 , 10^7 , 10^8 K and 10^9 K, respectively.

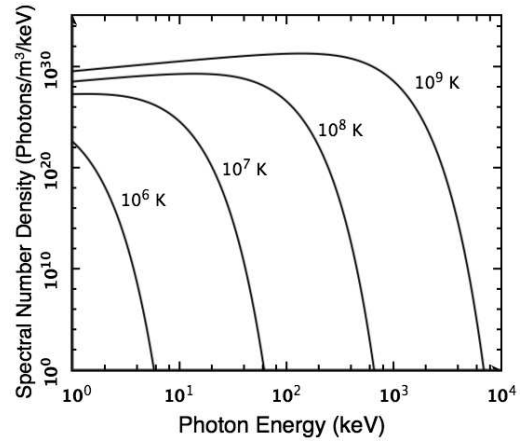


Fig. 2: The spectral number density of blackbody radiation as a function of radiation energy at temperature equal to 10^6 , 10^7 , 10^9 K and 10^{12} K, respectively.

with temperature of $10^7 - 10^8$ K (e.g. a massive black hole with millions of solar masses), the blackbody radiation dominates at the frequency of X-rays with photon energy in the range of 1 – 200 keV. The spectral photon number density $f(\nu, T) \equiv u(\nu, T)/\epsilon$ is plotted in Figure 2

Integrating the spectral energy density (Eq. 2) with respect to the frequency of radiation in the entire range, we have the energy density of the blackbody radiation inside a black hole including the black hole universe,

$$\rho_\gamma \equiv \int_0^\infty u(\nu, T) d\nu = \beta T^4, \quad (3)$$

where the constant β is given by $\beta \equiv 8\pi^5 k^4 / (15h^3 c^3) \simeq 7.54 \times 10^{-16} \text{ J/m}^3/\text{K}^4$. Inside a black hole with temperature $\sim 10^7 - 10^8$ K, the energy densities of radiation are $\sim 10^{13} - 10^{17} \text{ J/m}^3$.

As a black hole including the black hole universe accretes its outside matter and radiation, it expands and cools down. Considering that the increase of the Planck radiation energy within the black hole equals to the radiation energy inhaled from the outside space, we have [23]

$$\frac{dT}{dR} = -\frac{3T}{4R} \left[1 - \left(\frac{T_p}{T} \right)^4 \right]. \quad (4)$$

where T is the temperature inside the black hole and T_p is the temperature outside the black hole. This equation determines the temperature inside a black hole in accordance with its size. The solution of Eq. (4) for the dependence of T on R depends on T_p or on the relation between T and T_p . In the early studies [23, 29], Eq. (4) was solved for the present black hole universe that grew up from a hot star-like black hole through a supermassive black hole.

For star-like or supermassive black holes, the temperatures inside should be much greater than the temperatures

outside, i.e., $T \gg T_p$. In this case, Eq. (4) can be simply solved as

$$R^3 T^4 = C, \quad (5)$$

where C is a constant. Zhang [26] has assumed this constant to be the same for all size star-like or supermassive black holes and quantitatively explained the measurements of GRBs as emissions of dynamic star-like black holes. The value of the constant was determined according to the radius R_s and temperature T_s of a particular (or reference) black hole as $C = R_s^3 T_s^4$. For a three-solar-mass black hole ($M_s = 3M_{\text{Sun}}$) to be the reference black hole, its radius is about $R_s = 2GM_s/c^2 \sim 8.89$ km. Choosing its temperature to be $T_s = 10^{12}$ K, we have $C \sim 7 \times 10^{59} \text{ m}^3 \text{ K}^4$. The temperature of a star-like or supermassive black hole decreases as it expands in size according to $T \propto R^{-3/4}$.

Figure 3 plots the temperature of a black hole as a function of the radius or mass of the black hole. The the temperature of a three-solar mass black hole is chosen to be $T_s = 5 \times 10^{11}$ K and 10^{12} K. For Sgr A* with mass of 4.5 million solar masses or radius of 1.33×10^{10} m, the temperature is $\sim 10^7 - 10^8$ K. The frequency of blackbody radiation at the peak to this temperature range is $\sim 10^{18} - 10^{19}$ Hz (or the energy of X-rays at the peak is $\sim 4 - 40$ keV).

From Eqs. (3) and (5), we obtain the total radiation energy U inside a black hole with volume V or radius R to be a constant and independent of its size or mass,

$$U \equiv \rho_\gamma V = \frac{4}{3} \pi \beta R^3 T^4 = \text{Constant}. \quad (6)$$

It is seen that the total radiation energy inside a black hole (either a star-like or supermassive black hole) remains the same or is conserved. A black hole can grow its size by accreting mater from the outside space or merging with other black holes, but cannot increase its total radiation energy.

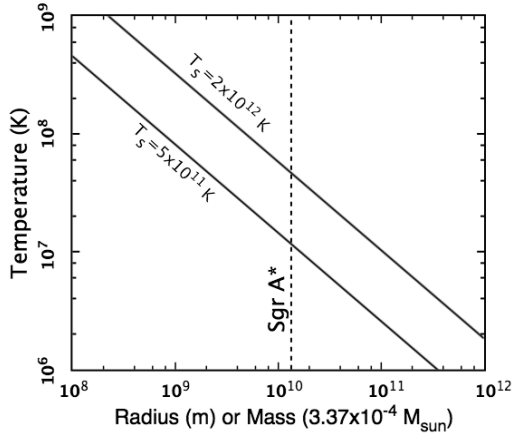


Fig. 3: The temperature of a massive black hole as a function of the radius or mass of the black hole with $T_s = 10^{12}$ K or 5×10^{11} . The vertical dashed line represents the radius, mass, and range of temperature.

A star-like black hole with several solar masses holds the same amount of radiation energy as a supermassive black hole with billions of solar masses does. The difference is only the temperature or frequency of the radiation. Dynamic star-like black holes with thousand billions of Kelvins radiate gamma rays [26], while dynamic massive or supermassive black holes with millions to billions of Kelvins radiate X-rays such as X-ray emissions from quasars [15] and X-ray flares from Sgr A*, a massive black hole at the Milky Way center as shown in this study.

3 Energy and energy spectrum of X-ray flares from Sgr A*

According to the black hole universe model, X-ray flares from the Milky Way center are the emissions of the dynamic massive black hole, Sgr A*, which is accreting objects that fail to orbit around Sgr A*.

The energy emitted by Sgr A* with mass M and radius R , after it has accreted an object with mass m and radius r , can be determined by the difference of gravitational potential energies subtracting all other losses or dissipations during the falling of the object towards Sgr A*

$$E = U_M + U_m + U_{Mm} - U_{M+m} - E_{\text{loss}}, \quad (7)$$

where U_M is the gravitational potential energy of Sgr A* before the object is accreted,

$$U_M = -\frac{3GM^2}{5R} = -\frac{3}{10} Mc^2; \quad (8)$$

U_m is the gravitational potential energy of the object (e.g. an asteroid),

$$U_m = -\frac{3Gm^2}{5r} = -\frac{3}{10} \frac{r_g}{r} mc^2, \quad (9)$$

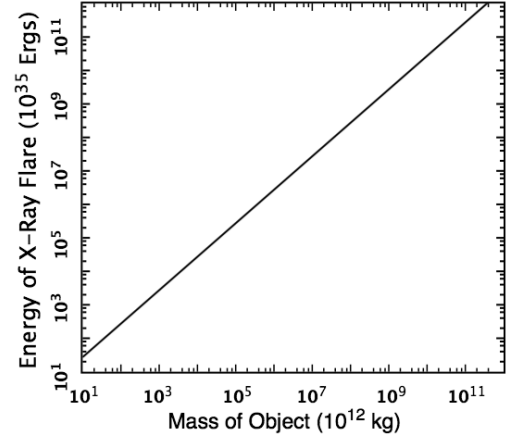


Fig. 4: The energy of X-ray flares from Sgr A* versus the mass of the object accreted.

with $r_g = 2Gm/c^2$ is the Schwarzschild radius of an object with mass m ; U_{M+m} is the gravitational potential energy of Sgr A* after the object is accreted,

$$U_{M+m} = -\frac{3G(M+m)^2}{5(R+\delta R)} = -\frac{3}{10} (M+m)c^2; \quad (10)$$

and U_{Mm} is the gravitational potential energy between Sgr A* and the object when the object is initially on the orbit,

$$U_{Mm} = -\frac{GMm}{R_{\text{orbit}}} = -\frac{1}{2} \frac{R}{R_{\text{orbit}}} mc^2, \quad (11)$$

with R_{orbit} is the radius of asteroid's initial orbit around Sgr A*; and E_{loss} is the energy lost or dissipated during the object is falling into Sgr A*. Substituting Eq. (8) through Eq. (11) into Eq. (7), we have

$$E = \frac{3}{10} \left(1 - \frac{r_g}{r} - \frac{5R}{3R_{\text{orbit}}} \right) mc^2 - E_{\text{loss}}. \quad (12)$$

Since $r_g \ll r$ and $R \ll R_{\text{orbit}}$, Eq. (12) simply reduces to

$$E \sim \frac{3}{10} mc^2, \quad (13)$$

if the loss or dissipation is negligible in comparison with the rest energy of the object. Therefore, the energy of X-ray flares from Sgr A* approximately depends on the mass of the object that Sgr A* has accreted from outside. Figure 4 plots the energy of X-rays emitted by the massive black hole Sgr A* when it accretes an object as a function of the object mass. It is seen that Sgr A* emit more X-rays if it accretes more massive object. For instance, Sgr A* can emit up to 10^{39} ergs of X-rays if it accretes an asteroid with mass of 10^{17} kg.

Table 1 lists the energies of X-ray flares from Sgr A* by accreting some particular objects. Hourly accreting some small-sized asteroids can explain the faint and steady emissions of Sgr A* ($\sim 10^{33}$ ergs/s). Daily accreting one medium-sized asteroid can explain the present observations of X-ray

Type of Object	Mass (kg)	Energy (erg)
Asteroid (small size)	10^{13}	3×10^{36}
Asteroid (medium size)	10^{16}	3×10^{39}
Asteroid (large size)	10^{20}	3×10^{43}
Planet (Pluto size)	1.3×10^{22}	4×10^{45}
Planet (Earth size)	6×10^{24}	2×10^{48}
Planet (Jupiter size)	2×10^{27}	6×10^{50}
Star (1 solar mass)	2×10^{30}	6×10^{53}
Star (100 solar mass)	2×10^{32}	6×10^{55}

Table 1: Mass of various objects and energy of X-ray flares from Sgr A* when it accretes these objects.

flares (about hundred times more luminous than the steady emission) from Sgr A* at a rate of once a day. Occasionally accreting of large-sized asteroids or pluto-sized planets can explain the X-rays outbursts of a million times brighter than the normal emission of Sgr A*, which occurred during the past few hundred years. For big size planets, this may also explain the X-ray outbursts from some other inactive galactic centers. In future, when Sgr A* accretes a star including neutron star daily (or yearly for a large star), an active galactic nucleus (AGN) or quasar will form or is born in our galaxy. It should be noted that the G2 cloud with 3 Earth masses, if it is accreted by Sgr A*, will produce a super X-ray flare, billions times brighter than the normal emissions.

The spectral energy flux $S(\nu, T)$ of the blackbody radiation from a dynamic black hole can be determined by,

$$S(\nu, T) = cu(\nu, T). \quad (14)$$

Dividing the spectral energy flux $S(\nu, T)$ by the energy of photon, we have the spectral photon flux as,

$$J(\nu, T) \equiv \frac{S(\nu, T)}{h\nu} = cf(\nu, T). \quad (15)$$

For the radiation observed at the Earth, the spectral flux of an X-ray flare produced by the dynamic massive black hole Sgr A*, when it accretes an object, is given by,

$$J(\nu, T) = cf(\nu, T) \left(\frac{r_0}{d_L} \right)^2, \quad (16)$$

where d_L is the luminosity distance and r_0 is the radius of radiation area, which is the area of the horizon broken. The temperature T of Sgr A* can be estimated, according to Eq. (5), by

$$T = T_s \left(\frac{R_s}{R} \right)^{3/4} = T_s \left(\frac{c^2 R_s}{2GM} \right)^{3/4}, \quad (17)$$

where M is the mass of Sgr A* and equals to about 4.5 million solar masses. As mentioned above or in [25–26], R_s is the radius of the three-solar-mass black hole and is equal to ~ 8.89 km; T_s is the temperature of the three-solar-mass black

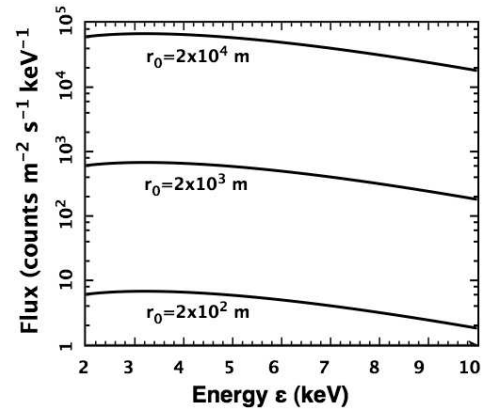


Fig. 5: The spectral flux of dynamic massive black hole Sgr A* as a function of radiation photon energy.

hole and is usually chosen to be around one trillion Kelvins, i.e. $T_s \sim 10^{12}$ K. Then we have the temperature of inside Sgr A* is $T \sim 2.3 \times 10^7$ K.

For the massive black hole Sgr A*, $d_L \sim 2.46 \times 10^{20}$ m or 26,000 light-years. The radius of radiation area r_0 can be considered to be about the radius of the object accreted by Sgr A* times a factor, $r_0 = br$. The factor b is equal to the unity if the full area of radiation faces towards to the observer or the Earth. Otherwise, we have $b < 1$ or $r_0 < r$. In addition, since the object is usually broken by the tidal force during the falling, the factor b should be smaller. An X-ray flare occurred at the opposite side of Sgr A* cannot be directly observed by an observer on the Earth. In this case, the factor b is zero. The 400 brighter than normal emission X-ray flare caught by Chandra on September 14, 2013 flares its X-rays in the upright direction according to the image [9,19]. Considering that an asteroid, whose density is usually given by about 2000 kg/m^3 , has mass of 10^{17} kg, we can find its radius $r \sim 23$ km and choose r_0 equal or less than 23 km. Figure 5 plots the average spectral flux of an X-ray flare from Sgr A* as a function of the X-ray photon energy. In this plot, we have chosen $r_0 = 200, 2000, 20000$ m, respectively, and $T_s = 10^{12}$ K. It is seen that the spectral flux of X-ray flares from Sgr A*, according to this new mechanism, increases with r_0 . Increasing T_s also increases the spectral flux especially in high energy end. Quantitatively, the spectral flux of X-ray flares from Sgr A* obtained from this study as emissions of dynamic massive black hole can be consistent with the measurements [39].

4 Discussion and conclusion

According to this new mechanism, the duration or time scale of an X-ray flare is the time needed for the broken horizon to be recovered. It depends on the size of the object accreted and also the rate or speed of matter diffusion. In general, the bigger the events are, the longer the flares can last, which agrees

with the measurements. The rate of matter diffusion depends on the state of matter. The rate of diffusion is faster if the matter is hotter and/or less dense. The falling of the object is usually dissipated due to radiation of lower frequencies such as near infrared as measured usually prior to the X-ray flares. In addition, the observed spectral flux of X-ray flares from Sgr A* may be significantly affected by the gravitational redshift. In future, we will address these issues in more details.

We have developed a new mechanism for X-ray flares from Sgr A*, in accordance with the black hole model of the universe that Zhang [21–22] recently proposed. According to this new mechanism, we can understand X-ray flares from Sgr A* as emissions of dynamic massive black hole at the Milky Ways center. A black hole (from star-like with several solar masses through supermassive with billions of solar masses), when accreting matter, becomes dynamic and breaks its event horizon, which leads to the inside hot (or high-frequency) blackbody radiation leaking out of it and produces an X-ray flare or burst. We calculate the energies and spectra of X-rays emitted by the galactic center massive black hole when various sized objects from asteroids through comets and planets to stars fall into Sgr A*. Then, through these calculations, we explain the current measurements of X-ray flares from Sgr A* including its steady emissions, predict big events that possibly occurred in the past or will possibly occur in future at our galactic center, and compare the predicted intensive events with the measurements of strong X-ray flares from other normal and active galactic centers. This study develops a possible mechanism for the origin of the X-ray flares from galactic centers and deepens our understanding to the black hole dynamics, galactic activities, and cosmological evolutions.

Acknowledgments

This work was partially supported by the NSF HBCU-UP, REU, and AAMU Title III programs.

Submitted on December 10, 2015 / Accepted on December 12, 2015

References

- Balick B., Brown R.L. Intense sub-arcsecond structure in the galactic center. *Astrophysics and Space Science*, 1974, v. 194, 265–270.
- Schödel R. et al. A star in a 15.2-year orbit around the supermassive black hole at the centre of the Milky Way. *Nature*, 2002, v. 419, 694–696.
- Gillessen S., Eisenhauer F., Trippe S., Alexander T., Genzel R., Martins F., Ott T. Monitoring stellar orbits around the massive black hole in the galactic center. *Astrophysical Journal*, 2009, v. 692, 1075–1109.
- Degenaar N., Miller J.M., Kennea J., Gehrels N., Reynolds M.T., Wijnands R. The X-ray flaring properties of Sgr A* during six years of monitoring with Swift. *Astrophysical Journal*, 2013, v. 769, article id. 155, 7 pages.
- Baganoff F.K. et al. Rapid X-ray flaring from the direction of the supermassive black hole at the Galactic Centre. *Nature*, 2001, v. 413, 45–48.
- Porquet D. et al. XMM-Newton observation of the brightest X-ray flare detected so far from Sgr A*. *Astronomy and Astrophysics*, 2003, v. 407, L17–L20.
- Neilsen J. et al. A Chandra/HETGS census of X-ray variability from Sgr A* during 2012. *Astrophysics Journal*, 2013, v. 774, article id. 42.
- Nowak M.A. et al. Chandra/HETGS observations of the brightest flare seen from Sgr A*. *Astrophysical Journal*, 2012, v. 759, article id. 95.
- Haggard D. et al. An update on Chandra/VLA galactic center campaigns targeting Sgr A* and G2. *American Astronomical Society 225th Meeting*, 2015, Abstract #102.09.
- Clavel M. et al. The reflection of two past outbursts of Sagittarius A* observed by Chandra during the last decade. *Proceedings of the International Astronomical Union*, 2014, v. 303, 344–348.
- Komossa S., Greiner J. Discovery of a giant and luminous X-ray outburst from the optically inactive galaxy pair RX J1242.6-1119. *Astronomy and Astrophysics*, 1999, v. 349, L45–L48.
- Saxton R.D. et al. An X-ray and UV flare from the galaxy XMMSL1 J061927.1-655311. *Astronomy and Astrophysics*, 2014, v. 572, article id. A1, 9 pages.
- Bahcall J.N., Kirhakos S., Saxe D.H., Schneider D.P. Hubble space telescope images of a sample of 20 nearby luminous quasars. *Astrophysical Journal*, 1997, v. 479, 642–658.
- Begelman M.C., King A. R., Pringle J. E. The nature of SS433 and the ultraluminous X-ray sources. *Monthly Notices of the Royal Astronomical Society*, 2006, v. 370, 399–404.
- Zhang T.X. Quasar formation and energy emission in black hole universe. *Progress in Physics*, 2012, v. 8, issue 3, 48–53.
- Kusunose M., Takahara F. Synchrotron blob model of infrared and X-ray flares from Sagittarius A*. *Astrophysical Journal*, 2011, v. 726, article id. 54, 6 pages.
- Yusef-Zadeh F. et al. An Inverse compton scattering origin of X-ray flares from Sgr A*. *Astronomical Journal*, 2012, v. 144, article id. #1, 10 pages.
- Liu S.M., Fulvio M., and Yahe F. Stochastic electron acceleration during the near-infrared and X-ray flares in Sagittarius A*. *Astrophysical Journal*, 2006, v. 636, 798–803
- Sagittarius A*: NASA Chandra Detects Record-Breaking Outburst from Milky Way's Black Hole (2015). Accessed from: <http://chandra.harvard.edu/photo/2015/sgra>
- Li Y.P. et al. Statistics of X-Ray Flares of Sagittarius A*: Evidence for Solar-like Self-organized Criticality Phenomena. *Astrophysical Journal*, 2015, v. 810, article id. 19, 8 pages.
- Zhang T.X. A new cosmological model: Black hole universe. *American Astronomical Society 211st Meeting*, 2007, Abstract #152.04.
- Zhang T.X. A new cosmological model: Black hole universe. *Progress in Physics*, 2009a, v. 2, 3–11.
- Zhang T.X. Cosmic microwave background radiation of black hole universe. *Astrophysics and Space Science*, 2010a, v. 330, 157–165
- Zhang T.X. Key to the mystery of dark energy: Corrected relationship between luminosity distance and redshift. *Progress in Physics*, 2013, v. 5, issue 3, 1–6.
- Zhang T.X. A new mechanism for gamma ray bursts: Emissions of dynamic black holes. *Proceeding of Gamma Ray Burst 2013 Symposium*, 2013b, SNSN-323-63.
- Zhang T.X. Gamma ray bursts of black hole universe. *Astrophysics and Space Science*, 2015, v. 358, article id. #14, 8 pages.
- Zhang T.X., Frederick C. Acceleration of black hole universe. *Astrophysics and Space Science*, 2014, v. 349, 567–573.
- Zhang T.X. Anisotropic expansion of the black hole universe. *American Astronomical Society 213rd Meeting*, 2009b, Abstract #357.03.
- Zhang T.X. Cosmic microwave background radiation of black hole universe. *American Astronomical Society 214th Meeting*, 2009c, Abstract #303.01.

30. Zhang T.X. Observation evidences of black hole universe. *American Astronomical Society 215th Meeting*, 2010b, Abstract #313.06.
 31. Zhang T.X. Black hole universe model and dark energy. *American Astronomical Society 217th Meeting*, 2011, Abstract #404.05.
 32. Zhang T.X. Mechanism for gamma-ray bursts and black hole universe. *American Astronomical Society 219th Meeting*, 2012b, Abstract #310.02.
 33. Zhang T.X. Acceleration of black hole universe. *American Astronomical Society 220th Meeting*, 2012c, Abstract #321.07.
 34. Zhang T.X. Key to the mystery of dark energy: Corrected relationship between luminosity distance and redshift. *American Astronomical Society 221st Meeting*, 2013c, Abstract #323.06.
 35. Zhang T. X. Evidences for supporting the black hole universe model. *American Astronomical Society 222nd Meeting*, 2013d, Abstract #103.02.
 36. Zhang T.X. Black hole universe model for explaining GRBs, X-ray flares, and quasars as emissions of dynamic star-like, massive, and supermassive black holes. *American Astronomical Society 223rd Meeting*, 2014a, Abstract #427.05.
 37. Zhang T.X. The black hole universe model. *American Astronomical Society 224th Meeting*, 2014b, Abstract #304.03.
 38. Yakovlev D.G., Gnedin O.Y., Kaminker A.D., Levenfish K.P., Potekhin A.Y. Neutron star cooling: Theoretical aspects and observational constraints. *Advances in Space Research*, 2004, v. 33, 523–530.
 39. Barrière N.M. et al. NuSTAR detection of high-energy X-ray emission and rapid variability from Sagittarius A* flares. *Astrophysical Journal*, 2014, v. 786, article id. 46, 10 pages.
-

On an Apparent Resolution of the Catt Question

Stephen J. Crothers

Tasmania, Australia. E-mail: steve@plasmaresources.com

Over a number of years there have been some attempts to answer the Catt Question within the context of classical electromagnetic theory. None of the authors of these attempts agree on the answer to the Catt Question, even though they all invoke the very same theory. An attempt at answering the Catt Question appeared in the journal *Physics Education* in 2013, penned by M. Pieraccini and S. Selleri, as a mathematical rendition of their earlier non-mathematical version published in *IEEE Antennas and Propagation Magazine*, 2012. The explanation by these two Authors contains violations of classical electromagnetic theory, although they claim to have satisfactorily answered the Catt Question by means of classical electromagnetic theory. The arguments adduced by Pieraccini and Selleri are therefore invalid.

1 Introduction

In their article [1] “An apparent paradox: Catt’s anomaly”, the Italian authors Pieraccini and Selleri* refer to the Catt Question as “Catt’s Anomaly”. Their earlier paper is titled ‘Catt’s Anomaly’ [2]. Although until 2001 “The Catt Question” was called “The Catt Anomaly”, it was in fact *always* a question, to be answered.

The Catt Question [3] pertains to the propagation of a Transverse Electromagnetic (TEM) wave along a transmission line. Upon closure of a switch, the TEM wave (step) travels at the speed of light between the conducting wires of the transmission line, from battery to load, as depicted in Fig. 1.

An electric field \mathbf{E} appears between the conductors, directed from the top wire to the bottom wire. This electric field is orthogonal to the two parallel wires and moves towards the load; thus there are positive charges on the top conductor and negative charges on the bottom conductor in the region of the transverse electric field. The Catt Question is: *Where does this new charge come from?* [3].

2 Electron current

According to classical electromagnetic theory and circuit theory, electric current in metallic wires is the flow of electrons in the wires (conductors), and a magnetic field is generated around the conducting wires according to the Right-Hand Rule. Since the TEM step travels at the speed of light towards the load, how does the current in the conducting wires keep pace with the TEM wave, if electrons cannot travel at the speed of light? The Authors [1] give the following answer,

“The key idea of the explanation of this apparent paradox is related to the great number of electrons in metal. Although each single electron is

*Massimiliano Pieraccini, Associate Professor, Department of Electronics and Telecommunications, University of Florence; Stefano Selleri, Assistant Professor, University of Florence.

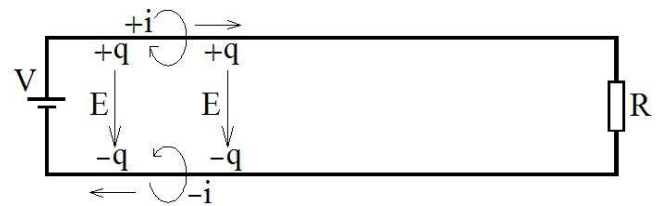


Fig. 1: An electric field points directly from the top conductor to the bottom conductor (from positive charge to negative charge). It is therefore orthogonal to the top and bottom parallel conductors. The transverse electric field travels from battery to load at the speed of light, subject to the dielectric medium between the wires.

not able to travel at the speed of light, a great number of slow electrons are able to produce a current as fast as an electromagnetic wave travelling at the speed of light in the conductor.”

What do they mean by “current”? They say here that electrons “produce a current”. However, the Authors actually assume the classical electron flow along wires as the meaning of electric current in wires, and claim that this current travels along the conductors at the speed of light even though the drift speed of electrons in the wires is a snail’s pace (e.g. 2mm/s in 1.0mm copper wire [1]). Strangely, the flow of electrons, although very slow, produces an electron current that is “as fast as an electromagnetic wave travelling at the speed of light in the conductor” [1]: after all, a current of electrons is an electron current. This impossible duality occurs, they say, because the free electron density in the conductors is very high, and they derive an equation for electron drift “velocity”.

Electron drift velocity in a wire is proportional to the vector electric field \mathbf{E}_w in the wire, which supposedly causes the electron drift,

$$\mathbf{v} = -\mu\mathbf{E}_w \quad (0)$$

and so the electron drift velocity and the electric field in the wire are collinear but point in opposite directions. The constant of proportionality μ is called the *mobility*.

The Authors begin with the following equation for electron current,

$$I = \pi a^2 v q N, \quad (1)$$

where a is the radius of the conductors, v “the drift velocity of the charges (in practice electrons, and the speed is much lower than the speed of light)” [1]*, q the elementary charge, and N the free electron density in the conductors.

Since the current, they say, travels at the speed of light, in time $\Delta t = \Delta x/c$ they obtain a passage of charge ΔQ along the top conductor, given by,

$$\Delta Q = I \Delta t = I \frac{\Delta x}{c}, \quad (2)$$

where Δx is the distance travelled by the TEM step in time Δt . This charge ΔQ the Authors call “an imbalance of charge” [1] because they say it is confined to a leading volume element of length Δx in the top conducting wire, and induces equal but opposite polarity charge on the bottom conducting wire.

Using a cylindrical Gaussian surface they next apply Gauss’ Law to calculate the magnitude E of the electric field \mathbf{E} due to ΔQ in the top conductor,

$$\frac{\Delta Q}{\epsilon_0} = (2\pi a \Delta x) E, \quad (3)$$

where ϵ_0 is the permittivity of free space. Substituting ΔQ from equation (2) and I from equation (1) the Authors obtain,

$$v = \frac{2c\epsilon_0 E}{qNa}. \quad (4)$$

From equation (4) they conclude,

“The notable point of this result is that the necessary speed decreases with the number of electrons per volume unit N . Therefore, a great number of slow electrons are able to generate enough unbalanced charge to follow an electromagnetic wave travelling at much higher speed.”

Thus electrons flow slowly in the conducting wires but the electron current in the wires is nevertheless flowing along the conductors at the speed of light.

Although equation (4) follows from equations (1), (2) and (3) by purely mathematical operations, the transverse electric field \mathbf{E} cannot drive electrons along the inside or outside of the wires. Equations (1), (2) and (4) imply flow of electrons along the wires, but the transverse electric field at equation (3) is orthogonal to the parallel axes of the top and bottom wires. According to classical electrodynamics, free electrons in a metallic conductor flow in the direction opposite to the direction of the electric field, according to equation (0), not orthogonal to the electric field ($\mathbf{E} \neq \mathbf{E}_w$). The Authors confound battery EMF[†] with the transverse electric field, and so

*The Authors confound velocity with speed; the latter denoted by $|v| = v$

†What EMF is, is another question.

make the transverse electric field the battery EMF to drive electrons along the wires; at equation (4).

Then they introduce the “skin effect” [1]:

“Up to this point, the current has been considered constant in the wire section, but in reality the current flow tends to be bound to the portion of the conductor closer to the surface.”

The equation for current in the wires they then give as,

$$I = 2\pi a \delta v q N, \quad (1b)$$

where δ is the skin depth, which is frequency dependent. With the “skin effect” they still argue that electrons flowing along the wire is electric current, orthogonal to the electric field they calculated at equation (3), and continue to make that transverse electric field the driver of the electrons in the conducting wires. Using equations (1b), (2) and (3) they then obtain the electron drift speed,

$$v = \frac{2c\epsilon_0 E}{qN\delta} \quad (5)$$

although the 2 in the numerator should not in fact appear.

3 Conclusion

Pieraccini and Selleri have not answered the Catt Question. On the one hand they treat current in the conducting wires as electron current but on the other hand they invoke the transverse electric field between the conducting wires to drive this electron current at the electron drift speed. Their analysis violates the classical electromagnetic theory they use in their attempt to prove that what they call “Catt’s Anomaly” is merely an “apparent paradox” [1]. The real paradox here is their claim that very slowly flowing electrons in the wires of a transmission line produce an electron current in those wires that travels at the speed of light, driven by an electric field orthogonal to those wires.

“If I have promised to deliver one dozen eggs to Oxford, one hour from now, Oxford being 100 miles away, there is no point in despatching ten dozen eggs in a vehicle which travels at only ten miles/h” [4].

Submitted on December 13, 2015 / Accepted on December 14, 2015

References

1. Pieraccini M. and Selleri S. An apparent paradox: Catt’s anomaly. *Physics Education*, 2013, v. 48 (6), 718–722.
2. Pieraccini M. and Selleri S. Catt’s anomaly. *IEEE Antennas Propag. Mag.*, 2012, v. 54, no. 6, 242–244.
3. Catt I. The Catt Question. <http://www.ivorcatt.co.uk/x54c1.htm>
4. Catt I. The death of electric current. *Wireless World*, December 1982, 79–81. Accessed from <http://www.ivorcatt.co.uk/x18j100.pdf>

LETTERS TO PROGRESS IN PHYSICS

The Roland De Witte Experiment, R. T. Cahill, and the One-Way Speed of Light

Joseph Catania

E-mail: jcatania1@verizon.net

In “The Roland De Witte 1991 Experiment (to the Memory of Roland De Witte)” (*Progr. Phys.*, 2006, v. 2(3), 60–65), R.T. Cahill gives us a briefing on his view that interferometer measurements and one-way RF coaxial cable propagation-time measurements amount to a detection of the anisotropy in the speed of light. However, while I obtain first order propagation delays in calculations for one-way transit which would show geometric modulation by Earth’s rotation, I do not agree with Cahill’s simplistic equation that relates the modulation solely to the projection of the absolute velocity vector \mathbf{v} on the coaxial cable, called v_p by Cahill (*ibid.*, p. 61–62). The reader should be warned that Cahill’s equation for Δt (*ibid.*, p. 63) is crude compared with a full Special Relativistic derivation.

1 Introduction

In *The Roland De Witte 1991 Experiment (to the Memory of Roland De Witte)* [1], R. T. Cahill gives us a briefing on his view that interferometer measurements and one-way RF coaxial cable propagation-time measurements amount to a detection of the anisotropy in the speed of light. This startling conclusion is difficult to swallow in the face of rigorous light speed in vacuo measurements which are reproducible and flaunt good experimental controls. For instance, in [2] Eisele et. al. were able to limit anisotropy in c to a fractional uncertainty of 10^{-17} . It would seem apparent that, to this precision, there is no first or second order anisotropy in the two-way speed of light.

2 The one-way speed of light

As regards the one-way speed of light, a point of confusion in regard to spurious claims of anisotropy might be exemplified by measurements with the Global Positioning Satellite (GPS) system, which can measure the rotational speed of the Earth, v , by the way it affects the propagation time of an electromagnetic signal used in the GPS system [3]. Thus, the *apparent* velocities $c + v$ and $c - v$ would be measured instead of c . But, certainly, GPS is not to be interpreted as capable of measuring c itself. As further clarification, let us say that, through some means I could set a train moving at 20 miles per hour along a railroad track in a due Easterly direction. At some point on the track to the East of the train I have stationed a measurement instrument which reads exactly 20 mph. If I now move this measuring instrument in an Easterly direction at 5 mph I should only measure the train speed as 15 mph. If I give the measuring instrument a Westerly motion of 5 mph, I should measure for the train 25 mph. Most of us have an intuitive familiarity with this situation. In no way should there be a temptation to assign the 15 or 25 mph speed to the train velocity which is obviously 20 mph. We should

not confuse actual velocity with apparent velocity. Likewise, one-way propagation times of electromagnetic signals cannot be used to calculate c , which has already been assumed constant, but they would be useful in calculating the v in $c + v$ or $c - v$, if the distance of propagation were known.

Similarly, the Michelson-Morley interferometer measurements Cahill refers to in [1] were not developed to measure the speed of light, c , but to measure relative motion, v to a postulated luminiferous ether. That Cahill admits this measurement of v was successful [4] on the one hand would seem to defy his light speed anisotropy conclusion on the other. So, I find it difficult to reconcile propagation time calculations used in interferometer measurements which assume c , a well-known constant of nature, as the speed of light in vacuo, and the explicit solution for the variable v , the motion with respect to the ether, with light-speed anisotropy in any form.

3 First order effects

Nevertheless, as pointed out, there are fringe-shifts measured in many interferometers and there is De Witte’s propagation time delay (which is correlated to sidereal time). It has been established in Michelson-Morley type interferometer measurements that there is a correlation of measurements of \mathbf{v} with cosmic velocity (similar to the CMB dipole velocity) accompanied with amplitude modulations with respect to rotation and revolution of the Earth. This is expected on the basis of current theory which explains fringe-shifts in interferometers as due to dielectric in the light path (no fringe-shifts are expected in vacuum interferometers) [4]. However, while I obtain first order propagation delays in calculations for one-way transit which would show geometric modulation by Earth’s rotation, I do not agree with Cahill’s simplistic equation that relates the modulation solely to the projection of the absolute velocity vector \mathbf{v} on the coaxial cable, called v_p by Cahill [1, p. 61–62]. The reader should be warned that

Cahill's equation for Δt [1, p. 63] is crude compared with a full Special Relativistic derivation. Also the period of the modulation based on a fixed absolute motion vector in the Miller direction would not be 12 sidereal hours but 24 as can be plainly seen from the geometry. Also apparent from the geometry is that Cahill's v_p would never go negative and indeed does not attain zero. In fairness Cahill states in (ibid., p. 63) that DeWitte's data is plotted with a false zero making the periodicity appear to be 12 hours sidereal. As well, there does not seem to be sufficient support of Cahill's use of $n = 1.5$ for De Witte's coaxial cable. It's more likely that $\epsilon = 1.5$.

4 Conclusion

In conclusion I can only say that although Cahill understands De Witte's result is first order and shows correlation to the Miller direction we must be cautious in ascribing this result to unconfirmed phenomena such as light speed anisotropy especially since SR would seem to be an apt predictor of the effect.

Submitted on December 30, 2015 / Accepted on December 31, 2015

References

1. Cahill R.T. The Roland De Witte 1991 Experiment. *Progress in Physics*, 2006, v. 2, issue 3, 60–65.
2. Eisele Ch., Nevsky A.Yu., Schiller S. Laboratory test of the isotropy of light propagation at the 10^{-17} level. *Physical Review Letters*, 2009, v. 103 (9), 090401.
3. Gift S.J.G. One-way speed of light relative to a moving observer. *Applied Physics Research*, 2013, v. 5, no. 1.
4. Cahill R.T. and Kitto K. Michelson-Morley experiments revisited. *Apeiron*, 2003, v. 10(2), 104–117.

A Non-anthropocentric Solution to the Cosmological Constant Problem

Robin James Spivey

Biological Sciences, Bangor University, Brambell, Deiniol Road, Bangor, Gwynedd, Great Britain
E-mail: y.gofod@gmail.com

Accelerating cosmological expansion is driven by a minuscule vacuum energy density possibly seeking opportunities to decay to a true ground state. Quasar characteristics imply their central engines possess an intrinsic magnetic field compatible with the presence of an electrically charged toroidal dark hole, an eternally collapsing structure lacking an event horizon. The possibility is consistent with the inability of black holes to capture particles in a universe of finite age, Einstein's dismissal of the Schwarzschild metric as unphysical and the implausibility of the various paradoxes invoked by black hole existence. The unclocked innards of these dark holes would expose immense vacuum accelerations at their cores, inevitably tempered by Planck scale physics. The Unruh effect predicts that intense yet highly localised heating should occur there. As thermal energy gradually amasses and dissipates, radiation would eventually start to escape into the surrounding environment. Virtual from the dark hole perspective, the emissions could not decrease the dark hole's mass: the energy source must instead be the universal vacuum, the likely repository of dark energy. In analogy with core-collapse supernovae, neutrinos should dominate the cooling flows. Red-shifting to low energies upon escape, quantum degenerate haloes should form predominantly around the largest galaxies. This mechanism is promising from the perspective of enabling the future universe to efficiently sustain aquatic life before stars become scarce, offering a biological yet decidedly non-anthropocentric solution to the cosmological constant problem.

1 Introduction

Despite tremendous interest in the composition, distribution and interactions of dark matter particles, the existence of only one of the candidates presently transcends speculation. This accolade belongs to the neutrino — a fermion which, by virtue of its non-zero mass [1], is capable of gravitational condensation to form quantum degenerate galactic haloes [2]. With cosmological constraints already implying hierarchical neutrino mass eigenstates, the similarity of $kT_{H_2O(aq)}$ and $|\Delta m_{13}|c^2$ is most striking. Neutrino oscillations require physics beyond the Standard Model but renormalisable extensions likely demand the existence of sterile varieties. Intriguingly, these facts could be hinting at the perpetuation of advanced aquatic lifeforms well beyond the stelliferous era [3].

Dark matter was recently overshadowed by the discovery of dark energy, a yet more pervasive and enigmatic phenomenon causing universal expansion to accelerate. Its spatial energy density is some 120 orders of magnitude smaller than quantum physics can comfortably explain [4]. Although dark energy's influence is locally imperceptible it dominates the cosmos already [5,6] and consequently represents a formidable new frontier in cosmology. Parallels can be drawn with theories of cosmic inflation, whose accelerating expansion purportedly terminated as an underlying energy field decayed into high energy particles. Whereas Mercury's orbital peculiarities provided both an impetus for Einstein's development of general relativity and a means of experimentally validating corrections to Newtonian mechanics, dark energy is far

more inscrutable. Thus, insights of any kind are potentially valuable and merit careful investigation.

The goal of this work is to revisit the cosmological constant problem following the advancement of a novel model of the universe predicting the future decay of dark energy. This framework happens to incorporate the first scientific hypothesis concerning the long-standing mystery of extraterrestrial silence, yielding testable predictions for particle physics [3]. There is a very real prospect that the future universe might sustain aquatic life for $\sim 10^{25}$ years in certain locales via the annihilation of gravitationally condensed neutrinos within hexagonally close-packed iron (hcp-Fe), a material that dominates the cores of oceanic planets up to $\sim 15 M_{\oplus}$ [7]. Active neutrinos may well have sufficient mass to maintain liquid oceans since oscillations [8] and cosmological considerations [9] imply that Σm_{ν} lies in the range 58–230 meV. Moreover, the hcp/fcc boundary in iron's phase diagram conveniently lends itself to planetary thermoregulation almost independently of planet size [3]. Key to the scenario is the finding that the cosmic abundance of neutrinos must first be hugely augmented, implicating the future decay of dark energy primarily to galaxy-engulfing active neutrino halos of a mass approaching $10^{21} M_{\odot}$ within ~ 60 Gyr [10].

This particular line of cosmological investigation has not previously succeeded in venturing any suggestion as to a physical process by which dark energy might decay to neutrinos, an eventuality implied by the propensity of neutrinos to sustain aquatic life with remarkable efficiency [3]. Other avenues of enquiry have similarly failed to pinpoint specific

mechanisms for vacuum discharge capable of ending the current phase of cosmic acceleration, although a model of dark energy interacting with a neutrino-like fermion field has been considered [11]. The present approach draws heavily on developments in black hole research and observational cues from the contrasts between active and inactive galactic nuclei. A promising mechanism for dark energy discharge shall be identified here but its quantitative analysis is likely to remain challenging for some time, in large part due to the continuing lack of a theory of quantum gravity and knowledge of physics at the highest energies. The concluding discussion reflects upon the capability of this mechanism to fulfil its cosmological motivations and thereby offer a radical new approach to comprehending the minute energy density of the vacuum.

2 Theoretical motivations

2.1 The physics of biology

Life is reliant on complex biochemical interactions involving only three subatomic particles whose arrangements are stabilised by only two forces: electromagnetism and the strong interaction. The neutron is marginally more massive than the combined rest mass of a proton and an electron, allowing protons and neutrons to coexist without prohibiting the formation of neutron degenerate matter within dense stars. The strong interaction conveniently allows the assembly of heavy atomic nuclei despite intense electromagnetic repulsion between protons. Of the elements up to lead, only three lack unconditionally stable isotopes, yet most possess only one or two stable isotopes. Remarkably minor adjustments to several physical constants could radically shorten the periodic table or rule out chemistry altogether. Space might be populated mainly by neutron stars and black holes. Stars might be incapable of nuclear fusion, too short-lived to support complex evolutionary processes or so dim that planets orbiting within their habitable zones soon become tidally-locked. Supernovae might never scatter the ashes of stars into space, so that their ejecta might form elements necessary for planets and life.

Ascertaining why nature's constants might possess the values they do has been traditionally regarded as the preserve of mathematical physics — yet the approach has met with little success. One should therefore remain open to alternative possibilities. Due to the improbable compatibility of the physical laws with long-term biological evolution the 'anthropic principle' has been advanced. Although the universe existed well before life on Earth commenced, our existence imposes retrospective constraints on the physical laws and the natural constants. However, the anthropic principle does not allow one to conclude that physics would have been any different had chance chemical interactions never led to life on this planet. Furthermore, the Copernican revolution provides a historical precedent that the innate sense of human self-importance does not always provide a reliable founda-

tion for cosmological extrapolation. Moreover, appeals to the precondition of human existence are at odds with a multitude of life-promoting characteristics in nature falling comfortably outside the gamut of the anthropic principle.

Nevertheless, the traditional perception has been that the universe is rather ill-suited to life. The Earth's living organisms only harness some 0.1% of the insolation, in turn amounting to just one billionth of the Sun's total radiation. No star liberates more than 0.008% of its rest mass energy through fusion processes. The Sun burns hydrogen to helium, yet 90% of its hydrogen will remain by the time it becomes a red giant. Planets orbiting low mass red dwarves are never habitable for very long. These considerations seem to paint a picture of a universe largely inhospitable to life. However, there is now reason to believe that impression was premature. Active neutrinos may be capable of internally heating iron-cored oceanic planets on galactic scales, sustaining aquatic life long after the stars have died with impressive efficiency [3, 10]. The fact that a technological species has evolved on this planet provides no plausible explanation for this, and neither does happenstance.

For oceans to be maintained in a liquid state by neutrino annihilation, haloes are required of a mass approaching the threshold for gravitational implosion, some 4~7 orders of magnitude larger than the mass of a galaxy cluster. Synthesis of the available information points to dark energy decaying at a suitable juncture predominantly to active neutrinos that form dense haloes. This is expected somewhat prior to the disappearance of the last stars capable of cultivating life on orbiting planets — when the universe is approximately five times its present age. Accordingly, the continuity of life need not be endangered and there would be ample time for the evolution of technologically and ethically advanced colonising civilisations before widespread colonisation could be attempted.

The former solar neutrino anomaly was resolved when it was found that neutrinos undergo spontaneous flavour oscillations [1], demonstrating their possession of mass. The diminutive neutrino mass scale closely coincides with the energy scale associated with the temperature of liquid water. Furthermore, it is small enough to ensure that neutrinos can condense under gravity to form galaxy-enveloping structures supported by fermionic quantum degeneracy [3, 10].

The likelihood of a neutrino mutually annihilating with other neutrinos depends on the ambient neutrino concentration, but the probability of a neutrino scattering with nucleons does not. In a dense neutrino halo, annihilation events can be frequent in the presence of hcp-Fe at temperatures compatible with the presence of a 4s electron receptive to some of the annihilation energy [3, 7]. Whilst even high energy neutrinos can travel through light years of lead without scattering, low energy neutrinos are unlikely to emerge from an iron-cored planet without annihilating if the planet is immersed in a sufficiently dense neutrino halo. If, as cues from cosmology

and oscillation experiments suggest, the neutrino mass scale lies in the vicinity of ~ 0.05 eV, a halo density of just one picogram per cubic kilometre can sustain liquid oceans. A neutrino mass just one order of magnitude smaller would be incapable of maintaining liquid oceans, even with assistance from a thick insulative crust of ice.

2.2 Biotic reasoning

Appreciation of the inadequacy of the weak anthropic principle as an explanation for the fine-tuning of physics inspired an investigation into whether dark matter particles might be capable of sustaining aquatic life. This led to the discovery that neutrino annihilation is capable of targeting 4s electrons in hcp-Fe, a phase transition in iron providing a natural thermoregulation mechanism as the 4s electrons transfer to the 3d subshell, assuring that the thermal flux through a subglacial ocean is essentially independent of planetary mass for relatively dense, rocky planets [3, 10].

Being polytropic, a neutrino halo expands upon depletion and, due to the resulting decline in neutrino concentration, the heating capacity eventually falls below that needed to maintain liquid oceans. A sizeable fraction of the halo energy might thereby go to waste. The energy of a neutrino halo approaching the gravitational implosion limit is inversely related to the mass of an individual neutrino. Hence, a smaller neutrino mass might support aquatic life for longer. This likely explains why the neutrino mass scale is at least one order of magnitude lower than required merely for haloes to fully surround a galaxy — reducing their ambient concentration, yet not to the degree that aquatic life cannot be maintained. Although this permits a lengthy aquatic era, the wastage this incurs as the aquatic era ends is not insignificant. This may be mitigated by another consideration, one that is potentially relevant to the current composition of dark matter.

Half the Earth's atmosphere is concentrated at altitudes below 6 km, less than 0.1% of the planet's radius. If the mass of the Earth were somehow abruptly reduced, say to the mass of the Moon, the atmospheric scale height would increase a hundred-fold. Many species, including our own, would soon die of asphyxiation. The gravitational load on the Earth's atmosphere is clearly vital to our minute-by-minute survival. By analogy, if oceanic planets are pictured as inhaling neutrinos and exhaling infrared photons, gravitationally loading an excessively large halo could locally boost the neutrino concentration over galactic scales. This could be very useful at late times when the neutrino halo would otherwise be quite rarefied within the galaxy. An inner halo of relatively low mass, roughly twice the diameter of the contained galaxy but of far greater mass than the galaxy itself, would apply an effective additional load. Ideally, this auxiliary halo would also support its own weight through fermionic repulsion but its constituent particles would be highly inert, virtually immune to all forces except gravity.

The weak interaction maximally violates parity so that right-handed particles and left-handed antiparticles are insensitive to it. Hence, particles resembling conventional neutrinos but having opposite chirality and a somewhat larger mass would be advantageous. Prior to the realisation that such particles could be biologically useful, anomalies in neutrino oscillation experiments were already alluding to the existence of sterile neutrinos at the eV-scale [12, 13]. Furthermore, gravitational lensing data for the Abell 1689 galaxy cluster strongly hinted at the presence of a cloud of degenerate 1.5 eV fermions [14, 15], inconsistent with cosmological constraints on active neutrinos but in keeping with the expectation that eV-scale sterile neutrinos would be well-suited to concentrating active neutrinos on galactic scales [3, 10].

Whilst the discovery of sterile neutrinos has not yet been formally announced and their mass remains loosely constrained, the statistical evidence for their existence already stands at 3.8σ . Active neutrinos may well have sufficient mass to maintain liquid oceans since $58 < \Sigma m_\nu < 230$ meV [16]. Moreover, the hcp/fcc boundary in iron's phase diagram beautifully lends itself to planetary thermoregulation in a manner almost independent of planet size [7, 10]. This picture testifies to the utility of biotic reasoning: a cohesive new approach to cosmology has emerged that dispenses with unsatisfactory anthropic explanations for fine-tuning and yields the first scientific resolutions of the Fermi paradox [3]. Before proceeding to apply similar logic to dark energy decay, attention shall be drawn to some other pertinent considerations.

2.3 Inferences and expectations

The potential sustainment of aquatic life by neutrinos annihilating within iron-cored oceanic planets would be sufficiently efficient as to bear the hallmarks of cosmic design, in turn implying that some coordinated strategy for life could operate at all levels throughout the universe. A swift overview of the envisaged scenario is provided here so as to facilitate expectations concerning the manner and timing of dark energy decay. The model anticipates that, following the decay of dark energy to neutrinos, oceanic planets will be populated by advanced civilisations adept at installing aquatic biospheres free of welfare-endangering perils such as carnivorous predation and avoidable disease. Photosynthesis has oxygenated the Earth's atmosphere but photochemistry would not be possible in subglacial oceans deprived of sunlight. This may not be problematic since many have speculated that complex chemosynthetic lifeforms could have evolved in Europa's dark and relatively anoxic oceans [17, 18].

Habitable planets capable of evading tidal-locking invariably orbit stars within the mass spectrum that terminate their lives as red giants, incinerating or absorbing any potentially habitable planets that may have orbited their progenitors. Given the cosmological context, this may be telling: it could

imply that lifeforms incapable of interstellar relocation are deemed too primitive to be granted survival beyond the early universe. More advanced, space-faring civilisations are likely to be skilled geneticists, especially if they have wrested control of their own biology from the clutches of haphazard evolutionary processes whether for purely ethical reasons or in an attempt to safeguard their ongoing survival [3, 19].

Galaxies frequently undergo mergers within galaxy clusters. Potentially introducing alien cultures to one another, collaboration and competition might ensue. If each galaxy spawns roughly one colonising civilisation then the ultimate outcome of a process of galactic mergers is expected to be a supercivilisation which could be confidently entrusted with colonisation [3]. The welfare of post-evolutionary lifeforms inhabiting skilfully designed aquatic biospheres could comfortably exceed that of the Earth's present lifeforms. Hence, the cosmic arrangement may seek to maximise opportunities for more advanced lifeforms subject to the need to first cultivate responsible colonists through natural selection. This impression is reinforced by the fact that formerly habitable orbiting planets would be incinerated during the red giant stage of their host stars, prohibiting the later revival even of dormant microbial organisms interred deep underground.

Statistical modelling of this scenario constrains to within a factor of two or so the rarity of advanced civilisations, not only now but also at other times [3]. This leads to three novel yet related resolutions of Fermi's paradox, all involving the future decay of dark energy to active neutrinos predominantly in galaxy clusters when the universe is ~ 5 times its present age. A small fraction of life-cultivating stars will remain active until then, assuring survival for civilisations capable of interstellar relocation. It is striking that the measured energy density of empty space is compatible with this timescale, offering a hitherto elusive explanation for its tiny yet non-zero value where the $\Lambda \approx m_p^4$ guesstimate for the value of the cosmological constant has failed so spectacularly, m_p being the Planck mass. This attempt to calculate the value of the cosmological constant from quantum theory alone has yielded what is notoriously regarded as the '*worst prediction in all physics*'. Note, however, the claim that "although the magnitude of the vacuum energy remains a profound mystery, it seems clear that an understanding of how quantum-mechanical matter behaves in curved spacetime will play an important role in any eventual resolution to the puzzle" [20].

In summary, the universe may keep a tight rein on its available resources, restricting their expenditure except when it supports life — in particular post-evolutionary aquatic life. The temporary, relatively inefficient sustainment of evolutionary life during the early universe can be amortised by the vastly more efficient ($\sim 99\%$) and lengthy ($\sim 10^{25}$ year) aquatic era. Life is reliant on energy but energy conservation is a cornerstone of physics. Thus, energy cannot be the underlying currency of the universe. However, the universe could be strategically arranged so that entropy-increasing processes

are restricted *unless* they either engender (via abiogenesis and evolution by natural selection) or support (via the direct internal heating of oceanic planets) advanced aquatic lifeforms.

2.4 The necessity of dark energy & its timely decay

If neutrinos are capable of efficiently sustaining aquatic life, why did the universe not provide dense neutrino haloes from the outset? Had the question instead been why did the universe not provide habitable planets from the outset, the answer would have been obvious: the primordial elements hydrogen and helium cannot form rocky planets or biomolecules. Answering the original question concerning the biological necessity for dark energy may not be so straightforward.

From a design perspective, a substantial postponement in the widespread provision of habitable environments for life could be a prudent precaution against incompetent colonisation. There may therefore be no urgency associated with the delivery of neutrinos until life-cultivating stars are becoming scarce. If dark energy must decay so that neutrino haloes capable of planetary heating can form then it can represent a temporary repository for the fuel needed by a forthcoming aquatic era. The accelerating expansion of the universe by an incongruously small cosmological constant may well be heralding the future delivery of active neutrinos.

Although some currently regard the cosmological constant as being literally responsible for cosmic acceleration, it requires an inexhaustible energy supply and its minuscule value defies theoretical explanation. Thus, independently of biotic reasoning, dynamical models of dark energy have been favoured. However, that leaves completely open the fate of the cosmic expansion. Biotic reasoning can assist here, offering clear hints concerning the future decay of dark energy, its timing, the particles it will yield and their distribution in space. A mechanism with considerable potential for satisfying all these various expectations shall now be sketched.

3 Gravitational collapse

Annual modulation in the timing of eclipses of Jupiter's moon Io allowed Ole Rømer to infer in 1676 that light travels at a finite speed. In 1783 John Michell argued for the existence of "dark stars", objects of sufficient mass that their escape velocity would exceed the speed of light. The Michelson-Morley experiment of 1887 found that light always travelled at the same speed regardless of the orientation of the apparatus relative to the Earth's passage through space. This spurred Einstein to conceive his 1905 theory of special relativity which ushered in the concept that clocks in relative motion are subjected to time dilation. When relativity was generalised a century ago to include gravitation Einstein showed that matter and energy could also affect the passage of time and indeed the entire network of temporal relationships amongst world-lines populating a spacetime manifold. Prior to this there was

no reason to suspect that nature might be capable of evading Michell's dark star expectation. We now understand that gravitational time dilation can grow without limit in general relativity: the proper time along one timelike worldline can cease to advance relative to the proper time along another. Combinations of the constants c , \hbar and G cannot impose any Planck-scale restriction upon time dilation, a dimensionless quantity. It is therefore interesting to consider whether time dilation effects might be sufficient to ensure that gravitationally imploding matter is incapable of vanishing from view and becoming forever lost to the universe.

Supermassive black holes are by now widely thought to inhabit galactic nuclei, their masses occupying the range $10^6 \sim 10^{10} M_{\odot}$ [21]. A Schwarzschild black hole has a surface area $A_{\bullet} = 4\pi R_{\bullet}^2 = 16\pi G^2 M^2 / c^4$ which ostensibly governs its growth rate when immersed within a degenerate cloud of matter. In a galaxy hosting a million black holes of stellar mass, their combined area might be ten orders of magnitude less than that of a single supermassive black hole. Thus, if supermassive black holes did exist they would unacceptably sap neutrino haloes of biologically vital energy [3]. A mechanism for the eradication of eternal black holes is known involving the separation of virtual particle pairs via quantum tunnelling effects near the event horizon, the escape of one particle coming at the black hole's expense [22, 23]. However, the timescale for black hole evaporation via Hawking radiation is $5120\pi G^2 M_{\bullet}^3 / \hbar c^4$ so astrophysical black holes require upwards of 10^{67} years to fully evaporate.

Rotating black holes are invariably plagued by the presence of closed timelike curves within their event horizons. The information loss paradox remains another stubborn complication [24] and locations of supposedly infinite mass density, *singularities*, hardly seem physically realistic — for example on energy conservation grounds. In addition, it has long been known that infalling particles, whether following timelike or lightlike trajectories, require infinite time to reach the event horizon of a black hole according to any arbitrarily-moving clock situated anywhere external to the event horizon. As the worldlines within a spacetime manifold must satisfy a global network of temporal interrelationships, black holes cannot grow through particle capture — rendering their dynamical formation implausible too [25–32]. No particle is better suited to the challenge of penetrating a Schwarzschild black hole event horizon than a radially ingoing photon but the metric then informs us that $|dr/dt| = c(1 - 2m/r)$ so that $dr/dt \rightarrow 0$ as $r \rightarrow 2m$ with attention confined to the regular coordinate region $r > 2m$. Evidently, the photon's motion is halted before it can reach the event horizon at $r = 2m$. It is possible to insert a mirror between the photon and the event horizon at arbitrarily late times and have it reflect back out along a radial geodesic, confirming that it never entered the black hole. Since nothing can be captured through an event horizon, the defining characteristic of a black hole, one can safely infer that gravitational collapse will always be safely

arrested by the phenomenon of gravitational time dilation.

Given the enthusiasm for black hole research within modern science it may be difficult to accept that these objects are merely mathematical curiosities. Some further elaboration may thus be warranted. *Any* useful theory of gravity should be capable of predicting the trajectories of test particles in the vicinity of a gravitating point mass. If there is some maximum speed which no particle can exceed then matter straying too near the point mass will inevitably be incapable of escaping. It should therefore come as no surprise whatever that general relativity yields a stationary solution matching this expectation. But whereas Newtonian gravity would predict the existence of dark stars, general relativity departs radically since it predicts that time dilation can grow arbitrarily large even at a finite distance from the point mass responsible. Caution must hence be exercised since the fact that the Schwarzschild metric exists by no means guarantees that the solution is actually attainable through any physical process from realistic initial conditions in a universe of finite age.

Analytical solutions to Einstein's field equations can only be derived in certain idealised situations. The metrics describing the familiar eternal black holes have all been obtained by imposing the condition of stationarity: an assumption prohibiting any temporal evolution of the spacetime geometry, including of course any evolution that might be initially required to obtain the stationary configuration in question. Tracing the full *dynamics* of gravitational collapse in general relativity is hindered by the nonlinearities of the field equations. However, a pioneering work tackled this for the spherically symmetric case of a homogeneous sphere of pressureless matter [33]. If the advancement of proper time along all worldlines satisfies a very obvious constraint [31] this solution is well-behaved and time dilation asymptotically halts the collapse process just prior to event horizon formation. This constraint is compatible only with the exterior perspective on Oppenheimer-Snyder collapse — the interior perspective requiring the physically impossible advancement of proper times along *all* external worldlines. Though aware that neutron degeneracy pressure cannot always resist gravitational collapse, Oppenheimer & Snyder did at least appreciate that “it is impossible for a singularity to develop in a finite time” [33]. Hence, their collapse did not form a Schwarzschild black hole. Accordingly, gravitational collapse is expected to generate “*dark holes*”, objects that may superficially resemble black holes in many circumstances but due to their lack of event horizons are free of their various pathologies. Whereas the situation considered by Oppenheimer and Snyder pertained to a particular mass distribution, a straightforward yet general proof now exists that black holes can neither form nor grow based on the inability of the Schwarzschild black hole to capture test particles of any description in a universe of finite age [31]. Furthermore, recent independent studies of dynamical collapse have also confirmed the non-formation of event horizons [27, 32].

Assertions that objects with event horizons exist cannot be verified even in principle [34] although the detection of Hawking radiation could arguably provide a counterexample. Whether or not black holes lie strictly outside the scope of science, nothing can prohibit the collection of evidence that specific black hole candidates *lack* rather than *possess* event horizons. The finite lifetimes ($10^7 \sim 10^8$ years) and the collimated jets of relativistic charged particles produced by quasars strongly suggests that their central engines have an intrinsic magnetic field — probably a dipole created by a spinning electrically charged torus [31, 35]. This interpretation calls into question the physical relevance of the *Principle of Topological Censorship*, a mathematical theorem constructed upon the assumption that trapped surfaces are present within some given spacetime [36] — a condition that no dark hole will satisfy [31] but which also belies the singularity theorems [37–39]. That is likely why, through the accrual of angular momentum, dark holes are free to adopt toroidal geometry. The torus can then amass a significant net electrical charge, its rotation inducing a poloidal magnetosphere defending against charge neutralisation from the plasma of an orbiting accretion disk. Toroidal dark holes can explain the formation of relativistic jets of charged particles, the extreme energetics and the finite lifetimes of quasars [35]. Astronomers have found evidence of intrinsic magnetic fields in several black hole candidates, consistent with the absence of event horizons both in galactic black hole candidates [40–42] and in quasars [43]. When evaluating solutions of the field equations, the need to ensure that those configurations can be realistically attained without falling foul of constraints on global relationships has been generally overlooked: their formation must not involve the physically impossible advancement of time along any worldline within the spacetime manifold [31].

4 Dark energy from dark holes

The intersection of quantum mechanics and black hole physics led to the field of black hole thermodynamics. If, however, gravitational collapse is incapable of realistically producing objects endowed with event horizons, it may be more fruitful to consider the implications of quantum physics for dark holes. The complete absence of an event horizon precludes the emission of any Hawking radiation but a closely related process, the Fulling-Davies-Unruh effect [44–48], could be highly relevant to this discussion. Regarded as a fundamental and inescapable consequence of quantum field theory [49], the Unruh effect teaches us that the concept of a particle is observer dependent and that what may seem to exist in one reference frame may not exist at all in another [44]. It predicts that an accelerating detector coupled to a quantum field should perceive empty space to be seething with particles whose temperature is proportional to the acceleration of the detector [50].

According to Einstein's equivalence principle, a uniform acceleration is locally indistinguishable from a constant gravitational field. Hence, Unruh radiation is also expected if the detector/observer is stationary and, due to the presence elsewhere of a gravitating body, space is accelerating. Unruh and Hawking temperatures both share the common form $T = \hbar a / 2\pi c k_B$ where T is the temperature of the perceived thermal bath of a vacuum field undergoing relative acceleration a . Although the value of the scaling factor $\hbar / 2\pi c k_B$ is minute, $\sim 4 \times 10^{-20} \text{ }^\circ\text{K/g}$, it is generally accepted that the Unruh effect has already been experimentally confirmed in the observed depolarisation of electrons in storage rings [51, 52]. More sensitive measurements should be possible by exploiting Berry's phase [53].

Black body radiation from nearby galaxy clusters peaks in the X-ray spectrum, betraying the fact that gas there has been intensely heated by gravitational contraction. In the rarefied and hence transparent conditions of the intracluster medium, X-rays provide cooling. In contrast, matter exists in a dense state within stars, making their interior regions opaque to electromagnetic radiation. During core collapse supernovae, stars release large amounts of gravitational binding energy that drive runaway thermonuclear reactions. In such circumstances, cooling occurs almost exclusively through neutrino emission [54]. Even at energies above $2m_e c^2 \approx 1 \text{ MeV}$ at which electron/positron pairs are readily produced, neutrinos continue to dominate supernova cooling processes [55]. Some 10% of the rest mass of a collapsing star can be converted into neutrinos within a ten second interval [56]. The total luminosity during that period is $\sim 10^{46} \text{ W}$ or $10^{19} L_\odot$, which greatly exceeds the power output of an entire galaxy. Radiated neutrinos are ultrarelativistic, a fact exploited by the Supernova Early Warning Systems to alert optical telescopes of impending supernova activity [57].

Likewise, neutrino escape will represent the main cooling mechanism for dark holes. They will copiously radiate neutrinos during their initial implosion stages but these formative outflows will soon cease as gravitational time dilation mounts, and are of no interest to this discussion. From the perspective of a stationary external observer, the internal vacuum of a dark hole whose collapse is arrested by time dilation will appear to undergo extreme acceleration — and hence, via the Unruh effect, should appear to be extremely hot. Over astronomical timescales, this intense but highly localised heating can deposit considerable thermal energy as heat percolates from the core of a dark hole to its periphery. The ordinarily prohibited proton decay process $p^+ \rightarrow n^0 + e^+ + \nu_e$ might be perceptible to dark hole onlookers whereas in the local frame it appears to be $p^+ + e^- \rightarrow n^0 + \nu_e$. The neutrino-related supernova processes $e^- + p^+ \leftrightarrow \nu_e + n^0$ and $e^+ + n^0 \leftrightarrow \bar{\nu}_e + p^0$ should also be important. Ultimately, via the Unruh effect, temperatures should become so elevated throughout the dark hole that some of the neutrinos generated by the thermal bath would satisfy the dark hole's escape requirements. A state of

pseudo-equilibrium might exist in which the neutrino cooling rate approximately balances the power in the Unruh effect.

For an observer accelerating through Minkowski space it has been speculated that the energy in Unruh radiation comes courtesy of the work that maintains the observer’s acceleration [20]. Hawking radiation is thought to come at the expense of the black hole which captures negative energy virtual particles, reducing its mass. However, neither explanation satisfactorily explains the origin of the Unruh-related radiation emanating from a dark hole. According to general relativity, distortions of spacetime influence the motions of all objects because gravitation is, like the vacuum, a *global* phenomenon. Energy conservation may therefore be possible if the vacuum represents a quantum gravitational energy reservoir coupling both to gravity (consistent with accelerating cosmic expansion) and quantum mechanics (consistent with the Unruh effect). If indeed the vacuum acts as a dynamical repository for dark energy, the Unruh effect precipitated by extreme accelerations within dark holes may be uniquely capable of tapping into the cause of the accelerating cosmic expansion and eventually halting it.

Although neutrinos could dominate the cooling processes both within core collapse supernovae and dark holes, the dynamics of the latter case would be profoundly influenced by time dilation. Neutrinos escaping from dark holes would necessarily be red-shifted to low energies. This could be most advantageous to aquatic life: if the emerging neutrinos are at most mildly relativistic they could be easily retained by the gravity of the dark hole’s host galaxy — thereby forming dense, inhabitable haloes.

4.1 Acceleration scales

In order to quantify the Unruh effect within dark holes there is a need to determine the acceleration of the vacuum due to gravity from the perspective of the surrounding universe. Although the Schwarzschild metric describes a black hole, by Birkhoff’s theorem its exterior region can accurately represent the spacetime outside any spherically symmetric mass distribution, including a dark hole. Consider a timelike particle momentarily at rest in Schwarzschild coordinates $x^\lambda = [x^t, x^r, x^\theta, x^\phi]$. The metric reads $d\tau^2 = (1 - 2GM/c^2r)dt^2$ such that $dt/d\tau = 1/\sqrt{1 - 2GM/c^2r}$ and the particle’s 4-velocity u is simply

$$u = \frac{dx^\lambda}{d\tau} = \dot{x}^\lambda = \left[\frac{1}{\sqrt{1 - 2GM/c^2r}}, 0, 0, 0 \right]. \tag{1}$$

To find the particle’s acceleration, $a^\lambda = \ddot{x}^\lambda$, the components of the covariant derivative of u are needed. Using the fact that dx^λ is non-zero only for dx^t and making use of the Christoffel symbols of the second kind, Γ^i_{kl} where

$$\Gamma^i_{kl} = \frac{g^{im}}{2} \left(\frac{\partial g_{mk}}{\partial x^l} + \frac{\partial g_{ml}}{\partial x^k} - \frac{\partial g_{kl}}{\partial x^m} \right) \tag{2}$$

this simplifies to

$$du^\lambda = \left[\frac{\partial u^\lambda}{\partial x^t} + u^\sigma \Gamma^\lambda_{\sigma t} \right] dx^t. \tag{3}$$

Since u^t is the only non-zero component of u^λ and $\Gamma^t_{tt} = 0$, it follows that $du^t = 0$. The only non-zero component of $\Gamma^r_{\sigma t}$ is $\Gamma^r_{tt} = GM(1 - 2GM/c^2r)/r^2$ and so

$$du^r = u^t \Gamma^r_{tt} dx^t = \left(\frac{GM(1 - 2GM/c^2r)}{r^2 \sqrt{1 - 2GM/c^2r}} \right) dt. \tag{4}$$

As Γ^t_{tt} and Γ^r_{tt} are both zero, the covariant derivative sought is $du = [0, GMr^{-2} \sqrt{1 - 2GM/c^2r} dt, 0, 0]$. The proper acceleration of the test particle can now be obtained using the fact that $dt/d\tau = 1/\sqrt{1 - 2GM/c^2r}$.

$$a^r = \dot{u}^r = \frac{du^r}{d\tau} = \sqrt{1 - 2GM/c^2r} \left(\frac{GM}{r^2} \right) \frac{dt}{d\tau} = \frac{GM}{r^2}. \tag{5}$$

Hence, the 4-acceleration is $a = [0, GM/r^2, 0, 0]$ and for this momentarily stationary particle the magnitude of the outwardly directed acceleration is $a_s = \sqrt{a_\mu a^\mu} = \sqrt{g_{rr} a^r a^r} = \sqrt{g_{rr}} GM/r^2$. Since $g_{rr} = (1 - 2GM/c^2r)^{-1}$,

$$a_s \equiv \frac{d^2r}{d\tau^2} = \frac{GM}{r^2 \sqrt{1 - 2GM/c^2r}}. \tag{6}$$

This acceleration corresponds to that of the vacuum at $x^r = r$, as perceived by remote observers. The Unruh temperature which this acceleration would predict, neglecting for now the influence of time dilation, would be

$$T_u = \frac{\hbar a_s}{2\pi c k_B} = \frac{\hbar GM}{2\pi c k_B r^2 \sqrt{1 - 2GM/c^2r}}. \tag{7}$$

Both a_s and T_u diverge as $r \rightarrow 2GM/c^2$, the radius of the event horizon. At $x^r = r$, the time dilation relative to distant objects can be readily derived from the Schwarzschild metric by setting $dr = d\theta = d\phi = 0$ to obtain $d\tau/dt = \sqrt{1 - 2GM/c^2r}$. Applying this correction factor to T_u , a finite temperature is obtained at the event horizon, T_{hor} . Inversely related to mass, this is the usual Hawking-Unruh temperature of a black hole:

$$T_{hor} = T_u \left(\frac{d\tau}{dt} \right) = \frac{\hbar c^3}{8\pi k_B G M}. \tag{8}$$

Some appreciation of the variation of the matter distribution within a dynamically forming dark hole would be useful. Oppenheimer & Snyder considered the scenario of uniform density [33]. More realistically, one would expect density to decline towards the periphery of a dark hole. The mean density within the event horizon of a black hole decreases quadratically with mass, $\bar{\rho}_\bullet = 3c^6/32\pi G^3 M_\bullet^2$, and

with radius, $\bar{\rho}_\bullet = 3c^2/8\pi GR_\bullet^2$. The addition of a mass δM to a Schwarzschild black hole increases its radius by $\delta R = 2G\delta M/c^2$ and hence the density of a thin shell at radius R is $\delta M/4\pi R^2\delta R = c^2/8\pi GR^2$. This is again inversely quadratic in R , justifying the expectation that the mass density within a dark hole should generally decline with radius and be most concentrated at the core.

When the square root term in (6) is small the acceleration grows large, permitting a simplifying approximation:

$$r \approx \frac{2GM}{c^2} + \frac{c^6}{8GMa_s^2}. \quad (9)$$

The coordinate time of a photon falling from a modest distance outside the event horizon to this radius satisfies

$$\Delta t > \frac{2GM}{c^3} \ln\left(\frac{8GMa_s^2}{c^6}\right). \quad (10)$$

In the case of a Planck mass black hole this gives

$$\Delta t \gtrsim 2 \times 10^{-44} \ln(3 \times 10^{-69} \times a_s^2). \quad (11)$$

If some 10^{18} seconds (30 Gyr) are allowed to elapse after an infalling particle starts its descent, the apparent acceleration of the vacuum at the particle's final location would be approximately $10^{(10^{62})} \times$ the surface acceleration of a neutron star. It is extremely doubtful that such a huge acceleration is physically attainable. Using dimensional analysis, a quantity constructed using the constants c , G and \hbar must be proportional to $c^{7/2}\hbar^{-1/2}G^{-1/2}$ in order to have the same units as acceleration. An estimate for the Planck acceleration, a_p , is therefore given by

$$a_p \sim \sqrt{\frac{c^7}{\hbar G}} \approx 10^{51}g. \quad (12)$$

The Planck temperature, T_p , is usually considered to be $T_p = m_p c^2/k_B = \sqrt{\hbar c^5/Gk_B^2}$. This tallies with the Unruh temperature for an acceleration of $2\pi\sqrt{c^7/\hbar G}$. However, the Hawking temperature, $\hbar c^3/8\pi k_B GM$, of a Planck mass black hole is normally assumed to be $T_p/8\pi$, yielding a Planck acceleration of $a_p \approx \frac{1}{4}\sqrt{c^7/\hbar G}$. This conforms to the Newtonian acceleration of a Planck mass from a distance matching its Schwarzschild radius. One may quibble over the best definition of a_p but it is apparent that $a_p \ll 10^{10^{62}}g$. Notice also that increments in proper time less than the Planck time, $t_p = \sqrt{\hbar G/c^5}$, are likely to be meaningless and, therefore, time dilations exceeding 10^{60} are essentially infinite within a universe less than 14 Gyr old.

If trans-Planckian accelerations are unattainable in nature then, independently of gravitational time dilation, this consideration alone would prohibit both the formation and growth of black holes. For a black hole of mass $M \gg m_p$, the ratio of the radius at which a stationary particle would experience the

Planck acceleration to the radius of the event horizon would be $1 + m_p^2/M^2$. The time dilation at the Planck acceleration radius is given by

$$\frac{d\tau}{dt} = \sqrt{1 - 2GM/rc^2} = \sqrt{1 - \frac{1}{1 + m_p^2/M^2}} \approx m_p/M. \quad (13)$$

The perceived temperature of the Unruh heat bath, T_b , at radius $r > 2GM/c^2$, as reported by observers remote from the Schwarzschild black hole, requires correction for time dilation:

$$\begin{aligned} T_b &= T_u \times \left(\frac{d\tau}{dt}\right) = \left(\frac{\hbar a_s}{2\pi c k_B}\right) \left(\frac{d\tau}{dt}\right) \\ &= \frac{\hbar GM \times \frac{d\tau}{dt}}{2\pi c k_B r^2 \sqrt{1 - 2GM/rc^2}} = \frac{\hbar GM}{2\pi c k_B r^2}. \end{aligned} \quad (14)$$

For a given black hole, T_b is a function of radius and declines as $1/r^2$. According to the Stefan-Boltzmann law for an ideal radiator, the radiative power, P_r , is given by the product of the area, $A = 4\pi r^2$, the Stefan-Boltzmann constant, $\sigma = \pi^2 k_B^4/60\hbar^3 c^2$, and the fourth power of the temperature:

$$P_r = A\sigma T_b^4 = 4\pi r^2 \left(\frac{\pi^2 k_B^4}{60\hbar^3 c^2}\right) \left(\frac{\hbar GM}{2\pi c k_B r^2}\right)^4 = \frac{\hbar G^4 M^4}{240\pi c^6 r^6}. \quad (15)$$

Evidently, this power is highly localised since $P_r \propto 1/r^6$. Bearing in mind the Shell Theorem, it makes little difference how the mass distribution within a spherically symmetric dark hole declines with radius (whether as $\sim 1/r^2$, $1/r$, $1/\sqrt{r}$ etc) since the radiated power will be almost entirely sustained by quantum activity in the immediate vicinity of its core where the density is maximal and the gravitational acceleration of the vacuum is strongest.

By setting $r = r_s = 2GM/c^2$, the Schwarzschild radius, in (15) one recovers the power obtainable through Hawking evaporation, $P_\bullet(M_\bullet) = \hbar c^6/15360\pi G^2 M_\bullet^2 \approx (M_\bullet/M_\odot)^{-2} \times 10^{-28}$ W. For a $10^{10} M_\odot$ black hole, this comes to some 10^{-48} W, roughly 98 orders of magnitude short of what aquatic life would need. Even if a dark hole of this mass were composed of a set of concentric spherical shells, each of a thickness comparable to the Planck length ($\sim 10^{-35}$ m) and each radiating the same power, there would still be a shortfall of around 50 orders of magnitude.

The maximum power available from Hawking evaporation occurs when the black hole's mass approaches the Planck scale. The Compton wavelength of a particle of Planck mass is comparable to its Schwarzschild radius, $\hbar/cm_p \approx 2Gm_p/c^2$. Classical physics breaks down at this scale because $\hbar \neq 0$. It is customary in gravitation to work with the reduced Planck mass, $m_p \approx \sqrt{\hbar c/8\pi G}$. A black hole of this mass will be a nebulous, fuzzy object referred to here as a 'reduced Planck particle' (**rpp**). Its radiated power would be roughly $P_{\text{rpp}} \approx 2 \times 10^{49}$ W, though it might be somewhat larger as the Planck power is usually taken to be, $c^5/G \approx 4 \times 10^{52}$ W.

It is generally thought that Planck particles are incapable of evaporating since their high Hawking temperatures preclude the black body radiation of significantly lighter particles. Hence, many imagine them to be quasi-stable remnants of black hole evaporation which is why they are now included amongst the panoply of dark matter candidates [58]. They also represent the most likely outcome of collapse processes that might otherwise result in naked singularities and the violation of cosmic censorship [59]. An **rpp** interred within a dark hole may be invulnerable to evaporation as long as the dark hole continues to exist. Thus, it is conceivable that power might be sustainably radiated at a level approaching P_{rpp} for spherically symmetric dark holes. Although this is very much an upper limit, it is encouraging that it yields a crude prediction that dark energy decay might terminate just as the last life-cultivating cease to be active.

4.2 Angular momentum injection

The Kerr metric represents a stationary, rotationally symmetric and asymptotically flat rotating black hole. It accommodates angular momentum through an extended singularity located within the plane $z = 0$, lying along the circle $x^2 + y^2 = a^2$ in Kerr coordinates. Its radius, $a \equiv J/m$, depends on the angular momentum, J , of the black hole. At extremality, $a \rightarrow m$ and $J \rightarrow m^2$, the radius of the singularity coincides with that of the two event horizons, $r_{\pm} = m \pm \sqrt{m^2 - a^2}$. For $a^2 < m^2$ the singularity lies internal to both event horizons.

At high angular momentum, self-gravitating fluids bifurcate from the Maclaurin spheroids, yielding toroidal configurations [60, 61] reminiscent of the prototypical Dyson rings [62]. With analytical solutions confined to relatively simple cases, numerical techniques have now been deployed to better explore the space of axisymmetric configurations [63–67]. The assumption of homogeneity has been relaxed, differential rotation has been allowed and realistic equations of state have been modelled. Qualitatively similar results have been obtained in both Newtonian analyses and general relativity [68–70]. Ergoregions can arise even in the absence of event horizons [71], which may be of some relevance to jet formation in quasars [35].

Since topological censorship does not apply to spacetimes lacking trapped surfaces, the gravitational collapse of a rotating body can result in a toroidal mass distribution, analogous to the circular source of the Kerr geometry although visible to the surrounding universe. Whilst the angular momentum of a Kerr black hole is bounded, $a^2 \leq m^2$, there is no such restriction for a dark hole: the major radius of a self-gravitating torus can be arbitrarily larger than its minor radius. The axisymmetric Kerr geometry cannot dissipate rotational kinetic energy via gravitational waves. Moreover, since gravitational waves are incapable of superluminal propagation, any gravitational radiation due to perturbations of the singularity would necessarily remain imprisoned within

the event horizon. However, deviations from axisymmetry deep within a dark hole could generate rather strong gravitational waves, and their radiation into space would sap the dark hole's energy and angular momentum.

Suppose a dense ring of radius $r = m$ is quantised by subdivision into a circular arrangement of N particles, each of roughly the reduced Planck mass, such that $N = m/m_p$. Since the ring's circumference is $C_r = 2\pi Gm/c^2$, each reduced Planck particle would then be separated from its two neighbouring particles by a distance

$$\frac{C_r}{N} = \frac{C_r m_p}{m} = \frac{2\pi G}{c^2} \sqrt{\frac{\hbar c}{8\pi G}} = \sqrt{\frac{\pi \hbar G}{2c^3}} \approx \sqrt{\frac{\pi}{2}} \ell_p. \quad (16)$$

The mean particle separation should decline as J decreases but if separations below the Planck length ℓ_p are unattainable, the idealised circular arrangement may be disrupted, resulting in localised thickening of the ring. It may help to picture the interior of the toroidal dark hole as a dense circular arrangement of knotty density existing at extreme densities approaching the Planck scale. Due to this granularity and its chaotically fluctuating nature, gravitational waves should be produced which dissipate both angular momentum and rotational energy. Ultimately, these losses should result in a topological collapse of the core.

For the purposes of this discussion, we might simply regard the core of a rapidly spinning dark hole as a circular collection of reduced Planck particles. In the case of a toroidal dark hole they would number m/m_p , a huge number. Toroidal dark holes should therefore receive enormously more internal heating via the Unruh effect than purely spheroidal dark holes of the same mass. Thus, the discharge of vacuum energy would be strongly biased towards the most massive and rapidly spinning dark holes of the cosmos — even if such objects are comparatively short-lived in astronomical terms.

Following galactic mergers, the supermassive dark holes introduced by each galaxy are generally expected to coalesce relatively swiftly since they occupy locations of least gravitational potential within their respective host galaxies. Inspiral supermassive black hole binaries provide prime targets for gravitational wave astronomy [72]. A supergalaxy harbouring an ultramassive remnant dark hole would be the inevitable outcome of hierarchical galaxy mergers. Just as the coalescence of a pair of co-orbiting black holes is able to create a rapidly rotating black hole due to the conversion of orbital angular momentum to rotational angular momentum [73], a pair of coalescing spheroidal dark holes will often combine to produce a more massive dark hole of internally toroidal structure with a dense filamentary core. Violent galactic mergers within galaxy clusters should hence be capable of sporadically inducing episodes of intensively accelerated heating and dark energy discharge until the resulting dark holes lose their toroidal inner structure via the shedding or redistribution of internal angular momentum.

4.3 Discharge timeframes

The details of the physical cooling processes operating within core collapse supernovae are still the subject of ongoing research but it is known that even neutrinos cannot free stream away from an innermost region termed the neutrinosphere. Although the circumstances deep within dark holes will be yet more complex and involve energies well above those probed by any practical particle collider, neutrinos generated there will also be unable to free stream away into space, hindered by the exclusion principle and large interaction cross sections. In order to accurately model these situations, a working theory of quantum gravity will be needed along with an understanding of how matter behaves at near-Planckian temperatures and densities. Also, the influence of strong time dilation must be taken into account, a problem which modern numerical approaches to general relativity still grapple with. Even order of magnitude estimates to the processes involved may currently lie beyond our reach. Nevertheless, it is incumbent upon us to consider the viability of this scenario.

At energies below 1 GeV, electron neutrinos scatter onto neutrons, $\nu_e + n \rightarrow e^- + p^+$, with cross section

$$\sigma_n = \frac{(\hbar c G_F E_\nu)^2 (g_V^2 + 3g_A^2)}{\pi} \approx 10^{-47} \left(\frac{E_\nu}{1 \text{ MeV}} \right)^2 \text{ m}^2. \quad (17)$$

The mean free path of a neutrino can be estimated using

$$\lambda_\nu \approx \left(\frac{\rho}{10^{18} \text{ kg} \cdot \text{m}^{-3}} \right)^{-1} \left(\frac{E_\nu}{10 \text{ MeV}} \right)^{-2} \text{ metres}. \quad (18)$$

Within a supernova the neutron number density may be as high as $\rho_n \sim 10^{45} \text{ m}^{-3}$. For a typical supernova neutrino energy of 30 MeV, the cross section would be $\sim 10^{-44} \text{ m}^2$ and the free path, $\lambda = 1/\rho_n \sigma_n$, may be as short as ten metres. Cooling occurs as neutrinos emerge from a thin shell surrounding a rather constipated, diffusion-limited neutrinosphere. The volumetric luminosity within that spherical escape shell could approach $10^{36} \text{ W} \cdot \text{m}^{-3}$. Deep within a dark hole, degeneracy is also likely to have a profound impact on the dynamics, for instance blocking neutrino production via the Unruh effect deep within the neutrinosphere.

The limiting mass of a halo of 0.05 eV neutrinos is estimated to be $8 \times 10^{20} M_\odot$ [10], equating to an energy in excess of 10^{68} J . The power due to Unruh radiation from a reduced Planck particle was determined earlier to be $P_{\text{rpp}} \approx 2 \times 10^{49} \text{ W}$ so it would take some 7×10^{18} seconds to inflate a habitable neutrino halo, roughly 230 Gyr. Encouragingly, this crude and simplistic estimate has the right order of magnitude: dark energy is anticipated to decay before the universe reaches $\sim 75 \text{ Gyr}$ in age. Pauli blocking and impedance of thermal transport within the time-dilated neutrinosphere will slow the discharge, but episodic input of angular momentum generating ultra-dense rings might easily compensate by hugely accelerating the process, if only briefly.

If, by analogy with Hawking radiation from black holes, the Unruh radiation from deep within supermassive dark holes came entirely at the expense of their dark hole hosts then the lifespan of a supermassive dark hole evaporating at the rate P_{rpp} would be $\sim Mc^2/P_{\text{rpp}}$. This is just a few hours for a $10^6 M_\odot$ black hole and no more than a few years for a $10^{10} M_\odot$ black hole. The observational evidence for the ongoing existence of supermassive black hole candidates in this mass range within galactic nuclei confidently rules out this possibility. It instead points to the dark energy vacuum being the origin of the Unruh radiation which, according to quantum field theory, is mandatory — so much so that it needs no experimental confirmation [49].

Consider now the case of an ultramassive remnant dark hole of a galaxy cluster of a mass $\sim 10^{11} M_\odot$ that ultimately generates a neutrino halo of mass $10^{21} M_\odot$. The Unruh effect provides the dark hole with intense but localised heating. Over time, thermal energy accumulates and steadily diffuses throughout the dark hole. Once peripheral temperatures are sufficient to permit neutrino escape, a galactic halo can start to form. One can envisage neutrino cooling approximately balancing heating from the Unruh effect until vacuum energy is exhausted. If, instead, one assumes that neutrinos barely escape until dark energy is almost fully depleted, then the mass of the dark hole from the galactic perspective must increase by ten orders of magnitude. From the dark hole's vantage, however, its mass will not have changed since there was no Unruh effect attempting to increase the temperature of its constituent matter.

Ignoring the initial thermal energy of the dark hole, in order that it can eventually form a dense neutrino halo from the thermal energy deposited through the Unruh effect, its particles must attain Lorentz factors, γ , of $\sim 10^{10}$ where γ represents the relativistic mass ratio m/m_0 . Temperature is synonymous with kinetic energy and relativistic kinetic energy is proportional to $\gamma m_0 c^2$. The Lorentz factor is closely tied to relativistic temperature according to the relationship, $T = 2(\gamma - 1)m_0 c^2 / 3k_B$. If $\gamma \gg 1$, it follows that $\gamma \approx 3k_B T / 2m_0 c^2$. Thus, for any given temperature, it is much easier for lighter particles such as neutrinos to attain large Lorentz factors. Consequently, irrespective of temperature, neutrinos should dominate the cooling outflows of dark holes. For a neutrino mass of 0.05 eV, a Lorentz factor of 10^{10} corresponds to a temperature of some $4 \times 10^{12} \text{ K}$, comfortably below the Planck temperature $\sqrt{\hbar c^5 / G k_B^2} \approx 10^{32} \text{ K}$. Hence, there is much latitude for dark holes to discharge dark energy by only temporarily adopting internally toroidal matter distributions. Dark holes will of course undergo heating via gravitational contraction during their initial formation, and this energy will contribute to their effective mass, pushing the required Lorentz factors and temperatures for neutrinos to escape somewhat higher. Nevertheless, there seems to be ample scope to accommodate this particular consideration.

5 Discussion

Via the Unruh effect, dark holes may well be capable of tapping into the energy of the vacuum and, in due course, fostering the total discharge of dark energy. A minority of class K stars will continuously host habitable planets until the universe is five times its present age. As the neutrino haloes produced would be capable of efficiently sustaining aquatic life, the model offers a new and biological resolution of the cosmological constant problem. This provides a long-sought alternative to the relatively loose bounds imposed by anthropic arguments [4] which, if neutrinos are well-suited to the task of planetary heating, would be as untenable as the Ptolemaic system. However, this new approach can only explain the value of the present vacuum energy density, not how it might have been tuned to 120 decimal places. That question is akin to asking how the constants of physics in general might have been manipulated to be propitious towards life — something perhaps for string theorists to mull over.

The supermassive dark holes of galaxy clusters are likely to play a prominent role in the decay of dark energy due to their frequent adoption of an internally toroidal structure following violent coalescence events pursuant to galaxy mergers. With circular ‘heating elements’ operating at temperatures potentially approaching the Planck scale, $T_p \approx 10^{32}K$, these rapidly spinning dark holes would accumulate thermal energy far more rapidly than their counterparts in field galaxies. Such extreme conditions will help combat the intense gravitational time dilation and Pauli-blocking deep within dark holes, in time facilitating a radiative flux from their cores. Eventually, peripheral temperatures should rise sufficiently to provide opportunities for neutrinos to escape completely, albeit after redshifting to low energies as they do so. Dense haloes should thereby form around the remnant galaxies of galaxy clusters — in accordance with the expectation that neutrinos might sustain aquatic life into the distant future [3].

During the initial phase of dark hole heating the neutrino luminosity is likely to remain negligible for billions of years. This is no cause for concern: a lengthy delay would be biologically advantageous, usefully prohibiting the widespread colonisation of the universe until ethically mature civilisations are on hand to undertake such daunting responsibilities. Very loosely, the situation might be likened to the conversion of liquid water within a lake into steam by the vigorous agitation of a single water molecule over a prolonged period. It is not inconceivable that galactic nuclei within galaxy clusters may be currently generating gentle outflows of neutrinos. It may even be that changes in the dynamics of galaxies orbiting within clusters may be perceptible over time.

A promising line of enquiry has been outlined concerning dark energy without any radical departure from the scientific method. Whilst alternative proposals capable of predicting the timing, outcome and mechanism of dark energy

decay have not been forthcoming, this scenario dovetails remarkably well with a recently advanced cosmological framework, reinforcing its potential to unravel the composition of dark matter, anticipate the fate of the accelerating cosmic expansion and decipher the mystery of extraterrestrial silence. This same framework offers much scope for understanding why the constants of nature assume the values they do without recourse either to mathematical arguments or anthropic reasoning [74]. Physical fine-tuning influences all aspects of the universe — from the simplest microscopic scales to the most complex macroscopic scales, including multicellular lifeforms, symbiotic ecosystems and the imponderable workings of the human mind. If the fine-tuning of physics cannot be apprehended through mathematical physics alone then alternatives can and should be explored, even if that entails a holistic synthesis of all scientific knowledge. Support has emerged here for the contention within superstring theory that there may exist a vast underlying landscape of physical configurations. A biological resolution of the cosmological coincidence problem, the naïvely surprising similarity between Ω_Λ and Ω_M is also apparent.

Although this dark energy decay scenario must be regarded as tentative for now, it exhibits many compelling features and the remaining uncertainties mainly pertain to timescales. Vacuum discharge by dark holes fulfils the original cosmological expectation that dark energy might decay predominantly to neutrinos of sufficiently low energy as to permit their retention by host galaxies. Whereas black holes have an unhealthy appetite for neutrinos, dark holes are incapable of recapturing the neutrinos they discharge on account of the Unruh effect: those particles belong to a different reality. Dark energy decay should strongly track supermassive, rapidly-rotating dark holes and hence galaxy clusters where collisions between galaxies and supermassive dark holes are commonplace events. There is no reason at present to suppose that significant errors exist in the basic timing constraints based on the measured vacuum energy density, calculated neutrino halo implosion threshold and the necessity of habitable neutrino haloes before the last life-cultivating stars expire. However, much work remains before decay timescales can be confidently calculated. In the meantime, as long as neutrinos continue to bear the hallmarks of cosmic design the efficient sustenance of aquatic life remains a very real possibility and the timely decay of dark energy just before life-cultivating stars die out is a likely outcome of cosmic evolution.

In the field of black hole thermodynamics, the entropy of a black hole is given by $S = kA/4\ell_p^2$. With the entropy of a Sun-like star being $\sim 10^{35} \text{ J} \cdot \text{K}^{-1}$ [75] a single black hole of some 10^4 solar masses would possess as much entropy as all the stars of all the galaxies within the visible universe. Therefore, the existence of even one supermassive black hole in nature would be catastrophic for a universe attempting to judiciously manage entropy-increasing processes for the benefit of advanced lifeforms [3]. Dark holes may not chime

with the scientific orthodoxy of recent decades but they accord with the original ‘frozen star’ interpretation of stellar collapse and dispense with the theoretical shortcomings of black holes. It is not that the stationary black hole metrics are mathematically invalid, merely that they are unobtainable via physically admissible processes: global constraints on the evolution of spacetime manifolds have been generally overlooked [31]. Although one expects any useful theory of gravity to possess within it a solution resembling that obtained by Karl Schwarzschild in 1916, i.e. a bizarre object describing a point mass surrounded by a region from which light cannot escape, the architect of general relativity did not rush to dismiss it. His considered opinion was offered after decades of careful reflection. That his views on black holes now carry so little weight within academic science is disturbing.

On a far more positive note, it comes as some surprise that particles which are able to propagate unperturbed through light years of lead may be of any potential benefit to life. That sterile neutrinos, their yet more inert counterparts, might provide further assistance also defies intuition. However, if this universe is exquisitely configured to host life, all natural phenomena would ideally have something positive to contribute. It would nevertheless be astonishing if the objects lurking at the heart of each galaxy, which many currently believe to be destructive black holes, can serve as portals to a crucial biological energy resource capable of efficiently sustaining aquatic life far into the distant future. We learnt from special relativity that mass and energy are interrelated, a breakthrough necessary to explain how stars could remain active for billions of years, sufficient time for the Sun to support the evolution of complex organisms. Ultimately, the take-home message from general relativity, if only apparent at present to extraterrestrial civilisations, may be that gravity is benign and free of pathologies precisely because time dilation provides a robust mechanism preventing the formation and growth of trapped surfaces — essential for the discharge of dark energy so that aquatic lifeforms might thrive long after the expiry of the stars, harnessing the full promise of $E = mc^2$. If Einstein were still with us he might regard the current fascination with black holes as a pathological science, further affirmation of his 1920 remark to Marcel Grossmann that the world is a “strange madhouse” [76]. It very much seems there is now a contagious misunderstanding of his theoretical legacy. It may be preventing humanity from collectively converging towards a comprehension of the universe capable of providing much-needed guidance for future policy-making.

Submitted on January 3, 2016/Accepted on January 5, 2016

References

1. Fukuda Y., Hayakawa T., Ichihara E., Inoue K., Ishihara K., Ishino H. et al. Evidence for oscillation of atmospheric neutrinos. *Phys. Rev. Lett.*, 1998, v. 81(8), 1562.
2. Cowsik R., McClelland J. Gravity of neutrinos of nonzero mass in astrophysics. *ApJ*, 1973, v. 180, 7.
3. Spivey R. J. A cosmological hypothesis potentially resolving the mystery of extraterrestrial silence with falsifiable implications for neutrinos. *Physics Essays*, 2015, v. 28(2), 254–264.
4. Weinberg S. Anthropic bound on the cosmological constant. *Phys. Rev. Lett.*, 1987, v. 59(22), 2607.
5. Riess A. et al. Observational evidence from supernovae for an accelerating universe and a cosmological constant. *ApJ*, 1998, v. 116, 1009.
6. Perlmutter S. et al. Measurements of Ω and Λ from 42 high-redshift supernovae. *ApJ*, 1999, v. 517, 565.
7. Stixrude L. Structure of Iron to 1 Gbar and 40,000 K. *Phys. Rev. Lett.*, 2012, v. 108, 055505.
8. Olive K. A., & Particle Data Group. Review of particle physics. *Chinese Physics C*, 2014, v. 38(9), 090001.
9. Planck Collaboration. Planck 2015 results. XIII. Cosmological parameters. 2015, arXiv:1502.01589.
10. Spivey R. J. Planetary heating by neutrinos and possible long-term habitats for aquatic life if dark energy decays favourably. *J. Mod. Phys.*, 2013, v. 4(12A), 20–47.
11. De la Macorra A. Interacting dark energy: Decay into fermions. *Astroparticle Physics*, 2007, v. 28(2), 196–204.
12. Kusenko A. Sterile neutrinos: the dark side of the light fermions. *Phys. Reports*, 2009, v. 481(1), 1–28.
13. Kopp J., Maltoni M., Schwetz T. Are there sterile neutrinos at the eV scale? *Phys. Rev. Lett.*, 2011, v. 107(9), 091801.
14. Nieuwenhuizen T. M. Do non-relativistic neutrinos constitute the dark matter? *Europhysics Lett.*, 2009, v. 86(5), 59001.
15. Nieuwenhuizen T. M., Morandi A. Are observations of the galaxy cluster A1689 consistent with a neutrino dark matter scenario? *MNRAS*, 2013, v. 434(3), 2679–2683.
16. Bouso R., Katz D. M., Zukowski C. Anthropic origin of the neutrino mass from cooling failure. *Phys. Rev. D*, 2015, v. 92, 025037.
17. Jackson B., Barnes R., Greenberg R. Tidal heating of terrestrial extrasolar planets and implications for their habitability. *MNRAS*, 2008, v. 391(1), 237–245.
18. Chyba C. F. Energy for microbial life on Europa. *Nature*, 2000, v. 403(6768), 381–382.
19. Savulescu J. Procreative beneficence: why we should select the best children. *Bioethics*, 2001, v. 15(5–6), 413.
20. Carroll S. M. Spacetime and Geometry. An Introduction to General Relativity (Vol. 1). *Addison Wesley*, 2004.
21. Celotti A., Miller J. C., Sciamia D. W. Astrophysical evidence for the existence of black holes. *Class. Quant. Grav.*, 1999, v. 16(12A), A3.
22. Hawking S. W. Black hole explosions. *Nature*, 1974, v. 248(5443), 30–31.
23. Hawking S. W. Particle creation by black holes. *Comm. Math. Phys.*, 1975, v. 43(3), 199–220.
24. Mathur S. D. The information paradox: a pedagogical introduction. *Class. Quant. Grav.*, 2009, v. 26(22), 224001.
25. Einstein A. On a stationary system with spherical symmetry consisting of many gravitating masses. *Annals of Mathematics*, 1939, v. 40, 4.
26. Kiselev V. V., Logunov A. A., Mestvirishvili M. A. Black holes: theoretical prediction or fantasy? *Physics of Particles and Nuclei*, 2006, v. 37(3), 317–320.
27. Vachaspati T., Stojkovic D., Krauss L. M. Observation of incipient black holes and the information loss problem. *Phys. Rev. D*, 2007, v. 76(2), 024005.
28. Kiselev V. V. E., Logunov A. A., Mestvirishvili M. A. The physical inconsistency of the Schwarzschild and Kerr solutions. *Theor. and Math. Phys.*, 2010, v. 164(1), 972–975.

29. Weller D. Five fallacies used to link black holes to Einstein's relativistic space-time. *Prog. Phys.*, 2011, v. 7, issue 1, 93.
30. Chafin C. E. Globally Causal Solutions for Gravitational Collapse. 2014, arXiv:1402.1524.
31. Spivey R. J. Dispelling black hole pathologies through theory and observation. *Prog. Phys.*, 2015, v. 11, 321–329.
32. Piñol M. A model of dust-like spherically symmetric gravitational collapse without event horizon formation. *Prog. Phys.*, 2015, v. 4, 331.
33. Oppenheimer J. R., Snyder H. On continued gravitational contraction. *Phys. Rev.*, 1939, v. 56(5), 455.
34. Abramowicz M. A., Kluzniak W., Lasota J. P. No observational proof of the black-hole event horizon. *Astron. Astrophys.*, 2002, v. 396, L31.
35. Spivey R. J. Quasars: a supermassive rotating toroidal black hole interpretation. *MNRAS*, 2000, v. 316(4), 856–874.
36. Friedman J. L., Schleich K., Witt D. M. Topological censorship. *Phys. Rev. Lett.*, 1993, v. 71(10), 1486.
37. Penrose R. Gravitational collapse and space-time singularities. *Phys. Rev. Lett.*, 1965, v. 14(3), 57.
38. Hawking S. W. The occurrence of singularities in cosmology. III. Causality and singularities. *Proc. Roy. Soc. A*, 1967, v. 300(1461), 187.
39. Hawking S. W. and Penrose R. The singularities of gravitational collapse and cosmology. *Proc. Roy. Soc. A*, 1970, v. 314(1519), 529.
40. Robertson S. L., Leiter D. J. Evidence for intrinsic magnetic moments in black hole candidates. *ApJ*, 2002, v. 565(1), 447.
41. Robertson S. L., Leiter D. J. On intrinsic magnetic moments in black hole candidates. *ApJ Lett.*, 2003, v. 596(2), L203.
42. Robertson S. L., Leiter D. J. On the origin of the universal radio–X-ray luminosity correlation in black hole candidates. *MNRAS*, 2004, v. 350(4), 1391–1396.
43. Schild R. E., Leiter D. J., Robertson S. L. Observations supporting the existence of an intrinsic magnetic moment inside the central compact object within the quasar Q0957+ 561. *ApJ*, 2006, v. 132(1), 420.
44. Fulling S. A. Nonuniqueness of canonical field quantization in Riemannian space-time. *Phys. Rev. D*, 1973, v. 7(10), 2850.
45. Davies P. C. Scalar production in Schwarzschild and Rindler metrics. *J. Physics A*, 1975, v. 8(4), 609.
46. Unruh W. G. Notes on black-hole evaporation. *Phys. Rev. D*, 1976, v. 14(4), 870.
47. Unruh W. G. Origin of the particles in black-hole evaporation. *Phys. Rev. D* 1977, v. 15, 365.
48. Unruh W. G., Schützhold R. Universality of the Hawking effect. *Phys. Rev. D*, 2005, v. 71(2), 024028.
49. Matsas G. E., Vanzella D. A. The Fulling–Davies–Unruh effect is mandatory: the Proton's testimony. *Int. J. Mod. Phys. D*, 2002, v. 11(10), 1573–1577.
50. Crispino L. C., Higuchi A., Matsas G. E. The Unruh effect and its applications. *Rev. Mod. Phys.*, 2008, v. 80(3), 787.
51. Bell J. S., Leinaas J. M. The Unruh effect and quantum fluctuations of electrons in storage rings. *Nucl. Phys. B*, 1987, v. 284, 488.
52. Akhmedov E. T., Singleton D. On the physical meaning of the Unruh effect. *JETP Lett.*, 2008, v. 86(9), 615–619.
53. Martin-Martinez E., Fuentes I., Mann R. B. Using Berry's phase to detect the Unruh effect at lower accelerations. *Phys. Rev. Lett.*, 2011, v. 107(13), 131301.
54. Bahcall J. N., Piran T., Press, W. H., Spergel D. N. *Nature*, 1987, v. 327, 25.
55. Hartmann D. H., Woosley S. E. The cosmic supernova neutrino background. *Astroparticle Physics*, 1997, v. 7(1), 137–146.
56. Woosley S., Janka T. The physics of core-collapse supernovae. *Nature Physics*, 2005, v. 1(3), 147–154.
57. Antoniolli P., Fienberg R. T., Fleuret F. et al. SNEWS: The supernova early warning system. *New Journal of Physics*, 2004, v. 6(1), 114.
58. MacGibbon J. H. Can Planck-mass relics of evaporating black holes close the Universe? *Nature*, 1987, v. 329, 308–309.
59. Christodoulou D. Violation of cosmic censorship in the gravitational collapse of a dust cloud. *Comm. Math. Phys.*, 1984, v. 93(2), 171–195.
60. Bardeen J. M. A reexamination of the post-newtonian maclaurin spheroids. *ApJ*, 1971, v. 167, 425.
61. Eriguchi Y., Sugimoto D. Another equilibrium sequence of self-gravitating and rotating incompressible fluid. *Prog. Theor. Phys.*, 1981, v. 65, 1870.
62. Dyson F. W. The potential of an anchor ring. *Phil. Trans. Roy. Soc.*, 1893, v. 53, 372–375.
63. Hachisu I. A versatile method for obtaining structures of rapidly rotating stars. *ApJ Suppl.*, 1986, v. 61, 479–507.
64. Ansorg M., Kleinwächter A., Meinel R. Relativistic Dyson rings and their black hole limit. *ApJ Lett.*, 2003, v. 582(2), L87.
65. Petroff D., Horatschek S. Uniformly rotating homogeneous and polytropic rings in Newtonian gravity. *MNRAS*, 2008, v. 389(1), 156–172.
66. Horatschek S., Petroff D. A Roche model for uniformly rotating rings. *MNRAS*, 2009, v. 392(3), 1211–1216.
67. Horatschek S., Petroff D. Uniformly rotating homogeneous rings in post-Newtonian gravity. *MNRAS*, 2010, v. 408(3), 1749–1757.
68. Ansorg M., Fischer T., Kleinwächter A., Meinel R., Petroff D., Schöbel K. Equilibrium configurations of homogeneous fluids in general relativity. *MNRAS*, 2004, v. 355(3), 682–688.
69. Fischer T., Horatschek S., Ansorg M. Uniformly rotating rings in general relativity. *MNRAS*, 2005, v. 364(3), 943–947.
70. Meinel R., Ansorg M., Kleinwächter A., Neugebauer G., Petroff D. Relativistic Figures of Equilibrium. *Cambridge Univ. Press*, 2008.
71. Butterworth E. M., Ipser J. R. On the structure and stability of rapidly rotating fluid bodies in general relativity. *ApJ*, 1976, v. 204, 200–223.
72. Enoki M., Inoue K. T., Nagashima M., Sugiyama N. Gravitational waves from supermassive black hole coalescence in a hierarchical galaxy formation model. *ApJ*, 2004, v. 615(1), 19.
73. Buonanno A., Kidder L. E., Lehner L. Estimating the final spin of a binary black hole coalescence. *Phys. Rev. D*, 2008, v. 77(2), 026004.
74. Livio M., Rees M. J. Anthropoc Reasoning. *Science*, 2005, v. 309(5737), 1022.
75. Bekenstein J. D. Black holes and entropy. *Phys. Rev. D*, 1973, v. 7(8), 2333.
76. van Dongen J. On Einstein's opponents, and other crackpots. 2011, arXiv:1111.2181.

Further Insight Relative to Cavity Radiation III: Gedanken Experiments, Irreversibility, and Kirchhoff's Law

Pierre-Marie Robitaille

Department of Radiology, The Ohio State University, 395 W. 12th Ave, Columbus, Ohio 43210, USA
E-mail: robitaille.1@osu.edu

Recently, gedanken experiments have been proposed in order to examine the validity of Kirchhoff's Law of Thermal Emission (*P.-M. Robitaille, Further Insight Relative to Cavity Radiation: A Thought Experiment Refuting Kirchhoff's Law, Prog. Phys., 2014, v. 10, no. 1, 38–40; P.-M. Robitaille, Further Insight Relative to Cavity Radiation II: Gedanken Experiments and Kirchhoff's Law, Prog. Phys., 2014, v. 10, no. 2, 116–120*). In the second of these works, real materials (i.e. graphite and silver) were utilized in order to construct two separate cavities at the same temperature which are then placed in thermal contact with one another. It was hypothesized that the graphite cavity initially contained blackbody radiation and that the silver cavity was devoid of radiation. In the case of the silver cavity, all of the energy of the system was assigned to the phonons in its walls. When the cavities were brought together and a small hole introduced between the cavities, it was hypothesized that thermal contact between the cavity walls would enable the transformation of phonon energy into photon energy, eventually resulting in filling the silver cavity with black radiation. Energy contained within the wall of the silver cavity was believed to be *reversibly* trapped. However, in allowing energy to flow reversibly out of the walls of the silver cavity in this context, it has been assumed that the silver conduction bands could be neglected and that only phonon energy need be considered. However, the reflectivity attributed to the silver cavity should be considered uniquely as a result of energy associated with the formation of its conduction bands. Such formation must be considered *irreversible*. It will be demonstrated that under these conditions Kirchhoff's law, once again, does not hold. The lack of thermal radiation within the silver cavity does not lead to a violation of the second law of thermodynamics.

If a space be entirely surrounded by bodies of the same temperature, so that no rays can penetrate through them, every pencil in the interior of the space must be so constituted, in regard to its quality and intensity, as if it had proceeded from a perfectly black body of the same temperature, and must therefore be independent of the form and nature of the bodies, being determined by temperature alone. . . In the interior therefore of an opaque red-hot body of any temperature, the illumination is always the same, whatever be the constitution of the body in other respects.

Gustav Robert Kirchhoff, 1860 [1]

1 Introduction

Gedanken experiments have played a major role in building support for Kirchhoff's Law of Thermal Emission [1, 2]. If this is the case, it is because Kirchhoff proposed his law without any experimental verification [1, 2]. This remains a significant departure from the other laws of thermal emission [3–6] which have been confirmed through the construction of laboratory blackbodies. In addition, The Law of Equivalence, first formulated by Balfour Stewart [7], has also been confirmed experimentally. However, Kirchhoff's law, namely the

belief that the radiation contained within an arbitrary cavity will always be black, or normal, independent of the nature of the cavity wall, has never been demonstrated experimentally [8–12]. Furthermore, Kirchhoff's law knows no proper theoretical proof [13]. Even Max Planck's theoretical proof of Kirchhoff's law can be shown to be invalid [14]. As such, the real justification for Kirchhoff's law falls on thought experiments, all of which can be shown to contain logical omissions and errors.

A powerful sentiment remains in the physics community that should Kirchhoff's law be invalid, then a violation of the second law of thermodynamics would exist and perpetual motion machines of the second kind could be constructed. The arguments typically involve the consideration of two cavities isolated from the outside world by exterior adiabatic walls. The inner walls of the first cavity are then constructed from a perfect absorber (emissivity $\epsilon = 1$ and reflectivity $\rho = 0$) and should therefore contain black radiation. The inner walls of the second cavity are constructed from a perfect reflector (emissivity, $\epsilon = 0$ and reflectivity, $\rho = 1$). Both cavities are theorized to be at the same temperature. It is then argued that if the second cavity is empty of radiation, that the second law of thermodynamics would be violated as photons could

travel from the first cavity into the second cavity and do net work, even if the temperatures of the two cavities were equal. As such, the conclusion is immediately made that the second cavity cannot be devoid of radiation and indeed must contain black radiation, even if a perfect reflector has no means of generating such radiation. Obviously, a logical error exists in such arguments. The question remains to identify the error.

2 Cavity radiation revisited — reversibility

Recently, the author has proposed two gedanken experiments in order to revisit Kirchhoff's law [15, 16].

In the first of these works, two cavities are considered, wherein a perfectly reflecting cavity is placed within a perfectly absorbing cavity (see Figure 1 in [15]). The experiment demonstrates that arbitrary cavities can indeed be permanently filled with arbitrary radiation [15]. This reinforces Max Planck's statement: "... *in a vacuum bounded by totally reflecting walls any state of radiation may persist*" [6, § 51]. This gedanken experiment and Planck's statement point to a direct contradiction of Kirchhoff's law, as the radiation within all cavities is supposed to be black, independent of the nature of the walls.

In the second of these works, two cavities are once again considered (see Figure 1 in [16]). This time however, the concern is centered on the nature of the cavities themselves. Of particular significance is the realization that the perfectly reflecting cavity cannot be made solely from a theoretical adiabatic wall. That is because such a wall cannot be characterized by any temperature [16]. As such, the author moved to create the second cavity from silver, although importantly, within a footnote, he emphasized that he had neglected the conduction bands of the metal. The idea was that all of the energy of the second cavity could be placed reversibly within its walls and phonons. Thus, the interior of the second cavity would be devoid of any photons. Thermal contact could then be made with the perfectly absorbing first cavity, and the energy contained within the phonons from the second cavity could be released, such that the second cavity becomes eventually filled with black radiation through the action of the first cavity [16].

The idea of this thought experiment was to consider what would happen within the perfectly reflecting cavity, if all of the energy within this system was initially reversibly contained within the phonons of its walls. No energy was permitted to be trapped in the conduction bands.

It could be argued that this was not a proper representation of the silver cavity. As such, it is also possible to build the second perfectly reflecting cavity from a material devoid of conduction bands, but now, to enclose both its inner and outer surfaces with adiabatic walls. In this case, all of the energy of the perfectly reflecting cavity can indeed be contained within its phonons. When the second cavity is placed in thermal contact with the first cavity, by removing part of

the outer adiabatic walls, the energy will flow reversibly out of its phonons. This energy would move into the walls of the first cavity, enabling a photon to be produced and then to cross through a small opening into the second cavity. Both cavities end up being filled with black radiation. No net work is done as the displacement of phonons out of the second cavity, is exactly balanced by the entry of photons into its interior space. No net temperature change is experienced by the second cavity or by the first. All that has happened is that energy initially trapped in the walls of the second cavity has been released into the radiation field. Both cavities still possess the same energy as they did initially.

In hindsight, the reversible experiment was probably not well suited to represent a perfectly reflecting cavity. In fact, it could be imagined that if one removed the inner adiabatic lining from the second cavity, that the phonons could have been used to fill the cavity directly with photons. The first cavity was not even required in this case. This serves to emphasize Max Planck's approach, in that the energy of the system could be accounted for simply through the generation of the radiation field [6]. This has now been shown to be correct when the process involved in creating the field was reversible and no other processes are involved. However, not all processes in materials are reversible and this is why Kirchhoff and Planck have stumbled. Given the state of knowledge at the time, they were unable to properly consider the effect of conduction bands.

3 Cavity radiation revisited — irreversibility

This brings us to the question of what happens when the energy of the second cavity is irreversibly trapped within the conduction bands of the silver.* Let us once again state that the exterior of the first and second cavities are surrounded by adiabatic walls. The first cavity, constructed from graphite acting as a perfect absorber [16], is assumed to be filled with black radiation. The second cavity, constructed from silver acting as a perfect reflector [16], will be assumed to be devoid of any radiation. Then, let us place the cavities in contact, but this time permitting only a small hole to link the interior of the two cavities.

It is often argued that, under these circumstances, photons can flow from the first cavity into the second cavity. However, such a proposal in itself violates the second law. The problem is evident when one considers what happens to a photon which would enter the second cavity. It is clear that at some point, such a photon would interact with the wall of the second cavity. Since a photon contains both energy and momentum, it would impart momentum and energy momentarily to

*This is a structural question, as the presence of conduction bands becomes critical to the structure of silver. It is not possible to manipulate the energy associated with the formation of these bands without destroying the very nature of the metal. Hence, the existence of the conduction bands will be considered irreversible. As for the phonons, they are now assumed, within silver acting as a perfect reflector, to contain no energy.

the wall of the silver cavity. This is strictly forbidden by the second law, because heat would be moving into the wall of the second cavity, not only within the cavity void. Alternatively, consider the entry of the second photon from cavity 1 into cavity 2. This presents a substantial problem now, since cavity 2, having already gained the first photon, has a higher energy content than cavity 1. This is because *both* the cavity wall and the radiation field are used to define the system. Movement of the second photon into cavity 2 must be strictly forbidden by the second law, because heat would be moving from a cavity with a lower temperature to a cavity with a new higher temperature.

Still, our instinct desires that photons can enter the second cavity without violating the second law. The secret to resolving this problem involves the natures of the walls themselves. Let us divide the walls of each cavity into many elements. Within the perfectly absorbing cavity, each of the elements selected possessed at one time the energy contained in the photon at the frequency of interest. However, this energy has now flowed to the interior of cavity 1, as required by Max Planck [6]. The wall elements of the first cavity can be thought of as devoid of energy, but able to absorb the energy of the photon of interest. Conversely, the elements in the silver cavity can be thought of as containing the same amount of energy as the photon of interest. That is because for the silver cavity, all of the energy is initially confined to the wall elements.

Now, the only way to permit a photon to enter the second cavity without violating the laws of thermodynamics is to simultaneously permit an element from cavity 1 to interchange with an element from cavity 2. In this way, when the photon hits the wall of the second cavity, it will actually momentarily impart its momentum and energy to a wall which has now a reduced energy by the value contained in one element of the silver cavity. The photon can enter, but the net result is that the emissivity of the second cavity has begun to rise. Simultaneously, the emissivity of the first cavity, now short one photon and with one perfectly emitting element replaced with a perfectly reflecting element, has begun to fall. Should the cavities be of equal dimensions and contain equal numbers of elements, the net result would be that the total emissivity of both cavities becomes a weighted average of the joint emissivities. Both cavities now contain gray radiation and the second law was never violated.

It is evident that when the small hole was made between the two cavities, that their walls, from a thermodynamic point of view, became one. It is in neglecting this important fact that some physicists attempt to state that the second law of thermodynamics has been violated. In fact, the law is violated only when the experiment is not fully presented. The truth is that the net emissivity of the total cavity simply becomes gray. Photons can exist anywhere within this new cavity, but their net density will not be black.

At the same time, if it is possible to drive additional heat

into this system, one can built up black radiation in these two cavities, as highlighted long ago by Stewart [7] and as re-emphasized recently by the author [17, 18].

4 Summary

In the end, arbitrary cavities are not necessarily filled with black radiation. Laboratory blackbodies are specialized objects always made from relatively good emitters of radiation over the frequency range of interest, as well illustrated by the facts (see references within [8–12]). No valid theoretical proof of Kirchhoff's law has been formulated and no gedanken experiments can properly account for the existence of this law.

Dedication

This work is dedicated to my second grandchild, Daniel.

Submitted on: January 6, 2016 / Accepted on January 7, 2016
First published online on: January 7, 2016

References

1. Kirchhoff G. Über das Verhältnis zwischen dem Emissionsvermögen und dem Absorptionsvermögen der Körper für Wärme und Licht. *Poggendorfs Annalen der Physik und Chemie*, 1860, v. 109, 275–301. (English translation by F. Guthrie: Kirchhoff G. On the relation between the radiating and the absorbing powers of different bodies for light and heat. *Phil. Mag.*, 1860, ser. 4, v. 20, 1–21).
2. Kirchhoff G. Über den Zusammenhang zwischen Emission und Absorption von Licht und Wärme. *Monatsberichte der Akademie der Wissenschaften zu Berlin*, sessions of Dec. 1859, 1860, 783–787.
3. Wien W. Über die Energieverteilung in Emissionsspektrum eines schwarzen Körpers. *Ann. Phys.*, 1896, v. 58, 662–669.
4. Stefan J. Über die Beziehung zwischen der Wärmestrahlung und der Temperatur. *Sitzungsberichte der mathematisch-naturwissenschaftlichen Classe der kaiserlichen Akademie der Wissenschaften*, Wien 1879, v. 79, 391–428.
5. Planck M. Über das Gesetz der Energieverteilung im Normalspektrum. *Annalen der Physik*, 1901, v. 4, 553–563 (English translation by ter Haar D.: Planck M. On the theory of the energy distribution law in the normal spectrum. The old quantum theory. Pergamon Press, 1967, 82–90; also Planck's December 14, 1900 lecture *Zur Theorie des Gesetzes der Energieverteilung in Normalspektrum*, which stems from this paper, can be found in either German, or English, in: Kangro H. Classic papers in physics: Planck's original papers in quantum physics. Taylor & Francis, London, 1972, 6–14 or 38–45).
6. Planck M. The theory of heat radiation. P. Blakiston's Son & Co., Philadelphia, PA, 1914.
7. Stewart B. An account of some experiments on radiant heat, involving an extension of Prévost's theory of exchanges. *Trans. Royal Soc. Edinburgh*, 1858, v. 22, no. 1, 1–20 (also found in Harper's Scientific Memoirs, edited by J.S. Ames: The Laws of Radiation and Absorption: Memoirs of Prévost, Stewart, Kirchhoff, and Kirchhoff and Bunsen, translated and edited by D.B. Brace, American Book Company, New York, 1901, 21–50).
8. Robitaille P.-M. On the validity of Kirchhoff's law of thermal emission. *IEEE Trans. Plasma Sci.*, 2003, v. 31, no. 6, 1263–1267.
9. Robitaille P.-M. A critical analysis of universality and Kirchhoff's law: A return to Stewart's law of thermal emission. *Progr. Phys.*, 2008, v. 3, 30–35.

10. Robitaille P.-M. Blackbody radiation and the carbon particle. *Progr. Phys.*, 2008, v. 3, 36–55.
 11. Robitaille P.-M. Kirchhoff's law of thermal emission: 150 Years. *Progr. Phys.*, 2009, v. 4, 3–13.
 12. Robitaille P.-M. Blackbody radiation and the loss of universality: Implications for Planck's formulation and Boltzmann's constant. *Progr. Phys.*, 2009, v. 4, 14–16.
 13. Schirmacher A. Experimenting theory: The proofs of Kirchhoff's radiation law before and after Planck. *Hist. Stud. Phys. Biol. Sci.*, 2003, v. 33, 299–335.
 14. Robitaille P.-M. and Crothers S.J. "The Theory of Heat Radiation" Revisited: A Commentary on the Validity of Kirchhoff's Law of Thermal Emission and Max Planck's Claim of Universality. *Progr. Phys.*, 2015, v. 11, no. 2, 120–132.
 15. Robitaille P.-M. Further Insight Relative to Cavity Radiation: A Tough Experiment Refuting Kirchhoff's Law. *Prog. Phys.*, 2014, v. 10, no. 1, 38–40.
 16. Robitaille P.-M. Further Insight Relative to Cavity Radiation II: Gedanken Experiments and Kirchhoff's Law. *Prog. Phys.*, 2014, v. 10, no. 2, 116–120.
 17. Robitaille P.-M. On the Equation which Governs Cavity Radiation I. *Prog. Phys.*, 2014, v. 10, no. 2, 126–127.
 18. Robitaille P.-M. On the Equation which Governs Cavity Radiation II. *Prog. Phys.*, 2014, v. 10, no. 3, 157–162.
-

LETTERS TO PROGRESS IN PHYSICS

Mansouri-Sexl Test Theory: The Question of Equivalence between Special Relativity and Ether Theories

Maciej Rybicki

Sas-Zubrzyckiego 8/27, 30-611 Krakow, Poland

E-mail: maciej.rybicki@icloud.com

The goal of this paper is drawing attention to a mistake confusing discussion upon the alternatives to special theory of relativity (STR). In the Mansouri-Sexl test theory utilized as a mathematical framework for testing the preferred frame theories, the Lorentz transformation of time has an erroneous form. This generates a false conclusion, namely that a theory based on Tangherlini transformation is empirically equivalent to STR.

Before the advent of STR, FitzGerald [1] and Lorentz [2] proposed a solution to the Michelson-Morley experiment, different from that resulting from the Einstein's theory. Their idea, extensively developed in the Lorentz's theory of electrons [3,4] (later known as Lorentz ether theory — LET) consisted in assumption that objects moving with respect to a postulated preferred frame of reference, determined by motionless "aether", are contracted in the direction of their motion. This idea, together with the introduced by Larmor assumption that clocks moving through ether slow down by a velocity dependent factor, sufficed also to explain the modified M-M experiment, i.e. the Kennedy-Thorndike experiment. Defined in these terms, length contraction and time dilation constitute real processes of dynamic origin, connected with the impact of absolute motion on molecular forces. However, after appearing of Einstein's 1905 paper on STR [5], this idea has been ignored and abandoned by the overwhelming majority of physicists. The reason was that, in spite of its different ontology LET did not formally differ from STR, neither led to specific empirical predictions. The underlying cause binds to the space-time transformations, in fact determining the shape of theory. Namely, the Lorentz transformation (to which Voigt, Larmor, Poincare and Lorentz contributed in various degree) evolved to a symmetrical form reflecting the STR founding postulates instead of the Lorentz's assumptions. Thus, paradoxically, Lorentz transformation became the main obstacle in evolving the original Lorentz's idea to a form of consistent autonomic theory. Eventually, LET gained the status of a superfluous ontology put upon the STR formalism (so-called "Lorentzian approach to relativity"), which made the choice between LET and STR the question of simplicity ruled by the Occam's razor. Neither the (much later) space-time transformation consistent with original assumptions (Tangherlini [6]), nor the Bell's exact calculations (Bell [7]) deriving "relativistic" effects from Maxwell's equations by means of classical physics and quantum mechanics, did alter this general opinion.

The today's version of LET takes the form of test theories verifying STR by introducing free parameters instead of these resulting from definite assumptions. They are in particular the Robertson's test theory [8] and Mansouri-Sexl theory [9–11] for their basic equivalence known by the common name of Robertson-Mansouri-Sexl test theory (RMS). We shall focus on the Mansouri-Sexl (M-S) transformation presented in [9], considered to be a proper mathematical framework for experiments verifying special relativity. While the Lorentz transformation (boost) is

$$\left. \begin{aligned} t' &= \gamma \left(t - \frac{vx}{c^2} \right), & t &= \gamma \left(t' + \frac{vx'}{c^2} \right) \\ x' &= \gamma (x - vt), & x &= \gamma (x' + vt') \end{aligned} \right\}, \quad (1)$$

where

$$\gamma = \frac{1}{\sqrt{1 - v^2/c^2}}$$

(while $y' = y$, $z' = z$, in all transformations here considered), Mansouri & Sexl introduced a generalization:

$$t = aT + \epsilon X, \quad x = b(X - vT) \quad (2)$$

The coordinates, X , T are the ones measured in the postulated preferred frame Σ in which the speed of light is axiomatically isotropic. Instead, x , t are the coordinates measured in frame S being in standard configuration with Σ . The idea consists in measuring independently the factors a and b (functions of v) in experiments, and to choose one of two alternative values of ϵ : $-v/c^2$ or 0 , corresponding to the alternative synchronization conventions. The first, Poincare-Einstein (P-E) "internal" synchronization, based on the axiom of isotropic one-way speed of light in any inertial frame (i.e. based on the postulate of invariant speed of light), relates to $\epsilon = -v/c^2$, a factor responsible for the relativity of simultaneity. The second, "external" synchronization, related to $\epsilon = 0$, consists in adjusting all inertial clocks to the clocks

synchronized in the preferred frame Σ according to the P-E synchronization, which entails absolute simultaneity. Beside these two, there exists a third possible convention, the (slow) clock transport, which can be classified as internal procedure. The clock-transport convention confirms P-E synchronization provided STR is correct; instead its relation with the theories involving absolute simultaneity is not unambiguous inasmuch as they basically may, or may not predict time dilation and length contraction.

Any observed deviations from the exact relativistic values of a and b in the first or second order experiments (according to Mansouri and Sexl, resulting in deviations from the isotropic two-way speed of light) would speak for the preferred frame alternatives to STR. Mansouri and Sexl state that for $a = b = 1$, $\epsilon = 0$, the Galilean transformation is obtained, which is correct. If, after employing the external synchronization, a and b equal to unity, it would mean that mechanical phenomena are ruled by Newtonian physics and subject to the Galilean principle of relativity, while the Maxwell equations (and the relevant constant speed of light) refer to the preferred frame (ether) only. This is exactly what Michelson and Morley (ineffectively) expected to detect in their experiments.

However, Mansouri and Sexl also claim that for $1/a = b = \gamma$ and $\epsilon = -v/c^2$, their transformation turns into the Lorentz transformation, which is obviously wrong. This mistake is coupled with the incorrect notation of the Lorentz transformation of time, written in their paper as:

$$t' = \frac{t}{\gamma} - \frac{vx}{c^2}, \quad (3)$$

whereas the correct form is

$$t' = \gamma \left(t - \frac{vx}{c^2} \right). \quad (4)$$

In fact, this mistake is not simply accidental; being trivial, it has however a deeper cause. Namely, Mansouri and Sexl intended to treat separately the questions of time dilation and simultaneity. This, however, is infeasible with respect to the Lorentz transformation in which relativity of simultaneity and relativistic effects are inseparably connected. This mistake entails false conclusion as to the question of equivalence between STR and the postulated ether theory. It also maintains a persistent myth, according to which the Michelson-Morley experiment, together with the Kennedy-Thorndike experiment provides an evidence for the invariant speed of light. What these (and other) experiments proved in fact with a high degree of probability is the isotropy of the two-way speed of light, which however is not tantamount to isotropy of the one-way speed of light. Mansouri and Sexl came to a false conclusion that the difference in one-way speed of light is a sole matter of choice of the synchronization convention. Consequently, they concluded that only violation of the two-way isotropy resulting in deviations from the rela-

tivistic values of a and b constitutes a challenge to STR.

From among various alternatives to special relativity, the preferred frame theory (PFT) here considered seems to be the only one consistent with the Lorentz's original idea (we treat PFT as a specific formulation of "ether theory"). It is based on the general assumption according to which there exists a physically substantial preferred frame of reference, of which the properties are:

1. In the preferred frame, the one-way speed of light is isotropic;
2. The bodies moving in the preferred frame shrink by the Lorentz factor in the direction of their motion; the clocks moving in the preferred frame slow down by the Lorentz factor.

The effects mentioned in the second postulate are interpreted as "real", which means that their relation to the preferred frame does not depend on the choice of reference frame in which they are described. Provided that, from these postulates one derives the following asymmetrical transformation between the preferred frame Σ (coordinates T, X) and frame S moving with respect to the preferred frame (coordinates t, x):

$$\left. \begin{aligned} t &= \frac{T}{\gamma}, & T &= t\gamma \\ x &= \gamma(X - vt), & X &= \frac{x}{\gamma} + vt\gamma \end{aligned} \right\}. \quad (5)$$

While using the notation used in M-S transformation, this would mean: $1/a = b = \gamma$, $\epsilon = 0$. Transformation (5) determines all dynamic and kinematical properties of PFT. Formally, the above transformation and Lorentz transformation do not convert to each other. Mansouri and Sexl quote this transformation in their paper [9], rightly attributing it to Tangherlini. However, they erroneously claim Tangherlini transformation differs from Lorentz transformation only with respect to the synchronization convention employed, which is a direct consequence of a basic mistake above-mentioned. They conclude that theories determined by these transformations (i.e. STR and PFT) are empirically equivalent to each other. According to this viewpoint, the ether system can be singled out in an arbitrary manner and thus respective predictions concerning experimental results in any inertial system are identical. This false conclusion confuses discussion on the Lorentzian approach for nearly forty years.

As a matter of fact, PFT shares some empirical predictions with STR. The main similarity is that PFT predicts length contraction and time dilation by the usual Lorentz factor, provided measurements are executed in the preferred frame (in more detail Rybicki [12]). It predicts e.g. the elongation of lifetime of muons crossing the atmosphere since the Earth frame is nearly identical (compared with the muon's speed) with the postulated preferred frame. It also gives identical to STR prediction (although different interpretation) to

the twin paradox, irrespectively of the choice of the observer's "rest" reference frame. This also refers to the "realistic" version of twin paradox, namely the Hafele-Keating experiment.

PFT predicts the isotropic two-way speed of light, which makes the M-S theory ineffective in testing this alternative to STR. To show this question in details, let us return to the usually used notation with primed and non-primed coefficients, here the latter attributed to the preferred frame (thus, below, S denotes the preferred frame and S' the frame in motion). From the fact that clocks and measuring rods moving with respect to S are distorted in the definite way by the Lorentz factor it follows that, in S' , the speed of light traveling along x -axis is, dependently on the (positive or negative) direction:

$$c'_1 = (c - v)\gamma^2, \quad c'_2 = (c + v)\gamma^2, \quad (6)$$

where v denotes the velocity of the observer with respect to the preferred frame along x -axis. (In the 2D and 3D depictions, the light wave front form ellipse and ellipsoid, respectively). The averaged two-way speed of light on path l' parallel to x -axis is constant (isotropic) since the respective time is

$$t' = \frac{l'}{(c - v)\gamma^2} + \frac{l'}{(c + v)\gamma^2}. \quad (7)$$

After simple algebra, one gets $t' = 2l'/c$, a result identical to that predicted by STR. While the speed of light defined according to STR determines the relativity of simultaneity, the speed of light defined according to Eq. (6) forms an alternative solution, in the sense that it determines absolute simultaneity.

In general, the concept of "relative velocity" between two frames, defined in STR as identical speed (the same for the observers in S' and S), is replaced in PFT by the concept of "mutual velocities". While S' moves against S with the velocity v , the speed of S measured in S' becomes

$$v' = v\gamma^2. \quad (8)$$

This involves significant consequences, e.g. such as the following one. Assume S' and S'' are the frames in motion to each other, and that their velocities with respect to the preferred frame S are identical. Since also the Lorentz factors described in S for the frames S' and S'' are identical, the mutual velocities measured in both frames must be identical either, thus constituting the "relative velocity" in the STR sense. However, contrary to the STR predictions, neither of these frames will manifest "relativistic effects" (length contraction and time dilation) when observed (measured) from the other one, since

$$\frac{\gamma'}{\gamma} = \frac{\gamma''}{\gamma} \implies \frac{\gamma'}{\gamma''} = 1. \quad (9)$$

This specific prediction of PFT, together with the characteristic "position" of the Earth with respect to the assumed

preferred frame enables experiment settling between STR and PFT. Namely, one assumes that, if the preferred frame exists, it is likely identical with the (local) frame in which the cosmic microwave background radiation (CMBR) is isotropic. Meanwhile, from the observed Doppler effect obtained from WMAP known as "dipole anisotropy" one deduces that Solar System moves with respect to isotropic CMBR with the velocity 368 ± 2 km/sec in the direction of galactic longitude $l = 263.85^\circ$ and latitude $b = 48.25^\circ$. This translates to the Lorentz factor:

$$\gamma = (1 - 1.52 \times 10^{-6})^{-1} \approx 1 + 7.6 \times 10^{-7}. \quad (10)$$

PFT predicts that an object moving with equal velocity with respect to the isotropic CMBR, in the direction (e.g.) opposite to that of Solar System (i.e. $l = 83.85^\circ$ and $b = 228.25^\circ$) will not exhibit any relativistic effects since $\gamma'/\gamma'' = \gamma''/\gamma' = 1$. This prediction is absolute, i.e. does not depend on the choice of synchronization conventions or any other assumptions. It is quite obvious that in the lab experiments with γ reaching the value of 1,000 (thousand) and higher, the difference between 7.6×10^{-7} and zero is not identifiable. To be detected, it thus demands employing subtle methods in the specially aimed experiments. Nevertheless, it does not seem to lie beyond the scope of the today's experimental capabilities.

Conclusion

We have shown that an incorrect notation of the Lorentz transformation of time in the Mansouri-Sexl test theory entails false claims, namely:

1. Only the theories predicting anisotropic two-way speed of light differ from STR;
2. A theory maintaining absolute simultaneity is equivalent to special relativity (Mansouri and Sexl call this a "remarkable result");
3. As far as prediction of experimental results is concerned, Tangherlini transformation is completely equivalent to Lorentz transformation.

These claims confuse the discussion upon the preferred frame alternatives to special relativity. Contrary to a common belief, a theory based on the preferred frame postulate and formalized by Tangherlini transformation (i.e. PFT) is not in whole experimentally equivalent to STR. Thus settling between them two in experiments is a feasible task. The present author aims to develop this subject in the subsequent papers.

Submitted on January 6, 2016 / Accepted on January 8, 2016

References

1. FitzGerald G.F. The ether and the Earth's atmosphere. *Science*, 1889, v. 13, 390.
2. Lorentz H.A. The relative motion of the Earth and ether (1892). In: *Collected Papers*, v.IV, Hague, 1937, 219–223.

3. Lorentz H.A. Attempt of a Theory of Electrical and Optical Phenomena in Moving Bodies. Leiden, E. J. Brill, 1895.
 4. Lorentz H.A. Simplified theory of electrical and optical phenomena in moving bodies. *Proceedings of the Royal Netherlands Academy of Arts and Sciences*, 1899, v. 1, 427–442.
 5. Einstein A. Zur Elektrodynamik bewegter Körper (On Electrodynamics of Moving Bodies). *Annalen der Physik*, 1905, Bd. 322(10), 891–921.
 6. Tangherlini F.R. *Nuovo Cimento Suppl.*, 1961, v. 20, 351.
 7. Bell J.S. Speakable and unspeakable in Quantum Mechanics. In: *Collected Papers on Quantum Philosophy*, Cambridge University Press, 2004.
 8. Robertson H.P. Postulate versus observation in Special Relativity. *Reviews of Modern Physics*, 1949, v. 21(3), 378–382.
 9. Mansouri R. and Sexl R.U. A test theory of Special Relativity I: Simultaneity and clock synchronization. *General Relativity and Gravitation*, 1977, v. 8(7), 497–513.
 10. Mansouri R. and Sexl R.U. A test theory of Special Relativity II: First order tests. *General Relativity and Gravitation*, 1977, v. 8(7), 515–524.
 11. Mansouri R. and Sexl R.U. A test theory of Special Relativity III: Second order tests. *General Relativity and Gravitation*, 1977, v. 8(10), 809–814.
 12. Rybicki M. Critical analysis of Special Relativity in reference to the energy transformation. *Apeiron*, 2008, v. 15, issue 3, 270–293.
-

Progress in Physics is an American scientific journal on advanced studies in physics, registered with the Library of Congress (DC, USA): ISSN 1555-5534 (print version) and ISSN 1555-5615 (online version). The journal is peer reviewed and listed in the abstracting and indexing coverage of: Mathematical Reviews of the AMS (USA), DOAJ of Lund University (Sweden), Scientific Commons of the University of St.Gallen (Switzerland), Open-J-Gate (India), Referential Journal of VINITI (Russia), etc. **Progress in Physics** is an open-access journal published and distributed in accordance with the Budapest Open Initiative: this means that the electronic copies of both full-size version of the journal and the individual papers published therein will always be accessed for reading, download, and copying for any user free of charge. The journal is issued quarterly (four volumes per year).

Electronic version of this journal: <http://www.ptep-online.com>

Advisory Board of Founders:

Dmitri Rabounski, Editor-in-Chief
Florentin Smarandache, Assoc. Editor
Larissa Borissova, Assoc. Editor

Editorial Board:

Pierre Millette
Andreas Ries
Gunn Quznetsov
Felix Scholkmann
Ebenezer Chifu

Postal address:

Department of Mathematics and Science, University of New Mexico,
705 Gurley Avenue, Gallup, NM 87301, USA
